Intracellular Logistics –

Sorting Nexins in Retrograde Transport of Endogenous and Exogenous Cargo

Miriam Verena Bujny
Diplom Biochemikerin

A dissertation submitted to the University of Bristol in accordance with the requirements of the degree of Doctor of Philosophy in the Faculty of Medical and Veterinary Sciences

Department of Biochemistry
University of Bristol

Word Count: 58,483

May 2007

Author's Declaration

I declare that the work in this dissertation was carried out in accordance with the regulations of the University of Bristol. The work is original, except where indicated by special reference in the text, and no part of the dissertation has been submitted for any other academic award. Any views expressed in the dissertation are those of the author and in no way represent those of the University of Bristol. This dissertation has not been presented to any other university for examination either in the United Kingdom, or overseas.

SIGNED: ..... DATE: .....

Abstract

The endosomal system and vesicular carriers derived from it are the membranous correlates of intracellular transport and serve as 'dynamic platforms' and 'vehicles' to sort and dispatch cargo and membrane to a variety of sub-cellular destinations. Proper endosomal sorting can be accomplished through the cargo's ability to interact with, or to avoid, cargo/destination-specific machinery, through retention and partitioning mechanisms. To recruit the sorting machinery needed, endosomal-membrane compartments dispose of defined identities that serve as binding cues, *inter alia* provided by phosphoinositides, the phosphorylated derivatives of phosphatidylinositol.

Here, I have investigated the role of members of the phosphoinositide-binding protein family of sorting nexins (SNXs) in intracellular sorting and membrane transport processes. The prototypical member of this family, SNX1, had originally been implicated in regulating receptor traffic to degradative organelles under conditions of its overexpression. Subsequent studies of the endogenous protein could however not confirm its pro-degradative role.

Here, using RNAi technology to selectively suppress SNX1 expression, the role of endogenous SNX1 in intracellular transport was re-examined. Using a variety of techniques, including live and fixed cell analyses, biochemical approaches and infection assays, I show that SNX1 is critically involved in promoting retrograde transport from endosomes to the *trans*-Golgi network of a variety of endogenous and exogenous cargos. This includes the cation-independent mannose 6-phosphate receptor, Shiga toxin B subunit and furthermore sortilin, which had not been identified as a recycling receptor before. In addition, these studies show that SNX1 is involved in remodelling early stages of *Salmonella*-containing vacuoles, exemplifying its capacity as a regulator of membrane transport.

I have furthermore examined the role of the highly related SNX2 in these processes; I come to the conclusion that under the experimental conditions used in this study, its role in retrograde transport of the examined cargo is less prominently developed.

Acknowledgements

Firstly, my sincere thanks to 'the boss' Professor Pete Cullen, for open ears and doors, support and advice – but foremost for providing a highly flexible spatio-temporal set-up allowing both, professional and personal development. Many thanks for that. I am thankful to my co-assessor Dr Mark Jepson, for reading and discussing my work over the years, for helpful comments and advice. I would also like to thank my two examiners, Dr Sean Munro and Dr David Stephens, for their time and efforts. I thank Perkin Elmer LAS, especially Patrick Courtney, the Department of Biochemistry, University of Bristol, and the European Molecular Biology Organization for financial help.

I am grateful to all our collaborators: Prof Judith Klumperman, Prof Hans Geuze and of course Dr Muriel Mari, who I would like to thank for both, the excellent EM studies and friendship. Dr Ludger Johannes and Mr Vincent Popoff must be thanked for the collaboration on the role of retromer in Shiga toxin traffic, and for providing Parisian bench space. I am grateful to Dr Matthew Seaman and Prof Paul Luzio for the never ceasing source of crucial antibodies and reagents, and to Prof Paul Gleeson and Dr Rohan Teasdale for providing the original clones, and hence starting the Lab on sorting nexin biology. In this light, in retrospect, thanks must go to Dr Kai S. Erdmann at the Ruhr-Universität Bochum, who once upon a time, in 2002, introduced me to these little 'beasts'.

Everyone, past and present, in the ISL EW labs and offices, staff and students, must be thanked for making these three years so productive and eventful. One may forgive me to single out Dr Thomas 'Mehr Seil' Wassmer, for subjecting me to the *'vertical rocks'* to take my mind of the science from time to time, and of course Dr Anna Rutherford, for the *schmience* and for introducing me to the art of apiculture. I have learned a lot.

A big 'thank you' goes to Ms Heike Bohländer for the printing this thesis – 25 years on from our first day at school – and to Dr Nicola 'Nanni' Ternette, for paper and friendship.

Lastly, thanks to all you lovely people I had the pleasure to meet during my time 'on the island', thank you for shared houses and lifes, head massages, helicopter rides, and dinners, and just being fantastic to live and laugh and cry with.

Absolutely definitively most of all, my deepest gratitude to my wonderful family and to my friends - for the tremendous support over the years, for believing in me and for making this life worthwhile.

Für ***die*** Eva - die beste Mutter der Welt,
und ein wirklich vernünftiger Mensch

Für Andreas – meinen *'partner in crime'*
und wissenschaftliches Gewissen

Danke.

List of Abbreviations

aa	Amino acid
AAA-ATPase	ATPase associated with a variety of cellular activities
A-ALP	ALP containing DPAP-A luminal domain
ADP	Adenosine di-phosphate
ALP	Alkaline phosphatase (Pho8p)
AOBS	Acousto-optical beam splitter
AOTF	Acousto-optical tuneable filter
AP	Adaptor protein
APS	Ammonium persulphate
Arf	ADP ribosylation factors
ASGPR	Asialoglycoprotein Receptor
ASM	Acid sphingomyelinase
ATCC	American Tissue Culture Collection
BAR	Bin/Amphiphysin/Rvs
BFA	Brefeldin A
BSA	Bovine serum albumin
cAMP	Cyclic adenosine-3', 5'-monophosphate
CCV	Clathrin-coated vesicle
CD-MPR	Cation-dependent mannose 6-phosphate receptor
CD	Cluster of differentiation
cDNA	Complementary deoxyribonucleic acid
C. elegans	*Caenorhabditis elegans*
CHX	Cycloheximide
CI-MPR	Cation-independent mannose 6-phosphate receptor
CK2	Casein kinase-2
COP	Coatomer protein
Ci	Curie (1 Ci = 3.7×10^{10} Becquerel)
Cpm	Counts per minute
CPS	Carboxypeptidase S (Cps1p)
CPY	Carboxypeptidase Y (Cpy1p)
CTx	Cholera Toxin
CTxB	Cholera Toxin B-subunit
Cy	Cyanine
DAG	Diacylglycerol
dATP	2'-deoxyadenosine 5'-triphosphate
dCTP	2'-deoxycytidine 5'-triphosphate
dGTP	2'-deoxyguanosine 5'-triphosphate
dH_2O	distilled H_2O
DHB	DMEM/Hepes/BSA
D. melanogaster	*Drosophila melanogaster*
DMEM	Dulbecco's modified Eagles medium
DMSO	Di-methyl sulfoxide
DNA	Deoxyribonucleic acid
DPAP-A	Dipeptidyl aminopeptidase-A
DsRed	*Discosoma coral* red
DTT	Dithiothreitol
E.coli	*Escherichia coli*
ECL	Enhanced chemiluminescence

ECV	Endosomal carrier vesicle
EDTA	1-(4-Aminobenzyl)ethylenediamine-N,N,N',N'-tetraacetic acid
EE	Early endosome
EEA1	Early endosomal antigen-1
EGF	Epidermal growth factor
EGFP	Enhanced green fluorescence protein
EGFR	EGF receptor
EGTA	Ethylene glycol bis-(β-aminoethyl) N,N,N',N' tetraacetic acid
EM	Electron microscope, or electron microscopy
ENTH	Epsin amino-terminal homology
EPEC	Enteropathogenic *E. coli*
ER	Endoplasmic reticulum
ERC	Endocytic recycling compartment
ES cells	Embryonic stem cells
ESCRT	Endosomal sorting complex required for transport
EspF	*E. coli* secreted protein F
ETC	Endosome-to-TGN carrier
EtOH	Ethanol
FBS	Fetal Bovine Serum
FERM	Band 4.1, ezrin, radixin, moesin
FITC	Fluorescein isothiocyanate
Fps	Frames per second
FRAP	Fluorescence recovery after photobleaching
FYVE	Fab1p/YOTB/Vac1p/EEA1
GAP	GTPase Activating Protein
GDP	Guanosine 5'-diphosphate
GEF	Guanine nucleotide exchange factor
GFP	Green fluorescence protein
GGA	Golgi-localised, gamma-ear-containing, Arf-binding protein
GLUT	Glucose transporter
GPCR	GTPase-protein coupled receptor
GPI	glycosylphosphatidylinositol
Grd19p	Golgi retention defective-19 protein
GS	Golgi SNARE
GTP	Guanosine 5'-triphosphate
GTPase	Guanosine 5'-triphosphatase
HBSS	Hanks' balanced salt solution
Hepes	1-Piperazineethane sulfonic acid, 4-(2-hydroxyethyl)- monosodium salt
HRP	Horseradish peroxidase
Hrs	Hepatocyte growth factor-regulated tyrosine kinase substrate
H.sapiens	*Homo sapiens*
IF	Immunofluorescence
IgG	Immunoglobulin G
$Ins(1,4,5,6)P_4$	D-myo-inositol 1,4,5,6-tetraphosphate
$Ins(1,3,4,5,6)P_5$	D-myo-inositol 1,3,4,5,6-pentaphosphate
Kex2p	Killer expression-2 protein
Lamp-1	Lysosomal membrane glycoprotein-1
LB	Luria-Bertani
LBPA	Lyso-bis-PtdOH
LCI	Live cell imaging
LDL	Low-density lipoprotein

LE	Late endosome
LM	Light microscope, or light microscopy
M6P	Mannose 6-phosphate
MeOH	Methanol
MEF	Mouse embryonic fibroblast
MPR	Mannose 6-phosphate receptor
mRFP	Monomeric red fluorescence protein
mRNA	Messenger RNA
MVB	Multivesicular body
Mvp1p	Multicopy suppressor of Vps1p protein
NADPH	nicotinamide adenine dinucleotide phosphate
NEM	N-ethyl maleimide
NMR	Nuclear magnetic resonance
NSF	NEM sensitive factor
OD	Optical density
PACS-1	Phosphofurin acidic cluster sorting protein-1
PAGE	Poly-acrylamide gel electrophoresis
PAR-1	Protease activated receptor-1
Para.	paragraph
PB	Phosphate buffer
PBS	Phosphate Buffered Saline
PCR	Polymerase chain reaction
PDGF	Platelet derived growth factor
PDGFR	PDGF receptor
PDZ	Post synaptic density-95/Discs-Large/Zona-Occludens-1
PFA	Paraformaldehyde
PGE	Post-Golgi endosome
PH	Pleckstrin homology
PI3K	PI 3-kinase
p.i.	*post* infection
PI	Phosphoinositide
pIgA	Polymeric immunoglobulin A
pIgR	Polymeric immunoglobulin receptor
PIKfyve	PI kinase with a specificity for the 5-position, containing a FYVE finger domain
PLC	Phospholipase-C
PMSF	Phenyl-methylsulfonyl fluoride
PPIn	polyphosphoinositide
PROPPIN	β-propeller(s) that bind PPIn
PSD	Post-synaptic density
PSF	Point-spread function
PtdIns	D-myo-phosphatidylinositol
PtdIns3*P*	D-myo-phosphatidylinositol 3-monophosphate
PtdIns4*P*	D-myo-phosphatidylinositol 4-monophosphate
PtdIns5*P*	D-myo-phosphatidylinositol 5-monophosphate
PtdIns(3,4)P_2	D-myo-phosphatidylinositol 3,4-bisphosphate
PtdIns(3,5)P_2	D-myo-phosphatidylinositol 3,5-bisphosphate
PtdIns(4,5)P_2	D-myo-phosphatidylinositol 4,5-bisphosphate
PtdIns(3,4,5)P_3	D-myo-phosphatidylinositol 3,4,5-triphosphate
PVDF	Polyvinylidene fluoride
PVE	Pre-vacuolar endosome
PX	Phox homology

RA	Ras Association
RE	Recycling endosome
RGS	Regulator of G-protein signalling
RIPA	RadioImmunoPrecipitation Assay
RNA	Ribonucleic acid
RNAi	RNA interference
ROI	Region of interest
RPE	Rhodamine-phycoerythrin
RS-ALP	Retention-sequence ALP
SAP	sphingolipid activator protein
S.cerevisiae	*Saccharomyces cerevisiae*
Sch. pombe	*Schizosaccharomyces pombe*
s.d.	Standard deviation
SDS	Sodium dodecyl sulphate
SH	Src-homology
sH_2O	Sterile H_2O
siRNA	Small interfering RNA
Sip	*Salmonella* invasion protein
SNARE	Soluble NSF-attachment protein
SNX	Sorting nexin
Sop	*Salmonella* outer protein
SptP	*Salmonella* protein tyrosine phosphatase
Ssp	*Salmonella* secreted protein
STx	Shiga toxin
STxB	Shiga toxin B-subunit
S. Typhimurium	*Salmonella enterica* serovar Typhimurium
SV40	Simian virus 40
TAE	Tris-acetate-EDTA
TAPP1	Tandem PH-domain containing protein-1
TCA	Trichloroacetic acid
TEMED	N,N,N',N'-tetramethylethylenediamine
TET	Tetracycline
Tf(R)	Transferrin (receptor)
TGN	*trans*-Golgi network
TIP47	Tail interacting protein of 47-kDa
TPST	Tyrosylprotein sulfotransferase
TRITC	Tetra methyl rhodamine isothiocyanate
TSE/TEN	tubular sorting endosomes/tubular-endosomal network
TSG-101	Tumour suppressor gene-101
TTSS	Type III secretion system
V	Volume
VAMP	Vesicle associated membrane protein
V_oH^+ATPase	Vacuolar H^+ATPase
Vps	Vacuolar protein sorting
Vti1	Vps ten interacting 1
W	Weight
WASp	Wiskott-Aldrich Syndrome protein
WB	Western blotting
WD40 repeat	Protein motif ~40 aa containing a conserved tryptophan (W) & aspartic acid (D)
WIPI	WD40 repeat protein Interacting with PhosphoInositides of 49kDa

Table of Content

Table of Figures

Chapter 1 - Introduction

Chapter 3 – Role of Retromer in Receptor Retrieval

Chapter 4 - Role of Retromer in Retrograde Toxin Transport

Chapter 5 - Role of Sorting Nexins in Salmonella Invasion

List of Tables

Chapter 1 - Introduction

Chapter 3 – Role of Retromer in Receptor Retrieval

Chapter 4 - Role of Retromer in Retrograde Toxin Transport

Index of Movies

Remarks: While in some cases, movies might be best viewed in 'double size'- or 'fit to screen'-modes, it was in other cases indispensable to reduce size of the movies to keep file size manageable, rendering movies rather coarsely pixelated upon enlargement.

Chapter 3 Role of Retromer in Receptor Retrieval

I. Movies 3.1 GFP-SNX1 overexpression – low and high expressors

HeLa cells were transiently transfected with a vector encoding for GFP-SNX1 for 22 hours, and cells expressing either low levels or high levels were chosen and imaged for 2 -3 minutes using a PerkinElmer Ultra*VIEW* LCI system. Movies were exported at 10 frames per second.

Movie 3.1.1 GFP-SNX1 in HeLa cells (low expressor)

Movie 3.1.1 GFP-SNX1 in HeLa cells (high expressor)

II. Movies 3.2 HeLa cells co-expressing GFP-VPS35 and RFP-SNX1

HeLa cells were transiently co-transfected with vectors encoding for GFP-VPS35 and RFP-SNX1 for 22 hours, and cells expressing low levels were imaged for 2 -3 minutes using a PerkinElmer Ultra*VIEW* LCI system. Movies were exported at 10 frames per second.

Movie 3.2.1 GFP-VPS35 (green) and RFP-SNX1 (red) in HeLa cells (merge)

Movie 3.2.2 RFP-SNX1 only (from Movie 3.2.1)

Movie 3.2.3 GFP-VPS35 only (from Movie 3.2.1)

III. Movies 3.3 CD8-uptake in cells stably expressing CD8-CI-MPR chimera

HeLaM cells stably expressing a CD8-CI-MPR chimeric protein were transiently transfected with a vectors encoding GFP-SNX1 for 22 hours. Cells were surface-labelled with RPE-coupled anti-CD8 antibodies (RPE-CD8), and uptake was imaged live (see para. 3.2.4 for details) using a PerkinElmer Ultra*VIEW* LCI system.

Movie 3.3.1 GFP-SNX1 (green) and RPE-CD8 (red) (merge)

Movie 3.3.2 GFP-SNX1 only (from Movie 3.3.1)

Movie 3.3.3 RPE-CD8 only (from Movie 3.3.1)

Movie 3.3.4 Region of interest (ROI2): GFP-SNX1 and RPE-CD8 (merge, from Movie 3.3.1)

Movie 3.3.5 Region of interest (ROI2): GFP-SNX1 only (from Movie 3.3.2)

Movie 3.3.6 Region of interest (ROI2): RPE-CD8 only (from Movie 3.3.3)

Chapter 4 Role of Retromer in Retrograde Toxin Transport

IV. Movies 4.1 Uptake of FITC-STxB into RFP-SNX1 transfected cells

HeLa cells, transiently transfected with a vector encoding for RFP-SNX1 fusion protein ,were surface-labelled with FITC-STxB. The toxin subunit was partially internalized at 19.5°C (see **para. 4.3.4** and **4.4.** for details). Uptake (early stage) was imaged live using a PerkinElmer Ultra*VIEW* LCI system. Movie was exported at 10 fps.

Movie 4.1.1 FITC-STxB (green) and RFP-SNX1-transfected HeLa cells (early stage)

Movie 4.1.2 A region of interest from Movie 4.1.1 is shown. Movie was additionally manipulated using ImageJ (see paragraph 4.234 for details)

V. Movies 4.2 Uptake of FITC-STxB into RFP-SNX1 transfected cells

HeLa cells, transiently transfected with a vector encoding for an RFP-SNX1 fusion protein, were surface-labelled with FITC-STxB. The toxin subunit was partially internalized at 19.5°C (see **para. 4.3.4** and **4.4.** for details), and intracellular transport to the TGN (late stage) was imaged live using a PerkinElmer Ultra*VIEW* LCI system, time is in seconds (10 fps).

Movie 4.2.1 FITC-STxB and RFP-SNX1 (merge, late stage)

Movie 4.2.2 RFP-SNX1 alone

Movie 4.2.3 FITC-STxB alone

Movie 4.2.4 Region of interest (ROI): FITC-STxB and RFP-SNX1 (merge, late stage)

Movie 4.2.5 Region of interest (ROI): RFP-SNX1 alone

Movie 4.2.6 Region of interest (ROI): FITC-STxB alone

Chapter 5 Role of Sorting Nexins in Salmonella Invasion

VI. Movie 5.1 3D-animated view of a *Salmonella*-induced membrane ruffle

Shown is a deconvolved, 3D-rendered and animated movie of a membrane ruffle with endogenous SNX1 labelled with anti-SNX1 (Alexa488, green), actin labelled using TRITC-phalloidin and bacterial DNA labelled using DAPI.

HeLa cells transiently transfected with GFP-SNX1 were infected with SL1344 for 15 minutes, then fixed and treated with TRITC-phalloidin (red) and DAPI (blue). Optical z-slices were acquired (z = 5.37, 12 sections) and, using Volo*city* V4.0.1, data sets were deconvolved (98% confidence, or 20 iterations), 3D-rendered, animated, and exported as .avi movie.

VII. Movies 5.2 GFP-SNX1 recruitment to infection sites

MDCK cells transiently transfected with a vector encoding for a GFP-SNX1 fusion protein were infected with the *S. Typhimurium* strain SL1344 (readily identifiable by the sudden increase in light-lucency in the fluorescent channel). Images were captured every 20 seconds for 24:20 minutes. Movies were compiled using Volo*city* software and exported at 10 frames per second (fps).

Movie 5.2.1 GFP-SNX1 in MDCK cells infected with wild type SL1344

Movie 5.2.2 Phase contrast of MDCK cells infected with wild type SL1344

Movie 5.2.3 GFP-SNX1; a region of interest from Movie 5.2.1

Movie 5.2.4 Phase contrast; a region of interest from Movie 5.2.2

VIII. Movie 5.3 GFP-SNX5 recruitment upon SL1344 infection

MDCK cells, transiently transfected with a vector encoding for a GFP-SNX5 fusion protein, were infected with the *S. Typhimurium* strain SL1344. Images were captured every 20 seconds for approximately 25 minutes. Movies were compiled using Volo*city* software and exported at 10 fps.

Movie 5.3.1 GFP-SNX5 in MDCK cells infected with wild type SL1344

Movie 5.3.2 Phase contrast of MDCK cells infected with wild type SL1344

IX. Movie 5.4 GFP-SNX1 meshwork

Shown is a 3D-rendered animation of deconvolved images of GFP-SNX1-meshwork in SL1344-infected cells (DNA in blue (DAPI stain), actin (red) visualized using TRITC-phalloidin).
HeLa cells transiently transfected with GFP-SNX1 were infected with SL1344 for 15 minutes, then fixed and treated with TRITC-phalloidin (red) and DAPI (blue). Optical z-slices were acquired ($z = 4.76$ µm, 29 sections) and, using Volo*city* V4.0.1, data sets were deconvolved (98% confidence, or 20 iterations), 3D-rendered, animated, and exported as .avi movie.

X. Movie 5.5 GFP-2xFYVE recruitment in HeLa cells infected with SL1344

HeLa cells, transiently transfected with a vector encoding for a GFP-2xFYVE, were infected with SL1344. Images were captured every 20 seconds for approximately 25 minutes. Movies were compiled using Volo*city* software and exported at 10 fps.

Movie 5.5.1 GFP-2xFYVE in HeLa cells infected with wild type SL1344

Movie 5.5.2 Phase contrast of HeLa cells infected with wild type SL1344

XI. Movie 5.6 RFP-2xFYVE and GFP-SNX1 recruitment in HeLa cells infected with SL1344

HeLa cells, transiently transfected with both, RFP-2xFYVE (red) and GFP-SNX1 (green), were infected with the SL1344 strain and imaged live with a 20-second delay between image capturing. Movie was compiled using Volo*city* software, showing first an overlay of all channels (phase contrast channel at 50% opacity, RFP-2xFYVE, GFP-SNX1), then an overlay of the two fluorescent channels, and finally the RFP-2xFYVE channel alone followed by the GFP-SNX1 channel (10 fps).

XII. Movie 5.7 GFP-SNX1 recruitment in HeLa cells infected with SL1344–ΔsigD

HeLa cells transfected with GFP-SNX1 were infected with a SL1344 mutant lacking the phosphatase SigD (ΔsigD). Images were captured every 20 seconds. Movies were compiled using Volo*city* software and exported at 10 fps.

Movie 5.7.1 GFP-SNX1 in HeLa cells infected with wild type SL1344-ΔsigD

Movie 5.7.2 Phase contrast of HeLa cells infected with wild type SL1344-ΔsigD

XIII. Movie 5.8 GFP-SNX1 recruitment in HeLa cells infected with a SL1344–Δsig-pSigD-pSigE strain

HeLa cells transfected with GFP-SNX1 were infected with a SL1344 strain carrying an isogenic sigD deletion (ΔsigD) but complemented with a plasmid encoding for SigD and its chaperone SigE (pSigDpSigE). Images were captured every 20 seconds. Movies were compiled using Volo*city* software and exported at 10 fps.

Movie 5.8.1 GFP-SNX1 in HeLa cells infected with wild type SL1344-ΔsigD-pSigD-pSigE

Movie 5.8.2 Phase contrast of HeLa cells infected with wild type SL1344-ΔsigD-pSigD-pSigE

Chapter 1 - Introduction

1.1. Preface - 'Intracellular Logistics'

Logistics, n, pl.
The organization of supplies, stores, quarters, etc., necessary for the support of troop movements, expeditions, etc.
(Oxford English Dictionary, 1989, 2nd Edition).

One of the central questions in cell biology is how cells organize and orchestrate intracellular transport processes. At any given time, cells receive incoming material at the plasma membrane that is 'packed' into 'carriers' and transported to a given destination. On the other hand, intracellularly produced material needs to be delivered to the appropriate target organelles. Depending on the cell type, these highly complex interconnected processes ensure proper cell function by fulfilling a broad range of tasks, such as uptake and delivery of nutrients, secretion of hormones or cell-surface proteins, antimicrobial defence and degradation of unwanted material.

A better understanding of 'intracellular logistics' is not only essential to further our knowledge about normal cell function, *id est* 'non-disease states', but may also help to better understand 'disease states' related to defects transport or exploits by extracellular pathogens. Thus, this knowledge may ultimately contribute to designing intracellularly-targeted therapeutic agents and further our understanding of - and how to interfere with - the itineraries of pathogens and toxins inside cells.

The intracellular correlate of transport is the endosomal system, which appears as sorting and dispatching system. It is comprised of a morphological heterogeneous and interconnected network of dynamic membranous compartments.. It is emerging that endosomal compartments are comprised of highly organised microdomains generated and maintained by finely tuned mechanisms to recruit small GTPases, to create lipid microdomains and to partition cargo into such subdomains. An immanent problem arising from the high turnover and dynamic properties is the accurate description of the system when studying it.

This thesis is primarily concerned with transport processes from endosomes to the *trans*-Golgi network and a group of peripheral membrane proteins that are transiently associated with endosomes (sorting nexins), members of which have been implicated in regulating endosomal sorting.

The following introduction is aimed at introducing some of the major concepts in intracellular sorting; further introduction to the specific subjects can be found at the beginning of the individual chapters, or will be introduced where appropriate.

Main concepts:

1. 'Mosaic-like organisation' of endomembranes, achieved by selective enrichment or generation of distinct molecules: high spatial and temporal control for transient, but precise targeting of peripheral membrane proteins ensures flexibility with high accuracy at the same time
2. Improved targeting through 'cascade effects' and 'coincidence detection': to ensure transient, but precise targeting, more than one recruitment cue is employed (this includes additional protein-protein interactions, additional lipid-binding domains, binding enhancement through conformational changes upon recruitment or geometry-based targeting)
3. Sorting is a process consisting of active removal and retention.

1.2. Endomembrane Organisation

For efficient sorting of proteins and lipids the different compartments need to have a defined identity. It is now well accepted that compartmentalization already starts at the organelle level: proteins (like small GTPases) and lipids appear enriched within distinct 'sub-organelle' membrane domains, thus creating a 'mosaic-like' structure that organises endosomal membranes (Gruenberg, 2001; Zerial and McBride, 2001; Miaczynska and Zerial, 2002).

1.2.1. Spatial organisation at lipid level

Spatial organisation and compartmental identity can be achieved by selective accumulation of lipids in membranes, which can occur at specific sites in the bilayer, as with phosphoinositides, or in discrete 'patches' or 'rafts', as has been proposed for cholesterol and sphingolipids.

1.2.1.1. Polyphosphatidylinositols and their binding modules

Polyphosphoinositides (PPIn)[1] are minor constituents of cellular membranes, and while PPIn have been implicated in "nearly all aspects of cell physiology" (Di Paolo and De Camilli, 2006), in this thesis I have mostly concentrated on their role in intracellular trafficking. As lipids, they appear as ideal cues to organize endomembrane identity as they are partitioned into bilayers, and hence often restricted to the site of their generation, while within the bilayer they can rapidly diffuse. Furthermore, they can be rapidly generated and decomposed and can be interconverted [see (Di Paolo and De Camilli, 2006) for a recent review].

The 'backbone' for the PPIn family of eight members is phosphatidylinositol (PtdIns), which consists of a *myo*-inositol-1-phosphate head group coupled, almost exclusively, to 1-stearoyl 2-arachidonoyl diacylglycerol (DAG) *via* a phosphodiester bond (**Figure 1. 1**). The lipophilic 'tail' allows PPIn to partition into the inner leaflet of cellular membranes leaving its charged sugar head group exposed to the cytosol. This inositol can be phosphorylated in 3-, 4- or 5-position through the actions of site-specific lipid kinases or phosphatases, giving rise to a total of seven derivates of PtdIns (see **Figure 1. 1** and (De Matteis and Godi, 2004) for review).

---

[1] The nomenclature for phosphoinositides in this thesis was adopted as outlined by Michell, Heath, Lemmon and Dove (Michel et al., 2006); see also http://www.chem.qmul.ac.uk/iupac/misc/phos2t8.html#t4 and http://www.chem.qmul.ac.uk/iupac/cyclitol/myo.html

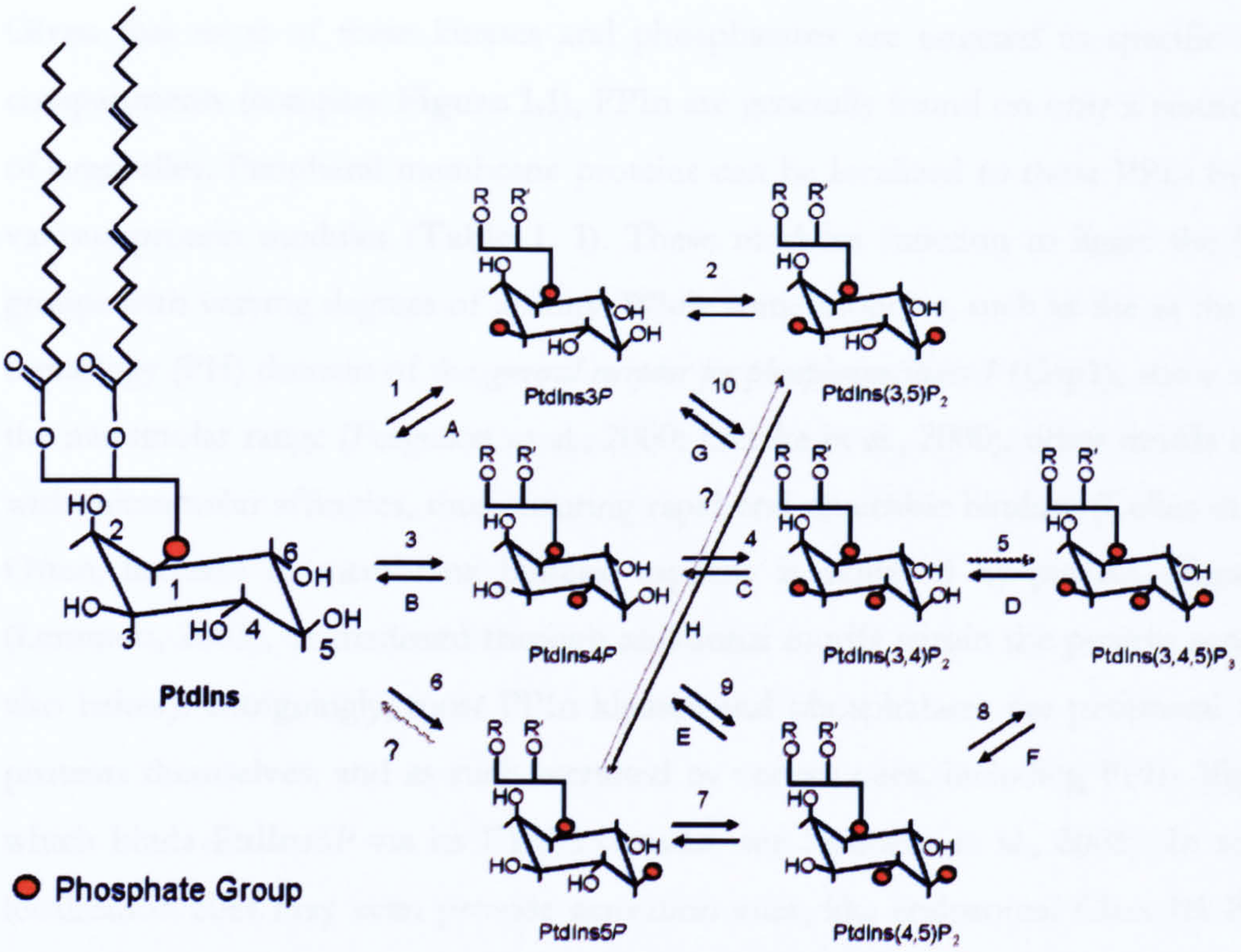

1 : PI3-kinase — Type II PI 3-kinase-C2 α (Golgi, endosomes; β (PM); γ (Golgi)
PI 3-kinase (Type III (Vps34) (Golgi, endosomes)

2 : PI3P 5-kinase — PIKfyve (endosomes)

3 : PI4-kinase — IIα (Golgi, endosomes); IIβ (Golgi, PM); IIIα (ER, Golgi); IIIβ (Golgi, Nu)

4 : PI4P 3-kinase — Type II PI 3-kinase-C2 α (Golgi, endosomes); β (PM); γ (Golgi)

5 : PI4P 5-kinase — PIP5Kα,β,γ (PM)

6 : PI5-kinase — PIKfyve (endosomes)

7 : PI5P 4-kinase — PIP4Kα,β (PM); γ (ER)

8 : PI 3-kinase — Type 1 α,β,γ (PM, nucleus)

9 : PI4P 5-kinase — PIP5Kα,β,γ (PM)

10: PI3P 4-kinase — PIP4Kα,β (PM), γ (ER)

A : PI3P 3-phosphatase — MTM1 (PM); MTMR1-8 (PM, and not determined)

B : PI4P 4-phosphatase — Synaptojanin 1, 2 (clathrin-coated vesicles, mitochondria), Sac1 (Golgi, ER)

C : $PI(3,4)P_2$ 3-phosphatase — PTEN 1, 2 (PM, Golgi, nucleus)

D : $PI(3,4,5)P_3$ 5-phosphatase — SHIP 1, 2 (PM, nucleus)

E : $PI(4,5)P_2$ 5-phosphatase — 5-phosphatase II (not determined); OCRL (Golgi, endosomes, lysosomes)
Synaptojanin (synaptic vesicles, mitochondria)

F : $PI(3,4,5)P_3$ 3-phosphatase — PTEN I, II –(PM, Golgi, nucleus)

G : $PI(3,4)P_2$ 4-phosphatase — Type I, II 4-phosphatase (not determined)

H : $PI(3,5)P_2$ 3-phosphatase — MTMR1-8 (not determined)

Figure 1. 1 Phosphoinositide metabolism in mammalian cells.

Reversible phosphorylation of the inositol ring of phosphatidylinositol (PtdIns) either singly or multiply at the 3-, 4- or 5- positions yields the phosphoinositides above. Arrows indicate the possible phosphorylations (numbers) and dephosphorylations (letters). Reactions indicated with grey/dotted arrows are unconfirmed *in vivo*, or have been shown *in vitro*, but their importance in living cells remains unclear. PM: plasma membrane; ER: endoplasmic reticulum; Nu: nucleus. Compiled and adapted from Hughes et al., 2000; Stephens et al., 2000; Cullen et al., 2001; De Matteis and Godi, 2004; Di Paolo and De Camilli, 2006.

Given that most of these kinases and phosphatases are targeted to specific subcellular compartments (compare **Figure 1.1**), PPIn are generally found on only a restricted subset of organelles. Peripheral membrane proteins can be localized to these PPIn by means of various protein modules (**Table 1. 1**). These modules function to ligate the PPIn head groups with varying degrees of affinity. While some modules, such as the as the pleckstrin homology (PH) domain of the *general receptor for phosphoinositides-1* (Grp1), show affinities in the nanomolar range (Ferguson et al., 2000; Lietzke et al., 2000), other motifs ligate PPIn with micromolar affinities, thus ensuring rapid and reversible binding (Cullen et al., 2001). Often, increase in membrane binding capacity is achieved by protein oligomerization (Lemmon, 2003), or mediated through additional motifs within the protein sequence (see also below). Intriguingly, most PPIn kinases and phosphatases are peripheral membrane proteins themselves, and as such recruited by certain cues, including PPIn (like PIKfyve which binds PtdIns3*P* via its FYVE domain; see Shisheva et al., 2001). In some cases, localization cues may even provide activation cues, like endosomal Class III PI 3-kinase that is localized and activated upon binding to GTP-Rab5 (Christoforidis et al., 1999).

PtdIns3*P* on endosomes and PtdIns(4,5)P_2 at the plasma membrane are probably by far the best characterized PPIn with regard to endomembrane organization. PtdIns3*P* is present on the limiting membranes of early endosomes and on internal vesicles of multivesicular bodies (MVB) (Gillooly et al., 2000) and is recognized by a wide variety of peripheral membrane proteins by means of different PtdIns3*P*-ligating domains. Most commonly, these proteins contain FYVE- or PX-domains (Xu et al., 2001c; Lemmon, 2003; Birkeland and Stenmark, 2004).

The FYVE domain – multiple cues

The FYVE domain, named after proteins it was originally identified in (Fab1p, YOTB, Vac1p and EEA1), exclusively ligates PtdIns3*P* (Gaullier et al., 1998; Patki et al., 1998). It is responsible for the localization of the early endosome antigen-1 (EEA1) (Stenmark et al., 1996), a protein involved in homo- and heterotypic fusion of early endosomal compartments. Additionally to the lipid cue, its ability to dimerize (Dumas et al., 2001) as well as binding to the small GTPase Rab5 (Lawe et al., 2000; Lawe et al., 2002) ensures effective recruitment to endosomal membranes. Hrs, another FYVE-domain containing protein, is involved in later events of endosomal processes and regulates sorting of cargo destined for degradation into MVBs. Importantly, it also provides an example how

transport and sorting can be uncoupled: while the sorting step of activated EGF receptors is dependent on PtdIns3*P*, the 'core' of endosome formation appears independent of PtdIns3*P* (Petiot et al., 2003).

The PX domain – multiple PPIns

Another PtdIns3*P*-ligating motif, the phox homology (PX) domain was originally identified as a conserved module in the p40phox and p47phox subunits of the phagocytic nicotinamide adenine dinucleotide phosphate (NADPH) oxidase (phox) complex (Ponting, 1996; Kanai et al., 2001). It is now clear that PX domains can be found in a wide range of proteins involved in transduction pathways and intracellular trafficking, including phosphatidylinositol 3-phosphate kinases (PI3-kinases), phospholipases, and, of particular interest in this study, sorting nexins (see also **Table 1. 1**). While a subset of PX domains solely binds to PtdIns3*P*, as do all yeast PX domain identified so far (Yu and Lemmon, 2001), PX domains of mammalian sorting nexins bind to a variety of PPIn, but with a bias toward 3-phosphoinositides (Worby and Dixon, 2002; Carlton et al., 2005a).

Interactions of PX domains with membranes are likely to be determined by a combination of electrostatic interactions with the bilayer, and structurally, likely to include insertions of hydrophobic loops into the membrane (Stahelin et al., 2003).

Module	Specificity	example of proteins
ENTH	PtdIns4*P*	epsinR
	PtdIns(3,5)*P*2	Ent3, Ent5, HIP1
	PtdIns(4,5)*P*2	AP180, epsin-1
PX	PtdIns3*P*	SNX1-4, SNX17
	PtdIns5*P*	SNX13
	PtdIns(3,4)*P*2	p47phox
	PtdIns(3,5)*P*2	SNX1
	PtdIns(4,5)*P*2	class II PI3 kinase
	PtdIns(3,4,5)*P*3	CISK
FYVE	PtdIns3*P*	EEA1, Hrs, PIKfyve
GRAM	PtdIns(3,5)*P*2	Myotubularins
PH	PtdIns4*P*	FAPP1/2
	PtdIns(3,4)*P*2	Akt/PKB
	PtdIns(4,5)*P*2	PLCδ1,dynamin
	PtdIns(3,4,5)*P*3	Btk, Akt/PKB, ARNO, Grp1

Shown are examples of phosphoinositides and identified –binding motifs. Binding is in most cases not restricted to one PPIn (see SNX1, which binds to PtdIns3*P* and PtdIns(3,5)P_2), but not all binding partners are indicated in all cases. Adapted from Di Paolo and De Camilli, 2006.

Table 1. 1 Phosphoinositides and their binding modules in some example proteins

It is noteworthy that most PX domains ligate PPIns with relatively low (micromolar) affinities. Given that many PX domain-containing proteins also contain additional domains such as PH domains (PLD1 and PLD2), or SH3 domains (SNX9, SNX18, p40phox and p47phox), or GTPase interacting domains like SNX13, SNX14, SNX25 or SNX27 [reviewed (Xu et al., 2001c)], it is likely that correct membrane targeting of PX domain-containing proteins arises due to oligomerization, or with aid of more than one domain.

Epsins and the ENTH domain – multiple destinations

Until recently, the ENTH domain was thought to specifically interact with 4-phosphoinositides. It was first identified in epsin-1, and its homologues AP180 and CALM, and shown to specifically bind to PtdIns(4,5)P_2 (Ford et al., 2001; Itoh et al., 2001). PtdIns(4,5)P_2 is enriched in the inner leaflet of the plasma membrane and concentrated into specialized domains (see McLaughlin et al., 2004; McLaughlin and Murray, 2005 for review). Here, at regions of endocytosis, it serves to co-ordinate the internalization process; consistent with the ability of AP180 and epsin-1 to bind to clathrin and the AP-2 complex, these PtdIns(4,5)P_2-binding ENTH domain-containing proteins are found in the invagination regions at the plasma membrane. Further still, dependent upon their binding to PtdIns(4,5)P_2, AP180 and epsin-1 polymerize flat clathrin lattices, while epsin-1 is furthermore capable of physically deforming PtdIns(4,5)P_2-enriched membranes (Ford et al., 2001; Ford et al., 2002).

The ENTH domain of epsinR, which is related to epsin-1, has been shown to bind to PtdIns4*P* (Hirst et al., 2003), a PPIn found at the Golgi/*trans*-Golgi network (Wang et al., 2003; Godi et al., 2004). In contrast, the ENTH domain of the yeast epsin orthologues, Ent3 and Ent5 (Friant et al., 2003; Eugster et al., 2004), which are localized to the vacuoles and associated membranes, have been shown to bind all PtdInsP_2 isomers with relatively low affinity ($K_D > 3\mu M$) (Michell et al., 2006). In these cases, their function appears to be in regulating traffic at endosomes and the trans-Golgi network. Thus, the ENTH domain constitutes a further PPIn-binding module that is active at a number of subcellular destinations.

PtdIns(3,5)P_2 – new kid on the block

The exact role and sub-cellular localization of PtdIns(3,5)P_2 in mammalian cells is currently being unraveled. So far, no mammalian protein has been identified that solely ligates this

PPIn making it difficult to discriminate its exact sub-cellular targeting. Based on the localization of PIKfyve, the kinase generating PtdIns(3,5)P_2, it has often been quoted as a late endosomal PPIn (Shisheva et al., 2001). It is now well accepted however that the FYVE-domain containing PIKfyve localizes in most cell types to an early, rather than a late endosomal compartment (Cooke, 2002; Rutherford et al., 2006). Lack of PtdIns(3,5)P_2-generating kinases (PIKfyve in mammals, Fab1 in yeast) causes grossly enlarged vacuoles as common phenotypes, suggesting that PtdIns(3,5)P_2 is needed for membrane homeostasis (Michell et al., 2006). Likewise, lack of effector proteins can cause a similar phenotype: in yeast, Svp18/Atg18 is a specific and high-affinity PtdIns(3,5)P_2-binding protein that has been localized to the limiting membranes of vacuoles and participates in retrograde membrane traffic (Dove et al., 2004). Evidence for a role of PtdIns(3,5)P_2 in mammalian retrograde pathways comes from the recent identification of the WD40 repeat protein interacting with phosphoinositides of 49kDa (WIPI49), renamed to PROPPIN-1 (Michell et al., 2006), a protein involved in endosome-to-TGN retrieval of the CI-MPR (Jeffries et al., 2004). PROPPINs is the proposed new name for a family of proteins found encoded for in almost all eukaryotic genomes, containing WD40-repeat-based seven bladed β-propeller(s) that bind PPIn. This includes Atg18 (see above), which is one of three yeast PROPPINs (Michell et al., 2006).

PtdIns(3,4)P_2 and PtdIns(3,4,5)P_3 – the second messengers

PtdIns(3,4)P_2 and PtdIns(3,4,5)P_3 are second messengers, hence generated in acute response to external signals. Localized production of PtdIns(3,4,5)P_3 from plasma membrane-localized PtdIns(4,5)P_2 occurs downstream of receptor activation through activation of class I PI 3-kinase (Stephens, 2000). PtdIns(3,4,5)P_3 is known to recruit a number of signalling molecules of the Akt/PKB pathways and thus to activate signalling cascades involved the mitogenic and cellular survival pathways (Brazil and Hemmings, 2001). Further still, it is involved in re-localizing and activating proteins involved in cytoskeletal rearrangements, including a number of RacGEFs (Han et al., 1998; Nimnual et al., 1998). A definitive physiological role for PtdIns(3,4)P_2 is as yet to be assigned, although it is thought to regulate mitogenic stimuli, similar to the proposed role of PtdIns(3,4,5)P_3. Notably, many PH domains that bind PtdIns(3,4,5)P_3 also bind PtdIns(3,4)P_2, for example, DAPP1 (Dowler et al., 1999) and PKB (Frech et al., 1997), thus proteins that are responsive to PI 3-kinase activation at the plasma membrane may be

recruited and thus activated dependent upon relative levels of PtdIns(3,4)P_2 and PtdIns(3,4,5)P_3, and their ability to bind these lipids.

1.2.1.2. Lipid rafts

The finding that glycosylphosphatidylinositol (GPI)-anchored proteins, certain glycolipids, sphingomyelin and cholesterol persist, and are enriched in, membrane fractions after non-ionic detergent extraction, was a first evidence that lipids and sterols do not heterogeneously mix, but form distinct microdomains in the plane of the bilayer (Brown and Rose, 1992). The general concept of 'rafts' is now well established: lateral membrane heterogeneity emerges as requirement of biological membranes; the exact nature remains notoriously debated (see Munro, 2003 for review), as it proves technically very challenging to study 'nanoscale ordered lipids' From a biophysical view, microdomain formation is a function of both, the chain length and degree of saturation of the hydrocarbon tails for each lipid species. It appears that saturated, long-chain lipids are more tightly packed and thus their rotational mobility within the hydrophobic region of the bilayer is decreased compared to unsaturated, short-chain lipids. Phase separation can be observed at physiological temperatures as long-chain, saturated lipids display gel-like properties (l_o phase) while unsaturated species are more fluid (l_d phase). These membrane l_o microdomains, or 'rafts' are primarily composed of cholesterol and highly ordered saturated glycosphingolipids [see (Jacobson et al., 2007) for a recent review].

Rafts are generally viewed as dynamic assemblies of cholesterol and sphingolipids that form in the exoplasmic leaflet of cellular membranes (Simons and Ikonen, 1997; Brown and London, 1998). These structures selectively incorporate - or exclude - proteins and thereby form 'dynamic platforms' for selective interactions. It is emerging that rafts do not only play important roles in sorting and vesicle formation, but also vesicle movement and cytoskeletal interactions, as well as docking and fusion events (Ikonen, 2001). Of wider interest for this study in the finding that lipid rafts also affect trafficking between endosomes and the TGN, as exemplified by the endosome-to-TGN transport defects in cholesterol storage diseases, like Niemann-Pick disease type C (NPC) (Mukherjee and Maxfield, 2004). There is also strong indication that receptor-binding of toxins, such as cholera toxin (CTx), correlates with its transport to the ER. The relationship between rafts and toxin traffic has been most well studied for CTx as its cellular receptor, the ganglioside GM1, strongly partitions into rafts and is often used as '*bona fide*' raft marker. Nevertheless, CTx endocytosis depends on both, clathrin-dependent and –independent mechanisms and

it appears that all forms of endocytosis identified so far may allow for CTx access to the Golgi/ER [(Orlandi and Fishman, 1998; Torgersen et al., 2001; Massol et al., 2004; Kirkham et al., 2005); see also below].

1.2.2. Spatial organisation at protein level – small Rab GTPases

Members of the Ras superfamily also emerge as regulators of membrane organisation: this prominently includes members of the family of Rab GTPases, and the Arf and Arl family. GTPases act as molecular switches that alternate between an activated, GTP-bound form and an inactive GDP-bound form. While in its active form, the GTPase becomes associated with membranes, the conformational changes associated with GTP-hydrolysis render the protein cytosolic (Vetter and Wittinghofer, 2001). The activation and inactivation cycle of these GTPases is governed by a number of regulatory proteins, which: keep the protein in its inactive form to prevent random association with membranes (GDP-dissociation inhibitor, GDI); which allow association with membranes by displacing GDIs (GDI displacement factor, GDF); which allow activation of the GTPase by aiding replacement of the GDP by GTP (guanine nucleotide exchange factor, GEF); which enhance the intrinsically low GTPase activity of the GTPase (GTPase activating protein, GAP).

Rab GTPases create unique 'Rab domains' on endosomal organelles, which serve to recruit distinct effector proteins, including peripheral membrane proteins and motors, and hence can regulate sorting to distinct destinations from these organelles (Zerial and McBride, 2001). As schematically illustrated in **Figure 1. 2**, GTP-bound active Rab proteins each associate with different membranous compartments within the endosomal system. Different Rab proteins are also seen to segregate into different regions of the same endosomal compartment. While Rab4, Rab5 and Rab11 are all present on the membranes of early endosomes, they each occupy a separate area of membrane as revealed by fluorescence microscopy, (Sonnichsen et al., 2000). The partitioning into separate subdomains also reflects the different functional roles of these Rab proteins: while, simplified, Rab5 covers the vesicular portion and recruits effectors regulating early endosome fusion, Rab4 is required for transport form the sorting endosome to the plasma membrane (van der Sluijs et al., 1992), and Rab11 for recycling of cargo from the sorting endosome and via the recycling endosome (Ullrich et al., 1996; Ren et al., 1998). Communication between the separate Rab domains is mediated by divalent Rab effectors

(de Renzis et al., 2002). Localization of and *via* Rabs also imparts temporal control, being activated by GTP exchange, and there is much evidence now to suggest that exact spatio-temporal targeting of Rabs is governed by the proteins regulating the GTP/GDP cycle of these Rabs. In this light, GEFs are peripheral membrane proteins and localized only to a specific set of organelles, thus amplifying the specificity and targeting [see (Behnia and Munro, 2005; Grosshans et al., 2006) for review].

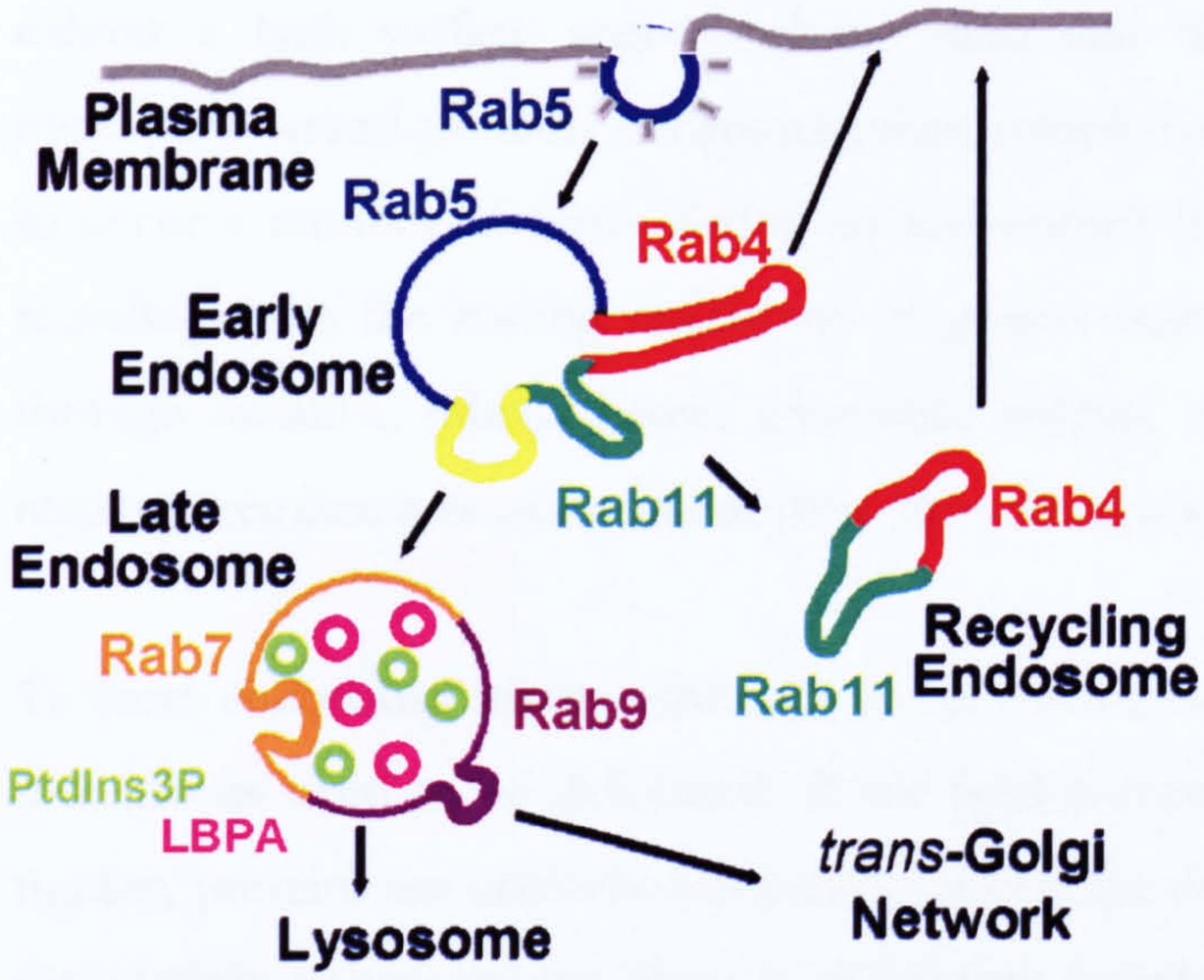

Simplified schematic illustration of the proposed non-uniform distribution of selected Rab GTPases throughout the endosomal system. Adapted from Miaczynsca and Zerial, 2002.

Figure 1. 2 Rab GTPases in the endosomal system

Crosstalk

Rabs and PPIn are cross-regulated and interconnected. For example, the presence of PtdIns3*P* is intimately linked to the presence of Rabs: On one hand, VPS34, the kinase that generates most PtdIns3*P* in the cell, is a direct Rab effector, meaning that synthesis of PtdIns3*P* is regulated by Rab5 (Shin et al., 2005). On the other hand, Rab effectors contain FYVE domain, which bind to PtdIns3*P* (see above).

1.2.3. Membrane tubules and their deformation by proteins

'Membrane geometry' might be, in a wider sense, regarded as another aspect of membrane organization. Endocytic organelles exhibit a complex morphological organisation and are characterised by vacuolar and tubular elements. Geometry-based sorting through narrow-diameter tubules is the predominant way in the sorting endosome to remove recycled membrane from soluble cargo of endosomal vacuoles [(Dunn et al., 1989; Mayor et al., 1993), reviewed in Maxfield and McGraw, 2004]: narrow diameter membrane tubules exhibit a high surface area-to-volume ratio and thus will more efficiently partition membrane bound proteins (receptors), than soluble content. Tubulation events are known to occur a number of times during an endosome's lifespan, improving the efficiency of recycling from the sorting endosome to greater than 99% (Mayor et al., 1993). Hence, through iterative, tubular-based, geometric sorting, membranous tubules can efficiently remove membrane bound content from the sorting endosomal body.

To form endosomal tubules (but also at the plasma membrane and at the TGN) vacuolar membranes need to be deformed. While lipid composition will determine its fluidity or rigidity, proteins are critically involved in aiding the deformation processes. It now seems that clathrin polymerisation alone is insufficient to induce membrane deformation (Nossal, 2001). Mechanistically, protein oligomerization and deformation according to the bilayer couple hypothesis have been proposed as mechanisms of inducing deformation. Oligomerization of certain proteins such as endophilin or amphiphysin is thought to physically deform the bilayer by forming a 3-dimensional structure that conveys rigidity, which is capable of deforming the 'elastic' membrane. Membrane deformation according to the bilayer couple hypothesis describes the effects when inserting an amphipathic helix into a one leaflet of the bilayer. This has the effect of forcing the opposing leaflet to deform in a concave manner to maintain hydrophobic and van der Waals forces between the monolayers, and hence, will result in induce membrane deformation [see (Farsad and De Camilli, 2003) for review].

Again, the ENTH domain of epsin-1 may serve as an example: while given its PtdIns(4,5)P_2-binding capacity (Itoh et al., 2001), it serves to recruit epsin-1 to the plasma membrane, subsequent studies have shown that upon PtdIns(4,5)P_2 ligation, conformational changes result in the insertion of an amino-terminal amphipathic α-helix (helix-0) into the bilayer resulting in membrane bending (Ford et al., 2002).

BAR domain

A recently discovered motif that, at least in some cases, mediates membrane tubulation is the BAR domain, named after the proteins it was first discovered in (Bin/amphiphysin/Rvs). The BAR domain can sense curvature, meaning that some BAR-containing proteins will only associate with liposomes of appropriate diameter, and in other cases, BAR domain-containing proteins are able to deform membranes. So far, BAR domains have been found in a variety of proteins including amphiphysins, centaurins, endophilins, nandrins, oligophrenins, and sorting nexins (Habermann, 2004; Peter et al., 2004). The domain spans approximately 250 amino acids, with highly charged regions, which folds into a kinked tripartite α-helix. Upon dimerization, these coiled-coil regions can form crescent shaped structures. The positively charged concave surface then allows binding to oppositely charged curved membrane surfaces. A subset of BAR domains also contains an amino-terminal amphipathic α-helix (the N-BAR helix), and it appears that these proteins are able to directly impose curvature upon membranes (Habermann, 2004; Peter et al., 2004). Mechanistically, a protein will induce curvature if the energetic stabilization upon binding to a curved surface over a flat surface is sufficient to overcome the energy required to deform the membrane. Biophysical calculations have shown, that for amphiphysin, the rigidity of the BAR domain and its charge alone are sufficient to overcome the membrane elastic modulus. Hence, the membrane can be deformed by the electrostatics between BAR domain and membrane (Zimmerberg and McLaughlin, 2004).

While BAR-domains are dimerization and membrane curvature sensors, most of the proteins with this domain also dispose other membrane-binding modules, such as PH domains (in oligophrenins and centaurins) or PX domains (in sorting nexins). Likewise, BAR-domains are often found adjacent to small GTPase-binding, or regulatory domains, such as RhoGAP, ArfGAP or ArfGEF domains (Habermann, 2004). Hence, a 'tandem structure' may regulate the correct sub-localization, or even influence the activation state of small GTPases at specific subcellular localizations, especially as the BAR domain can function as a small G-protein binding module (Habermann, 2004; Peter et al., 2004). Interestingly, a number of Arf-GTPase regulators (Centaurinβ, arfaptin) contain BAR domains and may thus localise the GTPase to sites of high curvature (Lee and Schekman, 2004; Peter et al., 2004). ArfGAP1 itself contains an ALPS (ArfGap1 lipid-packing sensor) motif. Like Bar domains, this motif responds to lipid curvature and it is necessary for coupling ArfGAP1 activity with membrane curvature (Bigay et al., 2003; Bigay et al., 2005).

1.3. The Endosomal System

The following paragraphs will give an overview over the endosomal system: the ways to enter it, the itineraries, the cargo and machinery associated with it that is most relevant to this thesis (for an overview, see **Figure 1.3**).

While a 'categorical description' of 'early' and 'late' endosome is often used, these refer to morphological most disparate characteristics of these organelles. However, within these categories a gradual change, or maturation is observed (see also below for discussion on maturation). Indeed, as proposed by Hopkins in 1990 (Hopkins et al., 1990), or more recently by Bonifacino and colleagues (Bonifacino and Rojas, 2006), *the* early endosome might morphologically be best described as a 'continuous reticulum', or more functionally as 'tubular sorting endosome', with various proteins associating with spatially distinct domains at different times to mediate differential sorting of cargo, and to allow for budding from these compartments and fusion events with other organelles.

1.3.1. Endocytosis

So how do molecules enter the sorting network? The classical concept that clathrin-mediated endocytosis (CME) provides the common mechanism for a variety of cargo has now been replaced by a picture where different molecules may utilize distinct entry mechanisms. Likewise, even when using the – nominally - same way of entry, different receptors may display dissimilar requirements for accessory and scaffolding proteins; for example, internalization of transferrin receptors (TfR) was shown to require both, clathrin and its adaptor AP-2, while epidermal growth factor receptors (EGFR) and low density lipoprotein receptors (LDLR) require clathrin but not AP-2 (Motley et al., 2003). Moreover, in some cases - especially for toxins - it appears that one given molecule may use more than one way of entering the cell, further adding on to the high complexity.

1.3.1.1. Macropinocytosis

Stimulation of cells with growth factors, such as EGF, induces actin-driven formation of plasma membrane ruffles that, upon contact with other membrane tips, will backfuse. In this process, extracellular liquid will become encapsulated in macropinosomes, which thus provides a route for non-selective endocytosis of solute macro-molecules (Swanson and Watts, 1995). Macropinosomes are heterogeneous in size and can be as large as 5 μm in

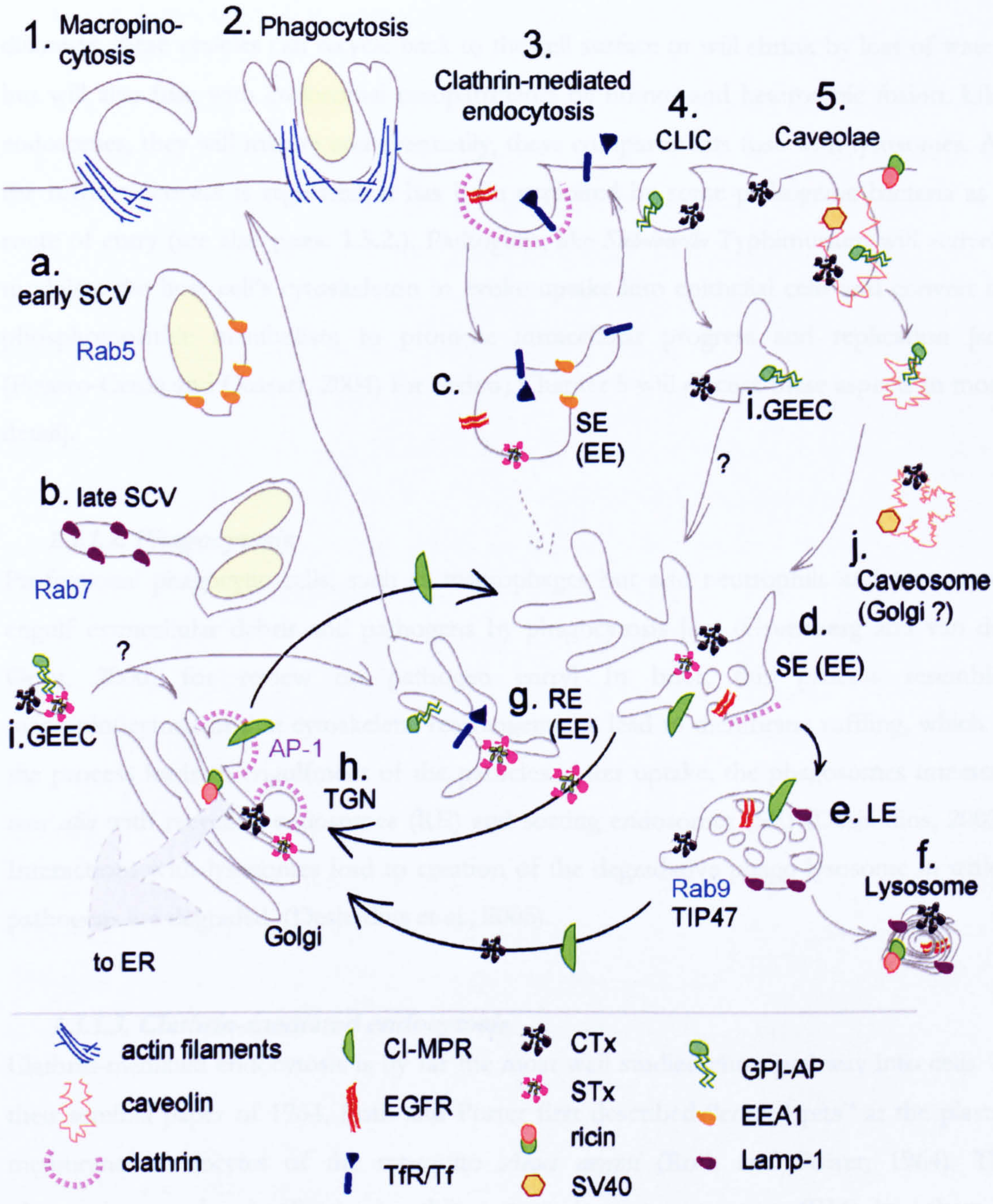

Figure 1. 3 The Endosomal System – some biosynthetic and retrograde routes.

Various endo- and exocytic routes and the endosomal network are depicted. For each itinerary a model cargo is shown. Some cargos might take more than one route. CLIC = non-clathrin, non-caveolae; GEEC = GPI-anchored protein-enriched early endosomal compartment; SE (EE) = sorting endosomes, also referred to as early endosomes (dashed line indicates maturation, and centripetal transport); RE (EE) = recycling endosomes; SCV = *Salmonella*-containing vacuole (broadly speaking, early SCVs resemble SEs, late SCVs resemble LEs); LE = late endosome; TGN = *trans*-Golgi network; ER = endoplasmic reticulum. CTx = cholera toxin; STx = Shiga toxin. Refer also to text for details. Adapted and modified from Perret et al., 2005.

diameter; these vesicles can recycle back to the cell surface or will shrink by loss of water, but will also fuse with endosomal compartments by homo- and heterotypic fusion. Like endosomes, they will mature and eventually, these compartments fuse with lysosomes. As the ruffling process is regulated, it has been exploited by some pathogenic bacteria as a route of entry (see also **para. 1.3.2.**). Pathogens, like *Salmonella* Typhimurium will actively modulate the host cell's cytoskeleton to evoke uptake into epithelial cells and convert its phosphoinositide metabolism to promote intracellular progress and replication [see (Pizarro-Cerda and Cossart, 2004) for review; Chapter 5 will discuss these aspects in more detail].

1.3.1.2. Phagocytosis

Professional phagocytic cells, such as macrophages but also neutrophils and monocytes engulf extracellular debris and pathogens by phagocytosis [see (Gruenberg and van der Goot, 2006) for review on pathogen entry] In brief, this process resembles macropinocytosis in that cytoskeletal rearrangements lead to membrane ruffling, which in the process leads to engulfment of the particles. After uptake, the phagosomes interact , *inter alia* with recycling endosomes (RE) and sorting endosomes (SE) (Desjardins, 2003). Interactions with lysosomes lead to creation of the degradative phago-lysosome in which pathogens are degraded (Desjardins et al., 2005).

1.3.1.3. Clathrin-mediated endocytosis

Clathrin-mediated endocytosis is by far the most well studied entry pathway into cells. In their seminal paper of 1964, Roth and Porter first described "coated pits" at the plasma membrane of oocytes of the mosquito *Aedes aegypti* (Roth and Porter, 1964). The observations made, visualized using thin-section electron microscopy (EM), lead them to propose that coated pits are membrane-invaginations that can pinch off from the plasma membrane to form coated vesicles, which following internalization, would uncoat to deliver their cargo to an intracellular target. Although 40 years ago the components of the coat were unknown, this study already described the crucial features of the process. For a more recent view on this topic see for example (Slepnev et al., 2000; Brodsky et al., 2001; Perrais and Merrifield, 2005).

1.3.1.4. Non-clathrin, non-caveolae endocytosis, CLIC

One way to internalize proteins associated with lipid receptors, for example cholera toxin and its receptor GM1, or GPI-anchored proteins, is thought to occur *via* through raft-like, Ø (diameter) 40 – 50 nm structures in a mechanism independent of clathrin and caveolin (see **par 1.3.1.5**), leading to what has been termed GPI-anchored protein-enriched early endosomal compartments (GEEC) (Sabharanjak et al., 2002; Kirkham et al., 2005; Kalia et al., 2006). These GEECs are initially negative for Rab5, and EEA1, but subsequently acquire these proteins and are thus competent to fuse with endosomes containing cargo from the clathrin-dependent endocytic pathway (Kalia et al., 2006). From ultrastructural studies using murine embryonic fibroblasts (EF) lacking caveolin, it appears that about 50% of CTx enters the cells in this cholesterol-sensitive, non-caveolae, non-clathrin-dependent pathway (Kirkham et al., 2005). Besides caveolin, flotillin-1 has been implicated in clathrin-independent endocytosis. While flotillin-1 is expressed in cells that lack caveolae and caveolins, the exact relationship between caveolins and flotillins is not clear (Lang et al., 1998; Santamaria et al., 2005). Flotillin-1 resides in specific subpopulation of endocytic intermediates defines a clathrin-independent endocytic pathway in mammalian cells. It has been shown that in cells depleted of flotillin-1 using siRNA, uptake of CTx and GPI-linked proteins is inhibited (Glebov et al., 2006). Intriguingly, coassembly of flotillin-1 and the related flotillin-2 into microdomains is sufficient to induce membrane curvature and formation of plasma-membrane invaginitations and the accumulation intracellular vesicles (Frick et al., 2007). This finding strongly suggests that flotillin proteins are defining structural components of the machinery that mediates a clathrin-independent endocytic pathway.

1.3.1.5. Caveolae-mediated endocytosis and caveosomes

Caveolae are lipid raft-enriched, flask-shaped, caveolin-containing membrane invaginations that have been described for many cell types (Anderson, 1998). Caveolae serve as 'anchored' multifunctional platforms for stimulated internalisation: caveolae are now thought to be relatively immobile organelles that do not partake in constitutive, endocytic uptake (Thomsen et al., 2002). Based on morphological studies, CTx has been proposed to be internalised via caveolae (Tran et al., 1987; Parton, 1994). It has however also been noted that the use of different cell lines and tools pose difficulties in comparing the relevance of the different entry mechanisms for this toxin. Exemplary for this, a recent study found that the mechanism of entry of a fluorescently-labelled CTxB probe was

directly dependent on the respective levels of cellular caveolin. While in cells displaying high levels of caveolin, uptake was found to be clathrin-independent, it was found to be dependent on clathrin in cells with low caveolin (Singh et al., 2003). And while CTx has been found in caveosomes, an intracellular, caveolin-1 positive membrane-bounded structure (Pelkmans et al., 2001), it appears possible that CTx can enter a caveolin-containing compartment after entry by caveolae-independent mechanisms: indeed, it appears that all forms of endocytosis identified so far may allow for CTx access to the Golgi/ER [(Orlandi and Fishman, 1998; Torgersen et al., 2001; Massol et al., 2004; Kirkham et al., 2005) see Kirkham et al., for a comparative study]. Interestingly, GM1-binding simian virus-40 (SV40) is transported differently to CTx: SV40 must reach the ER to infect the host cell and given the same receptor, somewhat expectedly, both are dependent on lipid rafts. However, there appear to be clear differences between the two. While CTx and SV40 can both enter cells using caveolae and move together to the caveosome, they subsequently partition away from each other. Whilst SV40 appears to be directly transported to the ER in separate vesicles, CTx reaches the Golgi (Pelkmans et al., 2004). In any case, this pathway appears to avoid the degradative endosomal-lysomal route (Pelkmans et al., 2001).

For completeness, the exotoxin of *Shigella dysenteriae*, STx, can also enter cells by both, clathrin-dependent and -independent mechanisms, and entry depends on binding to its glycolipid receptor, the globoside Gb3. Thus, like CTx, STx is sorted by lipids rather than proteins, and it has been proposed that the heterogeneity of the ceramide domains (Degroote et al., 2004) may ultimately influence their intracellular itinerary (Lencer and Saslowsky, 2005). Potentially, the CTx- and STx-induced clustering of their respective receptors might also contribute to their endocytosis and trafficking properties (see also Chapter 4).

1.3.2. Endosomal Transport Routes

After uptake from the plasma membrane, the first discernible organelles most cargo is delivered to, are early/sorting endosomes, which however also receive input from the TGN. Receptors like the transferrin receptor (TfR) and EFGR are internalized by CME into these highly fusogenic organelles whose ability to fuse with incident endocytic material and pre-existing sorting endosomes is regulated by Rab5 and EEA1 (Lawe et al., 2000; Lawe et al., 2002). Here, the receptors will segregate from their ligands due to the more acidic environment created through action of the V_o H^+-ATPase (Yoshimori et al.,

1991; van Weert et al., 1995). The major part of actively signalling receptors, such as the EGFR, are delivered to lysosomes, as they are retained in the sorting endosomes by ubiquitination (see below). Nutrient receptors, in their apo-form, are recycled back to the plasma membrane – either directly, or *via* recycling endosomes (RE) (Gruenberg and Maxfield, 1995; Maxfield and McGraw, 2004).

1.3.2.1. Recycling pathway to the plasma membrane

Recycling endosomes are composed of mainly tubular membranes of about 60 nm and are positioned juxtanculearly near the microtubule organizing centre (Hopkins et al., 1994). They are characterized by a more neutral pH (around pH 6.4) compared to sorting endosomes but considered part of the 'early endosome', as opposed to late endosomes, which are characterized by their commitment to the degradative route [see (Maxfield and McGraw, 2004) for review on endocytic recycling]. Tubular exit from the recycling endosome is thought to return both, cargo and membrane, to the plasma membrane with a $t_{1/2}$ of approximately 10-12 minutes (Mayor et al., 1993). It is to be noted that a faster phase of recycling is thought to occur directly from early endosomes with a $t_{1/2}$ of approximately 2 minutes (Stoorvogel et al., 1987). Given the speed at which this phase of recycling occurs, it has proved hard to study and little is known of its regulation. Sorting through the recycling endosome is thought to by tubule-based geometric sorting (see **para. 1.2.3**), and to occur independently of recycling motifs but it has been shown to require the small GTPases Rab4, Rab5 and Rab11, although their exact role in these processes is not clear.

1.3.2.2. Anterograde transport: TGN-to-endosome transport

The mannose 6-phosphate receptors

Besides input from the plasma membrane, sorting endosomes also receive input from intracellular organelles like the TGN. This pathway provides molecules from the biosynthetic routes, including lysosomal hydrolases that are delivered to endosomes by mannose 6-phosphate receptors. The cation-dependent (CD-) and the cation-independent (CI-) mannose 6-phosphate receptors (MPRs) are two transmembrane receptors involved in transport of lysosomal hydrolases (Kornfeld, 1992; Ghosh et al., 2003). These receptors recognize phosphomannosyl residues on the post-translationally modified hydrolases in

the TGN, and deliver these enzymes to prelysosomal compartments. For transport, MPR-hydrolase complexes are packed into clathrin-coated transport carriers, and the packing is thought to be mediated *via* AP-1, as this clathrin adaptor directly binds to a di-leucine motif in the cytoplasmic MPR tail (Johnson and Kornfeld, 1992). In support of this model is also the finding that clathrin, AP-1 and the MPRs co-localize on buds at the TGN (Klumperman et al., 1998), and that interfering with this interaction causes MPR mis-sorting in living cells (Hille-Rehfeld, 1995). In addition to the AP-1/MPR interaction, a second association involving the di-leucine motif in the MPR tail has been identified. Here, it has been found that Golgi-localizing, gamma-adaptin ear homology domain, ARF-binding (GGA) proteins also bind to this motif, and participate in the incorporation of the MPR into clathrin coated buds at the TGN (Doray et al., 2002; Shiba et al., 2002). GGAs are monomeric clathrin adaptor proteins, and it has been proposed that GGAs and AP-1 may act processively - with the GGAs retaining MPRs on non-clathrin-coated regions of the TGN and in a phosphorylation dependent process, and passing them on to AP-1 at bud sites (Doray et al 2002, Ghosh et al., 2003).

1.3.2.3. Retrograde transport: endosome-to-TGN retrieval

In addition to the anterograde transport of biosynthetic cargo from the TGN to endosomes, a retrograde pathway from endosomes exists to return receptors to the TGN: in contrast to their cargo, the MPRs do not enter the degradative pathway (Dahms et al., 1989). Once at the endosome, the hydrolase is released from the receptor, mediated by the relatively lower endosomal pH, and while the soluble enzymes remain in the luminal body of the endosome, the receptor is efficiently retrieved to the Golgi/TGN for further rounds of delivery (for mechanism see below). Besides the MPRs, receptors and molecules on this route also includes furin, a subtilisin-like dibasic endopeptidase, and orthologue of *S.cerevisiae* Kex2p [see (Molloy et al., 1999) for review], murine TGN38 and its human orthologue TGN46 (proteins of unknown function; see (Stanley and Howell, 1993) for review], the carboxypeptidase D, a metallocarboxypeptidase [see (Varlamov and Fricker, 1998) for review]. Furthermore, several bacterial exotoxins traffic on this retrograde route to eventually reach the ER [(Bonifacino and Rojas, 2006) for review; generally see Chapter 4 for details).

Molecular machinery involved in retrieval

The proteins thought to be involved in the retrieval steps of the MPRs include AP-1, which also participates in anterograde TGN-to-endosome: due to defective endosome-to-TGN transport, embryonic fibroblasts from mice deficient in the μ1A subunit of AP-1 exhibit a redistribution of MPRs to early endosomes (Meyer et al., 2000; 2001). Additionally, a novel adaptor protein, the phosphofurin acidic cluster sorting protein-1 (PACS-1), has also been implicated. Originally identified through its interactions with furin, PACS-1 also binds to clusters of acidic amino acids in the CI-MPR tail (Wan et al., 1998). RNAi-mediated PACS-1 depletion, caused redistribution of cellular furin and CI-MPR to peripheral compartments indicative of inhibited retrograde transport (Wan et al., 1998). PACS-1, an AP-1 binding protein, can ligate the acidic cluster motif within the cytosolic domains of proteins retrieved from endosomes to the TGN (Wan et al., 1998). In this manner, PACS-1 has been proposed to co-operate with AP-1 to package proteins containing acidic clusters (such as the CD- and CI-MPRs and furin) into transport intermediates.

A role for the clathrin adaptor epsinR has also been proposed. Overexpressed epsinR prevented the endosome-to-TGN retrieval of Shiga toxin, overexpressed CI-MPR, and TGN38/46 (Saint-Pol et al., 2004). EpsinR has recently been shown to interact with Vti1b (Chidambaram et al., 2004), a SNARE related to Vti1a, itself implicated in transport from the sorting endosome-to-TGN transport (Mallard et al., 2002).

Late endosome-retrieval

Besides the machinery described above, retrieval machinery from late endosomes appears also to exist for the CI-MPR: the GTPase Rab9 and its effectors tail interacting protein-47 (TIP47) and p40 have all been implicated in traffic from the late endosome. Rab9 associates with both late endosomes and the TGN destined vesicles that bud from them. Retrograde traffic is disrupted by expression of dominant negative Rab9 *in vivo* and stimulated by recombinant Rab9 *in vitro* (Lombardi et al., 1993) (Riederer et al., 1994). TIP47 is able to bind is able to bind GTP-Rab9 and CI-MPR via separate sites and it was proposed that Rab9 recruits TIP47 to late endosomes, where it may be involved in cargo recognition. Depletion of TIP47 was reported to inhibit CI-MPR transport in vivo (Diaz and Pfeffer, 1998). However it has recently been suggested that TIP47 plays no role in MPR retrieval (Medigeshi and Schu, 2003). Indeed, the finding that structurally, TIP47 is a member of a family of lipid droplet-binding proteins (Hickenbottom et al., 2004) is difficult to reconcile with a role in MPR retrieval (Bonifacino and Rojas, 2006).

1.3.2.4. The degradative pathway

Lysosomes are often referred to as the end-points of the endosomal system and are acidic, proteolytic compartments that receive degradative cargo and input from the biosynthetic route in the form of lysosomal hydrolases. Trough fusion of lysosomes with late endosomes, cargos retained in endosomes will become subject to degradation. Retention of cargo is achieved through specialised endosomal domains that are able to undergo a process of inward budding into the endosomal lumen, and thus cargos are incorporated into intraluminal vesicles. These intraluminal vesicle-containing endosomes are referred to as multivesicular bodies (MVBs), and are commonly thought to represent late endosomes. The molecular mechanism of intralumenal sorting is highly complex and only beginning to unravelled. Presently, the actual mechanistic basis for invagination into the endosomal lumen is unknown. Ubiquitin addition appears as dominant sorting signal for incorporation into the intraluminal vesicles of the MVB and subsequent degradation. And ubiquitinated cargo (Ub-cargo) is retained in a specialised PI 3-kinase sensitive, bi-layered, clathrin-containing coat upon sorting endosomes (Sachse et al., 2002b). This coat contains Hrs, a protein that is heavily phosphorylated upon activation of growth factor receptors and retention and concentration of Ub-cargo within the clathrin-containing bi-layered coat is dependent upon the interaction of the incorporated ubiquitin moiety with Hrs (Raiborg et al., 2002; Urbe et al., 2003). Hrs is able to interact with TSG101, which in turn acts to recruit the endosomal sorting complex required for transport-I (ESCRT-I), a multi-protein complex, to endosomal membranes. This in turn is required for correct recruitment of two other ESCRT complexes (ESCRT II and III), and it has been proposed that these complexes function in a sequential manner to coordinate the delivery of Ub-cargo to the intraluminal vesicles of the MVB (Katzmann et al., 2002).

Maturation versus vesicular delivery

Two mechanisms for progression between early and late endosomes have been proposed - maturation and vesicular delivery. The maturation hypothesis proposes that the endosome effectively matures around the cargo present within the endosome. As recycling proteins are removed from - and acid hydrolases are delivered to - this endosome, it matures into a late endosome (Murphy, 1991; Stoorvogel et al., 1991; Dunn and Maxfield, 1992; Futter et al., 1996; Hirst et al., 1998). The vesicular delivery hypothesis suggests that the detachment of membrane containing intraluminal vesicles from sorting endosomes gives rise to an

endosomal carrier vesicle (ECV), which subsequently fuses with a late endosome (Griffiths and Gruenberg, 1991; Gu and Gruenberg, 1999; Gruenberg and Stenmark, 2004). Recently a third model of maturation by "Rab conversion" has been proposed which integrates aspects of both models (Rink et al., 2005). This model, based largely on live-cell fluorescence microscopy, suggests that incoming vesicles from the plasma membrane undergo homotypic fusion to generate early endosomes. These Rab5-positive endosomes continue to accept incoming vesicles, while recycling cargo exits *via* Rab4-positive tubules. Continual fusion causes these Rab5 structures to increase in size and decrease in number as they move towards the cell centre, until a rapid mass replacement of Rab5 with the late endosome defining Rab7 occurs. This Rab conversion is mediated by the Rab5-dependent recruitment of a Rab7 nucleotide exchange factor, although the trigger for this has not been specified (Deretic, 2005; Rink et al., 2005). All three models incorporate the same mechanism of degradative sorting, and agree that once the late endosome has formed, it undergoes a heterotypic fusion with the lysosome (Futter et al., 1996; Mullock et al., 1998).

1.4. Sorting Nexins

The family of sorting nexins comprises a diverse group of PX domain-containing proteins, members of which have been implicated in regulating intracellular sorting (see also **Table 1.4**). Based upon sequence homology of this SNX-specific PX domain, there are currently 30 mammalian proteins assigned to this family [see (Worby and Dixon, 2002; Carlton et al., 2005a) for review; compare **Figure 1. 4**]. Sorting nexins can be found in species ranging from plants (Jaillais et al., 2006) to *Drosophila* (Worby et al., 2001), *Danio rerio* (Yoo et al., 2006) and yeast (10 members).

Given that the PX domain has been identified as PPIn-ligating motif, it is not surprising that the majority of studies have localized SNXs to endomembranes; in every SNX examined so far, its PX domain targets its host to phosphoinositide-enriched membranes, mostly ligating 3-phosphoinositides (see (Teasdale et al., 2001) for review; compare **Table 1.2**).

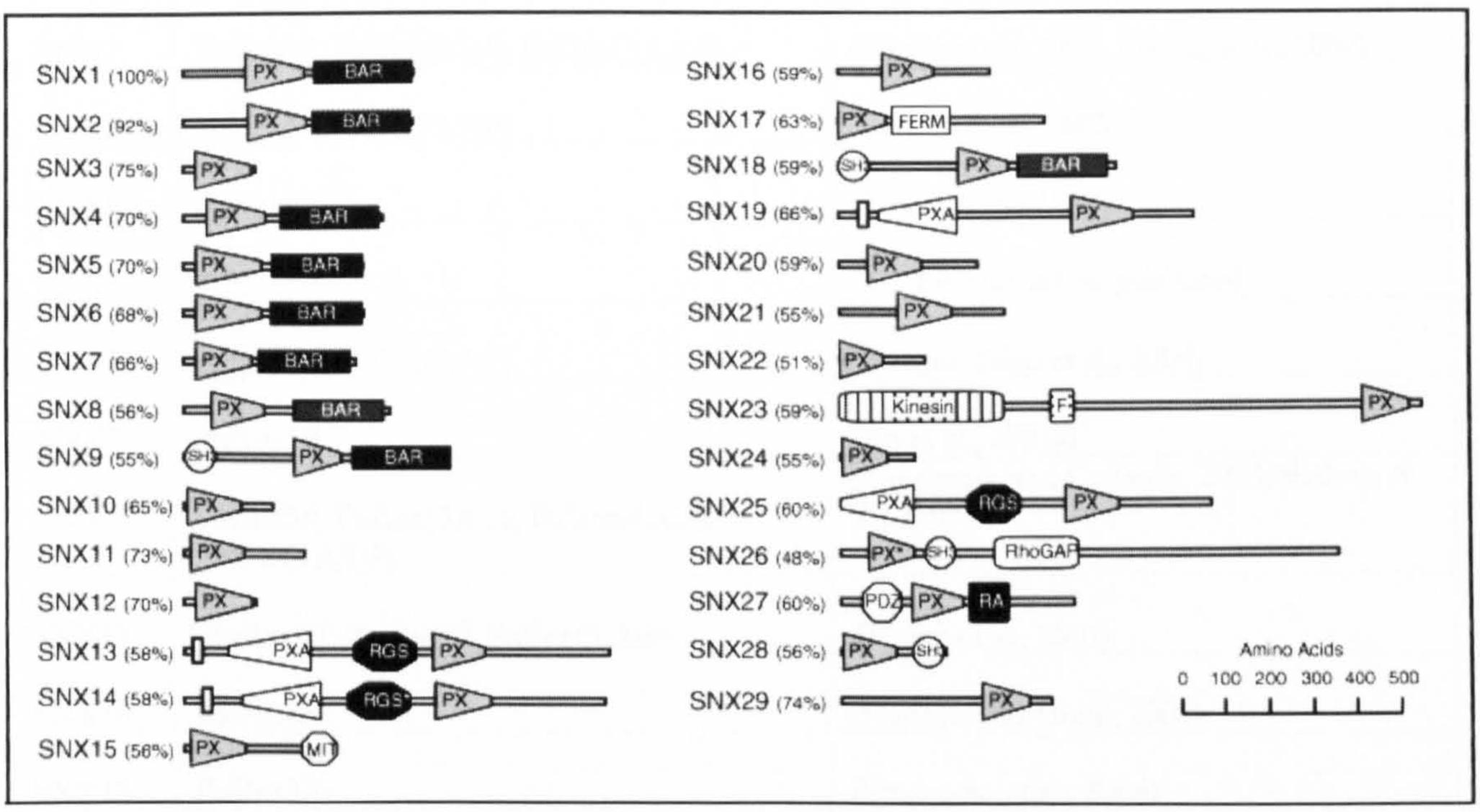

Figure 1. 4 Domain architecture of mammalian sorting nexins

Sequences for the mammalian SNXs (as deposited on NCBI) were analysed using the SMART (http://smart.embl-heidelberg.de) and Pfam (http://www.sanger.ac.uk/Software/Pfam) architecture research tools to generate predicted domain structures. Calculated percentage similarity between the SNX-PX domain and the SNX1-PX domain is given in brackets. BAR - Bin/Amphiphysin/Rvs, F - forkhead, FERM = 4.1, ezrin, radixin, moesin; GAP - GTPase activating domain, MIT - microtubule interacting and trafficking molecule domain, PDZ - PSD95/Dlg/ZO1/2; PX - Phox homology, PXA - PX associated, SH3 - Src homology 3, RA - Ras association, RGS - regulator of G-protein signalling. Asterisk (*) indicates that the domain is predicted, but is below threshold levels for identification. (Modified from a figure compiled by Jez Carlton)

Apart from their 'hallmark' PX domain, the sequence homology is generally low between SNXs. Solely based on further domain structures and predicted motifs, the sorting nexins may be further subclassified: members of group A contain C-terminal coiled-coil domains, and these may also be referred to as SNX-BAR proteins, although strictly speaking, in most cases a functional classification as 'BAR protein' (see **par. 1.2.3**) is still lacking. Members of group B have no recognisable motifs other than the PX domain. Sorting nexins in group C are 'multi-domain proteins' and contain a number of protein-protein interaction motifs, like Src homology (SH3) domains[2] or PDZ (postsynaptic density-95/ discs large/zona occludens-1) motifs, as well as motifs involved in cell signalling, like RGS (regulator of G-protein signalling) domains, or the RasGTP effector domain, RA.
Most members of this family are still poorly characterised, and it remains to be established whether they are all involved in sorting.

SNX	PPin-binding Specificity	Reference
SNX1	PtdIns3*P*, PtdIns(3,5)P_2, PtdIns(3,4,5)P_2	(Cozier et al., 2002; Zhong et al., 2002)
SNX2	PtdIns3*P*, PtdIns(3,5)P_2	(Carlton et al., 2005b)
SNX3	PtdIns3*P*	(Xu et al., 2001b)
SNX4	PtdIns3*P*	(AC Rutherford, unpublished)
SNX5	PtdIns3*P*, PtdIns(3,4)P_2	(Merino-Trigo et al., 2004)
SNX7	PtdIns3*P*	(Xu et al., 2001a)
SNX9	PtdIns3*P*, PtdIns(3,4)P_2, PtdIns(4,5)P_2, PtdIns(3,4,5)P_3	(Lundmark and Carlsson, 2003; Badour et al., 2007)
SNX13	PtdIns3*P*, PtdIns5*P*, PtdIns(3'.5)P_2	(Zheng et al., 2001)
SNX16	PtdIns3*P*	(Hanson and Hong, 2003)
SNX17	PtdIns3*P*	(Czubayko et al., 2006)
SNX23 (KIF16B)	PtdIns3*P*, PtdIns(3,4)P_2, PtdIns(3,4,5)P_3	(Hoepfner et al., 2005)
SNX27	PtdIns3*P*	(JG Carlton – unpublished)

Table 1. 2 Phosphoinositide-binding properties on mammalian SNXs

[2] So strictly speaking, SNX9 and SNX18 could be classified into 'group A' as well as 'group B'.

1.4.1. Sorting Nexin-1

SNX1 was originally identified in a yeast two-hybrid screen as binding partner for the cytoplasmic tail of the EGF receptor, and subsequently, in cells overexpressing SNX1, levels of EGFR were found to be markedly reduced compared to untransfected cells. SNX1 was thus proposed as a positive regulator of lysosomal sorting (Kurten et al., 1996). This proposed role was subsequently confirmed by a number of other groups (Chin et al., 2001; Cozier et al., 2002; Zhong et al., 2002). Overexpressed SNX1 was also shown to be capable of homo- and hetero-oligomerisation and was found to interact with a number of surface receptors (Haft et al., 1998; compare **Table 1.3**); this included Hrs, suggesting a possible mechanism whereby the EGFR could be passed from SNX1 onto Hrs for correct ESCRT dependent degradative sorting (Chin et al., 2001). Interestingly, besides the EGFR, SNX1 was shown to interact with receptors for PDGF under conditions of dual overexpression (Haft et al., 1998); in contrast to its role in EGFR degradation however, overexpressed SNX1 exerted no effect upon PDGFR degradation (Kurten et al., 1996).

Besides interaction with cargo destined for degradation, SNX1 was shown to interact with VPS35 (Haft et al., 2000; Gullapalli et al., 2004; Merino-Trigo et al., 2004; Rojas et al., 2007) and thus implicated in a different itinerary of endosomal sorting: the retrograde endosome-to-TGN retrieval (see below, **para. 1.5**).

1.4.2. Other Sorting Nexins

To exemplify the diversity of this family, some members of the sorting nexin family will be briefly introduced (see also **Tables 1.3 and 1.4**).

SNX16 and SNX17 – 'sorting SNXs'

SNX16 possesses both, a PX domain and C-terminal regions of coiled coil structure, both of which are involved in localising the protein to its early and late endosomal localizations (Hanson and Hong, 2003). SNX16 has been implicated in the early to late endosome sorting step of the EGFR: following EGF stimulation, SNX16 was shown to associate with the EGFR in COS-7 cells, and overexpression of SNX16 enhanced the rate of EGF-induced receptor degradation, whilst at the same time inhibiting downstream EGF signalling events (Choi et al., 2004). More recent studies have also implicated SNX16 in backfusion of intralumenal vesicles with the limiting membrane of the late endosome, and hence to participate in endosome-to-cytosol transport of viral nucleocapsids (Le Blanc et al., 2005).

SNX	Interaction	Reference
SNX1	EGFR	(Kurten et al., 1996; Haft et al, 1998)
	Enterophilin-1	(Pons et al., 2003; Pons et al., 2004)
	VPS35	(Haft et al., 2000; Gullapalli et al., 2004)
		(Merino-Trigo et al., 2004; Rojas et al., 2007)
	Hrs	(Chin et al., 2001)
	PAR-1 receptor	(Wang et al., 2002)
	PDGF receptor	(Haft et al., 1998)
	Transferrin receptor	(Haft et al., 1998)
	Leptin receptor	(Haft et al., 1998)
	D5-Dopamine receptor	(Heydorn et al., 2004)
	P-Selectin	(Williams et al., 2004)
SNX2	EGFR, PDGFR, Leptin receptor	(Haft et al., 1998)
	TGF-β receptor	(Barr et al., 2000)
	VPS35	(Rojas et al., 2007)
SNX4	Amphiphysin2	(Leprince et al., 2003)
	EGFR, PDGFR	(Haft et al., 1998)
	Leptin receptor	(Haft et al., 1998)
	TGF-β receptor	(Parks et al., 2001)
SNX6	Pim-1	(Ishibashi et al., 2001)
	TGF-β receptors	(Parks et al., 2001)
SNX9	Insulin and IGF receptor	(MaCaulay et al., 2003)
	AP-2 (α and β2 appendages)	(Lundmark and Carlsson, 2002)
	Clathrin	(Lundmark and Carlsson, 2003)
	Dynamin-2	(Lundmark and Carlsson, 2003)
	ACK2	(Lin et al., 2002)
	MDC9, MDC15	(Howard et al., 1999)
	Aldolase	(Lundmark and Carlsson, 2004)
	p85 (PI3-kinase)	(Badour et al., 2007)
	WASp	(Badour et al., 2007)
SNX15	VPS29*, VPS35*	(Barr et al., 2000)
	PDGFR	(Phillips et al., 2001)
SNX16	EGFR	(Choi et al., 2004)
SNX17	P-Selectin	(Florian et al., 2000; Williams et al., 2004)
	LDL receptor	(Stockinger et al., 2002; Burden et al., 2004)

Table 1. 3 SNXs and their interaction partners

The table illustrates the variety of proposed SNX interaction partners. Note that the list is not exhaustive and that several of the roles proposed from older studies, especially where based solely on overexpression data, may eventually be refined, or redefined (* documented but unconfirmed).

SNX	Proposed Functions	Reference
SNX1	Endosome-to-TGN retrieval of the CI-MPR Pro-degradative sorting of the EGFR Pro-degradative sorting of PAR-1	This study; Rojas et al., 2007 Kurten et al., 2002; Cozier et al., 2002 Gullapalli et al., 2006
SNX2	Pro-degradative EGFR sorting Endosome-to-TGN transport of ricin	Gullapalli et al., 2004 Skanland et al., 2007
SNX3	Recycling from the early endosome (early-to-recycling endosome TfR transport)	Xu et al., 2001
SNX4	Endocytosis? (amphiphysin interaction, TfR internalization inhibited) Endosome-to-ERC transport of Tf/TfR Endosome-to-TGN transport of ricin	Leprince et al., 2002 Rutherford/Traer, unpublished Skanland et al., 2007
SNX5	Inhibitory regulation of EGFR degradation Endosome-to-TGN transport of CI-MPR	Liu et al., 2006 Wassmer et al., 2007
SNX6	Nuclear traffic of Pim-1 Endosome-to-TGN transport of CI-MPR	Ishibashi et al., 2006 Wassmer et al., 2007
SNX9	GLUT4-translocation Co-ordination of endocytic machinery (dynamin, adaptor protein recruitment) Integration of signalling; endocytosis, actin cytoskeleton EGFR degradation	MaCauley et al., 2003 (Lundmark and Carlsson, 2004) Soulet et al., 2005 Badour et al., 2007 Lin et al., 2002
SNX13	GAP for $G_{\alpha s}$, pro-degradative EGFR sorting	Zheng et al, 2001
SNX15	Trafficking between endosomes and the TGN	Barr et al., 2000
SNX16	Early to late endosomal sorting (EGFR) Back fusion of MVB intraluminal vesicles	Hanson and Hong, 2003; Choi et al., 2004 Le Blanc et al., 2005
SNX17	Recycling of LRP from the early endosome Endosomal retention of P-Selectin (prevents entry into MVB vesicles)	Van Kerkhof et al., 2005 (Knauth et al., 2005)
SNX23	A kinesin that directs +end movement of early endosomes (thus regulates degradative traffic)	Hoepfner et al., 2005

Table 1. 4 Proposed Roles of SNXs in endosomal sorting
In some cases, very recent findings were included, and will be discussed at the appropriate chapters. Adapted and extended from AC Rutherford.

SNX17 might also be considered as a 'classical SNX' as it binds to PtdIns3*P*, and is primarily localized to early endosomal membranes and involved in endosomal sorting. Electron microscopy revealed the presence of SNX17 on both, the limiting membrane and recycling tubules of the early endosome (van Kerkhof et al., 2005). SNX17 appears mainly involved in endosome-to-plasma membrane recycling; by virtue of its FERM domain and C-terminal region, SNX17 interacts with several low-density lipoprotein (LDL) receptors (Stockinger et al., 2002; Burden et al., 2004): SNX17 binds to and promotes the recycling of the LDL receptor-related protein (LRP) from the early endosome, as siRNA mediated-knockdown of SNX17 causes a reduction in LRP recycling, and enhances the lysosomal degradation of LRP (Van Kerkhof et al., 2005). Additionally, SNX17 has been implicated in the internalisation and recycling of the leukocyte receptor P-selectin (Florian et al., 2001; Williams et al., 2004).

SNX9 – integration of actin cytoskeleton, endocytosis, and signalling?

In addition to its PX domain, SNX9 possesses an N-terminal SH3 domain, which is followed by a region of low complexity. Through these N-terminal regions, SNX9 is capable of interacting with core components of the CME machinery, including dynamin-2, AP-2 and clathrin itself (Lundmark and Carlsson, 2003). It has been proposed that SNX9 regulates CME by mediating dynamin recruitment to the plasma membrane (Lundmark and Carlsson, 2004), and knockdown of SNX9 inhibited transferrin internalisation in HeLa cells (Soulet et al., 2005). The substrate specificity of its PX domain remains a matter of debate (compare **Table 1.2**), and accordingly, besides a cytosolic distribution, it has been described to localize to plasma membrane, the TGN and endosomes.

Additionally, SNX9 has been recently implicated in bacterial invasion processes although its exact role is not yet clear. Here, SNX9 was identified as interaction partner for the bacterially secreted protein EspF (Marches et al., 2006), an effector protein of enteropathogenic *E. coli* (EPEC). Functionally, EspF is essential for F-actin assembly because it promotes recruitment of the host actin-nucleating machinery to sites of bacterial adherence, which is thought to be important for actin pedestal formation that are crucial for the invasion process (Campellone et al., 2004; Garmendia et al., 2004). SNX9 has also been recently shown to inducibly bind to Wiskott-Aldrich syndrome protein (WASp), and interact with the PI3-kinase regulatory subunit p85 and its product, to stimulate CD28

uptake in T-cells in a PI3-kiase-dependent manner, thus coupling cytoskeletal rearrangements to endocytic events and signalling function (Badour et al., 2007).

SNX23 – endosomal motility

Recent work has shown that KIF16B, a kinesin-3 (also known as SNX23), drives plus-end, as well as minus-end directed motility of sorting endosomes in a process dependent on Rab5 and PI3-kinase (Hoepfner et al., 2005). It appears that KIF16B directly modulates the steady state distribution of endosomes by regulating the 'switch' between centrifugal, plasma membrane-bound recycling, and centripetal late endosomal/lysosomal degradative transport. Overexpression of SNX23 caused a redistribution of early endosomes towards the cell periphery whereas SNX23 depletion caused the early endosomes to cluster in the perinuclear region. In terms of receptor trafficking, the former scenario inhibited degradative delivery (EGFR), whereas in the latter receptor recycling was delayed and degradation accelerated (Hoepfner et al., 2005).

SNX3

Although multiple domains are a feature of the SNX family, 'group B' SNXs are composed of very little sequence outside their PX domain. Of these smaller SNXs, SNX3 which is comprised largely of its PtdIns3*P*-binding PX domain, and thus does not oligomerize with other SNXs, is nevertheless implicated in endosomal function. SNX3 is localised to early and perinuclear endosomes (Xu et al., 2001b), where it is believed to function in the trafficking of membrane from the early endosome to the recycling endosome. SNX3 overexpression leads to endosomal swelling, and microinjection of anti-SNX3 antibodies into cells results in defective early endosome-to-recycling endosome TfR traffic (Xu et al., 2001b).

SNX13

The diversity within the SNX family is also illustrated by the domain architecture of SNX13. In addition to its SNX-PX domain, SNX13 possesses a RGS (regulator of G protein signalling) domain that can function as a GTPase activating protein. SNX13 enhances GTP hydrolysis upon G_{α_s}, thus attenuating signalling via G_{α_s}, and reducing adenylate cyclase mediated AMP production. SNX13 is targeted to endosomes and the presence of a G_{α_s} GAP on endosomes intriguingly suggests that it might function to

attenuate signalling from receptors, such as the β2-adrenergic receptor as they traffic through endosomes (Zheng et al., 2001). SNX13 might also provide a potential link between signalling and trafficking; as recently SNX13 has been shown to promote EGFR degradation in a G_{α_s} stimulated manner (Zheng et al., 2004).

1.5. Making the case - sorting nexins in cargo retrieval

1.5.1. Insights from yeast sorting nexins on retrieval

The consistent theme for all yeast sorting nexins identified so far is that they mediate retrieval of cargo from endosomes. The yeast retromer subunits Vps5p and Vps17p have been shown to function in the retrieval of the hydrolase receptor Vps10p [see also below; (Horazdovsky et al., 1997; Seaman et al., 1998; Hettema et al., 2003) and Pep12p (Hettema et al., 2003) from prevacuolar endosomes (PVEs). Snx4p, Snx41p and Snx42p, the predicted yeast orthologues of mammalian SNX4, are thought to control retrieval of the late-Golgi SNARE Snc1p from PGEs to the TGN. In the absence of Snx4p, Snc1p mis-localises to the vacuole (Hettema et al., 2003). Yeast Grd19p, the predicted orthologue of mammalian SNX3 is required for the retrieval of the late Golgi proteins Kex2p (the homolog of furin), Ste13p, Pep12p and A-ALP. These proteins are mis-localised to the vacuole in *grd19Δ* cells (Voos and Stevens, 1998; Hettema et al., 2003). Similarly, the predicted orthologue of mammalian SNX8, Mvp1p, is also required for the retrieval of late Golgi proteins from the degradative route, as it retrieves the carboxypeptidase Y (CPY) receptor Vps10p, and Kex2p from endosomes; *mvp*1Δ cells secrete an immature form of CPY, characteristic of a defect in the sorting of the CPY receptor (Ekena and Stevens, 1995)

1.5.2. The yeast retromer complex

The hydrolase receptor Vps10p, a receptor with analogous function to the CI-MPR, is efficiently retrieved from prevacuolar endosomes (PVE) to the late-Golgi complex with the aid of a multimeric protein complex called retromer (Seaman et al., 1997; Seaman et al., 1998). This pentameric coat complex consist of two sub-complexes; one half comprises the vacuolar protein sorting proteins Vps26p, Vps29p and Vps35p (Seaman et al., 1998), while the second sub-complex is formed by the sorting nexins Vps5p and Vps17p (Horazdovsky et al., 1997; Nothwehr and Hindes, 1997). These yeast sorting nexins associate with prevacuolar membranes by means of their phox homology (PX) domain being capable of ligating phosphatidylinositol 3-monophosphate, while the Vps26p-Vps29p-Vps35p sub-complex is cargo-selective due to the ability of Vps35p to recognize a (Y/F)XXΦ motif within the cytoplasmic tail of Vps10p. Additionally, Vps35p has been shown to directly interact with Vps5p, thus connecting both complexes (Nothwehr et al., 1999; Nothwehr et al., 2000).

1.5.3. The mammalian retromer complex

With the exception of Vps17p, mammalian orthologues of all retromer components have been identified (Haft et al., 1998). Like its yeast counterpart, the mammalian retromer complex is thought to be pentameric, with one sub-complex consist of VPS26, VPS29 and VPS35. In light of the lack of a mammalian orthologue of Vps17p, the composition of the second sub-complex is less clear. The mammalian proteins sorting nexin-1 (SNX2) and sorting nexin-2 (SNX2) show high sequence similarities with Vps5p, and as indeed, SNX1 binds to SNX2, as well as VPS35 (Haft et al., 1998), they have been proposed as orthologues of Vps5p.

VPS35 is a hydrophilic membrane protein that shows 43% identity to Vps35p (Edgar and Polak, 2000). Co-immunoprecipitation and yeast two-hybrid analyses have shown that VPS35-VPS29-VPS26 form a stable complex, with VPS35 being the core component of this complex. Interestingly, in co-elution experiments, when these components are co-expressed with either SNX1 or SNX, the majority of the sorting nexins elute at a size consistent with its monomeric or dimeric form, while expressing the sorting nexins alone or in combination, results in large oligomers. This suggests that the other forms compete with the ability of SNXs to form larger complexes. (Haft et al., 2000)

1.6. Perspectives and aims of this thesis

At the beginning of my PhD studies in October 2003, the literature on SNX1 was dominated by overexpression approaches mainly identifying its interactions with various receptors and other sorting nexins. Seven years after its discovery as regulator of pro-degradative transport, this role had been questioned, as it could not be confirmed under conditions of siRNA-mediated SNX1 suppression.

Thus, my primary aim was to scrutinize the proposed role of SNX1 as component of a potential cargo retrieval complex in more detail, a model that had been proposed through the discovery of potential mammalian orthologues of the yeast retromer complex.
Within the first six month of my PhD, through the work in the Bonifacino Labs and by Matt Seaman, a breakthrough in mammalian retromer biology had been made: this included identifying a functional mammalian retromer complex, and hence providing tools and models, with the aid of which this work swiftly progressed toward identifying and characterizing the role of SNX1 in endosome-to-TGN transport processes.

As the yeast retromer complex appeared as a 'multi-cargo' sorting complex, our interest was sparked as to whether SNX1 had more generalised role in retrograde transport, and hence we expanded our studies to include a variety of cargo.

This thesis may be further viewed under the aspect of attempting to analyse protein function in an integrative and synergistic approach: dissecting transport by studying endogenous cargo and utilizing exogenous molecules, by employing a broad range of techniques combining overexpression and RNA interference techniques with live and fixed cell approaches, and through collaborative efforts, to combine these with ultrastructural analysis, functional studies using biochemical assays, and infection models.

Chapter 2 – Material and Methods

2.1 Materials

This chapter lists all general material and contains a list of suppliers. Experiment-specific materials are also listed in individual chapters. If not stated, reagents were either purchased from SigmaAldrich (SIGMA) or Invitrogen.

2.1.1. Bacterial Strains

BL21-Gold (DE3)	(STRATAGENE) *E. coli* B strain, F- episome, *dcm*$^+$, The, *ompT*, *hsdS*(r_B- m_B-), *gal* Δ DE3), *endA*, Tet^r
XL-Blue	(STRATAGENE) *recA1, endA1, gyrA96, thi-1, hsd*R17, *sup*E44, *relA1 lac [F' proAB lacI^{q}ZΔM15 Tn10(Tet^r)].*
XL10-Gold	(STRATAGENE) Tet^r Δ*(mcrA)183 Δ(mcr*CB-*hsd*SMR-*mrr)173 endA1 sup*E44 *thi-1 recA1 gyrA96 relA1 lac* Hte [F' *proAB lacI^{q}ZΔM15 Tn10* (Tet^r) Amy Cam^r]^a
DH5α	(INVITROGEN) F$^-$ ϕ80d*lac*ZΔM15 Δ(*lac*ZYA-*arg*F) U169 *rec*A1 *end*A1 *hsd*R17(r_k^-, m_k^+) *pho*A *sup*E44 λ$^-$ *thi*-1 *gyr*A96 *rel*A1

Growth Media

Bacterial growth media were either provided by the Department of Cellular and Molecular Medicine, University of Bristol or purchased from Invitrogen.

Luria Bertani (LB)	10 g NaCl, 10 g tryptone (DIFCO), 5 g yeast extract (DIFCO); in 1 litre of sH_2O, pH 7.0, autoclaved
LB agar	20 g agar (DIFCO) added per 1 litre of LB prior to autoclaving
SOC Media	20 g tryptone (DIFCO), 5 g yeast extract (DIFCO), 0.5 g NaCl; in 980 ml of sH_2O pH 7.0 , autoclaved, then added to 20 ml of a sterile 1M glucose solution

Antibiotics

Ampicillin	(SIGMA) 100 μg/ml stock solution in dH_2O, 1:1000, stored at -20°C
Kanamycin	(SIGMA) 50 μg/ml stock solution dH_2O, 1:1000, stored at -20°C

2.1.2. Eukaryotic Cell Lines and Tissue Culture

HeLa Cells (CCl-2)	(ATCC) Epithelial, human, derived from cervical adenocarcinoma (Gey et al., 1952)
HeLaM Cells	A kind gift from Dr Matthew Seaman, CIMR, Cambridge, UK (Seaman, 2004) stably transfected with a CD8-CI-MPR chimera
HepG2M Cells	A kind gift from Prof Judith Klumperman, Cell Microscopy Center, University of Utrecht, The Netherlands Epithelial, human, derived from hepatocellular carcinoma
MDCK Cells	A kind gift from Dr Mark Jepson, University of Bristol, UK Epithelial (unpolarized), canine, derived from kidney cells by S.H. Madin and N.B. Darby (1958)
Growth Media	
DMEM- full (HeLa)	Dulbecco's Modified Essential Medium with 4.5g/l glucose, 1mM pyruvate, supplemented with 10% fetal calf serum (FCS), 2 mM L-glutamine, 100 units/ml penicillin, 100 µg/ml streptomycin (all INVITROGEN)
DMEM (HeLaM)	DMEM- full (HeLa), additionally supplemented with 0.5mg/ml geneticin (G418) (INVITROGEN)
MEM (HepG2)	Minimum essential medium containing Hank's salts, 2 mM L-glutamine 0.1 mM non-essential amino acids, 1.0 mM Na-pyruvate, supplemented with 10% FCS, 100 units/ml penicillin, 100 µg/ml streptomycin (all INVITROGEN)
EMEM (MDCK)	EMEM supplemented 10% FCS, 0.1 mM MEM non-essential amino acids, 2 mM L-glutamine, 100 units/ml penicillin, 100 µg/ml streptomycin (all INVITROGEN)
DH buffered medium (DHB)	DMEM with 4.5g/l glucose, 25 mM HEPES, 1mM pyruvate
OptiMEM	(INVITROGEN)
General Solutions for Tissue Culture	
1x PBS	4 g NaCl, 0.2 g KCl, 0.2 g KH_2CO_3, 0.144 g $Na_2HCO_3 \cdot 2H_2O$; to 1 litre, autoclaved
4x poly-D-lysine solution	100 mg/ml poly-D-lysine hydrobromide (SIGMA) in H_2O
Trypsin-EDTA solution	0.5 mg/ml porcine trypsin, 0.5 mM EDTA in HBSS
Transfection Reagents	
GeneJuice	(NOVAGEN)
Oligofectamine	(INVITROGEN)
10x HBS	5 g HEPES, 8 g NaCl, 0.37 g KCl, 0.9 g Glucose, 0.103 g Na_2HPO_4 to 100 ml, pH 7.05 - 7.12 (1N NaOH)

Cell lysis buffer	50 mM HEPES, 0.1 M NaCl, 1 mM EGTA pH8, 10 mM $MgCl_2$, 1% Triton X-100, 0.1 mM DTT, 5 µg/ml each of benzamidine, trypsin inhibitor, leupeptin, aprotonin pepstatin A and antipain, 0.5 mM PMSF, pH 7.5

2.1.3. Molecular Biology

Agarose gels	agarose (BIOLINE) x % (w/v) in 1x TEB 0.5 µl EtBr stock per 10 ml gel
1x TAE	0.8M Tris-acetate, 20mM EDTA, pH 7.8
Ethidium bromide (stock)	(BIORAD) 10 mg/ml ethidium bromide solution
DNA sample buffer (5x)	25% (w/v) Ficoll, 10 mM EDTA, 0.125% (w/v) bromophenol blue (MERCK), 0.125% (w/v) xylencyanole (MERCK)
DNA Molecular Weight Marker X (0.07 - 12.2 kbp)	(ROCHE)
DNA ladders	(NEW ENGLAND BIOLABS) 1Kb and100 bp DNA ladder
QIAprep Miniprep Kit™	(QIAGEN)
Plasmid Maxi Kit	(QIAGEN)
QIAEXII *Gel extraction Kit*	(QIAGEN)
WIZARD® SVGel and PCR Clean-Up System	(PROMEGA)

Oligonucleotide Primers (Sequences refer to **Appendix I)**
All oligonucleotides were synthesized by Sigma-Genosys (0.025 µM). Stock solutions were made to 100 µg/ml in sH_2O, prior to storage at -20 °C.

Restriction Enzymes
Restriction enzymes were purchased from MBI FERMENTAS, NEW ENGLAND BIOLABS, PROMEGA, ROCHE, and used according to manufacturer's instruction.

Other Enzymes

T4-DNA Ligase	(ROCHE)
dNTPs	(ROCHE)
KOD Hot Start DNA polymerase	(NOVAGEN)
Phosphatase, alkaline (1000U)	(ROCHE)

PCR Master Mix	(PROMEGA) Containing Taq polymerase 50U/ml in reaction buffer 400 µM dNTPs, 3mM Mg_2Cl_2
QuickStick Ligation Kit	(BIOLINE)

2.1.4. Commercial Plasmids

pEGFP-C1	(CLONTECH)

2.1.5. Donated Vectors

pEGFP-C1-SNX1	Dr Alex McGregor, former University of Bristol, Bristol, UK.
pEGFP-C1-SNX5	Dr Anna Rutherford, University of Bristol, Bristol, UK.
pEGFP-C1-2xFYVE	Prof George Banting, University of Bristol, Bristol, UK (Pattni et al., 2001)
pCMU-3xFLAG-SNX5	Dr Rohan Teasdale, University of Queensland, Brisbane, Australia
pCMU-3xFLAG-VPS26	
pCMU-3xFLAG-VPS29	
pCMU-3xFLAG-VPS35	
pmRFPC1	Dr Jez Carlton, University of Bristol, Bristol, UK (developed using the pEGFP-C1 from Clontech, and replacing the GFP-coding sequence of with RFP from the pGEXmRFP vector, a kind gift of Dr Roger Tsien, UCSD, La Jolla, USA)

2.1.6. GenBank Accession numbers (NCBI)

SNX1	ACCESSION NUMBER BC000357
SNX2	ACCESSION NUMBER BC003382
Vps35	ACCESSION NUMBER BC002414

2.1.7. Sequences of small interfering RNAs

siRNA duplexes	(DHARMACON) Option C, reconstituted at 40 µM in RNase free H_2O
SNX1	TARGET: AAGAACAAGACCAAGAGCCAC
SNX2	TARGET: AAGUCCAUCAUCUCCAGAACC
Control	TARGET: AAGACAAGAACCAGAACGCCA

2.1.8. Antibodies and Reagents

Key:
WB = Western blotting
IF = immunofluorescence, UA = IF Uptake Assays (fixed or Live Cell Imaging),
IP = immunoprecipitation experiments

Primary Antibodies

	Species	Dilution		Supplier
anti-β-actin	Mouse	1:5,000	WB	SigmaAldrich
anti-CD8 (UCHT4)	Mouse	1:200	IF	Ancell
anti-CD8	Rat	1:1000	IF	Serotec
		10 µg/ml	UA	
anti-CD8 (RPE-coupled)	Mouse	50 µg/ml	UA	Serotec
anti-CI-MPR	Rabbit	1:200	IF	Prof Paul Luzio, CIMR,
		1:1,000	WB	Cambridge, UK (Reaves et al., 1996)
anti-CI-MPR	Mouse	1:500	WB	Affinity BioReagents
anti-EEA1	Mouse	1:200	IF	BD Transduction Labs
anti-giantin	Rabbit	1:500	IF	Covance
anti-Lamp-1	Mouse	1:500	IF	Research Diagnositics
anti-*Salmonella* (LPS)	Rabbit	1:200	IF	Difco
anti-SNX1	Mouse	1:200	IF	BD Transduction Labs
		1:1,000	WB	
anti-SNX1	Rabbit	1:200	IF	Dr Matthew Seaman, CIMR, Cambridge, UK (Seaman, 2004)
anti-SNX1	Goat	1:200	IF	Santa Cruz Biotechnology
anti-SNX2	Mouse	1:200	IF	BD Transduction Labs
anti-sortilin (tail)	Rabbit	1:1000	IF	Gifts from Dr CM Petersen,
anti-sortilin (VpsD)	mouse	1:400	IF	Aarhus University, Denmark
anti-STxB (13C4)	Mouse		IP	Dr Ludger Johannes, Institut Curie, Paris, France (Johannes et al., 1997)
anti-TGN46	Sheep	1:500	IF	Serotec
anti-tubulin	Mouse	1:15,000	WB	SigmaAldrich
anti-VPS26-1	Mouse	1:200	IF,WB	Dr Matthew Seaman, CIMR, Cambridge, UK (Seaman, 2004)

Secondary Antibodies for Immunofluorescence and Western Blotting

JACKSON IMMUNORESEARCH Laboratories

Cy2-anti-mouse IgG	Donkey 1:500	Cy3-anti-mouse IgG	Donkey 1:500
Cy2-anti-rabbit IgG	Donkey 1:500	Cy3-anti-rabbit IgG	Donkey 1:500
TRITC-anti-goat	Rabbit, 1:200		

INVITROGEN

Alexa^{488} anti-goat IgG	Donkey 1:200	Alexa^{568} anti-mouse IgG	Donkey 1:200
Alexa^{488} anti-mouse IgG	Donkey 1:500	Alexa^{568} anti-mouse IgG	Goat 1:200
Alexa^{488} anti-rabbit IgG	Donkey 1:200	Alexa^{568} anti-rabbit IgG	Donkey 1:200
Alexa^{568} anti-sheep IgG	Donkey 1:500	Alexa^{647} anti-mouse IgG	Donkey 1:200
Alexa^{594} anti-rabbit IgG	Donkey 1:200	Alexa^{680} anti-sheep IgG	Donkey 1:200

HRP-anti-goat IgG	Donkey 1:2000	Santa Cruz Biotechnology
HRP-anti-mouse IgG	Sheep 1:5000	(GE HEALTHCARE)
HRP-anti-rabbit IgG	Sheep 1:5000	(GE HEALTHCARE)

2.1.9. Solutions for Immunofluorescence and Live Cell Imaging

PFA stock solution	20% paraformaldehyde (RIEDEL DE HAËN) in 1x PBS alkaline hydrolysis with 1 N NaOH at 60°C pH 7.0, stored at -20°C
4% PFA working solution	1:5 diluted PFA stock in DMEM or PBS
PBS-T	0.1% (v/v) TritonX-100 (SIGMA) in 1x PBS
P-BSA-T	1% (w/v) BSA (SIGMA), 0.1% (v/v) TritonX-100 in 1x PBS
P-BSA	1% (w/v) BSA (SIGMA) in 1x PBS
Mowiol mounting medium	6 g glycerol, 2.4 g Mowiol 4-88 (CALBIOCHEM), to 6 ml sH_2O; 12 ml 0.2 M Tris (pH 8.5). Stored at -20°C
DAPI	(HOECHST) 4', 6'-diamidino-2-phenylindole, 1:5000 (in H_2O)
TRITC-phalloidin	(INVITROGEN) 1:1000 in immunofluorescence analyses
Imaging buffer	125 mM NaCl, 42 mM HEPES, pH 7.4, 18 mM glucose, 5.4 mM KCl, 3 mM $NaHCO_3$, 1.6 mM $MgCl_2$, 1.3 mM EGTA

2.1.10. Protein Biochemistry

Material and Solutions for SDS-PAGE

Acryl amide solution	(SEVERN BIOTECH) 30% acrylamide, 0.8% bis-acrylamide
APS stock	10% (w/v) ammonium persulphate (ACROS) in H_2O, stored at -20°C
TEMED	N,N,N´,N´-tetramethylethylenediamine (RIEDEL DE HAËN)
SDS stock	10% (w/v) SDS in H_2O
Resolving gel Lower Tris stock	1.5 M Tris-HCl, pH 8.8
Stacking gel Higher Tris stock	1.0 M Tris-HCl, pH 6.8
SDS-electrophoresis buffer	125 mM Tris-HCl, pH 8.6 1 M glycine 0.5 % (w/v) SDS in H_2O
10x Sample loading buffer HCl,	0.72 M β-mercaptoethanol, 62.5 mM Tris- pH 6.8, 25% (v/v) glycerol, 2% (w/v) SDS, 0.02% (w/v) bromophenol blue
Coomassie Stain	0.2% (w/v) Coomassie Brilliant Blue R250 12.5% (v/v) acetic acid 20% (v/v) ethanol
Coomassie Destain	1:1 (v/v) mix of 10% (v/v) acetic acid and 100% (v/v) ethanol
Precision Plus Protein Pre-stained Standards	(BIORAD)
BRADFORD reagent	(BIORAD)
NuPAGE gel system	(INVITROGEN) Novex range of Bis-Tris polyacrylamide gels

Material and Solutions for Western Blotting

Blotting buffer	200 mM Tris-Base, 1.5 M glycine, 20% (v/v) methanol, in H_2O
Ponceau Stain	0.2% (w/v) Ponceau S 3% (w/v) Trichloroacetic acid 3% (w/v) Sulfosalicylic acid
PBS-Tween	4 g NaCl, 0.2 g KCl, 0.2 g KH_2CO_3, 0.144 g $Na_2HCO_3 \cdot 2H_2O$, 0.05% Tween-20, to 1 litre with sH_2O
Stripping buffer	62.5 mM Tris-HCl, pH 6.8; 2% SDS, 100 mM β-mercaptoethanol; heated to 56°C

Blot blocking solution A	10% (w/v) skimmed milk powder in 1x PBS-Tween
Blot blocking solution B	3% (w/v) BSA
ECL™-Hyperfilm	(GE HEALTHCARE)
ECL™ Western Blotting Detection Reagent	(GE HEALTHCARE)
Whatman-Papier (G-002)	(SCHLEICHER&SCHUELL)
PolyScreen PVDF Transfer Membrane (45µm pore)	(NEN LIFE SCIENCE PRODUCTS)

2.2. Additional Equipment

Incubators, *Laminar Flow cabinet*	HERAEUS
Shaker	NEW BRUNSWICK
ELISA-*Easy Reader* 400AT	SLT LAB INSTRUMENTS
PTC-100 thermal cycler	MJ RESEARCH LTD
Mini-Protean-II Slab Cell Apparatur	BIORAD
Gel electrophoresis equipment, power supplies	
Photometer; Benchtop centrifuges	EPPENDORF
Centrifuges	BECKMANN, JOUAN
Thermomixer	EPPENDORF
Vortex Whirlimixer	FISON
Scales	SARTORIUS

General plastic ware (various)

GREINER, FALCON, STARLAB, Bibby-Sterilin, CORNING, Nalgene, TPP, CORNING

Pipettors	GILSON, Bibby-Sterilin
Chemi-Doc imaging system	BIORAD
Curex 60 developing machine	AGFA

2.3. Suppliers

Adobe Systems PLC	Uxbridge, UK	LKB Wallac	Turku, Finland
AGFA	Mortsel, BEL	Marienfeld	Lauda-Königshofen,GER
Apple	Cupertino, CA, USA	Mattek	Ashland, MA, USA
Applied Biosystems	Warrington, UK	MBI Fermentas	York, UK
ATCC/GC Promochem	Manassas, VA, USA	Menzel Glaeser	Braunschweig, GER
BDH Chemicals Ltd	Poole, UK	Millipore	Watford, UK
Beckman Coulter	High Wycombe, UK	MJ Research	Reno, NV, USA
Becton Dickinson	Oxford, UK	Molecular Devices Corp.	Sunnyvale, CA, USA
Bibby Sterilin Ltd.	Stone, UK	Molecular Probes	Cambridge, UK
Bioline	London, UK	New Brunswick Scientific	St Albans, UK
BioRad Ltd.	Hemel-Hempstead, UK	New England Biolabs Ltd	Hitchin, UK
Cell Signaling Tech.	Beverley, MA, USA	National Institutes of Health	Bethesda, MD, USA
Cell Signals Inc.	Columbus, OH, USA	Novagen Ltd.	Abingdon, UK
Clontech Inc.	San Jose, CA, USA	Olympus Microscopes	London, UK
Corning Inc.	Corning, NY, USA	Packard Biosciences	Groningen, NL
Covance	Berkley, CA, USA	Perkin Elmer	Seer Green, UK
DAKO Cytomation	Carpenteria, CA, USA	Pierce	Rockford, IL, USA
Diagnostics Scotland	Edinburgh, UK	Promega Ltd.	Southampton, UK
Dharmacon	Lafeyette, CO, USA	Qiagen Ltd.	Crawley, UK
Dow Chemical Co.	Luddington, MI, USA	Roche	Lewes, UK
Du Pont NEN Ltd.	Stevenage, UK	Santa Cruz Biotech.	Santa Cruz, CA, USA
Eppendorf	Hamburg, GER	Sigma-Aldrich	Poole, UK
GE Heathcare UK Ltd	Little Chalfont, UK	Sigma-Genosys	Poole, UK
Gilson	Middleton, WI, USA	Somerfield Supermarkets	Bristol, UK
Improvision	Coventry, UK	Stratagene Ltd.	La Jolla, CA, USA
Invitrogen	Paisley, UK	Till Photonics	Gräfelfing, GER
Jouan	St-Herblain, France	TPP	Trasadingen, SUI
JacksonImmunoResearch Labs, Inc	West Grove, PA, USA	Upstate	Maidstone, UK
Leica Microsystems	Milton Keynes, UK	Vector Laboratories, Ltd	Petersborough, UK
Life Technologies Ltd.	Paisley, UK	Whatman International	Maidstone, UK

2.4. General Methods

The following paragraphs describe general molecular biology, protein biochemistry and tissue culture techniques. For more subject-specific techniques, one is referred to the individual chapters. Detailed information regarding buffer compositions, equipment and material can be found in the preceding paragraphs and was omitted for clarity.

2.4.1. Amplification of DNA by PCR

To amplify DNA, a PCR was routinely performed using KOD Hot-Start DNA polymerase (Novagen). Amplification was typically performed in a total volume of 50 µl. Each individual reaction was routinely composed of 50 ng template DNA, 0.3 µM sense and antisense oligonucleotide primers, and either a dNTP mix (dATP, dCTP, dGTP, dTTP; each at 0.2mM) 1.5 mM $MgSO_4$, and 5 µl of 10 x polymerase buffer (Novagen), or using a pre-mixed PCR Master Mix (Promega). Thermal cycling was performed at conditions optimized dependent on the sequences amplified. PCR commenced with an initial denaturing step at 94°C for 2 minutes, followed by 20 - 30 rounds of amplification cycles, comprising a 1-minute denaturing step at 94°C, followed by a 1-minute annealing step (~5 °C below the primer melting temperature), and finally a 68°C extension step (performed for 1 min per 1000 nucleotide amplification sequence). A final 10-minute extension step at 68°C was performed, before samples were cooled to 4°C. The reactions products were stored at -20°C, and an aliquot was separated by agarose gel electrophoresis to check successful amplification.

2.4.2. Restriction Digests

Vector and DNA were digested as required to generate complementary sticky ends at the conditions required for the respective restriction enzyme. Depending on the required scale, digests were either performed in 15 µl ('diagnostic digest') to 50 µl (PCR products, cloning). Restriction enzymes were used at a maximum of 10% of the total volume according to manufacturer's recommendations. After heat inactivating the enzyme, the cut vector was routinely subjected to gel-electrophoretic separation (**para. 2.4.2**) and subsequent gel purification (**para. 2.4.5**) to reduce the fraction of uncut vector, while cut PCR fragments were purified as described under **para. 2.4.3**.

2.4.3. Purification of DNA from PCR Reactions and Restriction digests

When no immediate electrophoretic separation step was required, DNA was purified directly from a PCR reaction or a restriction digests using the WIZARD®SVGel and PCR Clean-Up System (Promega), following the manufacturer's protocol. The DNA was routinely eluted in 2x 15 µl sH_2O and stored at -20°C.

2.4.4. Agarose Gel Electrophoresis

For most DNA separation problems, 1% (w/v) agarose gels were sufficient. Agarose was weighed and added to 1x Tris-Acetate-EDTA (TAE) buffer. The mixture was heated to dissolve the agarose, and left to cool. Once the solution had cooled to below 50°C, ethidium bromide was added to a final concentration of 5µg/ml. The gel was poured into the casting block and the comb inserted. Once set, the gel was transferred to an electrophoresis tank and immersed in 1x TAE buffer. The samples were mixed with 5x sample buffer prior to loading into the wells of the gel. Electrophoresis was generally performed at approximately 10 V/cm for 40 minutes. The DNA was visualized in the gel upon the excitation of the intercalated ethidium bromide by UV trans-illumination.

2.4.5. Purification of DNA from Agarose Gels

From an electrophoresis gel, the band of interest was rapidly excised under UV illumination using a clean razor blade. DNA was routinely extracted and purified using the QIAquick gel extraction kit (Qiagen), according to the manufacturer's instruction. The DNA was eluted using 2x 15 µl of sH_2O. Alternatively, the WIZARD SVGel and PCR Clean-Up System (Promega), following the manufacturer's protocol, was used.

2.4.6. DNA Ligation

Ligation reactions were routinely performed in 20 µl reaction volumes, usually at a 1:10 ration of vector to insert, with a minimum of 50 ng vector. As control, a reaction containing only vector, but no insert ('mock-ligation') was prepared. Routinely, 2 units of T4 DNA ligase were used (Roche) and ligations were incubated overnight at 16°C. Alternatively, a QuickStick ligation Kit (Bioline) according to the manufacturer's instructions was used, incubating ligation mix for 1 hour at room temperature.

2.4.7. Transformation of Chemically Competent Bacteria

From both, the ligation mix and 'mock ligation' (control), 5 µl were used to transform chemically competent *E. coli* strains (strains as listed under **para. 2.1.1**). Typically, a 50 µl aliquot was transferred to a pre-chilled 15 ml polypropylene tube. Where appropriate 2 µl β-mercaptoethanol were added (manufacturer's protocol) and the cells were left on ice for 10 minutes. To these bacteria, 100 ng DNA (either plasmid DNA, or a ligation mixture) was added and carefully mixed, before being incubated on ice for a further 30 minutes. Cells were then subjected to a heat shock (37°C for 30 seconds, or 42°C for 45 sec, depending on strain used, according to the manufacturer's manual), and quickly returned to ice for 2 minutes. Pre-warmed SOC media was added at a 10:1 ratio, and the mixture was incubated at 37°C for 1 hour. The mix was briefly centrifuged to concentrate bacteria, and 100 µl of a suspension in fresh SOC was plated onto LB-

agar plates containing the appropriate selection antibiotic. The plates were incubated at 37°C and growth of colonies was examined 12 - 16 hours later. These 'master plates' were used to inoculate liquid cultures, sealed with parafilm and stored at 4°C for up to 5 days.

2.4.8. Bacterial Culture

Liquid cultures of transformed *E. coli* strains were inoculated transferring one colony of a 'master' agar plate (see **para. 2.4.7**) per 5 ml LB broth supplemented with the appropriate selection antibiotic. Cultures were incubated at 37°C in an orbital shaker at 180 rpm for 16 - 20 hours. These cultures were either used for long-term *E.coli stock*-preparation (**para. 2.4.9**), small-scale DNA preparation ('miniprep'), or were used to inoculate larger culture volumes either at a 1:100 ratio (low copy plasmids), or 1:500 for high copy plasmids. Liquid cultures from pre-cultures were also incubated at 37°C in an orbital shaker at 180 rpm for 16-20 hours.

2.4.9. Freezing and Thawing of E.coli Stocks

Stationary-phase *E. coli* cultures were pelleted by centrifugation at 13,000 x g for 1 minute and resuspended in 30% sterile-filtered glycerol. The suspension was mixed, snap-frozen in liquid nitrogen and immediately transferred to -80°C for storage. To reconstitute frozen stocks, an aliquot of frozen culture was streaked onto an LB-agar plate containing the appropriate selection antibiotic that was subsequently incubated at 37°C overnight.

2.4.10. DNA Purification

DNA purification was routinely performed using the QIAprep spin Miniprep kit (small scale) or the Qiagen Plasmid Maxi Kit (large scale), according to the manufacturer's instructions. While small-scale purifications were usually performed using 5 ml of overnight cultures of *E. coli,* the large-scale preparations were performed from 100 – 500 ml cultured bacteria (see also **para. 2.4.8** for culture preparation). The principle of both purification protocols is similar: first, bacteria are harvested by centrifugation and subsequently resuspended in a Tris-EDTA buffer containing RNase A. Then an alkaline lysis is performed using a NaOH/SDS-containing buffer. The reaction is stopped by adding a potassium acetate-containing buffer to neutralize the solution. In the case of large-scale preparations, the mixture is incubated on ice for a further 20 min to enhance the precipitation of genomic DNA, proteins, cell debris and the added sodium dodecyl sulphate, while the plasmid DNA remains in solution. The precipitated debris is subsequently removed by centrifugation. The resulting supernatant is applied to a resin-loaded column that binds the plasmid DNA, and subsequently washed with a medium-salt buffer to further remove contaminants. The DNA is finally eluted with high-salt buffer containing low amounts of alcohol to eliminate non specific hydrophobic interactions. DNA from small-scale purifications was eluted using 2x 25 µl of sH_2O, typically yielding 5 µg of DNA at a concentration of approximately 100 ng/µl (see **para. 2.4.11**). In case of large-scale preparations, the eluted plasmid DNA was further desalted and

concentrated by isopropanol precipitation and subsequent high-speed centrifugation. The DNA pellet was washed with 70% ethanol to remove residual salt and isopropanol, briefly air-dried and redissolved in a small volume of TE buffer, pH 8.0, typically yielding a concentration of 1-2 µg/µl (see **para. 2.4.11**).

2.4.11. Determining DNA Concentrations

A dilution of DNA was prepared in a total volume of 1 ml, and transferred to a quartz cuvette for spectrophotometric analysis. The OD_{260} (absorption of DNA) and OD_{280} (absorption of Tyr and Trp residues of proteins) readings were taken, and an A_{260}/A_{280} ratio (hence DNA purity) between 1.8 - 2.0 was deemed acceptable. The DNA concentration was calculated as follows:

$$DNA\,[\mu g/ml] = OD_{260}\ x\ dilution\ \ factor\ x\ \varepsilon \quad (with\ \ \varepsilon(DNA) = 50\ \mu g/ml)$$

2.4.12. Sequencing of DNA

DNA was sequenced by MWG Biotech, London, UK using the "value read" option. Per reaction, one tube containing 1 – 2 µg air-dried plasmid DNA and a second tube containing 10µM sequencing primer were prepared and dispatched.

2.4.13. Determining Protein Concentrations

Protein content was determined using the Bradford assay and spectrophotometric analysis. A standard curve was constructed using samples containing between 0 - 50 µg of BSA. To these and the experimental sample 1ml of Bradford reagent was added. Samples were mixed, and incubated for 10 minutes prior to measuring the OD_{595} was measured. Values for known concentrations could subsequently be used to calculate protein concentration of unknown samples.

2.4.14. SDS-PAGE

SDS-PAGE was routinely used to separate and visualize proteins. Poly-acrylamide gels were either purchased pre-cast from Invitrogen or cast by hand. Poly-acrylamide resolving gels were routinely made using a final 5 - 12% acrylamide/bis-acrylamide stock solution in sH_2O depending on the separation problem. To this (to a final concentration) was added: 0.4 M Tris-HCL pH 8.8, 0.1% (w/v) SDS, 0.1% (w/v) APS and 0.04% (v/v) TEMED. The mix was poured into the cast and overlain with sH_2O to ensure flat surface and to create a barrier between gel and air. Once set, poly-acrylamide stacking gel was poured on top, consisting of 5% acrylamide/bis-acrylamide stock solution, 125 mM Tris-HCl pH 6.8, 0.1% (w/v) APS and 0.1% TEMED in sH_2O, and a comb was inserted to generate wells for protein loading. Once polymerized, the gels were immersed in SDS-PAGE running buffer. To required amount of samples, 10x SDS-PAGE loading buffer was added at 10% (v/v) and samples were denaturated at 100°C for 5 minutes before loading into the wells of the poly-acrylamide gels. Electrophoresis was performed at constant voltage of 90V for the initial 30 minutes, then at 180V until the dye front had migrated to the bottom of the gel. If required, to

visualize proteins, gels were immersed in Coomassie stain for 30 minutes. Staining was followed by repeated washes in destaining solution until protein bands were detected as clear blue bands over a transparent background.

2.4.15. Western Blotting and Immunodetection

Proteins separated by SDS-PAGE were transferred from the gel to PVDF membranes by Western blotting. Therefore, membranes were wet in methanol and placed over the gel. The gel and membrane were sandwiched together between six pieces of Whatman 3MM paper and two foam pads, all soaked in transfer buffer. The assembly was placed in a blotting cassette, and transferred to a mini-Trans Blot Cell (BioRad) electrophoresis tank containing transfer buffer. The transfer step was performed with the application of constant current (200 mA) across the cassette for 180 minutes at 4°C. Blots were, if required, stained using Ponceau stain to verify successful transfer. Membranes were then rinsed with PBS and incubated in blocking solution for 1 hour under gentle rocking. Primary antibodies (refer to **para. 2.1.8**) were added in PBS-T containing 5% (w/v) dried skimmed milk or 3% (w/v) BSA, at sufficient volumes to immerse blots entirely for at least 1 hour at room temperature or overnight at 4°C with gentle rocking. Blots were washed thrice for 30 minutes per wash in excess PBS-T. HRP-conjugated secondary antibodies (**para. 2.1.8**) diluted in PBS-T were added and blots were incubated for 30 minutes at room temperature with gentle rocking. Again, blots were washed thrice for 30 minutes per wash in excess PBS-T. For detection of immunolabelled protein, the enhanced chemo-luminescence (ECL)-plus system (GE Healthcare) was used according to the manufacturer's protocol. Membranes were subsequently wrapped in saran wrap and exposed to hyperfilm (GE Healthcare) for varying periods to detect the luminescence, before film was developed in a Curex 60 developing machine (AGFA).

2.4.16. Mammalian Tissue Culture

All work involving the eukaryotic cells listed in **para. 2.1.2,** were performed in sterile Class II vertical laminar flow cabinets until fixation or lysis of cells. Cell lines were cultured at 37°C in a humidified atmosphere maintained at 5% CO_2. Upon reaching confluency (every 2 -3 days), cells were passaged. Growth media was removed by aspiration, cells were washed in sterile PBS and incubated with 1 ml trypsin-EDTA solution per 75 cm^2 for 2 minutes at 37°C. Cells were suspended in 10 ml growth medium and dissociated by pipetting before being transferred into a sterile 15 ml reaction tube. After centrifugation for 3 min at 3,000 x g (at room temperature), the pellet was resuspended in 10 ml fresh growth medium, and required numbers of cells were transferred into new flasks (2 x 10^6 cells per 75$cm^{2\text{-flask}}$ containing 15 ml growth media).

2.4.17. Cryo-preservation and Reconstitution of Eukaryotic Cells

Routinely, cells from a confluent 150 cm^2-flask were detached and centrifuged as described under **2.4.16**. The cell pellet was resuspended in 10 ml of DMEM supplemented with 10% (v/v) DMSO and 25% (v/v) FBS. The cell suspension was transferred in 1-ml aliquots into cryovials (Nunc), stored at –20°C for 2 hours, then at -80°C for 16 hours before being transferred to liquid nitrogen for long-term storage. In the reverse thawing process, cells were removed from the liquid nitrogen storage, and thawed rapidly at 37°C. To remove DMSO, cells were washed by transferring them to 10 ml pre-warmed growth media and centrifuging for 3 min at 3,000 x g. The pellet was resuspended in 6 ml growth media and transferred into a 25 cm^2-flask.

2.4.18. DNA Transfection of Eukaryotic Cells

To introduce plasmid DNA into eukaryotic cells, lipid-based or polyamine-based transfection reagents were used according to the manufacturer's instructions. Routinely, per 150.000 –200.000 cells (50% -70% confluency), 2 µg of plasmid-DNA were used. Cells were cultured as per normal, and used 22 hours later. Larger constructs were transfected using a method based on calcium phosphate precipitation of DNA. Therefore, growth media was changed 3 hours prior to transfection to guarantee optimal pH. For transfection, 4 µg of plasmid DNA were diluted with sH_2O to a final volume of 135 µl. Subsequently, 15 µl of 125 mM $CaCl_2$ were added, and 150 µl of a 2x HBS solution were added into a second tube. Under gentle vortexing, the diluted DNA was transferred to the tube containing the HBS, and the transfection mixture was added drop-wise to 50% confluent cell. Cells were cultured as per normal, and used 12 – 24 hours later.

2.4.19. Transfection of Eukaryotic Cells with siRNA Duplexes

Routinely, cells were seeded at 9.5 x 10^5 cells per well (∅ 35 mm) of a 6-well plate (approximately 30% confluency following 16 hours growth). The next day, cells were then washed twice in PBS, covered in 800 µl OptiMEM and returned to the incubator. Depending on the experiment, 0.1 - 0.2 nmol of siRNA duplex (2.5 – 5 µl of a 40 µM stock) was combined with OptiMEM in a sterile microcentrifuge tube to yield a total volume of 185 µl. In a second tube, 2.5 µl Oligofectamine (Invitrogen) was added to 12.5 µl OptiMEM. Both tubes were briefly mixed and left for 15 minutes at room temperature. The tube contents were combined, mixed briefly and incubated at room temperature for a further 30 minutes. The transfection mixture was added drop-wise onto the cells and incubated at 37°C. After 6 hours, 500 µl ml of growth media containing 30% FCS was added, and cells were incubated for a further 66 hours.

2.4.20. Preparation of Whole-cell Lysates

Eukaryotic cells were washed once with ice-cold PBS before being lysed on ice using 60 µl cell lysis buffer per 9.5cm^2-dish by scraping cells from the bottom of the culture dish. Cells were transferred into a microcentrifuge tube, incubated on ice for 5 minutes and lysates were cleared by

centrifugation (13,000 x g, 10 minutes, 4°C). The protein concentration in the lysates was estimated using the Bradford assay (**para. 2.4.13**). Lysates were stored at -20°C until subjected to SDS-PAGE (**para. 2.4.14**).

2.4.21. Immuno-labelling for Light Microscopic Analysis

Unless stated otherwise, cells plated onto glass coverslips (Ø 22 mm) were washed once in PBS and fixed at 37°C for 15 minutes using 4% PFA. Cells were washed extensively in PBS to remove all traces of PFA and, if immunolabelling was required, permeabilized using 0.1% Triton X-100 (v/v). Following permeabilization, unspecific binding was blocked incubating cells in P-BSA, which was followed by incubation with primary antibodies (refer to **para. 2.1.8**) in 100 µl of P-BSA containing 1 hour. Cells were subsequently washed three times in P-BSA and incubated in the dark with secondary antibodies (**para. 2.1.8**) in PBS for 1 hour (if required, fluorescent drugs such as TRITC-phalliodin were added at this stage). Cells were washed thrice with PBS, and once with H_2O before mounting coverslips onto microscope slides using 5 - 10 µl Mowiol or Vectashield with DAPI (Vectorlabs). If 0.5% (v/v) saponin in PBS was used for permeabilization, all subsequent solutions contained 0.1% saponin, but TritonX-100 was omitted.

2.4.22. Fixed Cell Imaging

Fixed cell imaging was performed using either a PerkinElmer Ultra*VIEW* LCI spinning disc confocal scanner equipped with an Olympus IX-70 inverted epifluorescence microscope or a Leica AOBS-SP2 confocal microscope, equipped with an inverted Leica DMIRBE epifluorescence microscope. Lenses used were 40x (HCX Apo) with 1.25 numerical aperture (NA), or 63x (PL Apo BL) with 1.4 NA oil emersion objectives. Laser lines used (PerkinElmer Ultra*VIEW*) were: an Ar/Kr laser to excite all 'green' fluorophore (488-nm line) and the 568-nm line for 'red' fluorophores; emission was collected using 525 ± 50 nm bandpass filters and 600 nm longpass filter sets respectively. Laser lines used (Leica AOBS-SP2) were an Ar/Kr laser (488-nm line) to excite GFP, Cy2 and Alexa488 fluorophores. He/Ne laser (543-nm line) was used for mRFP, Cy3 or Alexa568; the 594-nm line and 633-nm line were used to excite Alexa594 and Alexa633/648 fluorophores, respectively. A 405 nm diode laser was used to visualize DAPI staining. Confocal images were typically acquired at 100 – 500 nm separation of z-sections, and 8 – 12 sections were routinely acquired. Images of single slices or maximum z-projections were initially processed using the respective Ultra*VIEW* or Leica software. Optional post-processing was carried out as described (**para. 2.4.24, 2.4.25**).

2.4.23. Live Cell Imaging

Live cell imaging was performed using an Ultra*VIEW* LCI spinning disc confocal scanner (Perkin Elmer) or a wide-field imaging system (controlled with Openlab 4 software (Impro*vision*), to operate electronic focus, shutters and excitation filter wheel). Specifications for the Ultra*VIEW*

system are listed under (**para. 2.4.22**). The wide-field system (in an environmental control chamber) equipped with a Leica DMIRB inverted microscope connected to a Hamamatsu CCD camera (ORCA ER Firewire; 12-bit digital) was used for digital imaging. A triple dichroic filter was used for DAPI/FITC/TRITC (460/20, 520/35, 600/40), and a 484/15 excitation filter for FITC/GFP. A 40x, (1.25 NA) objective and a 63x (1.4 NA) objective were used. For experiments, transfected cells grown on coverslips (Ø 22 mm), were transferred to holders and immersed in 1 ml pre-warmed imaging buffer. Low level expressors were selected for imaging. Imaging was routinely performed for 5 - 30 minutes, with capture rates of either 1 frame per second, or with a 20-second delay for long-term imaging.

2.4.24. Data Manipulation of Movies and Images

For post-processing, live cell data for the recorded channels was exported from PerkinElmer Ultra*VIEW* or Leica confocal software as uncompressed movies. Using ImageJ (NIH public domain software), background correction was performed, routinely using the 'rolling ball' (set to 50) option. The contrast was enhanced by setting the maximum of allowed saturated pixels to 0.5% and normalizing it for all frames, and entire images only, before an RGB merge was performed to yield an overlay of the channels. Typically, movies were exported as QuickTime movies or .avi files at a rate of 10 frames per second. Movies captured using Openlab software (Impro*vision*) were cropped and merged using the Openlab software, and compiled as QuickTime movies. To obtain .avi files, individual images were exported as .tif files, and, using Vol*ocity* software V4.0.1 (Impro*vision*), these were converted into .avi movies, typically using Sorensen (Sorensen Communications) compression at maximum quality and at 10 frames per second.

For image processing, obtained images from fixed cell analyses were merged using Leica confocal software (Leica Microsystems). Where applicable, contrast and brightness adjustments were made using Adobe Photoshop® 6.0 (Adobe Systems Inc.), but was strictly performed for entire images only.

2.4.25. Deconvolution of Imaging Data and 3D-rendering

Images, typically 20 - 30 confocally acquired z-slices at a z-separation 100 - 200 nm, or as indicated, were iteratively deconvolved using Vol*ocity* software V4.0.1 (Impro*vision*). A point spread function (PSF) was calculated for each channel to be deconvolved and was iteratively applied to the raw data for 20 cycles, or stopped at 98% confidence (yielding a high degree of deconvolution with a manageable degree of computation). The processed images were then rendered in 3D, and either exported as .avi files, or manipulated using AdobePhotoshop 6.0 (Adobe Systems, Inc.).

Chapter 3 – Role of Retromer in Receptor Retrieval

3.1. Introduction

This chapter describes the functional characterisation of endogenous SNX1 as part of a multimeric sorting complex, the retromer, and its role in sorting of endogenous hydrolase receptors. Besides SNX1, this chapter also describes an initial examination of the role of the closely related SNX2 in these processes.

When commencing my PhD studies, the previously described role for SNX1 in pro-degradative transport (Kurten et al., 1996; Cozier et al., 2002) was under debate, since despite extensive efforts, this data could not be confirmed for endogenous SNX1 (Kurten et al, 1996; JG Carlton, PhD thesis[3]; Carlton et al., 2004; Gullapalli et al., 2004). In 1996, SNX1 had been identified as an interaction partner for the lysosomal targeting region of the EGF receptor (Kurten et al., 1996). While this was an exiting find, as it had identified the first mammalian sorting nexin, it had heavily relied upon overexpressing the protein. Whilst protein overexpression has long been the method of choice to examine the roles of a given protein, with the later discovered capacity of the SNX1-BAR domain to stabilize membrane curvature, or even to tubulate membranes in a concentration-dependent fashion (Carlton et al., 2004), there was concern about the reliability of the overexpression data. Indeed, while the original study reported that deleting the SNX1 C-terminus prevented downmodulation of the EGFR (Kurten et al., 1996), this region was only later identified as part of the BAR domain (Peter et al., 2004). Hence, this suggested that the effect of promoting EFGR degradation could be an artefact of overexpression-induced membrane tubulation directly or indirectly mediated by the BAR domain.

Besides a pro-degradative function, a role for SNX1 in retrograde sorting - therefore away from the degradative route (Haft et al., 2000; Pfeffer, 2001) - had been discussed at the time. This model was based on identification of proposed mammalian orthologues of the yeast retromer complex (Edgar and Polak, 2000; Haft et al., 2000). In yeast, numerous studies had established an important role for this complex in the retrieval of late-Golgi complex resident proteins from a pre-vacuolar/endosomal compartment [see (Pfeffer, 2001; Seaman, 2005) for review]. Hence, the finding that the yeast retromer component

[3] JG Carlton, *Examining the Role of Mammalian Sorting Nexins*, Ph.D. thesis, University of Bristol, Bristol, 2004

Vps5p shared extensive sequence homology with SNX1 (Nothwehr and Hindes, 1997), and that SNX1 furthermore interacted with VPS35 (Haft et al., 1998; Gullapalli et al., 2004; Rojas et al., 2007), the proposed cargo-selective component of a mammalian retromer complex, gave rise to a model which implicated SNX1 in retrograde sorting. Nevertheless, when commencing these studies, there was no direct evidence for a conserved function of retromer in mammalian cells, as a cargo was still elusive. For these reasons, at the start of my PhD I embarked on a project scrutinizing the proposed role for SNX1 as part of a mammalian retromer complex, investigating the relationship of SNX1 to other components of the retromer and questing for possible cargo.

The commencement of this project was greatly aided by the preliminary work of members in the Cullen Lab, including Dr Alex McGregor, Dr Gyles Cozier, but particularly Dr Jez Carlton, who must be thanked for the elaborate characterization of SNX1, and his work rebutting a role for endogenous SNX1 in EGF receptor trafficking. All work performed by, or with, those other than myself is accordingly acknowledged.

3.2. Materials

General materials and methods, as well as exact media and buffer compositions and other reagents have been described in Chapter 2. We are indebted to Dr Muriel Mari, Prof Judith Klumperman and Prof Hans Geuze, Cell Microscopy Center, University of Utrecht, The Netherlands, for providing outstanding electron micrographs and in-depth ultrastructural analysis of endogenous SNX1, SNX2 and the characterization of endosome-to-TGN carriers. The anti-VPS26 and anti-SNX1 polyclonal antibodies and HeLaM cells were kind gifts from Dr Matthew Seaman and the anti-CI-MPR antibody was from Prof Paul Luzio, both Cambridge Institute for Medical Research, Cambridge, UK. The polyclonal anti-sortilin antibodies were kind gifts from Prof Claus M Petersen, Aarhus University, Aarhus, Denmark.

3.2.1. Co-localization Analysis

To quantify the co-distribution of SNX1 with other cellular proteins, cells were processed for immunofluorescence labelling (see **para. 2.4.21**) and imaged, capturing 8-10 optical z-slices per visual field (**para. 2.4.22**). Co-localization analysis of two vesicular proteins in maximum projections was performed using the co-localization plug-in in ImageJ (NIH Image), creating a composite image of co-localizing vesicles. Enumeration of vesicles was done using the Colony Counter tool of ImageQuant TL software (GE Healthcare) for individual channels and co-localization composite images obtained through ImageJ-aided analysis. Degree of co-localization is expressed as percentage of all vesicles positive for the marker over total number of vesicles.

3.2.2. Generation of pmRFP-SNX1

To obtain the red fluorescent protein (RFP)-SNX1 fusion construct, a pmRFP-SNX1 eukaryotic expression vector was generated that made use of the pmRFP-C1 plasmid consisting of the "backbone" of the commercially available pEGFP-C1 (Clontech) but with the coding region for GFP being replaced by the sequence for monomeric RFP1 (**para. 2.1.4**, originally developed by Dr Jez Carlton). A plasmid containing the mRFP1 coding sequence was a kind gift from Prof Roger Tsien, UCSD, La Jolla, USA, and mRFP1 was generated by stepwise evolution of DsRed (*Discosoma* coral) to a dimer and then to a true monomer designated mRFP1 (monomeric red fluorescent protein) with the excitation and emission peaks of 584 nm and 607 nm, which are ~25 nm red-shifted from DsRed (Campbell et al., 2002). The sequence encoding for SNX1 was subcloned into

pmRFP-C1 from a pEGFP-C1-SNX1 construct (originally developed by Dr Alex McGregor) using the EcoRI and SalI restriction sites (for a complete vector map refer to **Appendix II.1**; the resulting construct was sequenced (see **Appendix I** for primers).

3.2.3. Generation of pEGFP-C1-VPS35

To obtain a green fluorescent protein-VPS35 fusion protein (GFP-VPS35), first, the coding sequence of VPS35 was amplified by PCR using pCMU-3xFLAG-VPS35 as a template (a kind gift from Dr Rohan Teasdale, University of Queensland, Brisbane, Australia); the sequence of the primers, containing a XhoI (5'-primer) and BamHI (3'-primer) restriction site, can be found in **Appendix I.** Using the XhoI and BamHI restriction sites, the sequence for VPS35 was inserted into the commercially available pEGFP-C1 (Clontech) plasmid. For a complete vector map refer to **Appendix II.2**; the resulting construct was sequenced (see **Appendix I** for primers).

3.2.4. CD8-CI-MPR Trafficking Assays

HeLaM cells stably expressing a CD8-CI-MPR chimera were seeded onto coverslips (∅ 22 mm) in 9.5 cm^2-wells and treated with either control, or SNX1- and SNX2-specific siRNA duplexes as described in **par 2.4.19**. After 72 hours, cells were washed in ice-cold PBS, the coverslips were transferred to 3 ml pre-chilled DHB medium, and incubated at 4°C for 15 minutes to stop traffic. Cell-surface CD8-CI-MPR was labelled with 1 µg anti-CD8 in 100 µl DHB medium, incubating cells for 30 minutes at 4°C. Coverslips were washed thoroughly with ice-cold PBS, then either fixed directly (0-minute time point) or transferred to wells containing pre-warmed (37°C) complete growth medium, and incubated for indicated periods and then fixed. Cells were processed for immunolabelling (refer to **para. 2.4.21**). In any case, the anti-CD8 antibody was detected using an appropriate fluorescence-coupled secondary antibody to visualize the CD8-CI-MPR. Fixed cells were imaged taking routinely 8 confocal *z*-sections at the same *z*-separation (typically 480 nm) and applying identical microscope- and laser-settings to all samples. The amount of TGN-resident anti-CD8 was determined by additional immunofluorescence-labelling with anti-TGN46. Co-localization in confocal images was quantified using LCSLite (Leica).

3.2.5. CD8- uptake Assays

HeLaM cells stably expressing CD8-CI-MPR constructs were grown on coverslips and transfected with plasmid DNA at 50% confluency (see **para.2.4.18**). After 22 hours, cells

were washed with ice-cold PBS, the coverslips transferred to 3 ml pre-chilled DHB medium, and incubated at 4°C for 15 minutes to stop traffic. Cell-surface CD8-CI-MPR was labelled with 50 µg/ml RPE-coupled anti-CD8 (RPE-CD8) in DHB medium, incubating cells for 30 minutes at 4°C. Coverslips were rinsed with ice-cold PBS, then transferred to coverslip holders and mounted onto a heated microscope stage where pre-warmed (37°C) imaging buffer was added. Cells were inspected by epifluorescence, and uptake was followed for 10 minutes before confocal live cell imaging was started using a PerkinElmer LCI Ultra*VIEW* system.

3.2.6. Sortilin Stability Assays

Cells were transfected with the relevant control and SNX1-specific siRNA duplexes as outlined in **para. 2.4.19** for 72 hours, then the treatment was repeated, and 20 hours into the second treatment, control and SNX1-suppressed cells were either lysed directly or treated with a freshly prepared 40 µg/ml-cycloheximide (CHX) solution. Where appropriate, lysosomal protease inhibitors (PI) in the form of 1mg/ml leupeptin and 10 µg/ml E-64 were added. CHX and PI were replaced every 4 hours and cells were lysed after 12 hours. Of each sample, 20 µg protein, as determined by Bradford assay (**para. 2.4.13**), was subjected to SDS-PAGE (**para. 2.4.14**), Western blotting and immuno-detection (**para. 2.4.15**) using anti-sortilin, anti-SNX1 antibodies and anti-β-actin antibodies as loading control. Quantification was carried out by volume integration using ImageQuant software (GE Healthcare). Results were normalised by dividing the intensity values obtained for the sample by the intensity of the band for the respective loading control.

3.2.7. Preparation for Electron Microscopy

Untreated, control- or SNX1-siRNA treated HepG2 cells cultured in 6-well plates (**see para. 2.4.19**) were grown to 80% confluency and the media was changed the day before fixation. On the following day, half of the media was removed and replaced with 8% PFA solution (in PB: 0.1 M phosphate buffer, pH 7.4), by gently agitating the plate, yielding a final concentration of 4% PFA. Cells were fixed for 15 minutes at room temperature, and the solution was subsequently replaced by one volume of 4% PFA in PB. After 4 hours incubation at room temperature, the plates were sealed with parafilm and transferred to 4°C for 16 hours. The next day, cells were warmed to room temperature, the fixative was removed and cells were washed three times with 0.1M PB. The wells were then completely filled with 2% PFA in PB before being carefully sealed using parafilm and kept at 4°C until

being shipped at ambient temperature to Dr Muriel Mari at the laboratory of Prof Judith Klumperman and Prof Hans Geuze. All immuno-gold labelling, immuno-electron tomography and 3D reconstructions were performed by Dr Muriel Mari and Dr Dagmar Zeuschner as described previously (Slot et al., 1991; Zeuschner et al., 2006). Besides the listed antibodies (**para. 2.1.8**), these studies additionally used anti-AP-1 antibodies (Prof MS Robinson, CIMR, Cambridge, UK), anti-ASPGR (Prof AL Schwartz, Washington University, St Louis, MO, USA) and anti-Hrs (Dr S Urbé, University of Liverpool, Liverpool, UK). Furthermore, anti-CD63 (hybridoma cell line HSC6, obtained from the University of Iowa, Department of Biological Sciences, Iowa City, USA), anti-Alexa488 and anti-GFP (both Invitrogen), anti-GGA3 and anti-Rab4 (both BD Biosciences) antibodies were used.

3.3. Preliminary characterization of SNX1 and SNX2

3.3.1. Sequence alignment of the sorting nexins Vps5p, SNX1 and SNX2

My reasoning to analyse both sorting nexins, SNX1 and SNX2, stemmed from the finding that the two proteins share approximately 63% sequence identity, and both are highly similar to yeast Vps5p (**Figure 3. 1**): a search of the whole yeast genome against a data base of all human expressed sequence tags returned SNX1 and SNX2 as best matches suggesting orthology of these proteins (Haft et al., 1998). As there appears to be no mammalian homologue for the second yeast sorting nexin (Vps17p) it was argued that SNX2 might fulfil this role in a mammalian retromer complex as indeed, previous studies had established that SNX1 and SNX2 can form hetero- and homo-oligomers (Haft et al., 2000).

As can be seen from **Figure 3. 1**, when comparing sequences of all three proteins (Vps5p, SNX1 and SNX2), a high degree of similarity is found – expectedly - over the length of the PX domain, which is the 'selection criteria' or hallmark for the sorting nexin family. Besides the central PX domain, the three proteins also show extensive sequence homology at the C-termini containing the predicted coiled-coil/BAR domains. In contrast, the sequence conservation at the N-termini is relatively poor. Overall, SNX1 and Vps5p share ~22% identity over 498 amino acids, while SNX2 and Vps5p are 21% identical over a stretch of 503 amino acids.

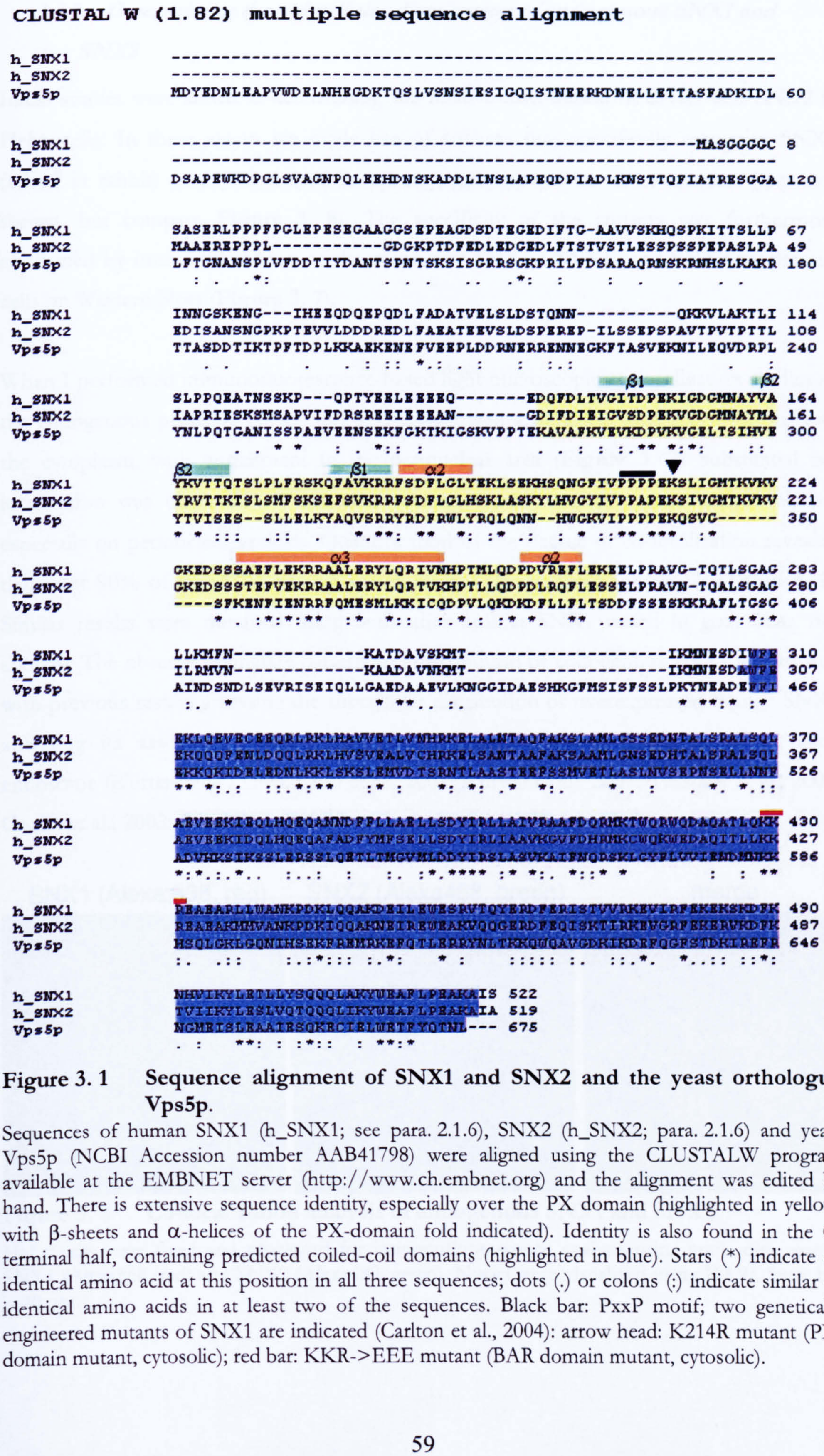

Figure 3. 1 Sequence alignment of SNX1 and SNX2 and the yeast orthologue Vps5p.

Sequences of human SNX1 (h_SNX1; see para. 2.1.6), SNX2 (h_SNX2; para. 2.1.6) and yeast Vps5p (NCBI Accession number AAB41798) were aligned using the CLUSTALW program available at the EMBNET server (http://www.ch.embnet.org) and the alignment was edited by hand. There is extensive sequence identity, especially over the PX domain (highlighted in yellow, with β-sheets and α-helices of the PX-domain fold indicated). Identity is also found in the C-terminal half, containing predicted coiled-coil domains (highlighted in blue). Stars (*) indicate an identical amino acid at this position in all three sequences; dots (.) or colons (:) indicate similar or identical amino acids in at least two of the sequences. Black bar: PxxP motif; two genetically engineered mutants of SNX1 are indicated (Carlton et al., 2004): arrow head: K214R mutant (PX-domain mutant, cytosolic); red bar: KKR->EEE mutant (BAR domain mutant, cytosolic).

3.3.2. Determining the subcellular distribution of endogenous SNX1 and SNX2

Initial studies were aimed at determining the relative distribution of SNX1 and SNX2 in HeLa cells. In these assays we made use of antisera that specifically recognize SNX1 (raised in rabbit) or SNX2 (raised in mouse) that showed no cross-reaction (data not shown, but compare **Figure 3. 8**). The specificity of the antisera was furthermore confirmed by immunodetection of the respective SNX in SNX1- and SNX2-suppressed cells on Western blots (**Figure 3. 7**).

When I performed immunofluorescence-based light microscopic co-localization studies of the endogenous proteins, SNX1 and SNX2 displayed a punctate distribution throughout the cytoplasm, with enrichment in the perinuclear area (**Figure 3. 2**) Substantial co-localization was observed on vesicular structures on both, the more peripheral, but especially on perinuclear vesicles. Quantification of the degree of co-localization revealed that over 90% of all SNX1-positve structures Ire also positive for SNX2 (**Table 3. 1**). Similar results were obtained using antibodies against SNX1 raised in goat (data not shown). The observed punctate pattern and distribution of endogenous SNX1 agreed well with previous results assessing the subcellular distribution of overexpressed human SNX1 analysing its association with vesicular and tubulo-vesicular structures of an early endosome (Kurten et al., 1996; Chin et al., 2001; Kurten et al., 2001; Teasdale et al., 2001; Cozier et al., 2002; Pons et al., 2003).

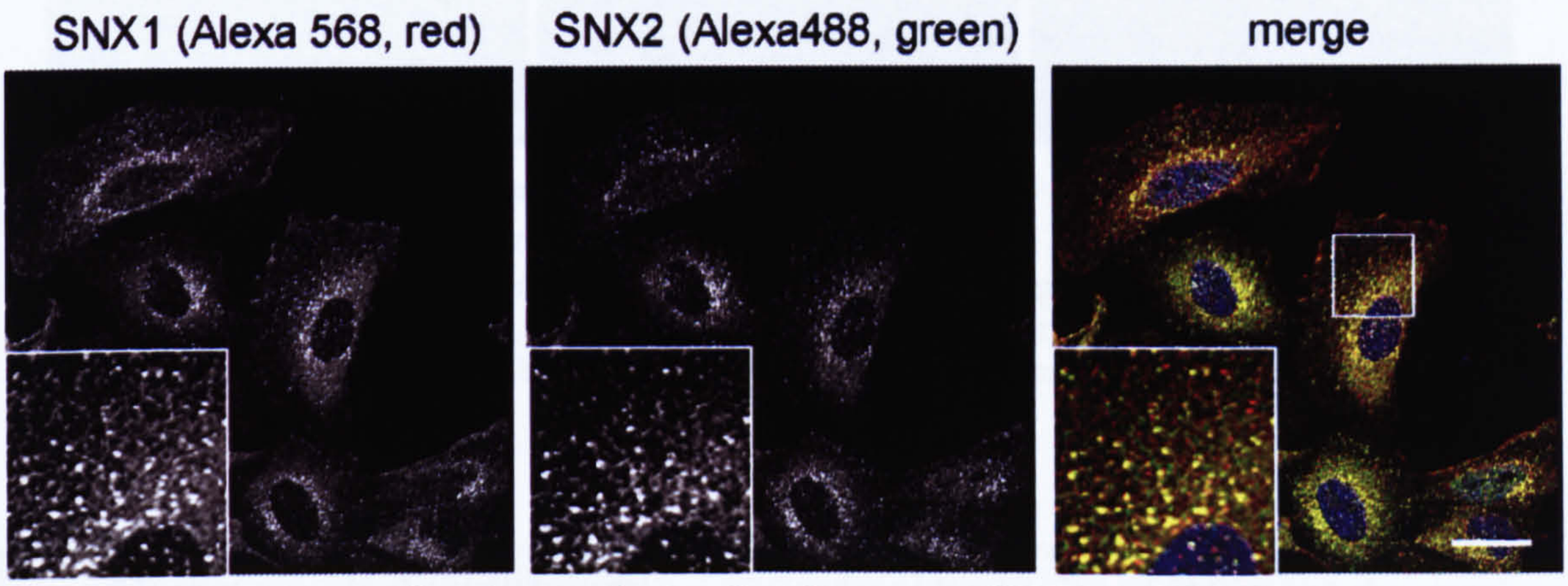

Figure 3. 2 Co-localization analysis of endogenous SNX1 and SNX2

HeLa cells were fixed and processed for immunofluorescence analysis using antibodies against SNX1 (Alexa568, red) and SNX2 (Alexa488, green). Nuclei were visualized using DAPI. Scale bar is 20 μm.

It is of note that previous immunofluorescence-based analyses of the subcellular distribution of endogenous SNX1 in HeLa cells had yielded conflicting results regarding the degree of co-localization with the early endosomal resident protein EEA1 (Gullapalli et al., 2004; Wang et al., 2004). I thus sought to analyse co-localization of SNX1 and EEA1; as part of this analysis, I also analysed co-localization with lysosomal-associated membrane protein-1 (Lamp-1), a protein localized to multivesicular bodies (MVBs) and lysosomes. As can be seen in **Figure 3. 3** and from **Table 3.1**, while there is substantial, but not complete overlap of endogenous SNX1 with EEA1, SNX1 showed virtually no co-localization with Lamp-1.

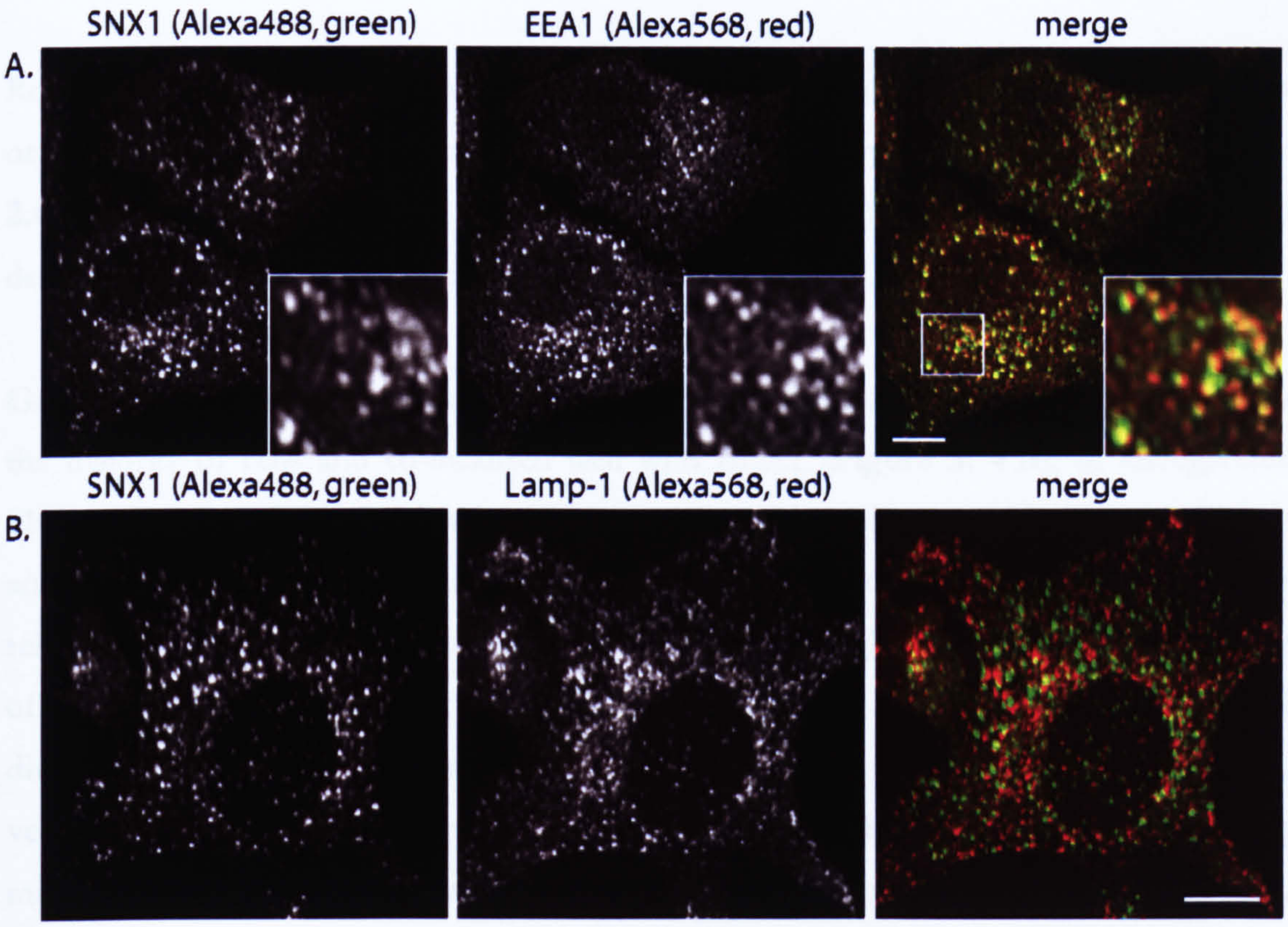

Figure 3. 3 Co-localization analysis of SNX1 with early endosomes and MVB / lysosomal markers.

HeLa cells were processed for immunofluorescence labelling using anti-SNX1 (Alexa488, green) and either anti-EEA1 (Alexa568, red) or anti-Lamp-1 (Alexa568, red) antibodies. Images shown captured using a PerkinElmer Ultra*VIEW* LCI system are maximum projections of 10 – 12 z-sections. Scale bar is 10 μm.

Marker	Co-localization
SNX2	88.3 ± 2.5
EEA1	65.8 ± 3.0
LAMP1	3.3 ± 1.1

Co-localization was analysed by eye as coincidental localization of SNX1 with the given marker on every vesicle on at least five cells for individual z-sections of confocal images and given as percentage of the total number of vesicles counted in a given cell.

Table 3. 1 Co-localization analysis of SNX1 with different endosomal proteins

3.4. Overexpression of SNX1

Besides analysing the localization of endogenous SNX1 in fixed cells, I also sought to examined the intracellular dynamics of fluorescently-labelled SNX1 fusion proteins to better understand the spatio-temporal 'behaviour' of SNX1.

Another aspect this chapter is the succinct illustration of the effects of strong overexpression on endosomal morphology, and examination of the effect of exposure to low temperatures on the association of GFP-SNX1 with intracellular membranes, as these findings have implications on experimental design.

Routinely, in these assays cells were transfected with fluorescent GFP-SNX1 (**para. 2.1.5**) or RFP-SNX1 (**para. 3.2.2**) for 22 hours, then analysed by live cell imaging (LCI, **par 2.4.23**), or fixed and processed for immunofluorescence (IF) analysis using the previously described antibodies as reference markers (SNX1, SNX2, EEA1, Lamp-1).

Generally, after 22 hours of expression, GFP-SNX1 displayed a vesicular appearance in the majority of cells and co-localized well with EEA1 (**Figure 3. 4 B**), or endogenous SNX2 (data not shown) indicating the correct targeting of the probe. In a qualitative analysis of the LCI, I found these vesicles to be very motile (**Movie 3.1.1**), with the relatively smaller SNX1-decorated structures showing the highest motility. Over the course of short distances, movement of these structures is best described as 'burst-like' and directional, and often accompanied by sudden changes in direction. The directionality, velocity and non-random quality of movements might suggest transport along microtubules. Larger structures appear more inert and movement is rather oscillatory. Fusion of vesicles and emergence of more tubular SNX1-decorated structures from these punctae was frequently observed. Unfortunately, analysis of vesicle movement in a more quantitative way by utilizing conventional single-particle tracking programs available to us proved to be not feasible, as the tracking problem is not trivial: changes occur, often simultaneously, at the level of directionality, signal intensity (factor and variation), velocity, as well as in size and shape of the particle due to tubulation out of the vesicle. It is not clear to us at this point, whether the more inert structures are a result of the higher protein content of the structure due to overexpression, or whether they represent less motile endosomal structures (Lakadamyali et al., 2006).

Besides the vesicular phenotype in low expressing cells, some cells exhibited extensive GFP-SNX1-decorated tubules (**Figure 3. 4 C**), the fraction of which increased when the period of GFP-SNX1 expression was prolonged. The predominant occurrence of the 'tubular phenotype' with increased expression time correlates with the finding that in *in vitro* assays, SNX1 tubulates (or stabilizes) liposomes in a concentration-dependent fashion (Carlton et al., 2004). Thus, one would imply that longer expression time leads to accumulation of more GFP-SNX1, hence occurrence of increased tubulation.

According to the intensity of green fluorescence and virtual absence of tubulation, cells displaying a vesicular appearance were deemed 'low expressors'. In these cells, GFP-SNX1 co-localized with EEA1 (**Figure 3. 4 B**) to a similar extent observed for endogenous proteins (**Figure 3. 3 A**), indicating that at these levels, membrane homeostasis is not detectably perturbed. In contrast, when examining cells that displayed notable tubulation, the EEA1-labelled compartment appeared on one hand partly enlarged (**Figure 3. 4 C,** arrows) compared to low expressors (**Figure 3. 4 B**), or non-transfected control (**Figure 3.** 3 **A**). On the other hand, on contiguous GFP-SNX1-labelled tubules, the discrete EEA1-positive vesicles appeared almost as 'beads on a string' (**Figure 3. 4 C**, boxed area). Strikingly, even in cells displaying high levels of GFP-SNX1 overexpression I found virtually no co-localization with Lamp-1 (**Figure 3. 4**) in accord with the results for endogenous SNX1 (**Figure 3. 3**). From this data, it appears that SNX1 selectively tubulates early endosomal membranes, or at least membranes inaccessible to Lamp-1. In strongly overexpressing cells, most of these tubules are rather 'stable', meaning that when analysed by live cell imaging (**Movie 3.1.2,** which shows an example of an extensively overexpressing cell), tubules did not disintegrate and appeared as continuous membranes. Preliminary EM studies have indicated that strong overexpression of SNX1 can result in membrane-'superfolds' showing GFP-SNX1 localized beneath layers of endosomal membrane (Prof Judith Klumperman, personal communication). Likewise, preliminary FRAP experiments have shown that 'stable' tubules are rather inert to fluorescence recovery after photobleaching (data not shown). This might indicate that under these conditions, photo-bleached GFP-SNX1 is not freely accessible to the cytoplasm, either by entrapment between membrane layers or by stable complexation, indicated by its ability to form large-size aggregates *in vitro* (Haft et al., 1998; Haft et al., 2000). I have however chosen not to investigate this in further detail, but to concentrate on more physiological conditions.

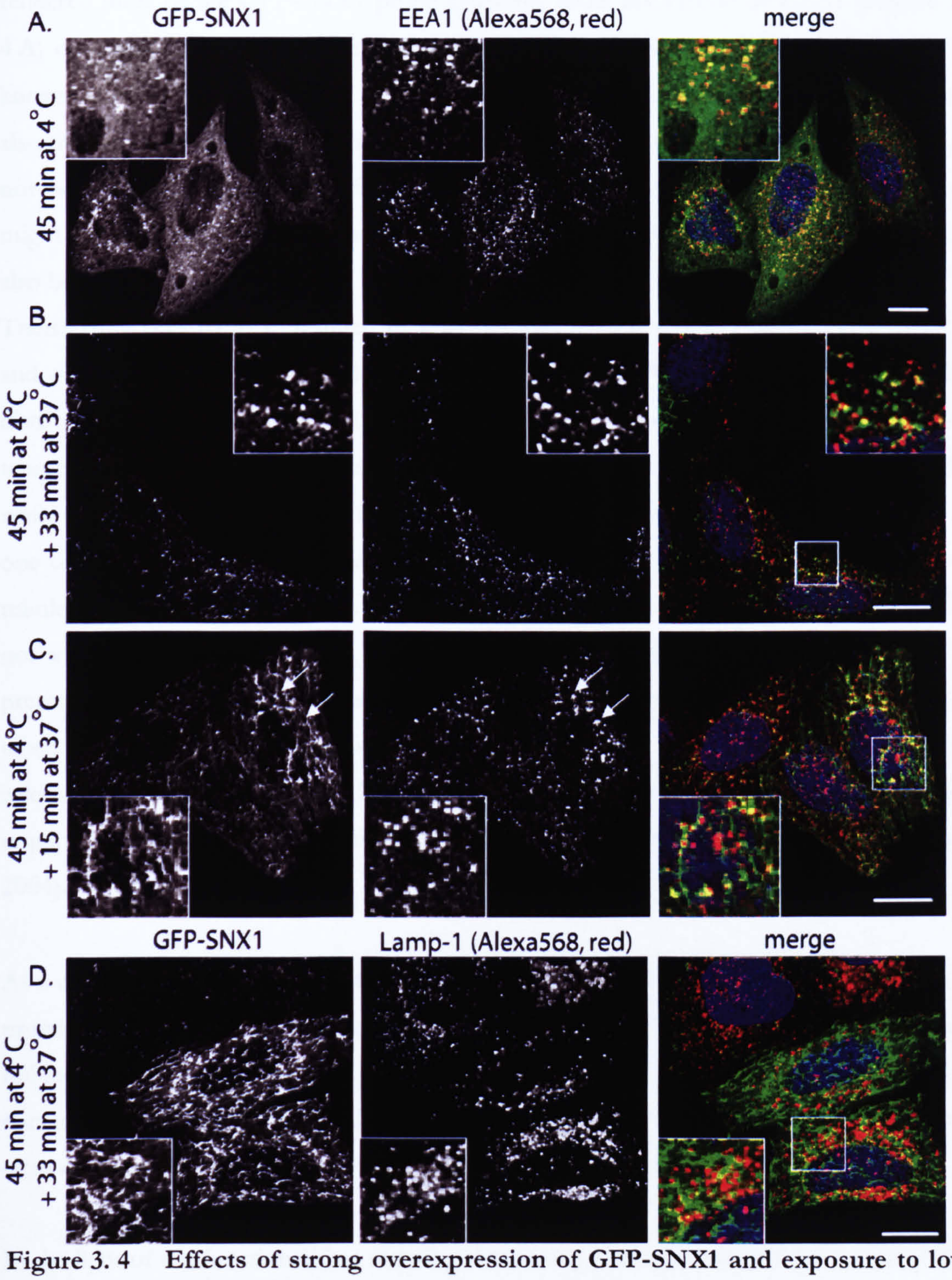

Figure 3. 4 Effects of strong overexpression of GFP-SNX1 and exposure to low temperatures.

HeLa cells transfected with GFP-SNX1 for 48 hours were transferred into ice-cold DHB medium for 45 min, and either fixed directly or following incubation in normal growth medium at 37°C for indicated times. Cells were processed for immunolabelling using the indicated antibodies and DAPI to stain nuclei. Exposure to 4°C rendered GFP-SNX1 largely cytosolic, while after 15 min at 37°C, SNX1 had reassociated and displayed a vesicular distribution. Different degrees of overexpression are shown. Note enlarged EEA1-positive structures in strongly overexpressing cells (C), and GFP-tubules with associated EEA1 (boxed area, C). Lamp-1 is virtually absent from tubules (D). Scale bar is 10 μm.

Another important results of this study was the finding that prolonged incubation at 4°C rendered most of the GFP-SNX1 probe cytosolic, while association of EEA1 (**Figure 3. 4 A**) or Lamp-1 (data not shown) with vesicular structures appeared unaltered. It is well known that EEA1 localizes - by means of its FYVE domain (Stenmark et al., 1996), but also through interaction with Rab5 (Simonsen et al., 1998) - to the vesicular body and has not been found on tubular profiles. So besides increased affinity, membrane-geometry might be factor, as tubules might not be effectively preserved at lower temperature (see also below).

Transferring cells to 37°C resulted in vesicular and tubular reassociation of GFP-SNX1, and was as a function of time and temperature (**Figure 3. 4 B, C, D**); after 15 minutes, the distribution pattern in these cells was indistinguishable from cells not exposed to low temperature. At 4°C however, the protein was observed to be cytosolic in virtually all cells, while with increased time and temperature, I did observe GFP-SNX1-'tubulated' cells: if one considers these findings together with the observed relative inertness of membrane-tubules harbouring high amounts of GFP-SNX1, this suggests that the tubular profiles do not withstand cold temperatures. This notion was further reinforced when attempting to preserve tubules decorated with endogenous SNX1 (Chapter 5), which was only achieved when fixing cells at physiological temperatures. This would correlate with the interpretation that the SNX1-BAR domain equips the protein with a curvature sensor that requires a certain geometry to effectively associate with curved membranes (Carlton et al., 2004).

As a control, I additionally generated a vector encoding for a red fluorescent SNX1 fusion protein, consisting of a monomeric red fluorescent protein (RFP) and C-terminally of this, full-length SNX1 (refer to **para. 3.2.2** and **Appendix II.1**). At low expression levels, this construct exhibited identical localization compared to GFP-SNX1, confirming that effects were not caused by the properties of the GFP moiety (compare also **para. 3.4**).

In the light of the functional data showing that strong overexpression of full length SNX1 does enhance endosomal degradation (Kurten et al., 1996; Cozier et al., 2002), these data put into perspective the problems arising when not carefully monitoring levels of overexpression. Nevertheless, these results also demonstrate that given low expression levels and physiologic temperatures, overexpressed SNX1 appears not to grossly perturb endosomal morphology as examined by light microscopy.

3.5. Subcellular localization of retromer components

With these considerations in mind, I embarked on a project where I wished to examine the relative subcellular localization of SNX1 and SNX2 to other retromer components using live cell imaging (LCI) analyses and immunofluorescence-based co-localization studies. Although membrane association of SNX1 and binding to VPS35 had been shown biochemically (Haft et al., 1998; Haft et al., 2000), at commencement of these studies the subcellular localization of individual mammalian retromer components at microscopic level had not yet been established.

I reasoned that this analysis could provide me with information about the nature of a retromer-resident subcellular compartment and provide cues about the itinerary of structures labelled with these proteins and potentially give insights into the function of a mammalian retromer complex.

In case of VPS26, an antibody was available (a kind gift from Dr Matthew Seaman, CIMR, Cambridge, UK) allowing examination at endogenous protein levels. With the lack of an antibody recognising VPS35, I decided to generate a fluorescently-labelled VPS35 fusion protein. To do so, I genetically engineered a eukaryotic expression vector encoding for a green fluorescent protein (GFP) N-terminally ligated to the sequence encoding for VPS35 (see **para. 3.2.3** and **Appendix II.2**). This furthermore provided me with a tool to examine intracellular dynamics of VPS35 employing live cell imaging analyses.

VPS35

In fixed cells studies, I found GFP-VPS35 localised to punctate intracellular structures (data not shown, but see **Figure 3. 5**). When analysing cell co-expressing GFP-VPS35 and RFP-SNX1 using LCI analysis, both proteins co-localized well on vesicular structures as well as tubular profiles (**Movies 3.1.1 – 3.1.3, Figure 3. 5 A**), which were not preserved in the fixed cell studies. The inspection of more than five cells (examined for at least 2 minutes) also showed that in all cases, both proteins moved conjointly on vesicular structures in the cytoplasm, with the most highly motile structures moving toward the perinuclear area (top left corner, labelled as 'Nu' in **Figure 3. 5** A).

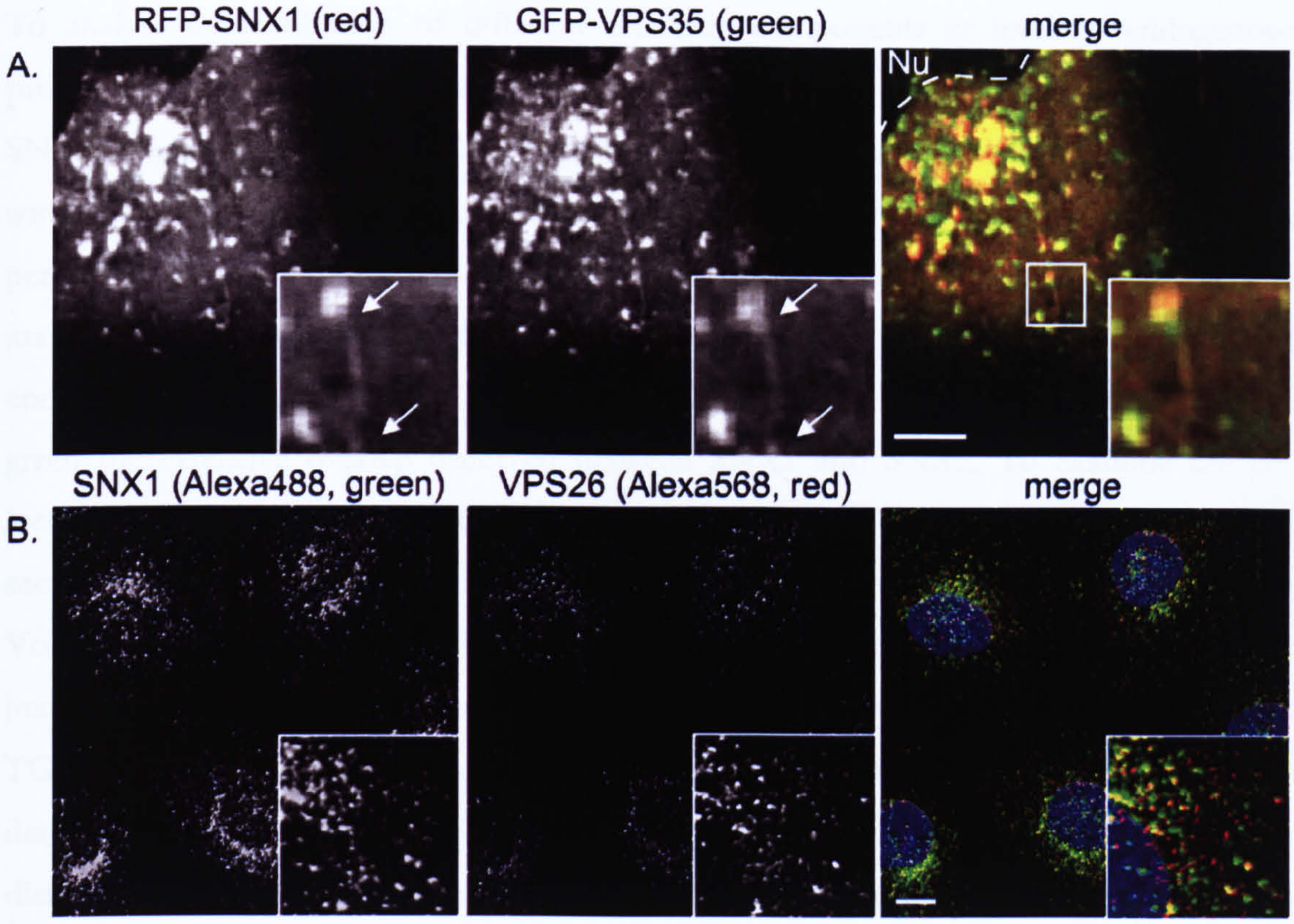

Figure 3. 5 SNX1 co-localizes with retromer components VPS35 and VPS26
(A) HeLa cells were transiently transfected with RFP-SNX1 (red) and GFP-VPS35 (green) for 22 hrs and imaged live (see also Movies 3.2.1 -3.2.3). One frame of the movie is presented showing only the perinuclear area of a cell with 'Nu' (merge) denoting nucleus, the edge of which is demarcated by a dashed line. Both proteins co-localize on punctate structures but also tubular profiles (arrows). (B) HeLa cells were fixed and processed for immunolabelling using anti-SNX1 (Alexa488, green) and anti-VPS26 (Alexa568, red). Scale bar is 10 μm.

Generally, as also described in **para. 3.3** and Chapter 5, tubular profiles are notoriously difficult to preserve, whether at endogenous or low overexpression levels. Thus, I suggest that the poor detectabilty of tubular profiles at fixed-cell level is mainly due to the transient nature of the tubular compartment, as illustrated by LCI, as well as the documented instability of membrane association of SNX1 under certain fixation conditions (see **para. 3.3**).

To analyse co-distribution of different retromer components at level of endogenous proteins, cells were fixed and immunolabelled with antibodies recognizing VPS26 and SNX1 (**Figure 3. 5 B**) or SNX2 (**Figure 3. 6**), respectively. In these assays I observed some degree of co-localization between SNX1 and VPS26 on vesicular structures on peripheral structures, but co-localization was most prominent on vesicles in the juxtanuclear area (**Figure 3. 5 B**). Likewise, I observed extensive co-localization of endogenous SNX2 and VPS26 (**Figure 3. 6 A, B**). This result was somewhat expected given the extensive overlap observed between SNX1 and SNX2. To examine the co-localization on vesicular structures in more detail, images consisting of 16 confocal z-sections, at a z-separation of 122 nm, were deconvolved and 3D reconstructed using Volo*city* software (Impro*vision*) (**Figure 3. 6 B**). This type of analysis also revealed that juxtanuclear vesicles labelled for VPS26 and SNX2 were in very close proximity to the TGN (**Figure 3. 6 B**; shown in magenta, some ribbons specified by asterisks), as determined by labelling for TGN46 (Ponnambalam et al., 1996). It was noticeable that distribution of both, the green and red fluorescence signal, often appeared 'polarized' on vesicles (**Figure 3. 6 B**). At the level of immuno-light microscopy is it however not possible to decide whether this truly represents sub-domain targeting. In this context, later immuno-electron microscopy studies examining the localization of SNX1 and VPS26 at ultrastructural level have indeed demonstrated that distribution on sorting endosomes is not identical (compare **para. 3.6.7** and Arighi et al., 2004).

Hence, in HeLa cells, the sorting nexins SNX1 and SNX2 co-localize with the VPS-components in fixed cells and at a dynamic levels. While these co-localization studies do not provide insights into a functional relationship, they demonstrate that individual retromer components are closely spatio-temporally linked.

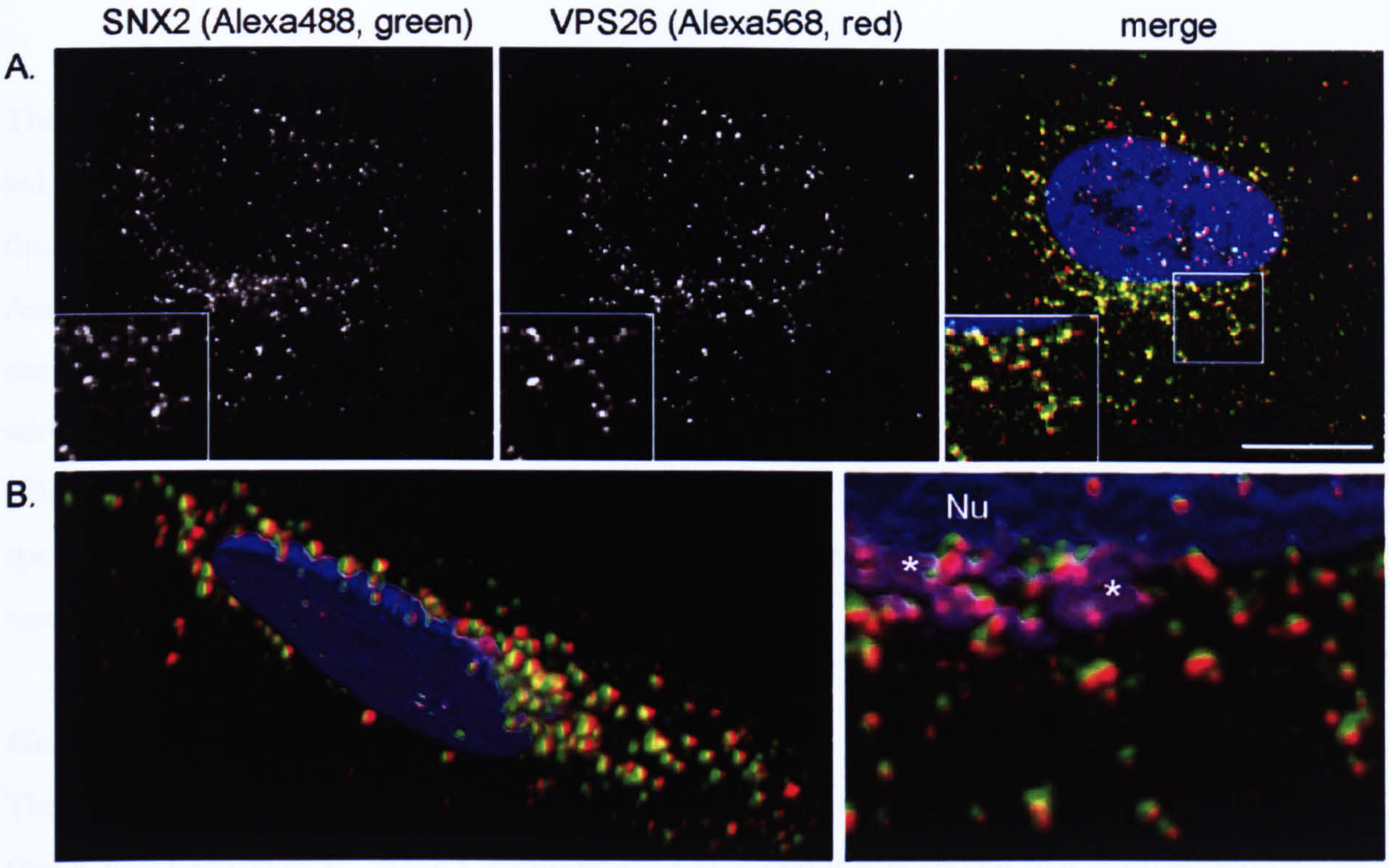

Figure 3. 6 Co-localization analysis of SNX2 and VPS26

(A) HeLa cells were fixed and processed for immuno-labelling using anti-SNX2 (Alexa488, green) and anti-VPS26 (Alexa568, red). (B) The 16 confocal z-sections, each at 122 nm z-separation, of the maximum projections shown in (A), were deconvolved and 3D-rendered using Volo*city* software (Improvision). A tilted and rotated view and a magnification, largely corresponding to the ROI shown in (A), is shown. 'Nu' denotes nucleus; asterisks are placed on selected TGN ribbons as labelled by anti-TGN46 (Alexa633, magenta). Scale bar is 10 μm.

3.6. RNAi approach to investigate SNX1 and SNX2 function

The finding that overexpression of SNX1 caused a dramatic tubulation of early endosomes led us to seek for ways to examine SNX1 function under more physiological conditions. I thus employed an RNA interference-based approach. Briefly, this technique pioneered by Andrew Z. Fire and Craig C. Mello [see also article by (Montgomery, 2006)] is based on the natural cellular RNA interference response to introduction of short RNA duplexes, with an apparent optimal length of 21 - 22 nucleotides for mammalian culture cells (Elbashir et al., 2001). The introduction of these small interfering RNAs (siRNAs) leads to specific silencing of genes complementary to the introduced the siRNA-antistrand and as a result, to suppression of protein expression.

General remarks on the siRNA used in this study

The siRNAs used were designed and previously characterized by Dr Jez Carlton (PhD thesis[4] and Carlton et al., 2004; Carlton et al., 2005), and it was shown that suppression of SNX1 using these sequences does not result in global trafficking defects, as no effects on EGF/EGFR of Tf/TfR internalization, recycling or degradation were observed.

Results

When treating HeLa cell with these duplexes for 72 hours, expression of SNX1 or SNX2 was found to be markedly reduced as assessed by immuno-detection from whole-cell lysates (**Figure 3. 7**), or immunofluorescence analysis (**Figure 3. 8**). In cells treated with a non-targeted control siRNA, both, SNX1 and SNX2 were detected as 68-kDa band, respectively. Treatment with SNX1-specific siRNA routinely lead to 90% reduction of SNX1 protein levels, as determined by volume integration of Western blots (**Figure** 3. 7 **A**; compare Chapter 4, **Figure 4. 13** for further quantification). Likewise, when examining SNX1-suppressed cells by light microscopy, the fluorescence signal for immunofluorescence-detected SNX1 was very low or even undetectable indicating the absence of this protein in the treated cells (**Figure 3. 7; Figure 3. 8 e, m**). Likewise, SNX2-specific siRNA effectively suppressed SNX2 expression to greater than 80% (**Figure 3. 7 A** and Chapter 4, **Figure 4.13**). And when assessed by immunofluorescence analysis, I routinely found the signal for SNX2 to be markedly reduced (**Figure 3. 7 C, D; Figure 3. 8 j, n**). It is to be noted that in some but not all instances, cells treated with the SNX2-specific siRNA showed a pronounced 'triangular' shape, meaning that these cells

[4] JG Carlton, *Examining the Role of Mammalian Sorting Nexins*, Ph.D. thesis, University of Bristol, Bristol, 2004.

were thinner and longer (or, from a different perspective, had a reduced volume). Compared to cells treated with SNX1-specific or control siRNA, I furthermore noticed that SNX2-suppressed cells proliferated less well. These are qualitative observations, and I have not further investigated this. These effects could however be linked to the documented interaction of SNX2 with Abstrakt (Abdul-Ghani et al., 2005), a protein that, in *Drosophila*, has been involved in many developmental processes, including cell-shape changes, localization of RNA and apoptosis (Irion and Leptin, 1999; Schmucker et al., 2000; Irion et al., 2004). Its human homologue was shown to be ubiquitously expressed (Sekito et al., 2005) but has yet to be characterised in detail. Importantly though, previous studies using this siRNA duplex have found that trafficking steps, like TfR recycling and EGFR degradation were not perturbed, suggesting that global endosomal processes are not grossly altered in cells treated with the SNX2-specific siRNA (JG Carlton, PhD thesis; Carlton et al., 2005).

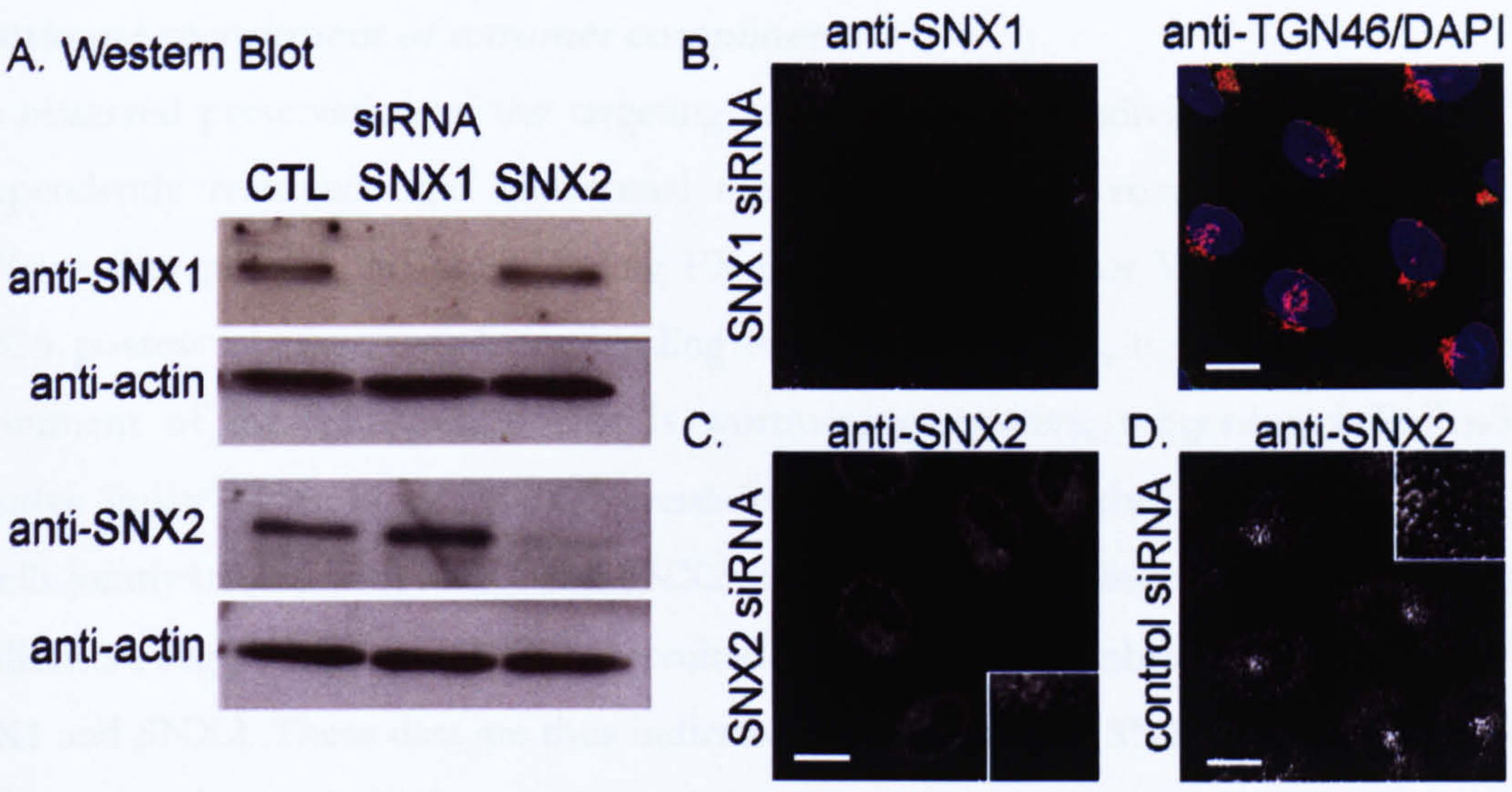

Figure 3. 7 Effect of siRNA-mediated suppression of SNX1 and SNX2
(A) HeLa cells were treated with control, SNX1- or SNX2-specific siRNA for 72 hours, before being lysed and subjected to SDS-PAGE. After Western blotting, membranes were probed with anti-SNX1, anti-SNX2 and anti-β-actin which served as loading control. (B-D) Cells plated on coverslips and treated with the respective siRNAs for 72 hours were processed for immunofluorescence detection. (B) Cells were simultaneously labelled with anti-SNX1 (Alexa488, green) and anti-TGN46 (Alexa594, red), nuclei were visualized using DAPI. The SNX1-signal is virtually absent, indicating successful suppression (TGN46 and DAPI serve as visual reference). (C) Cells treated with SNX2-specific siRNA were labelled with anti-SNX2 (Alexa488). The signal is markedly reduced compared to control cells (D.), in which cells treated with control siRNA were labelled with anti-SNX2 (Alexa488) and imaged under exactly the same conditions. Scale bar is 10 μm.

Effects of SNX1 suppression on endosomal integrity

Importantly, when treating cells with the SNX1-specific siRNA, the integrity of the Golgi complex and endosomes appeared not to be grossly affected, as examined at the level of light microscopy: in these assays I labelled the Golgi compartments using the TGN-enriched protein TGN46 (**Figure 3. 7 B**) or the *medial*- and *cis*-Golgi resident protein giantin (data not shown for HeLa cells, but compare **Figure 3. 20** for HepG2 cells yielding analogous results). When labelling SNX1-suppressed cells with anti-TGN46, the fluorescence pattern (**Figure 3. 7 B**) was comparable to the fluorescence pattern observed in control cells (**Figure 3. 9**), but maybe slightly 'sprawled'. EM studies using SNX1-suppressed HepG2 cells later confirmed that at ultrastructural level, the TGN morphology was indeed not grossly affected by the treatment (Dr Muriel Mari, personal communication). Likewise, I found no obvious alteration in the localization of EEA1 (data not shown, but compare Carlton et al., 2004), and localization of the respective other SNX was unaffected, as was the membrane association of VPS26 in these cells (**Figure 3. 8**).

Membrane recruitment of retromer components

The observed preservation of the targeting indicates that the individual proteins can be independently recruited onto endosomal membranes. This is somewhat expected for SNXs as they possess PtdIns3*P*-binding PX domains, but neither VPS26 nor VPS29 or VPS35 possess obvious membrane-binding motifs. Further still, it has been found that recruitment of the VPS-components is wortmannin-sensitive, suggesting a PtdIns3*P*-sensitive 'linker' (Rojas et al., 2007). Nevertheless, when assessing the localization of VPS26 in cells jointly treated with SNX1 and SNX2 siRNAs, I did not observe a markedly altered localization, suggesting that VPS26 is recruited to endosomal membranes independently of SNX1 and SNX2. These data are thus indicative for existence of SNXs and VPS26 in two separate complexes, as has been suggested for the yeast retromer complex and, from co-immunoprecipitation analysis, for a mammalian retromer complex (Haft et al., 2000). These results are however at odds with other findings showing that joint suppression ablates VPS26 membrane recruitment (Rojas et al., 2007). At this stage, I do not know the reason for this discrepancy. One possible explanation might be the different suppression levels achieved. Indeed, I observed appreciably lower suppression levels for SNX2 compared to SNX1, especially for jointly suppressed cells (an issue further discussed in **para. 3.7** and Chapter 4). Hence, interpreted in this light, my data could imply that a minimal but critical level of SNX2 is necessary for VPS26 recruitment.

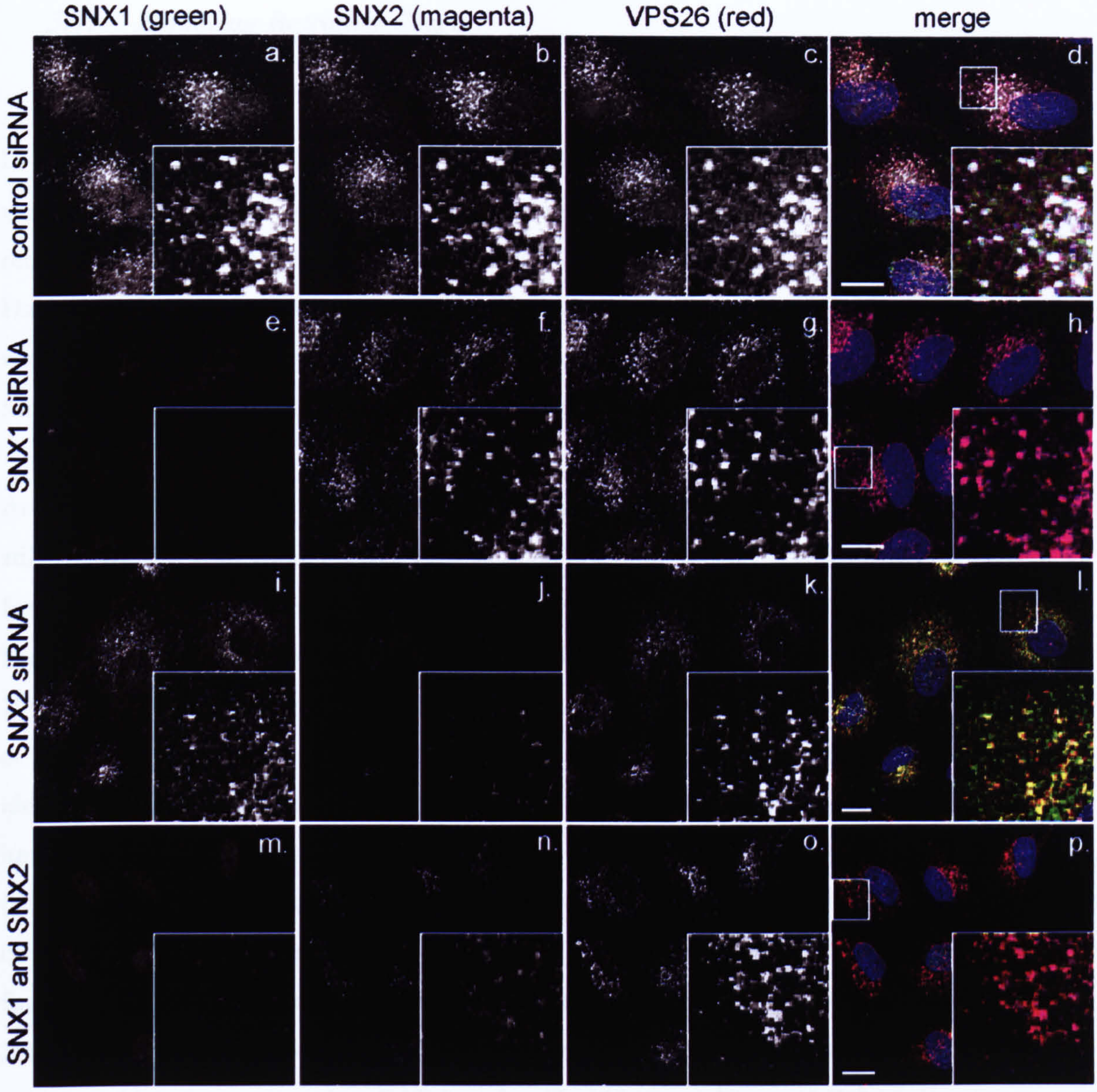

Figure 3. 8 Localization and targeting of retromer subunits following siRNA treatment

HeLa cells were treated for 72 hours with SNX1- and/or SNX2-specific siRNA (as indicated on the left). Cells were fixed and processed for IF analysis using anti-SNX1 (Alexa488, green), anti-SNX2 (Alexa647, magenta) and anti-VPS26 (Alexa568, red) antibodies. Scale bar is 20 μm.

3.7. Exploring Retromer Cargo

3.7.1. Introduction

In the preceding studies I established that SNX1 and other proposed orthologues of the yeast retromer complex co-localized on the same vesicular structures, and that individual retromer components were spatio-temporally 'coupled' on their intracellular itinerary. Having furthermore a tool to hand that allowed me to manipulate cellular SNX-levels without detectably perturbing endosomal sorting, it became pertinent to set out for a functional characterization of sorting nexins in retromer biology.

At the beginning of these PhD studies, a functional role for the mammalian retromer was still elusive. The yeast model served thus as reference point when exploring potential cargo for a mammalian retromer. In yeast, Ste13p/DPAP A (Matoba et al., 1997) - and Vps10p had been identified as 'retromer cargo' as they directly bind to Vps35p (Nothwehr et al., 1993; Marcusson et al., 1994; Cooper and Stevens, 1996; Nothwehr et al., 1999; Nothwehr et al., 2000). Possible homologues of Vps10p, a soluble hydrolase receptor, have been identified: this includes the multi-ligand receptor sortilin, which contains at its N-terminal luminal domain a stretch of amino acids that shows similarity to the yeast Vps10p domain (Westergaard et al., 2004; Ni et al., 2006). Sortilin, also identified as the non-G-protein coupled 100-kDa neurotensin (NT) receptor 3, has been associated with various cell functions ranging from cell migration, cell growth to cell death [for review see (Mazella, 2001)]. Sortilin has only been recently proposed to play a role in endosomal trafficking of sphingolipid activator proteins (SAPs) and acid sphingomyelinase (ASM) to lysosomes (Lefrancois et al., 2003; Hassan et al., 2004; Ni and Morales, 2006). Hence, like its yeast counterpart, sortilin also appears as a lysosomal hydrolase receptor; however the molecular machinery required for its intracellular transport was poorly defined at the beginning of these studies.

Much better documented is the role of the mannose 6-phosphate receptors (MPRs) as receptors for soluble lysosomal hydrolases in mammalian cells. Both, the cation dependent (CD-) and a cation–independent (CI-) MPR ligate their cargo *via* recognition of a mannose 6-phosphate (M6P) 'tag' added in the Golgi apparatus by the *N*-acetylglucosaminyl-1-phosphotransferase (Lang et al., 1984; Baranski et al., 1990; Baranski et al., 1991). In contrast to the mammalian system, vacuolar hydrolases of *S. cerevisiae* do

not appear to comprise M6P moieties, although a mannose 6-phosphate receptor-like protein (Mrp1p) has recently been identified (Whyte and Munro, 2001). Into these studies, the CI-MPR was indeed confirmed as retromer cargo by two independent studies (Arighi et al., 2004; Seaman, 2004). While both studies showed that suppressing VPS26 expression using an RNAi-based approach resulted in mis-localization of the receptor from the TGN to endosomes, one study additionally showed that VPS35 was capable of binding the CI-MPR (Arighi et al., 2004). A role for sorting nexins in this process had however been not addressed.

3.7.2. Studies into the role of SNX1 in retrograde CI-MPR transport

In line with previous studies, when examining the steady state distribution of the CI-MPR in HeLa cells at immunofluorescence level, the receptor is predominantly localized to the TGN (Waguri et al., 2003), as indicated by co-distribution with TGN46 (**Figure 3. 9**).

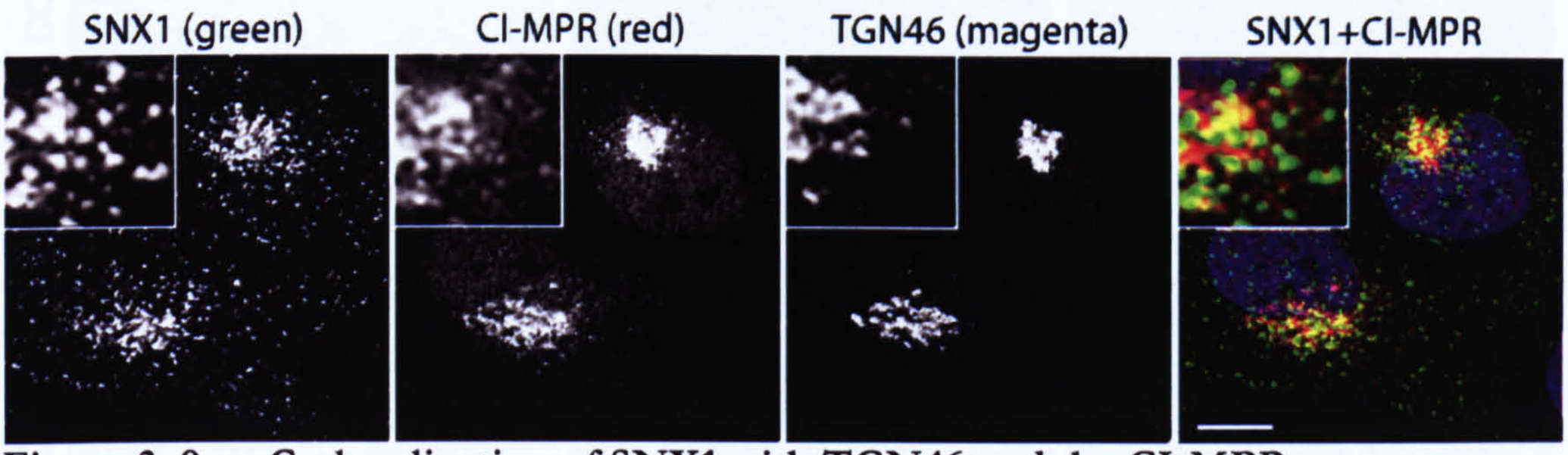

Figure 3. 9 Co-localization of SNX1 with TGN46 and the CI-MPR.
HeLa cells were processed for immunofluorescence labelling using anti-SNX1 (Alexa488, green), anti-CI-MPR (Alexa568, red) and anti-TGN46 (Alexa633, magenta) antibodies. Shown are maximum projections of 10 confocal z-sections at 500nm-separation each. The merged image shows an overlay of SNX1- and the CI-MPR-channel, while the 633-channel (TGN46) was omitted for clarity. The CI-MPR co-distributed with TGN46 and labelling of more peripheral vesicles was negligible Scale bar is 10 μm.

In contrast, in cells treated with SNX1-specific siRNA duplexes for 72 hours (fixed and immuno-labelled with anti-CI-MPR and anti-SNX1), the distribution of the CI-MPR is clearly altered (**Figure 3. 10**). In these cells, the receptor displayed a dispersed and punctate distribution, rather than TGN-like juxtanuclear enrichment. Importantly, this dispersal was unlikely due to disruption of the TGN itself, as I have previously shown that suppression of SNX1 did not grossly influence the appearance of this organelle (**Figure** 3. 7 **B**). Thus, given the precedent for VPS26, I reasoned that the CI-MPR-labelled structures could be of endosomal origin, indicating an endosome-to-TGN transport defect in the SNX1-suppressed cells. Indeed, when co-labelling SNX1-suppressed cells with EEA1, it was found that the CI-MPR on more peripheral structures co-localized partially with EEA1 (**Figure 3. 11**), demonstrating the endosomal nature of these punctae. Thus, the observed distribution was akin to the phenotype observed under VPS26-suppressed conditions (Arighi et al., 2004; Seaman, 2004).

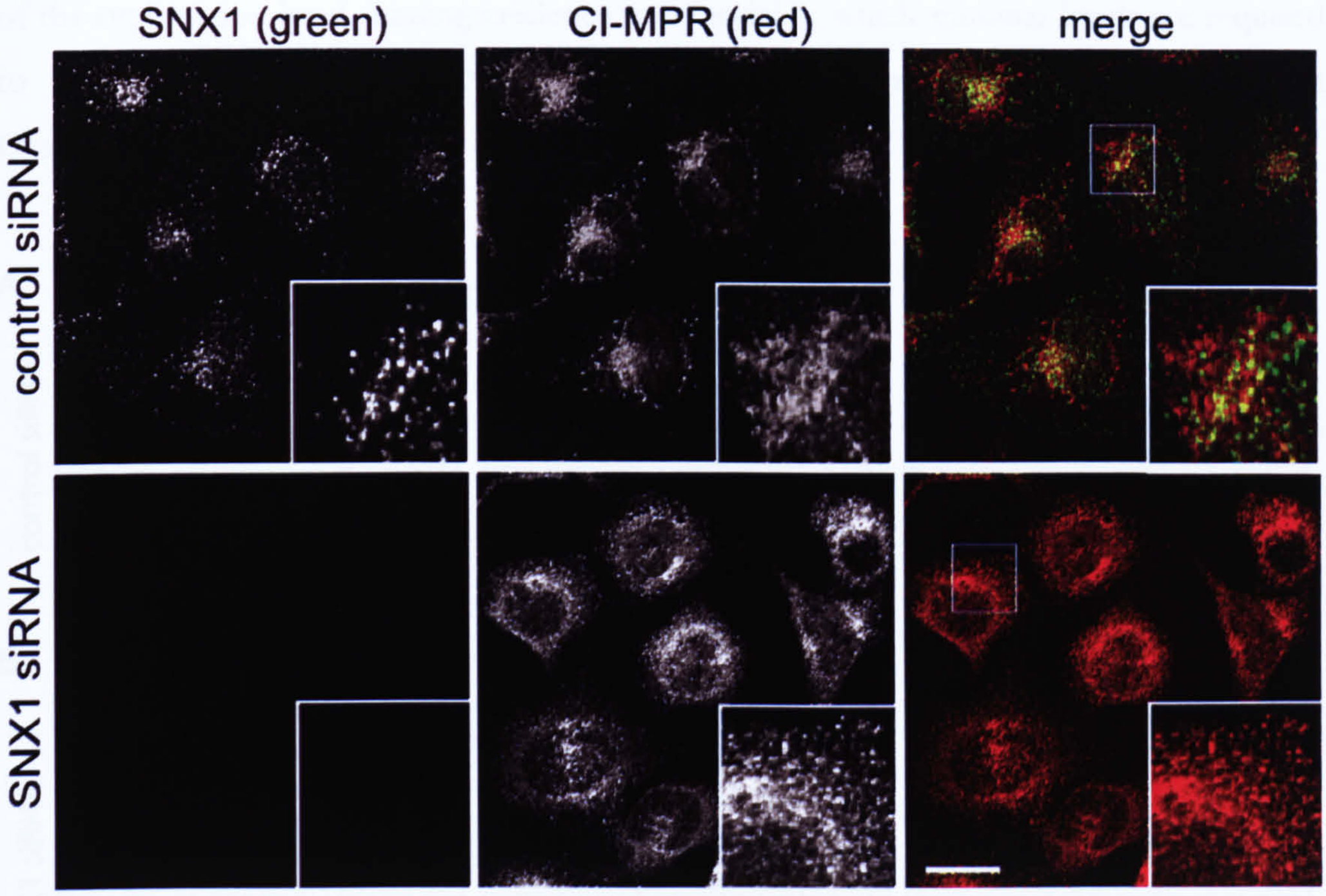

Figure 3. 10 Suppression of SNX1 leads to vesicular distribution of the CI-MPR. HeLa cells treated with control and SNX1-specific siRNA for 72 hours were processed for immunofluorescence labelling using anti-SNX1 (Cy2, green) and anti-CI-MPR (Cy3, red) antibodies. (A) In control cells, the CI-MPR shows predominantly a juxtanuclear concentration. (B) Upon SNX1-suppression, the distribution is shifted and CI-MPR appears punctate and dispersed. Scale bar is 10 μm.

Variations in the phenotype of CI-MPR redistribution

In spite of the clear phenotype in some cells, I noted that the degree of dispersal of CI-MPR was variable. In approximately 20% of all documented instances, suppression of SNX1 resulted in a strictly vesicular distribution as monitored by immunofluorescence labelling. It was then observed in virtually all cells that were clearly depleted of SNX1 (as judged by the absence of fluorescence signal). In other cases, simultaneously with a clear vesicular population, a partial TGN accumulation was observed. In rare cases, when inspecting populations of SNX1-suppressed cells, I observed 'islands' of cells having maintained unusually clear labelling for SNX1, indicating only minor or no suppression (**Figure 3. 12**). While these 'insular' cells showed the expected TGN-enrichment akin to control cells, a major population in these preparations also exhibited a TGN-enrichment in spite of a virtually absent SNX1 labelling. I thus propose that in these cells, SNX1 levels might not be suppressed to the highest level, but potentially below detection level of the antibodies. Hence, I suggest that the degree of dispersal directly correlates with the degree

of the suppression level, lending credence to a model in which minimal levels are required to maintain endosome-to-TGN transport, a concept that was further explored in Chapter 4.

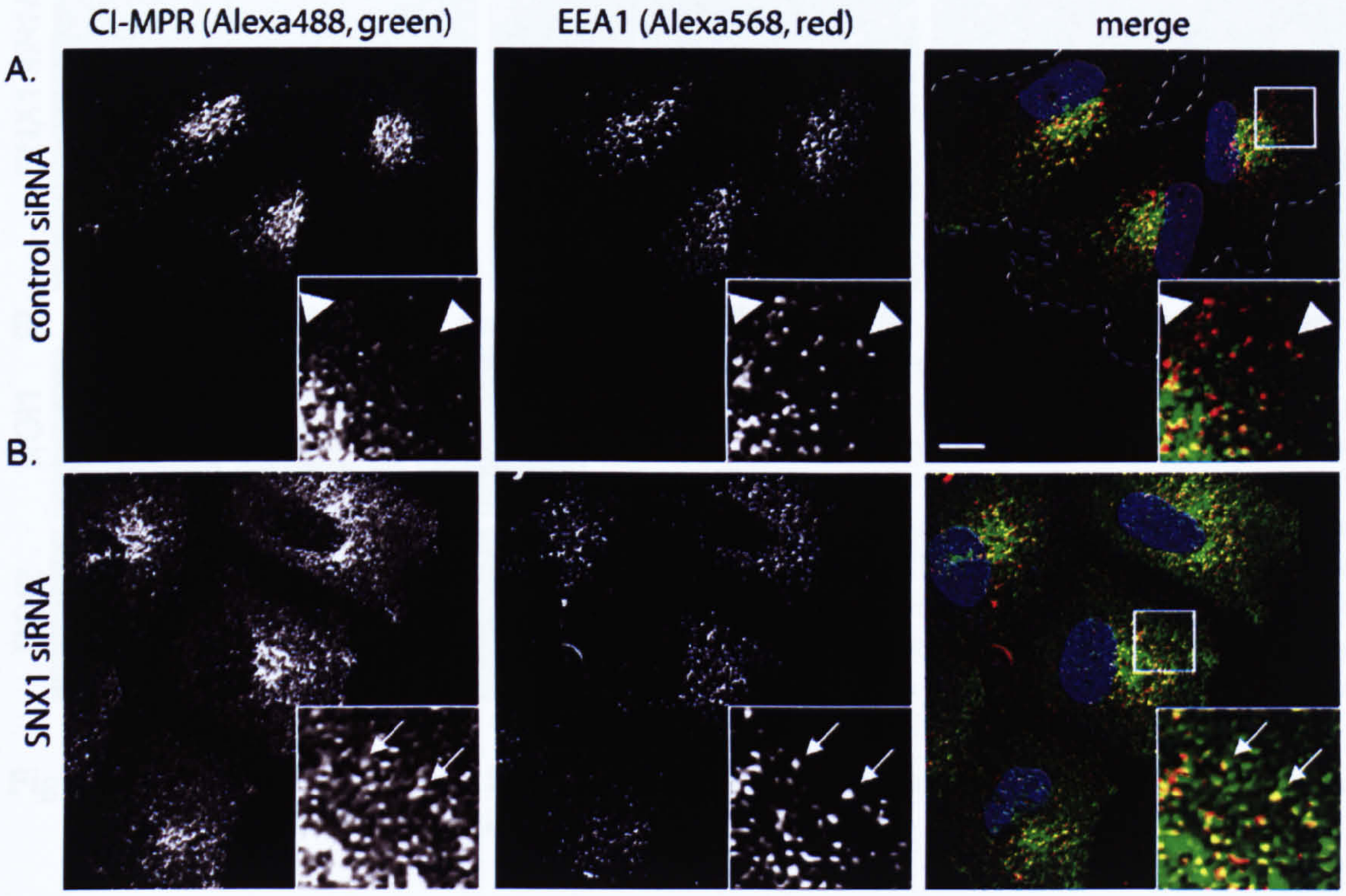

Figure 3. 11 SNX1 suppression results in endosomal redistribution of the CI-MPR.

HeLa cells treated with control and SNX1-specific siRNA for 72 hours were processed for immunofluorescence labelling using anti-CI-MPR (Alexa488, green) and anti-EEA1 (Alexa568, red) antibodies. In the merged image for control cells, the perimeter of a cluster of three contiguous cells is outlined. (A) In control cells, the CI-MPR shows predominantly a juxtanuclear concentration and more peripheral EEA1-positive vesicles are devoid of CI-MPR (arrowhead). (B) Upon SNX1-suppression, the distribution pattern of the CI-MPR is shifted toward dispersal throughout the cytoplasm, where the receptor localizes to EEA1-positive vesicles (arrows). Scale bar is 10 μm.

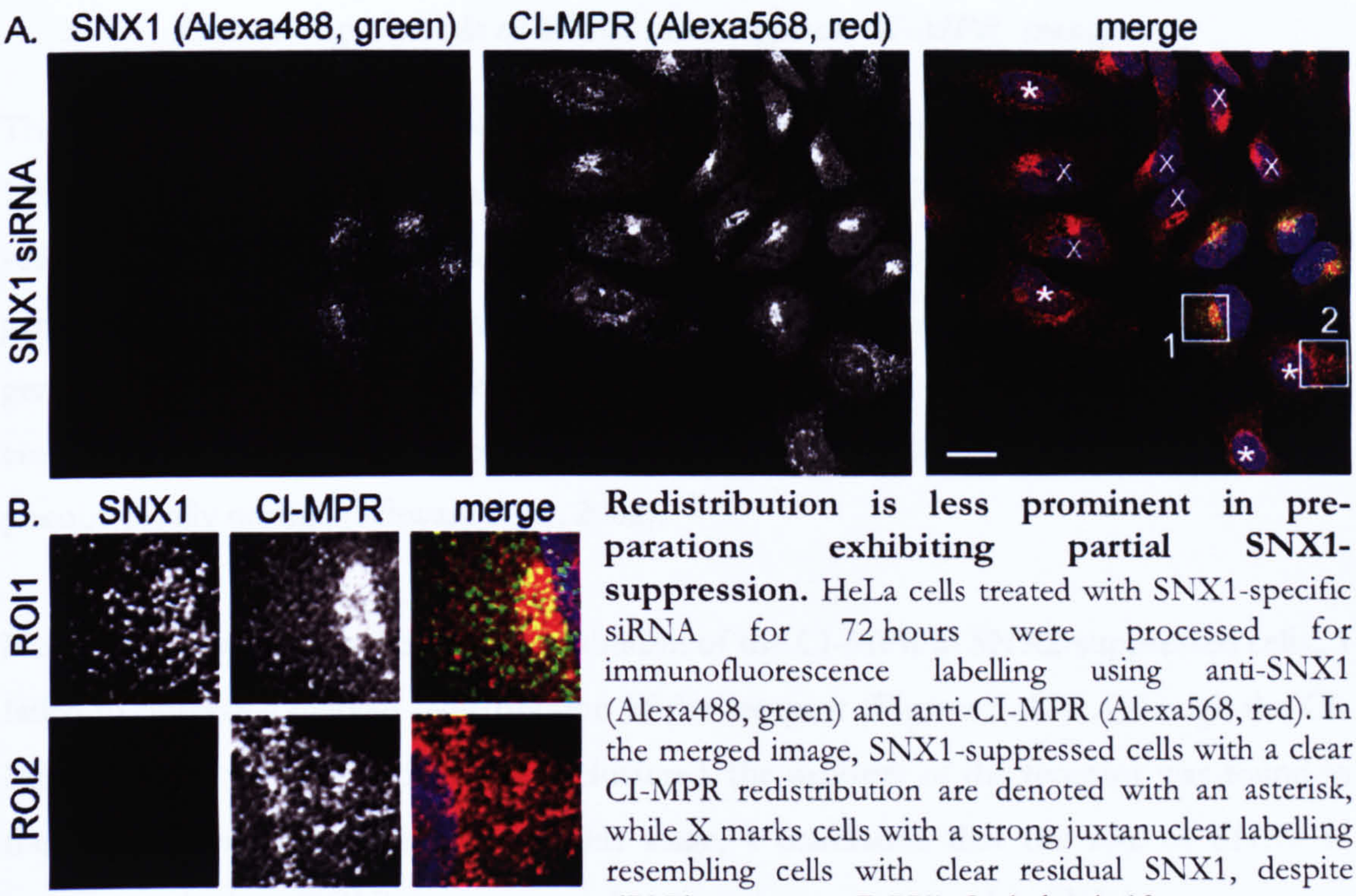

Redistribution is less prominent in preparations exhibiting partial SNX1-suppression. HeLa cells treated with SNX1-specific siRNA for 72 hours were processed for immunofluorescence labelling using anti-SNX1 (Alexa488, green) and anti-CI-MPR (Alexa568, red). In the merged image, SNX1-suppressed cells with a clear CI-MPR redistribution are denoted with an asterisk, while X marks cells with a strong juxtanuclear labelling resembling cells with clear residual SNX1, despite siRNA treatment (ROI1). Scale bar is 10 μm.

Figure 3. 12 Redistribution is less prominent in preparations exhibiting partial SNX1-suppression

3.7.3. Examining the role of SNX2 in retrograde CI-MPR transport

The finding that SNX1 and SNX2 have the capacity to hetero-oligomerize ((Haft et al., 1998) gave rise to a working model in which SNX2 might fulfil the role of Vps17p (the yeast component with no obvious homologue in higher eukaryotic cells). Further to this, a genetic precedent suggested that SNX1 and SNX2 might be functionally redundant: as gene knock-out studies in mice found that joint ($SNX1^{-/-}$; $SNX2^{-/-}$) gene deletion was embryonically lethal, while mice with single $SNX1^{-/-}$ or $SNX2^{-/-}$ gene knock out were phenotypically normal (Schwarz et al., 2002).

Nevertheless, when I analysed the distribution of the CI-MPR in SNX2-suppressed cells,, I failed to observe a marked redistribution of the receptor (**Figure 3. 13**). Although the CI-MPR appeared to be slightly less well clustered, the majority of the receptor was found in the juxtanuclear area. Therefore, at this stage, I concluded that the role of SNX2 in promoting the 'pro-TGN' transport was less prominent, compared to SNX1.

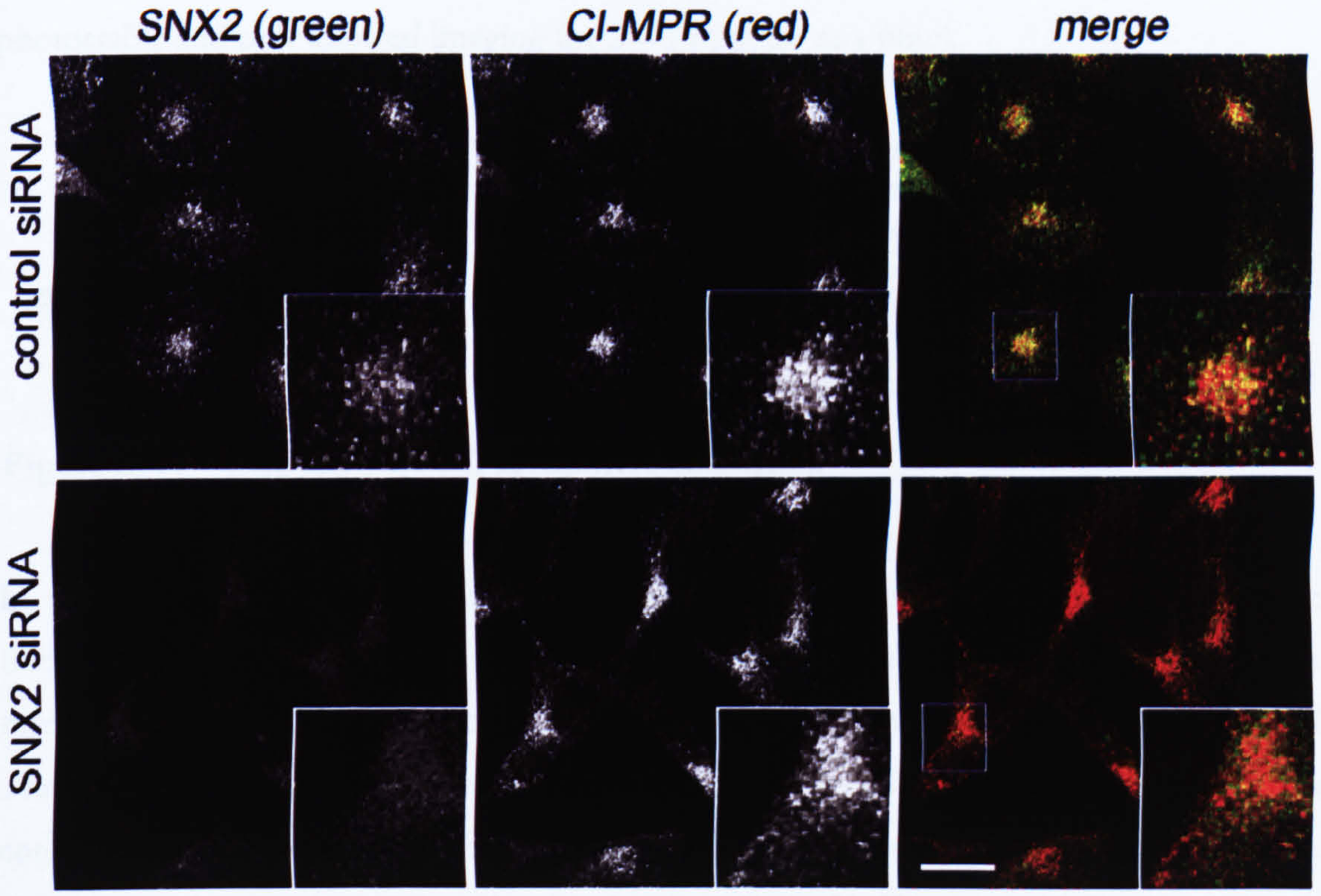

Figure 3. 13 SNX2 suppression does not markedly alter steady-state distribution of the CI-MPR.

HeLa cells treated with control and SNX2-specific siRNA for 72 hours were processed for immunofluorescence labelling using anti-SNX2 (Cy2, green) and anti-CI-MPR (Cy3, red) antibodies. (A) In control cells, the CI-MPR shows predominantly a juxtanuclear concentration. (B) Upon SNX2-suppression, the distribution of the CI-MPR is not markedly altered. Scale bar is 20 μm.

3.7.4. Kinetic Analysis of CI-MPR transport in cells suppressed for SNX1 and SNX2

The observation that in SNX1-suppressed conditions, the CI-MPR was redistributed to endosomal structures suggested that endosome-to-TGN transport step was blocked. To thus analyse the role of SNX1 in cargo flux, I chose an approach combining live cell studies and pulse-chase analyses: in absence of an experimentally suited ligand for the CI-MPR, I made use of a CD8-CI-MPR reporter construct stably expressed in a HeLaM cell line that has previously been shown to exhibit similar trafficking properties to the endogenous receptor [(Seaman, 2004); see also **Figure 3. 14**] [5].

The CD8-CI-MPR chimeric receptor consists of the cytoplasmic, trafficking signal-containing tail of the CI-MPR fused to the N-terminal domain of CD8, which makes it possible to use anti-CD8 antibodies to label cell-surface localized CD8-CI-MPR and track the receptor intracellularly. The availability of a fluorescently-labelled anti-CD8 (R-phycoerythrin-CD8; RPE-CD8) made it furthermore possible to visualize the transport of CD8-CI-MPR in living cells (although it is to be said that the fluorophore is not very photostable and only allowed imaging for 2 – 3 minutes at a time).

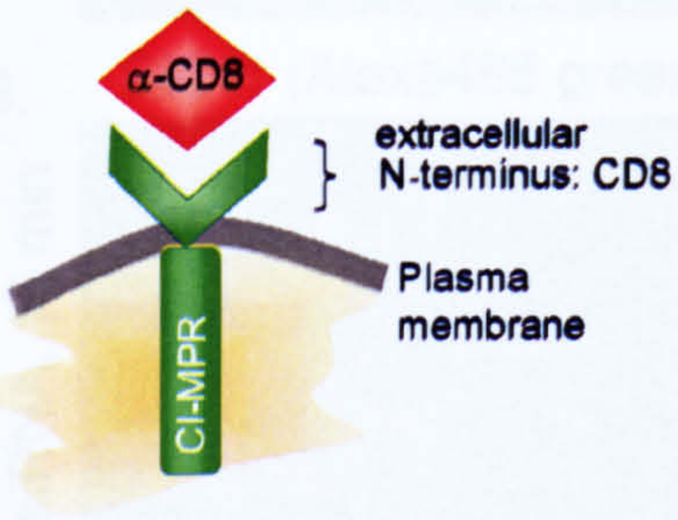

The CD8-CI-MPR reporter construct.
HeLaM cells were stably transfected with a CD8-CI-MPR chimera consisting of the cytoplasmic tail of the CI-MPR fused to the N-terminal domain of CD8. As CD8 is not expressed in HeLa cells, an anti-CD8 antibody can be used to selectively label CD8-CI-MPR at the cell surface and follow its transport inside the cell.

Figure 3. 14 The CD8-CI-MPR reporter construct.

In an initial analysis, antibody-uptake experiments were performed in which cells were fixed at different time points after internalization to analyse the kinetics of plasma membrane-to-TGN transport of the CD8-CI-MPR (see **para. 3.2.5** for experimental details). These assays compared transport in control and SNX1-suppressed cells; in controls, most of the antibody had reached the perinuclear area after 15 minutes (**Figure 3. 15 A**). At this time point, it co-localized well with SNX1 (**Figure 3. 15 B**), showing that the construct was delivered to SNX1-positive endosomes. After 25 minutes, virtually all anti-CD8 was clustered juxtanuclearly. In contrast, in SNX1-suppressed cells, the antibody was markedly less enriched in the perinuclear area (**Figure** 3. 15 **A**), providing a first

[5] developed and kindly provided by Dr Matthew Seaman

evidence that SNX1 was indeed involved in the endosome-to-TGN transport step of the cargo.

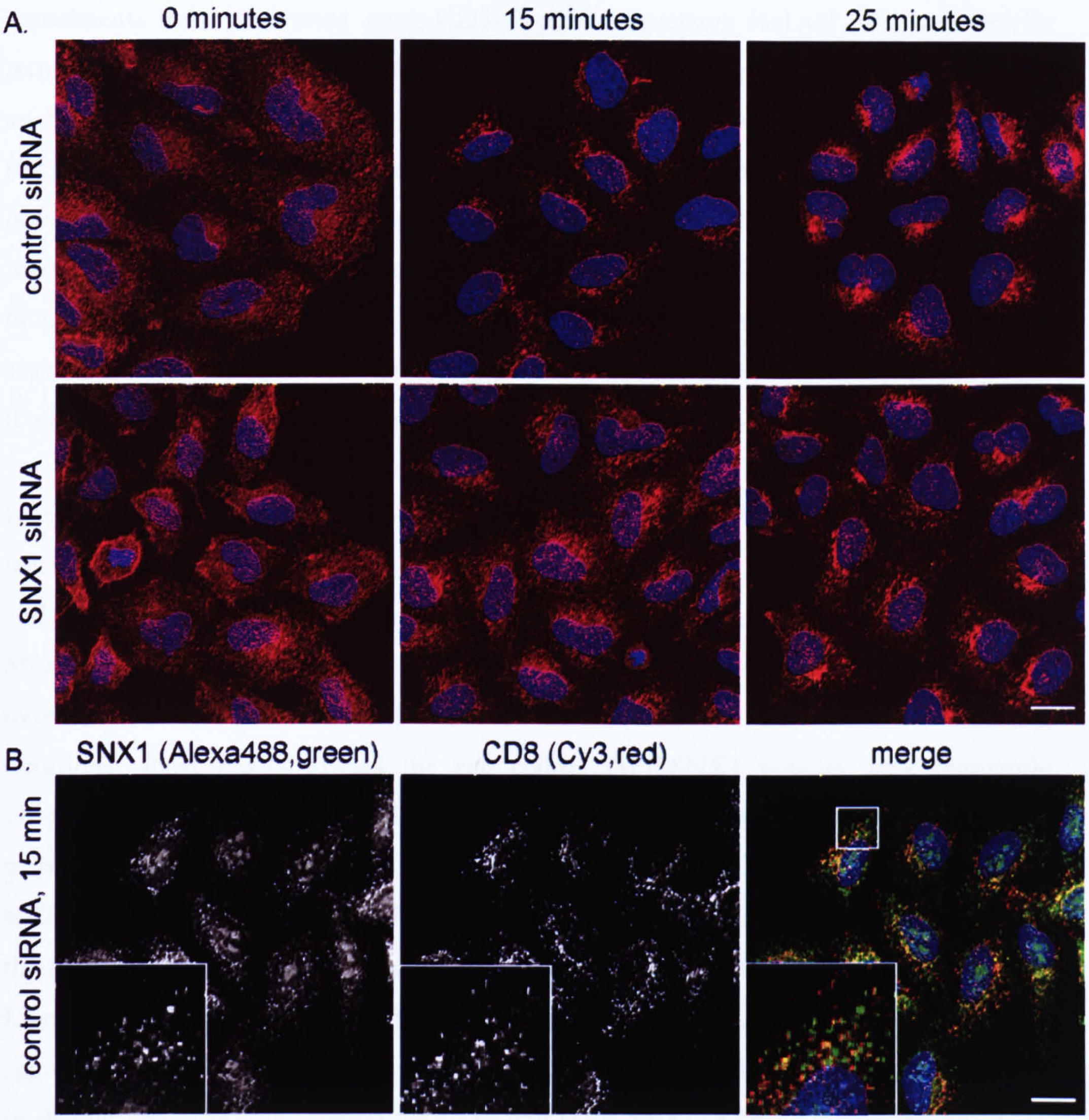

Figure 3. 15 Kinetic analysis of CD8-CI-MPR transport in SNX1-suppressed cells. HeLaM cells stably expressing a CD8-CI-MPR chimera were treated with control or SNX1-specific siRNA. After 72 hours, cells were surface-labelled with anti-CD8 at 4°C. Cells were either fixed directly to assess surface-labelling (0 minutes), or after 15 and 25 minutes respectively. While in control cells most of the CD8-CI-MPR had reached the perinuclear area within 15 minutes of internalization (A, control siRNA), in SNX1-suppressed cells, much of the receptor was still found on more peripheral vesicular structures (A, SNX1 siRNA). (B) The perinuclear receptor partially co-localizes with SNX1 after 15 minutes uptake. Scale bar is 20 μm.

Next, I sought to extend these studies examining whether the receptor traffics through, or is transported within SNX1-positive endosomes. I thus attempted to investigate the dynamics of this process employing a live cell imaging approach. Antibody uptake-experiments were performed using CD8-CI-MPR expressing HeLaM cells, additionally transiently transfected with GFP-SNX1. Cell-surface localized receptor was labelled using an R-phycoerythrin-coupled anti-CD8 antibody. Cells were then transferred to a heated stage and warmed for 10 minutes observing the process by epifluorescence microscopy before image capturing was started (**Movies 3.3.1 – 3.3.6**; **Figure 3.** 16). This way, reassociation of GFP-SNX1 was controlled (see **para. 3.4**) but it also allowed to select the time point when co-localization with the SNX1-labelled structures was maximal. As expected from the fixed cell analysis, after 10 minutes, CD8-positive structures were found to either co-localize or to be in conjunction with GFP-SNX1-decorates structures.

In these assays (n = 3), I frequently observed 'entry' of RPE-CD8 into GFP-SNX1-labelled structures of either tubular (**Figure 3. 16**) or more vesicular nature (**Figure 3. 17**), and movement of the two markers was often conjoined. I commonly observed GFP-SNX1 being located to, or moving to, the cell perimeter co-localizing with cargo. But overall, motion was multi-directional, with GFP-SNX1/RPE-CD8 structures showing occasional short bursts toward the cell centre. GFP-SNX1 vesicles were frequently observed to 'fuse' with other GFP-SNX1 decorated structures or come at least into close proximity. I also observed RPE-CD8 to exit a larger GFF-SNX1-labelled vesicle, and to traffic juxtanuclearly (**Figure 3. 17**). It was however not possible to unequivocally clarify at the level of light microscopy whether this vesicle was completely devoid of GFP-SNX1. Likewise, the fluorescent cargo often appeared as rather large punctae, maybe representing aggregates. Again, for the discussed difficulties (**para. 3.3**), these observations retain a qualitative character, but importantly show that GFP-SNX1/RPE-CD8 vesicles, like RFP-SNX1/GFP-VPS35 (**para. 3.4**) traffic conjointly with a bias toward the perinuclear area.

Taken together, the live cell analysis thus confirms and extends the fixed cell analysis, showing that RPE-CD8 is delivered to SNX1-positive structures. This data also shows that motile GFP-SNX1 vesicles move to the cell periphery, where they presumably take up RPE-CD8/CD8-CI-MPR. As the CI-MPR is believed to be internalised via clathrin-mediated endocytosis (Pearse and Robinson, 1990; Kornfeld, 1992), it is conceivable that

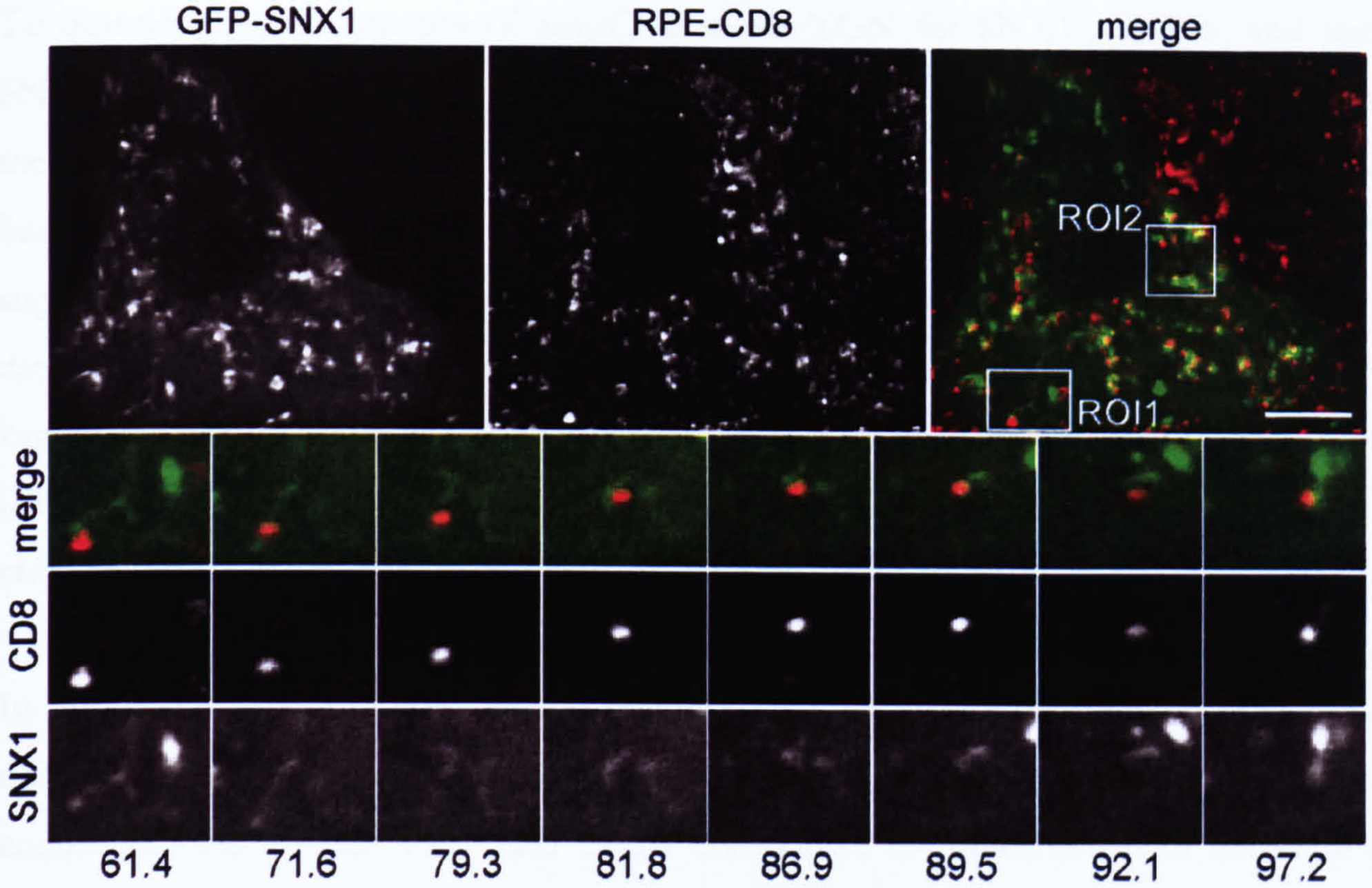

Figure 3. 16 CD8-uptake in live cells (ROI1).
HeLaM cells stably expressing the CD8-CI-MPR were transiently transfected with GFP-SNX1 (green) and surface-labelled with an R-phycoerythrin-coupled anti-CD8 antibody (RPE-CD8, red). Cells were transferred to a heated stage for 10 minutes before uptake of the antibody in one confocal section was imaged live (**Movies 3.2.1 – 3.2.6**). Stills of these movies are shown, time is in seconds. CD8-labelled structures co-localized with GFP-SNX1-positive compartments. A series of frames (ROI1) is shown, where a CD8-labelled structure appears to move 'at the tip' of a retracting SNX1-positive tubule, but not within the tubules. For ROI2 refer to **Figure 3. 17**. Scale bar is 10 μm.

---

the SNX1-postive endosomes receive cargo directly from CCVs in close proximity to the plasma membrane.

In contrast to the results for SNX1 suppression, when I investigated the effect of SNX2-suppression on the plasma membrane-to-TGN transport of the RPE-coupled anti-CD8 antibody, I found the RPE-CD8 to accumulate in the juxtanuclear area with only slightly slower kinetics compared to control cells (**Figure 3. 19**). In these SNX2-suppressed cells, after 25 minutes, most of the antibody had reached the juxtanuclear area, where it displayed a somewhat 'sprawled' distribution compared to the fairly tight accumulation in control cells, but was not found as clearly redistributed as the receptor in SNX1-suppressed cell – again showing that the effects of SNX2 suppression are less pronounced.

To quantify this, the amount of anti-CD8 at the TGN for SNX1-, SNX2-, and jointly SNX1- and SNX2-suppressed cells - judged by its co-localization with TGN46 - was measured (**Figure 3. 19**) and confirmed the qualitative analysis: markedly less anti-CD8 had reached the TGN after 24 minutes in SNX1-suppressed cells, while in SNX2-suppressed cells, co-localization was only slightly reduced compared to control cells. These data also show that jointly SNX1- and SNX2-suppressed cells 'behave' like SNX1-suppressed cells in that the joint suppression leads to reduced co-localization with TGN46 (**Figure 3. 19**) and a comparable vesicular dispersal of the CD8-CI-MPR (as well as of endogenous CI-MPR; data not shown).

In conclusion, the LCI and kinetic analyses thus furthered the previous steady-state observation in the way that they illustrate the flux of cargo through the SNX1-positive endosomes and, overall, these data clearly consolidate the involvement of SNX1 in the endosome-to-TGN transport step.

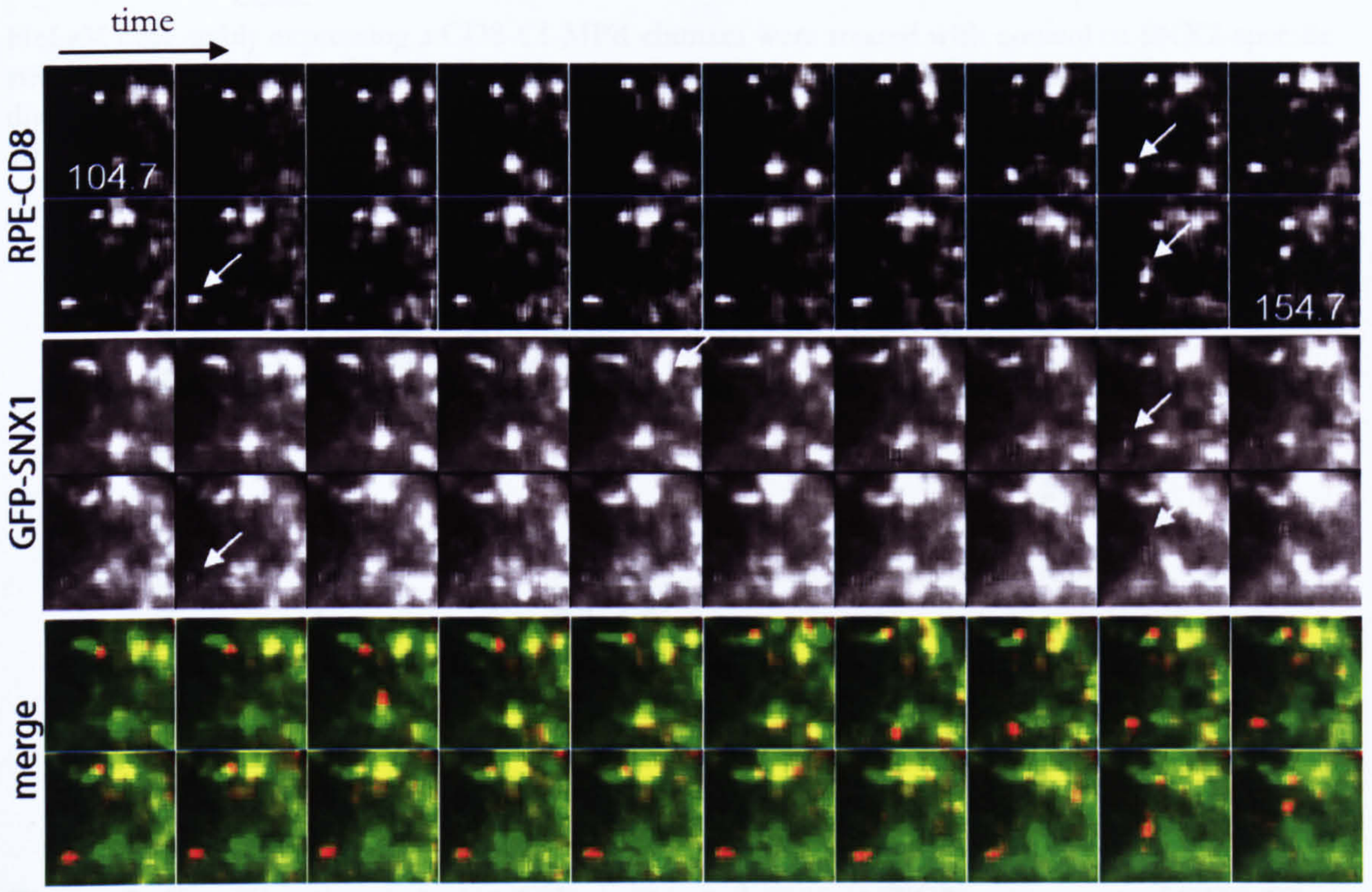

Figure 3. 17 CD8-uptake in live cells (ROI2).
HeLaM-CD8-CI-MPR cells transiently transfected with GFP-SNX1 (green) and surface-labelled with RPE-coupled anti-CD8 (RPE-CD8, red). Cells were transferred to a heated stage for 10 min before uptake of RPE-CD8 as imaged live (**Movies 3.2.1 – 3.2.6**). Stills of these movies are shown, time is in seconds for the first and last frame, and interval between images is 2.5 seconds. CD8-labelled structures are delivered to a GFP-SNX1-positive vesicle, which they subsequently appear to leave (arrows). (For scaling compare Figure 3.16)

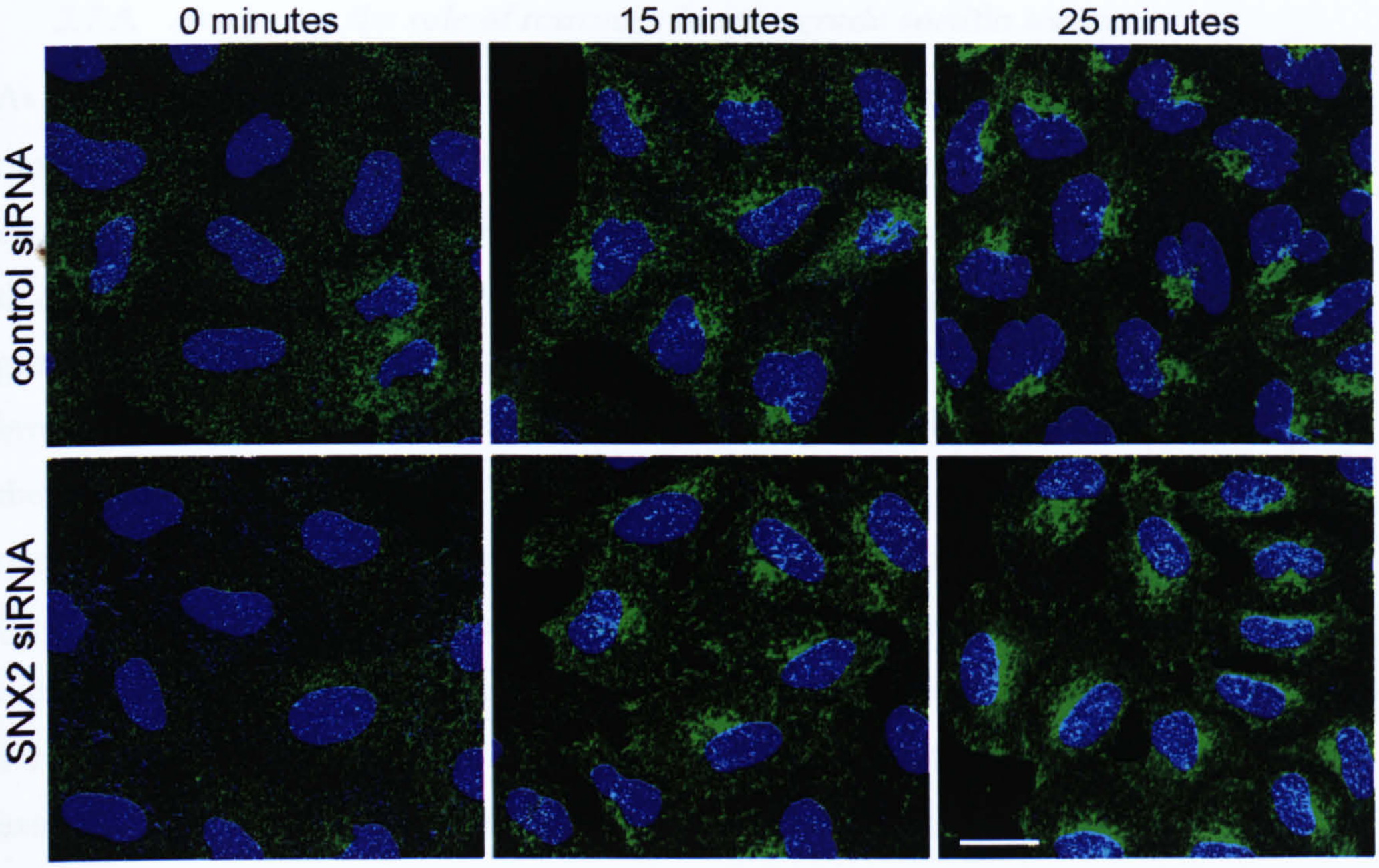

Figure 3. 18 Kinetic analysis of CD8-CI-MPR transport in SNX2-suppressed cells.

HeLaM cells stably expressing a CD8-CI-MPR chimera were treated with control or SNX2-specific siRNA. After 72 hours, cells were surface-labelled with anti-CD8 at 4°C. Cells were either fixed directly to assess surface-labelling (0 minutes), or after 15 and 25 minutes respectively. Scale bar is 20 μm.

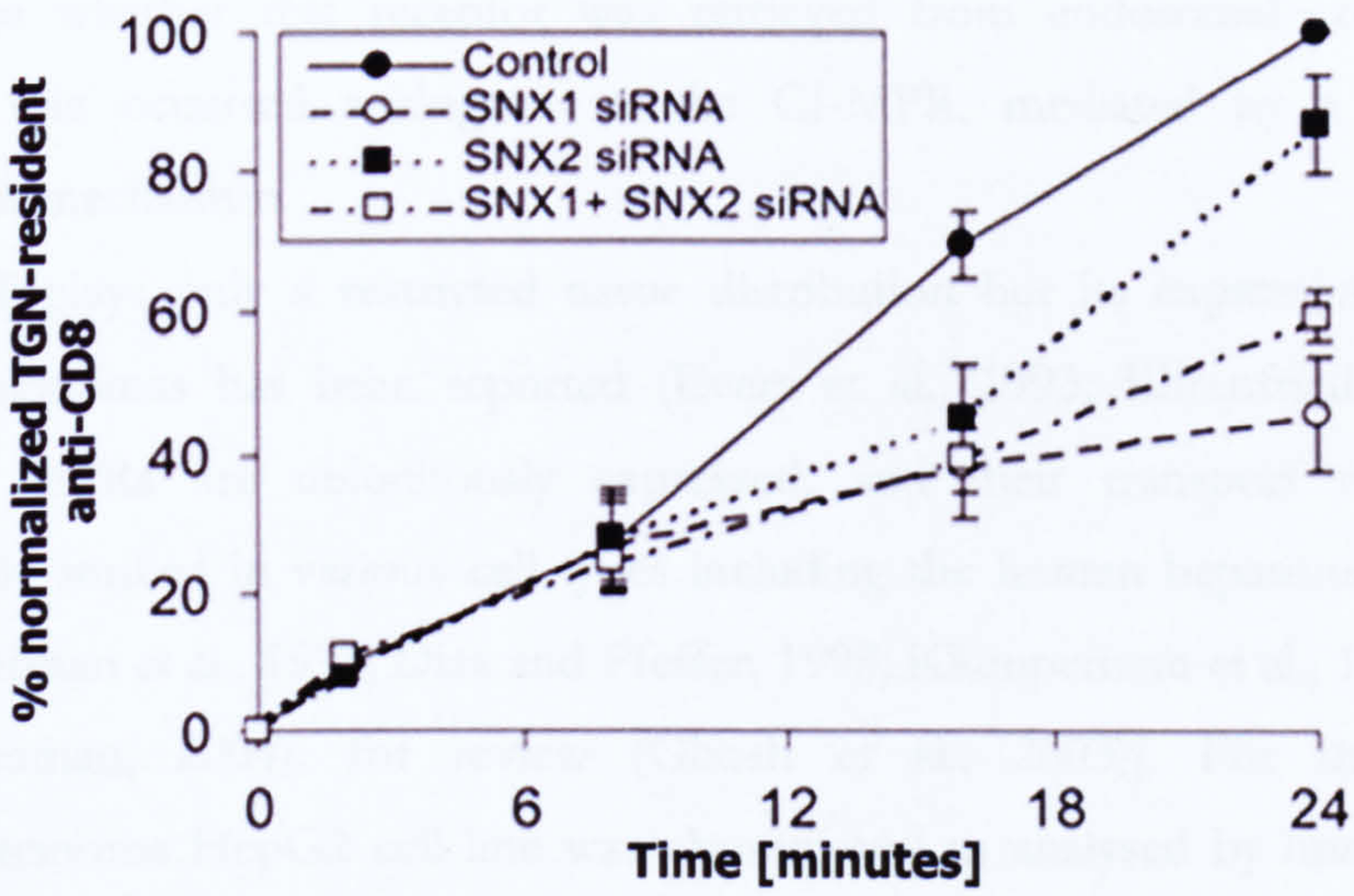

Figure 3. 19 Kinetic analysis of plasma membrane-to-TGN transport of CD8-CI-MPR.

HeLaM cells stably expressing CD8-CI-MPR were treated with the indicated siRNA for 72 hours. Cells were surface-labelled with anti-CD8, and either fixed directly, or after 2, 8, 16 or 24 minutes internalization. The amount of TGN-resident anti-CD8 was determined by labelling cells with anti-TGN46, and quantifying confocal images using LCSLite (Leica). Results are expressed ± the s.e.m. from three independent experiments (except the 2 minute time point, which is from two independent experiments; data courtesy of J. Carlton)

3.7.5. Analysing the role of retromer in retrograde sortilin transport

As discussed, the CI-MPR is structurally unrelated to Vps10p. Given that a role for M6P modifications in yeast hydrolases is still elusive, this suggests that mammalian retromer has evolved to a point where it interacts with cargo that differs from its yeast counterpart but that has analogous function and an analogous transport itinerary. But the mammalian genome does indeed contain homologous proteins of Vps10p. It was thus intriguing to investigate whether SNX1 was involved in a more general 'retrieval scheme' or whether the observed effect was CI-MPR-specific. As explained in **para. 3.7.1**, the function of mammalian sortilin as lysosomal hydrolase receptor had been recently discovered (Lefrancois et al., 2003; Hassan et al., 2004; Ni and Morales, 2006). Until now, the intracellular compartments harbouring sortilin and thus, its intracellular transport and sorting have not been described in detail. It is not yet clear on which itinerary the receptor exits the TGN to reach endosomal compartments, and it is not clear whether this receptor is a recycling receptor like the CI-MPR. Indication that it might be targeted to the same exit sites at the TGN comes from the finding that like the CI-MPR, sortilin contains binding motifs for clathrin-coat components (Nielsen et al., 2001; Takatsu et al., 2001). Interestingly, there is also indication that both receptors may share the same cargo (Ni and Morales, 2006), which might imply that they act on similar itineraries. I thus sought to investigate whether this receptor was retrieved from endosomal compartments, and whether this occurred analogous to the CI-MPR, mediated by a retromer/SNX1-dependent mechanism.

Sortilin displays only a restricted tissue distribution but its expression in fibrolamellar hepatocarcinomas has been reported (Evers et al., 1993; Ehrenfried et al., 1994). In contrast, MPRs are ubiquitously expressed, and their transport routes have been extensively studied in various cell types including the human hepatoma cell line HepG2 [(Klumperman et al., 1993; Diaz and Pfeffer, 1998; Klumperman et al., 1998; Waguri et al., 2003; Seaman, 2004); for review (Ghosh et al., 2003)]. For these reasons, the hepatocarcinoma HepG2 cell line was chosen, and as analysed by immuno-detection of whole-cell lysates using an anti-sortilin antibodies, it was revealed that this cell line indeed expresses high levels of the protein (**Figure 3. 22 A**). In immunofluorescence-based assays, I found sortilin to be localized to the juxtanuclear area in HepG2 cells, with noticeable, but comparatively little localization to endosomal structures (**Figure 3. 20 A**). Co-localization with SNX1 was almost exclusively restricted to vesicles in the perinulear area.

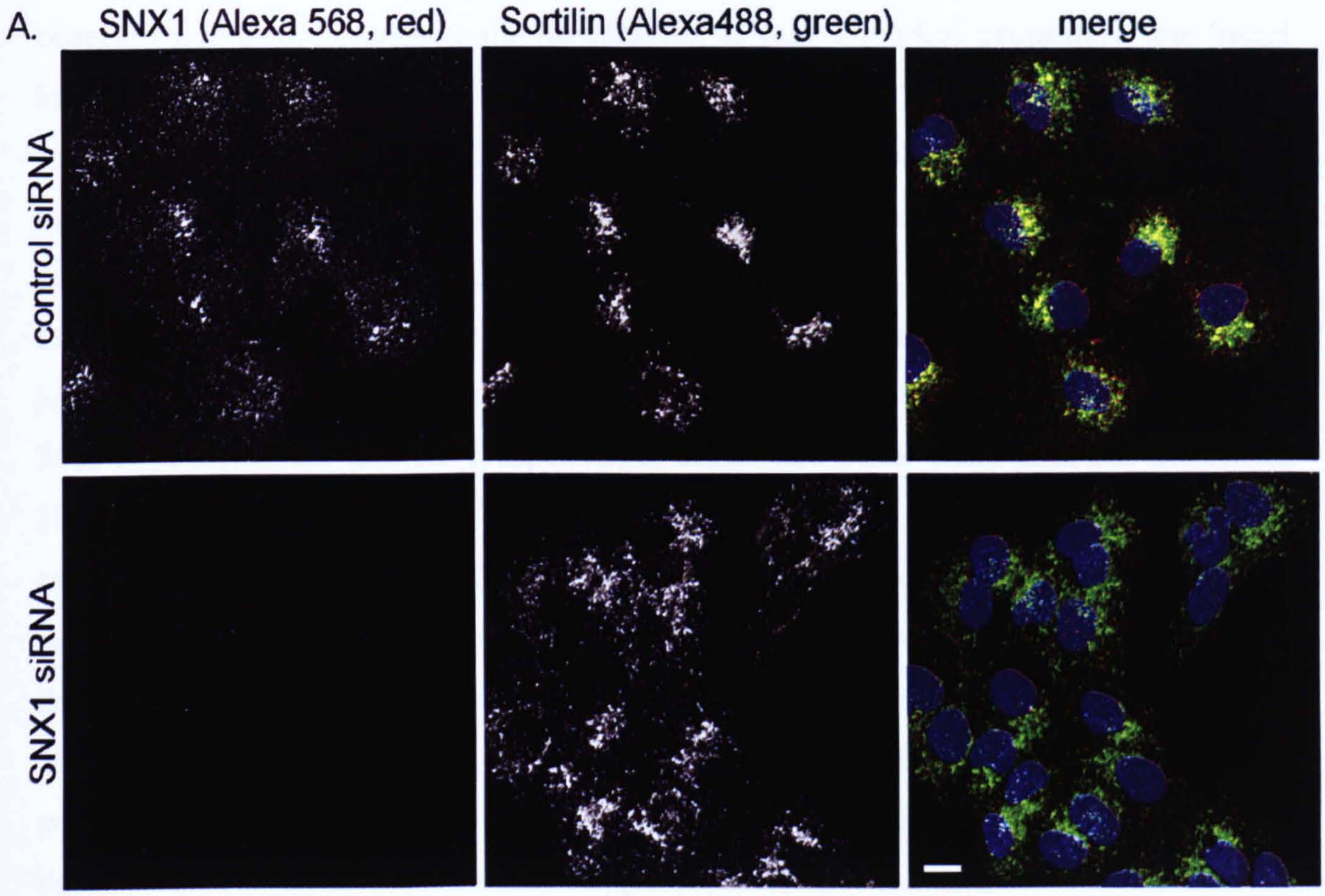

Analysis of sortilin distribution in control and SNX1-suppressed cells.

(A) HepG2 cells were treated with either control or SNX1-specific siRNA for 72 hours, fixed and processed for immunofluorescence analysis using anti-SNX1 (Alexa568, red) and anti-sortilin (Alexa488, green) antibodies. Nuclei (DNA) were visualized using DAPI (blue). Maximum projections of 10 – 12 z-sections are shown. In control cells, sortilin shows a relatively tight perinuclear distribution, while in SNX1-suppressed cells, the accumulation appears less concentrated, with a substantial amount still on vesicular, more peripheral vesicles. Note that in SNX1-suppressed cells, the contrast in the sortilin-displaying images was enhanced by ~ 20% compared to the respective control images, as the signal was dramatically reduced upon SNX1 suppression (see text). Scale bar is 20 μm.

(B) HepG2 cells from the same treatment conditions as in (A) were fixed and labelled with anti-giantin antibodies (Alexa568, red) to label the *medial-* and *cis*-Golgi complex. Nuclei were visualized using DAPI (blue). In SNX1-suppressed cells, the Golgi structures appear sometimes 'dilated' but not fragmented. Scale bar is 60 μm.

Figure 3. 20 Analysis of sortilin distribution in control and SNX1-suppressed HepG2 cells.

In contrast, when I examined the distribution of sortilin in SNX1-suppressed cells, I observed a dramatic change in the distribution, as now a marked proportion was found localized to vesicular structures (**Figure 3. 20 B**). It is to note that in the presented images for sortilin (in SNX1-suppressed cells), the contrast in was enhanced by ~20% compared to the level in controls, as the sortilin/Alexa488 fluorescence signal was markedly decreased in SNX1-suppressed cells (see also **para. 3.7.6**).

Like in HeLa cells, SNX1 suppression did not appear to affect Golgi morphology as judged by labelling SNX1-suppressed and control siRNA-treated cells for giantin (**Figure 3. 20 B**), a membrane-inserted component of the *cis*- and *medial*-Golgi (Linstedt and Hauri, 1993), or as detected using anti-TGN46 antibodies (**Figure 3. 21**). When I simultaneously assessed the distribution of the CI-MPR and sortilin in SNX1-suppressed cells, I found that both receptors were co-redistributed, indicating that both receptors failed to be delivered from an endosomal compartment to the TGN, as labelled by TGN46 (**Figure 3. 21**). Notably, redistribution was less prominent compared to HeLa cells, which correlated with the finding that in control cells at steady state, the sortilin distribution appeared less tight; hence, overall, 'visually' the effect appeared less dramatic.

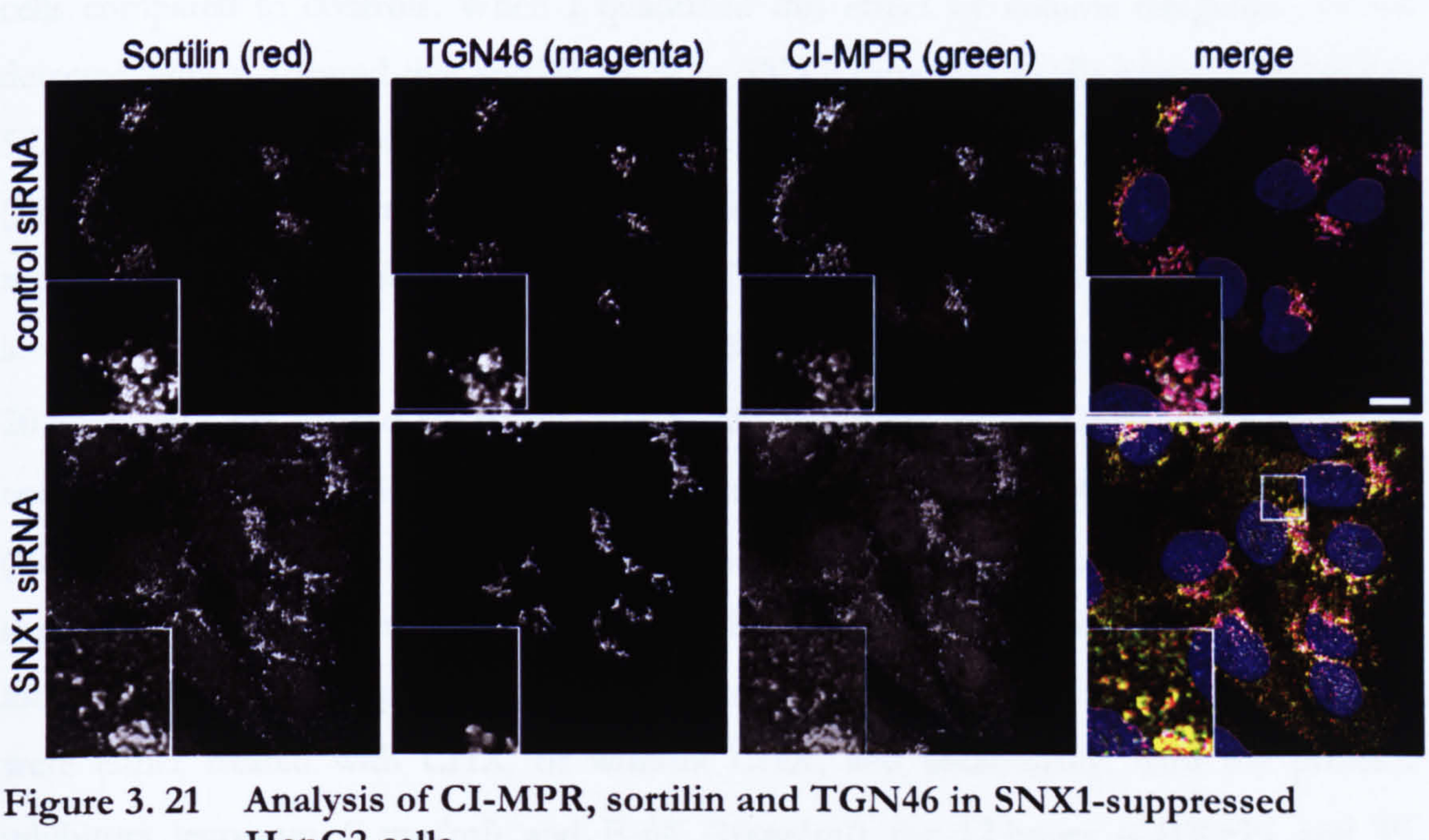

Figure 3. 21 Analysis of CI-MPR, sortilin and TGN46 in SNX1-suppressed HepG2 cells

HepG2 cells were treated with either control or SNX1-specific siRNA for 72 hours, fixed and processed for immunofluorescence analysis using anti-sortilin (Alexa568, red), anti-TGN46 (Alexa633, magenta), and anti-CI-MPR (Alexa488, green) antibodies. Nuclei were visualized using DAPI (blue). Maximum projections of 10 – 12 z-sections are shown. CI-MPR and sortilin show increased vesicular distribution in SNX1-suppressed cells while TGN46-fluorescence pattern appears unaltered compared to control cells. Scale bar is 10 μm.

3.7.6. Studies into the stability of sortilin in SNX1-suppressed cells

Having noticed that the immunofluorescence signal for sortilin was dramatically reduced upon SNX1 suppression, I wished to determine the 'fate' of the receptor under conditions of SNX1 depletion in more detail.

Given the precedent that in yeast cells lacking Vps5p (vps5Δ mutants), Vps10p is mis-localized to the vacuole, and that upon suppression of mammalian VPS26, internalised CI-MPR was shown to be diverted to the lysosome (Arighi et al., 2004), I reasoned that sortilin 'trapped' in endosomal vacuoles might become subject to lysosomal degradation. Indeed, the observed reduction of signal for sortilin upon immunofluorescence analysis of SNX1-suppressed cells was indicative for a possible degradation of the receptor; I thus sought to quantitatively analyse the stability of sortilin and investigate the involvement of lysosomal degradation using biochemical assays.

First, I analysed the steady-state levels of sortilin in whole-cell lysates cells by immuno-detection, and found that the receptor levels were markedly reduced in SNX1-suppressed cells compared to controls. When I quantified this effect by volume integration of the detected signals, I found that sortilin levels in SNX1-suppressed cells where decreased to 50.6% ± 10.07% (standard deviation, s.d., for n = 4 assays) of the control (**Figure 3. 22 A**). To further determine the proportion of *de novo* synthesized sortilin in the remaining fraction, a series of cycloheximide (CHX) treatment assays were performed, and levels of sortilin were re-assessed. Here, cells were treated twice with siRNAs, and 20 hours into the second treatment, 40 µg/ml CHX were added. Under these treatment conditions, sortilin levels were slightly more reduced (remaining 44.5% ± 4.25%, n = 3) (**Figure 3. 22 B, C**). To verify that the decrease in sortilin levels was caused by proteolytic degradation, I next examined the relative stability in cells treated with lysosomal hydrolase inhibitors [protocol adapted from (Arighi et al., 2004; Carlton et al., 2004)]. Again, cells were either treated with CHX, or without CHX, and additionally, with the protease inhibitors leupeptin (1 mg/ml) and E-64 (10µg/ml) for 12 hours (CHX+PI and PI, respectively), before levels of sortilin and SNX1 were immuno-detected as described. Compared to CHX-treated control cells (normalized to 100%), addition of protease inhibitors could stabilize the remaining levels of sortilin: treatment with CHX+PI resulted in a 24% increase in control cells (124.1% ± 3.22%, n=3) and sortilin levels reached 97.4% ± 8.81% for SNX1-suppressed cells compared to CHX-treated control cells

(**Figure 3. 22 C**). Likewise, as **Figure 3. 22 D** illustrates (a representative data set is shown), approximately 20% of the observed sortilin levels are a result from *de novo* synthesis (88.6%, from 'SNX1-CHX+PI', compared to 107.9% from 'SNX1-PI'). Thus, approximately 20% - 30% (net) are degraded as a result of SNX1 suppression, indicate that in these cells, sortilin is poorly retrieved back to the TGN, and its endosomal retention eventually leads to degradation by lysosomal hydrolases.

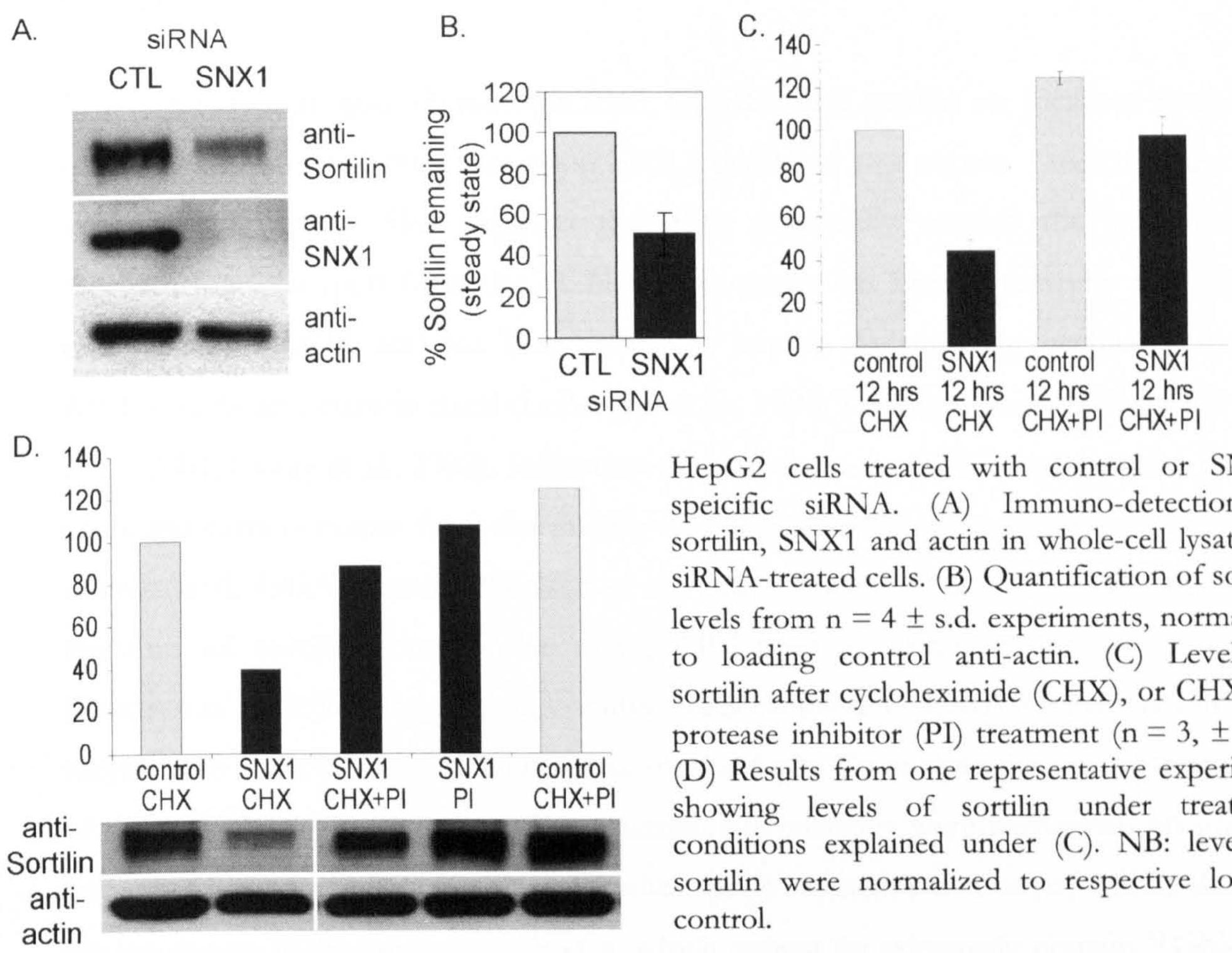

HepG2 cells treated with control or SNX1-speicific siRNA. (A) Immuno-detection of sortilin, SNX1 and actin in whole-cell lysates of siRNA-treated cells. (B) Quantification of sortilin levels from n = 4 ± s.d. experiments, normalised to loading control anti-actin. (C) Levels of sortilin after cycloheximide (CHX), or CHX and protease inhibitor (PI) treatment (n = 3, ± s.d.). (D) Results from one representative experiment showing levels of sortilin under treatment conditions explained under (C). NB: levels of sortilin were normalized to respective loading control.

Figure 3. 22 Biochemical studies into the stability of sortilin in SNX1-suppressed cells

3.7.7. Co-localization analysis of SNX1 and sortilin at ultrastructural level

All electron microscopic (EM) analyses presented in this paragraph were performed by Dr Muriel Mari in the Lab of Prof Judith Klumperman and Prof Hans Geuze, while I only provided the siRNA-treated cells, accordingly fixed for electron microscopic analysis. I feel that this data adds significantly to the understanding of a retrograde transport machinery involving SNX1, and hence I decided to include some of the data, provided by courtesy of Dr Muriel Mari[6].

In control cells, at light microscopic level, CI-MPR and sortilin are localized to the same organelle in untreated cells, but upon SNX1 depletion - as shown - redistributed to the same compartments. This suggests that they potentially employ the same transport mechanisms. Transport from the TGN to endosomes has been extensively studied in the case of the CI-MPR, and has been shown to require clathrin-coat machinery, including AP-1, GGAs and clathrin itself (LeBorgne et al., 1996; LeBorgne and Hoflack, 1997; Zhu et al., 2001; Doray et al., 2002). Indication that exit from the TGN might involve the same coats and carriers comes from the finding that in *in vitro* assays, sortilin has been shown to interact with GGA proteins (Nielsen et al., 2001; Takatsu et al., 2001), and that the C-terminus of sortilin contains the same, AP-1-binding sorting motif as the CI-MPR (Petersen et al., 1997). In contrast, possible coats on the endosomal site involved in sortilin recycling to the TGN had not been characterised yet. To analyse the identity the relation of this cargo to sorting nexins, ultrastructural EM analyses were performed on untreated and SNX1-suppressed cells. These studies led to characterization of SNX1-decorated 'endosome-to-TGN carriers', or ETCs, which appear to selectively contain TGN-bound cargo.

Initial EM analysis of the steady state distribution of receptors and SNX1 in control cells using immuno-gold labelling techniques (Slot et al., 1991) indeed showed that in HepG2 cells the majority of cellular sortilin was found at the TGN (data not shown). Nevertheless, a fraction of SNX1 and sortilin was also found co-localized on tubular extensions of endosomes and extensive co-localization was observed on small vesicles located in close proximity to the TGN (**Figure 3. 23 A, B, D, E**). These vesicles, as well as endosome-

---

[6] Mari M., Bujny M.V., Zeuschner D., Geerts W.J.C., Griffith J., Petersen C.M., Cullen P.J., Klumperman J., Geuze H.J. (2007) Sortilin and Mannose 6-phosphate Receptors define a novel exit from early endosomal vacuoles for SNX1-dependent recycling to the TGN. *Current Biology* (submitted)

associated tubules positive for SNX1 contained electron-dense material as seen in the darker content and did not only harbour sortilin and SNX1, but also SNX2 (**Figure** 3. 23 **C**), and the CI-MPR (data not shown). For the described defect in transport on the endosome-to-TGN route upon SNX1 suppression, these structures were named 'endosome-to-TGN carriers', or ETCs.

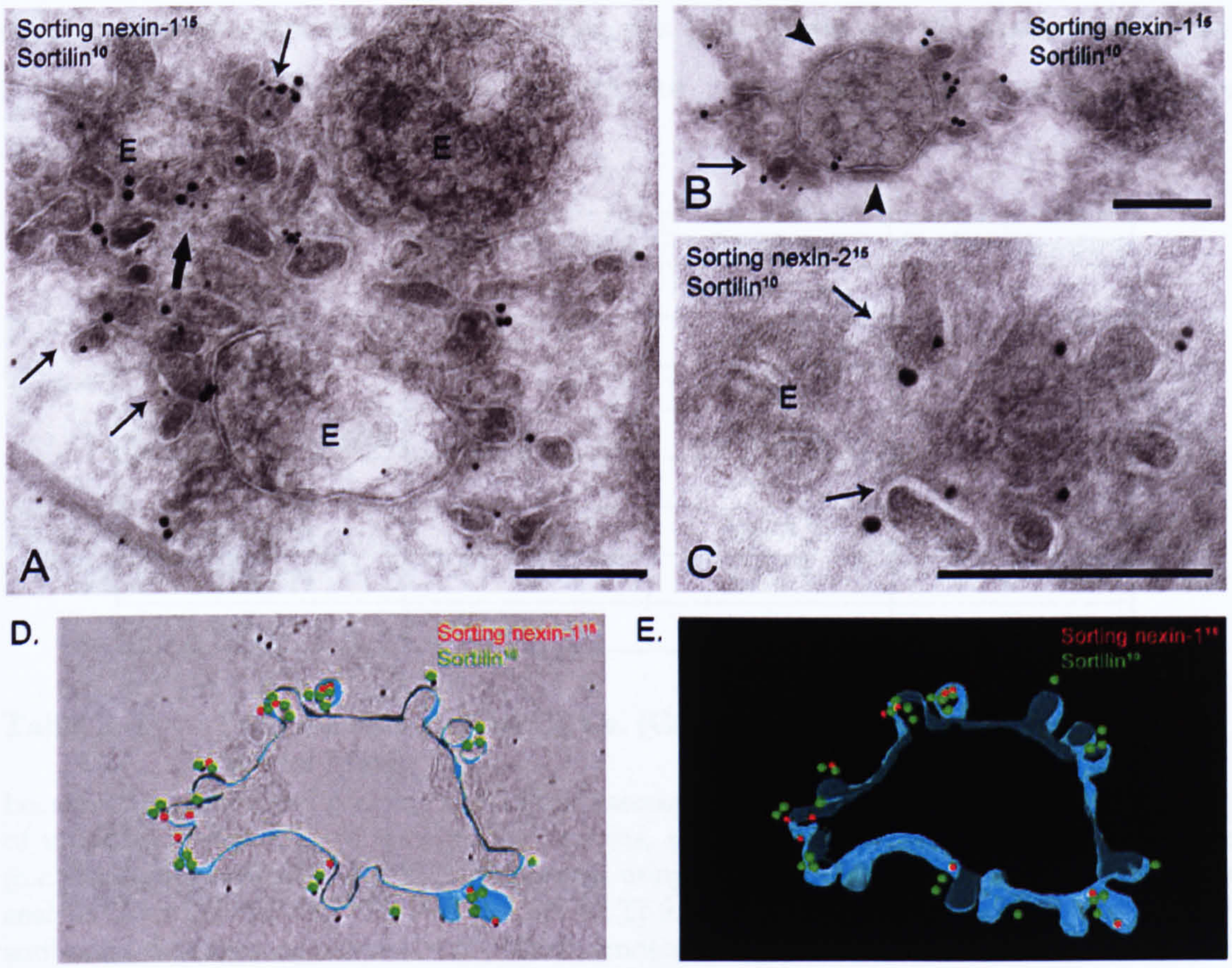

Figure 3. 23 Ultrastructural localization studies of SNX1, SNX2 and sortilin.
Cryosections of HepG2 cells were double-immunogold labeled for sortilin with 10nm gold and SNX1, or SNX2, with 15 nm gold. Arrows indicate co-localization, large arrow in (A) points to out discontinuity of membranes of individual vesicles. 'E' indicates endosomal vacuole. (A) Co-localization of both proteins on tubules emanating from endosomal structures, and on small vesicular, electron-dense carriers (endosome-to-TGN carriers, ETCs). (B) Clear co-localization on tubules emerging from an endosome containing internal vesicles, adjacent to the bi-layered clathrin-coat (arrowhead). (C) Co-localization of sortilin and SNX2 on ETCs. Scale bars are 200 nm. (D, E) Three dimensional models of sortilin- (10 nm gold, pseudo-coloured in green) and SNX1-positive endosome-associated tubules (15 nm gold, pseudo-coloured in red) were obtained by EM tomography of 250-500 nm thick cryosections as described in Zeuschner et al., 2006, demonstrating that the two proteins are clearly enriched on tubular profiles. Most profiles were non-branched tubules of 170 - 230 nm in length, and 20 – 50 nm in diameter, and vesicles. (Data courtesy of Dr Muriel Mari)

To judge whether these ETCs were indeed derived from endosomes, immuno-electron tomography was performed on thicker (250 nm) sections (Zeuschner et al., 2006), which increased the chance of detecting tubules attached to the endosomal vacuole (**Figure 3. 23 D**). As the 3D-reconstructions of the tomographs show (**Figure 3. 23 E**), the electron-dense, SNX1- and sortilin positive structures indeed show numerous connections with the endosomal vacuole, radiating out from the vacuole. Unlike the previously described tubular networks seen in recycling endosomes [for review see (Bonifacino and Rojas, 2006)], the ETCs labelled by SNX1 were not interconnected but formed individual elements.

Marker	Co-localization	Marker	Co-localization
SNX1	++)*	Rab11 (o.e.)	--
SNX2	++)*	Rab4	--
VPS26	++)**	Hrs	--
CI-MPR/CD-MPR	+	Clathrin	--
sortilin	+	AP-1	--
ASGPR	- (5%)	GGA3	--
TfR/Tf	--	CD63	--
EEA1	--	Lamp-1/2	--

Table 3. 2 Proteins localized to ETCs. (Compiled from data courtesy of Dr Muriel Mari)

Localization of indicated proteins to ETCs as assessed by immuno-gold labelling and EM analysis of ultrathin cryosections of endogenous proteins, apart from Rab11, which was overexpressed (o.e.) in the form of GFP-Rab11, and detected using an anti-GFP antibody. Tf distribution was analysed after internalising Alexa488-conjugated Tf for 30 min and detecting with an anti-Alexa488 antibodies. Scoring ranges from "++", which denotes strong/exclusive localization, to "- -", which denotes absence from ETCs. Levels of sortilin and CI-MPR are deemed "+" as only 20% of the total of detected receptor was found on ETCs (with the remainder at the TGN, on endosomes or at the plasma membrane), while SNX1, SNX2, VPS26 are found almost exclusively localized to ETCs (*): on ETCs and tubular profiles of endosomal vacuoles, but not body of the vacuole itself, (**): on tubules and on vacuole (Dr Muriel Mari, documented, but unpublished). Levels for asialoglycoprotein receptor (ASGPR) is deemed "-" as the minor amount of 5% of all cellular protein were found on ETCs.

Furthermore, a detailed analysis was performed revealing the nature of the endosomal vacuole from which ETCs were derived, *id est* whether they are of 'early endosomal' or 'late endosomal' origin. The distinction of these two structures is not trivial; endosomal organelles are highly dynamic structures with a constant in- and efflux of proteins, and hence lack truly resident proteins. One possible categorization of endosomes at ultrastructural level into early and late endosomes is by their accessibility to ligands like Tf

and BSA-gold. Endosomes accessible to internalized Tf and BSA-gold after a 10-minute uptake pulse can be considered as early endosomes (Stoorvogel et al., 1987; Stoorvogel et al., 1991). In contrast, endosomes that were inaccessible to endocytosed Tf and only reached by BSA-gold after a 15-minute pulse were deemed late endosomes. Applying these criteria, sortilin and CI-MPR were present on early and late endosomes with comparable amounts (6.3% and 5% normalised to the total sortilin present in the cell).

In a similar approach, combining characterisation with the number of internal vesicles [which reflect the maturation process of the endosomes; reviewed in (Sachse et al., 2002a)], 'early endosomal vacuoles' were deemed structures containing one to eight internal vesicles, while structures containing nine or more vesicles were considered late endosomes (**Table 3.3**). Applying these criteria, ETCs were increasingly observed as 'late stage early endosome'-associated (**Table 3.3**), with a sharp decline for vacuoles with nine or more vesicles. In similar assays, SNX1 was preferentially found on tubules of endosomes containing five to six internal vesicles. With the reference of EEA1 showing a clear-cut preference for endosomes with less than five vesicles (and a clear maximum for n = 2), SNX1 might be regarded as a 'late-stage early endosomal protein', which correlates with the clearly preferred association of ETCs with these 'late-stage early endosomes'.

Number internal vesicles	Tranferrin-positive (30 min pulse)	Characterisation
1 – 8	~ 75%	"early endosome"
9	~ 22%	"late endosomes"
10 or more	< 5%	"late endosomes"
	Max association	
SNX1	5 – 6 internal vesicles (~ 17% for each category)	
EEA1	2 internal vesicles (35%)	

Table 3. 3 Characterization of early and late endosomes (summary)

Numbers determined from cryosections of HepG2 cells incubated with Tf conjugated to Alexa488 for 30 min to saturate endosomal compartments with Tf. Endosomal vacuoles were subdivided in categories based on numbers of internal vesicle profiles. Vacuoles with up to about 8 vesicles had been reached by internalized Tf and were deemed early endosomes. From stage 8 internal vesicles onward, gradually less vacuoles were Tf-positive. These were deemed late endosomes. Likewise, form immuno-gold preparations (three grids), distribution of SNX1 and EEA1 was determined with regards to number of internal vesicles; maximum association is also shown as percentage of total of detected marker.

These ETCs are inaccessible to BSA-gold, and besides SNX1, sortilin and MPRs (both, the CD-MPR and CI-MPR), none of the 'classical markers' of early endosomes, late endosomes, or even previously described tubular networks from early endosomes were found on these structures (**Table 3. 2**). It thus appears that ETCs represent novel exit sites from late-stage early endosomes. ETCs are particularly distinct from the previously described tubular sorting endosomes (TSEs) (Peden et al., 2004), also referred to as tubular endosomal network (TEN), for example involved in recycling of the TfR (Bonifacino and Rojas, 2006); while the TEN appears as branched, and partially clathrin-coated, ETCs are non-branched, are negative for clathrin and moreover, do not contain Lamp-1 or CD63, which are found on 'classical' recycling tubules or TSEs (Peden et al., 2004). Most strikingly, ultrastructural analysis showed that the 'TSE-bound cargo' TfR (Bonifacino and Rojas, 2006) and the ETC-located cargos, sortilin and CI-MPR, are localized to different tubules emerging from the same endosomal vacuole (**Figure 3. 24**). It is furthermore of note that TSEs generally had a wider distribution around later stages of the early endosomes compared to ETCs.

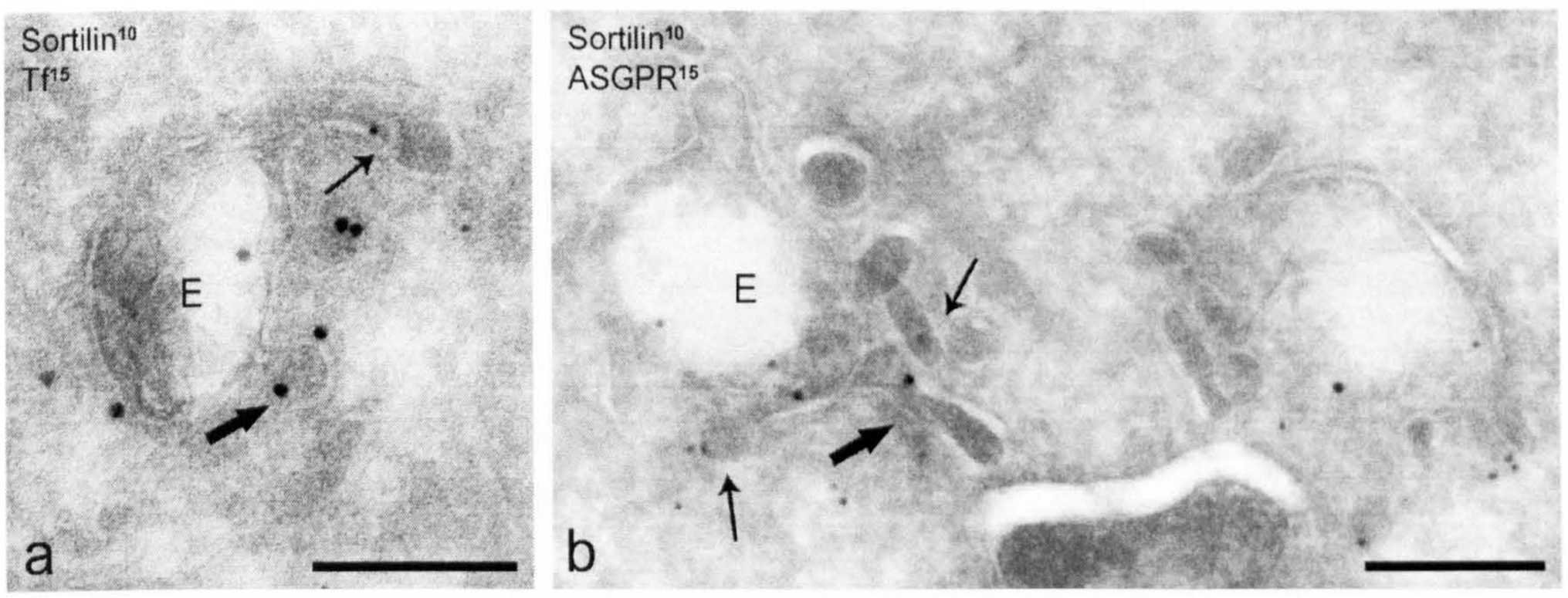

Figure 3. 24 Different tubular profiles with distinct cargo emerge from the same endosomal vacuole

(A) HepG2 cells incubated with Tf conjugated to Alexa488 for 30 min were sectioned and immuno-gold-labelled using anti-sortilin (10-nm gold), Tf was localized using anti-Alexa488 (15-nm gold). Sortilin (thin arrow) and Tf (thick arrows) co-localize to the same endosomal vacuole ('E') but are localized to different emerging tubules. (A) HepG2 cell-sections were co-labelled using anti-sortilin (10 nm gold) and antibodies against the cell-surface asialoglycoprotein receptor (ASPGR, 15-nm gold). Albeit present at the same endosomal vacuole ('E'), sortilin (thin arrow) and ASPGR (thick arrow) do not -localize to the same tubules. Scale bars are 200 nm. (Data courtesy of Dr Muriel Mari)

The importance of SNX1 in the ETC biogenesis was investigated analysing HepG2 cells in which SNX1 had been suppressed (**Figure 3. 25**). Strikingly, in these cells the number of endosome-associated ETCs (in a distance of < 100 nm from the endosomal vacuole) was reduced by almost 50% while the percentage of ETCs connected to the endosomal vacuole had almost doubled after SNX1- suppression. Overall, the amount of sortilin-gold was markedly decreased by approximately 58% compared to control cells, with the amount of TGN-resident sortilin most markedly reduced, while the levels of sortilin in endosome-associated ETCs were slightly increased. In SNX1-suppressed cells, the overall endosomal and TGN morphology was not markedly altered by the siRNA treatment, confirming and refining result obtained by immunofluorescence analysis (data not shown and **Figure 3. 7**)

While previous studies have shown that SNX1 localizes to endosomal, tubulo-vesicular structures in HeLa cells (Seaman, 2004) and HepG2 cells (Carlton et al. 2004), these studies extends this finding by showing that SNX1 and SNX2 both localize to tubular endosomal membrane profiles and vesicular carriers that contain TGN-recycling cargo, but not 'classical' recycling cargo or components of the clathrin-coat machinery. Interestingly, this distribution differs from the ultrastructural localization determined for VPS26 in HeLa cells (Arighi et al., 2004), as VPS26 does not only localize to tubular profiles but additionally localizes to the vacuole body. Further still, co-localization of VPS26 with TfR on tubular profiles was also detected. While this study has not directly explored co-localization of SNX1 with the TfR, coincidental evidence showing that Tf and sortilin label distinct profiles (while sortilin is localized to SNX1-tubules), suggests that localization of the two retromer components show subtle differences. Thus, the findings corroborate a model in which the cargo selection, comprising the VPS26-containing subunit takes could place in the endosomal body, and the complex then could targeted to more 'specialized' SNX-demarcated tubular profiles.

The finding that in SNX1-suppressed cells the number of tubular profiles is increased but the number of ETCs is decreased to almost reciprocal levels indicates an important function of SNX1 in the generation of the carrier. Whether this is a direct effect or achieved by engaging additional machinery remains to be established.

Figure 3. 25 SNX1 depletion causes increase in ETCs connected to the endosomal vacuole.

Ultrathin cryosections of SNX1-suppressed HepG2 cells were immuno-gold-labelled using (A) anti-SNX1 (15-nm gold) and anti-sortilin (10-nm gold) antibodies or (B) anti-CI-MPR (15-nm gold) and anti-sortilin (10-nm gold). After SNX1 suppression, sortilin is still present in ETCs (A, arrows) that are often connected with the endosomal vacuole ('E'). (B) Sortilin and the CI-MPR co-localize to the same endosome-connected ETCs also enriched with electron-dense material (arrows). Scale bars are 200 nm. (Data courtesy of Dr Muriel Mari)

3.8. Discussion

In this chapter, I have explored in detail the role of endogenous SNX1 in sorting and transport of the CI-MPR and sortilin. From this data, it appears that, SNX1 is indeed an orthologue of Vps5p in that it plays a conserved role mediating endosome-to-TGN retrieval of lysosomal hydrolase receptors.

Lysosomal degradation upon failed retrieval

The finding that addition of lysosomal protease inhibitors rescued the receptor from lysosomal degradation strongly indicates that upon failure to be retrieved to the TGN, the receptor becomes subject to degradation in lysosomes. I have however not succeeded in visualizing the receptor at this organelle. The hypothesis that upon SNX1 suppression, sortilin is targeted to lysosomal compartment arises from the parallels drawn with its yeast orthologue, Vps5p, as in *vps5*Δ cells, Vps10p is mis-localized to the degradative vacuolar compartment (Horazdovsky et al., 1997; Nothwehr and Hindes, 1997). In this context, suppression of VPS26 has previously been shown to result in endosomal redistribution of the CI-MPR, and in these cells, was indeed delivered to lysosomes, as determined by co-localization with Lamp-1 (Arighi et al., 2004). This correlates with the finding of Vps10p mis-localization to degradative vacuolar compartments in yeast *vps26*Δ (Seaman et al., 1998). Likewise, SNX1-suppression has been shown to lead to destabilization of the CI-MPR in HeLa cells as determined by biochemical assays (Carlton et al., 2004) and HepG2 cells resulting in reduced immuno-gold counts (Dr Muriel Mari, personal communication). Hence, there is correlative evidence for the lysosomal targeting of sortilin. Interestingly, another study found that upon siRNA-mediated VPS26-suppression, or in $VPS26^{-/-}$ ES cells, the CI-MPR was delivered to the plasma membrane (Seaman, 2004). In the EM studies presented here, it was indeed found that besides the marked overall-reduction of sortilin levels in SNX1-suppressed cells, plasma membrane levels of sortilin were slightly increased, showing another parallel between different components and cargo.

Retromer recruitment

Further parallels between the yeast and mammalian retromer can be drawn when comparing the ability of the SNX1-BAR domain to sense membrane curvature (Carlton et al., 2004) and to possibly induce membrane tubulation, which is similar to Vps5p (Seaman

et al., 1998). The SNX1-BAR domain is in a first instance a dimerization module and targets SNX1 to highly curved membranes. Whether it is a curvature sensor, or induces or stabilizes membrane tubulation was still a matter of debate: compared to other BAR domain-containing proteins, its tubulation capacity is relatively poorly developed. It is however one of the few curvature-sensing BAR domains, as in *in vitro* assays using recombinant SNX1, the extent of tubulation is strongly correlated with liposome diameter. Thus, the BAR domain provides a good cue for targeting of SNX1 to ETCs. In this context, the diameter of ETCs has been determined to 20 – 50 nm, which is consistent with liposome assays, in which a strong increase in binding was observed for liposomes with a diameter ≤ 50 nm. That the BAR domain is indispensable for association of SNX1 with membranes has been shown by localization studies using a GFP-SNX1 carrying a BAR-domain mutation SNX1 (KKR→EEE mutant, compare **Figure 3. 1**; Carlton et al., 2004), although one might interject that the mutations are quite drastic being a charge inversion [given that electrostatic interactions with membranes probably provide an important factor in the membrane association of BAR domains (Zimmerberg and McLaughlin, 2004)]. The data presented here showing that in SNX1-suppressed cells formation of endosome-associated tubules is not ablated, demonstrates that SNX1 is not crucially required for formation of these tubular profiles. The finding however that the number of ETCs is markedly reduced to 50%, strongly suggest that SNX1 is important in ETC formation. This is in line with the role of Vps5p in vesicle formation (Seaman et al., 1998), and opens the exciting possibility that SNX1 is directly or indirectly involved in the fission of vesicular carriers from endosome-associated tubules. Thus, there appear to be several lines of evidence not only suggesting the conserved function of retromer in mammalian cells, but also suggesting conservation of the mechanism. This might also hold true for the sub-complex association: in yeast, studies have shown that Vps26p-Vps29p-Vps35p and Vps5p-Vps17p exists as distinct sub-complexes (Seaman et al., 1998). And while it had previously been suggested that mammalian retromer is recruited as a stable pentameric complex from the cytosol (Haft et al., 2000), a more recent study showed by co-immunoprecipitation that mammalian retromer assembles from two distinct sub-complexes like its yeast counterpart (Rojas et al., 2007). Similarly, upon depletion of VPS26, levels of VPS29 and VPS35 are substantially decreased indicating sub-complex instability, while levels of SNX1 and SNX2 appeared largely unaffected (Arighi et al., 2004). Here, I show by IF analysis that in SNX1- and SNX2-suppressed cells association of a given SNX does not affect the membrane association of the respective other SNX

suggesting that membrane recruitment can occur independently of the respective other SNX. This could also be interpreted as an effect of the ability of SNX1 and SNX2 to form oligomers of alternate composition and existence as either homo- or hetero-oligomers (Haft et al., 1998; Rojas et al., 2007). Likewise, the finding that VPS26 stays associated with membranes upon suppression of SNX1 and SNX2 (whether individually or jointly) is indicative for the independent recruitment of both sub-complexes to endosomal membranes. This would in part also fit in with the observed differential localization at ultrastructural level. VPS26 was not only found localized endosome-associated tubules and ETCs (like SNX1), but (unlike SNX1) a substantial fraction was also found on endosomal vacuoles (Arighi et al, 2006). This differential localization might also include the TSE/TEN, as interestingly VPS26 was additionally found on TfR-positive tubules (Arighi et al., 2004), while previous EM studies have only found negligible co-localization between SNX1 and the TfR (Zhong et al., 2002), Likewise, Tf was prominently absent from ETCs but localized to tubules distinct from sortilin-decorated ETCs. One might thus hypothesize that VPS26 has a more extended distribution on endosomes and ETCs, which, admittedly is at first difficult to reconcile with a role for SNX1 in targeting the VPS-sub-complex to the vacuolar portion. Targeting to the vacuolar part might at least in part be mediated by other components- this could also include the receptor themselves, given these are transmembrane proteins.

Opposing to the findings presented here, a recent study reported that, in their hands, membrane recruitment of the VPS-subcomplex was dependent on the presence of either SNX1 or SNX2 (Rojas et al., 2007), which would also suggest that mammalian retromer differs from yeast in that regard. Unfortunately I do not know the reasons for these different findings, and it is obvious that the two studies furthermore differ in the conclusions whether suppression of SNX1 alone is sufficient for efficient CI-MPR retrieval. Here I present clear evidence that suppression of SNX1 is sufficient to markedly inhibit CI-MPR redistribution. While the abovementioned study argued that the difference might be cell type-specific, both studies appear to use the same cell type (HeLa), and furthermore, in this study I show that in HepG2 cells, the SNX1-specific siRNA used produces a similar phenotype with regards to the redistribution of the CI-MPR, but also with regards to a second unrelated cargo that appears to use the same pathway. It is worth mentioning that in agreement with Rojas and colleagues, I did indeed find markedly less redistribution in cell populations where SNX1 was only partially suppressed, even in cells

that had no detectable levels of SNX1. Based on the data presented, these appear to be the cells Rojas and colleagues have predominantly examined. These data could at least in part be reconciled with a model in which a minimal, but critical threshold level of SNX1 is required to maintain endosome-to-TGN transport (see also Chapter 4).

What about SNX2?

In our hands, SNX2 neither markedly influenced the steady state distribution of the CI-MPR, nor appreciably altered the kinetics of plasma membrane-to-TGN transport of a CD8-CI-MPR chimera.

1) On a technical note, it is possible that the SNX2-suppression levels achieved in this study are not effectual to induce redistribution comparable to the phenotype observed under SNX1-suppressed conditions. Indeed suppression levels achieved for SNX2 were consistently lower than for SNX1 (see also Chapter 4).

2) SNX2 might well be part of the retromer but simply 'less functional' than SNX1, *id est* less efficient in the retrieval to the TGN, which could be reconciled with the proposed redundancy as evidenced by genetic studies (Schwartz et al., 2002). These knockout studies in mice showed that both, $SNX1^{-/-}$ or $SNX2^{-/-}$ mice were phenotypically normal (Schwarz et al., 2002), while the simultaneous knockout was embryonically lethal and embryos died at midgestation. Likewise, $VPS26^{-/-}$ knock out mice die with a similar phenotype (Radice et al., 1991; Lee et al., 1992).

3) SNX2 might function at a different developmental stage. Furthering to the abovementioned knock out studies, mating studies with heterozygous mice indicated strong genetic interactions between SNX2 and VPS26, and weaker interactions between SNX1 and VPS26 (Griffin et al., 2005), highlighting the importance of SNX2 over SNX1 in embryonic development. It is of note though that this function does not necessarily relate to retromer function in its 'classical function' of a 'hydrolase retrieval complex': in all primary MEFs or permanent mutant-MEF cell lines derived from the various knock out mice, the CI-MPR was not mis-localised (Griffin et al., 2005), although in $VPS26^{-/-}$ MEFs the retromer assembly was clearly perturbed as evidence by depletion of VPS35. Likewise, tissues associated with high expression levels of the retromer components in embryonic development showed no alterations in the CI-MPR localization. These results are not only at odds with the findings in cultured epithelial cells, but also with findings from $VPS26^{-/-}$ embryonic stem cells, where the CI-MPR was redistributed to the plasma membrane

(Seaman, 2004; Griffin et al., 2005)[7]. Nevertheless, despite the lack of mis-localization of the CI-MPR, it is clear that VPS26- and simultaneous SNX1+SNX2-deletions are embryonically lethal. This might imply that SNX2, as well as other retromer components, may be involved in other functions than retrograde receptor retrieval. Specifically, this has recently been shown for SNX1 in the degradation of PAR-1 (Gullapalli et al., 2006), and potentially, for the VPS35-VPS26-VPS29 sub-complex in transcytosis of pIgR-pIgA (Verges et al., 2004) and for SNX2 regarding interaction with Abstrakt (Abdul-Ghani et al., 2005).[8]

4) Following from the previous argument, it is feasible that SNX2 has simply a different function in retromer biology compared to SNX1: despite the extensive sequence identity, both proteins show molecular differences, for example, recombinant SNX2 does not induce liposome tubulation (Carlton et al., 2005), and strong overexpression in mammalian cells does not lead to tubule formation but rather swelling of endosomal compartments (data not shown and JG Carlton, PhD thesis). Although highly speculative, SNX2 could thus act as 'negative regulator' by 'titrating' SNX1 tubulation though hetero-oligomerization or yet unidentified direct or indirect interactions. The kinetic analysis for the jointly suppressed cells did indeed show a slight enhancement of CD8-CI-MPR co-localization with TGN46, although a sound conclusion on this matter would certainly require further detailed investigations. Further coincidental evidence comes from a recent study showing that agonist-induced degradation of PAR-1 is SNX1-dependent, but independent of other retromer components, and, importantly, distinct from the Hrs/Tsg101-involving pathway. Strikingly, overexpression of SNX2, but not its suppression, markedly inhibited PAR-1 degradation. Further still, overexpressed SNX2, but not a PX-mutant (rendering SNX2 cytosolic) was capable of replacing SNX1 from endosomal membranes and prevent PAR-1 degradation (Gullapalli et al., 2006).

5) Given that mRNA levels of SNX1 and SNX2 are largely non-overlapping, although not directly comparatively tested (Haft et al., 1998), it is also possible that SNX1 and SNX2 act as tissue-specific orthologues. Specifically, leucocytes as an example have almost no mRNA for SNX1, but very high levels of SNX2, although a functional significance has not been established, and mRNA levels do not necessarily reflect protein levels.

---

[7] Although it has been argued that technical differences generating the respective gene knock out could be causative for this difference (Griffin et al., 2005).

[8] The two latter studies have however not conclusively excluded a role for the other proposed retromer components.

The finding that suppression of SNXs other than SNX1 and SNX2 can lead to redistribution of the CI-MPR also raises the distinct possibility that retromer biology might be much more complex than previously anticipated. A recent RNAi loss-of-function screen revealed that of all 29 sorting nexins, suppression of SNX5 and SNX6 led to marked redistribution of the CI-MPR (Wassmer et al., 2007). Further still, suppression of SNX5 resulted in decreased steady state levels of a CD8-sortlin chimera (Dr Thomas Wassmer, personal communication). Interestingly, the SNX1-targeted SMARTPool (Dharmacon) siRNAs used in this study were less effective with regards to inducing CI-MPR distribution, indicating how critical optimal suppression levels are to induce redistribution. It was furthermore found that simultaneous suppression of SNX5 and SNX6 resulted in destabilization of SNX1, probably amplifying the redistribution assuming that all three proteins are necessary for the retrieval step.

We have also presented evidence for a novel exit site from early endosomes, which appeared to exclusively contain cargo destined for retrieval to the TGN. These endosome-associated tubules were non-branched, 170 - 230 nm-long SNX1- and SNX2-decorated tubules, containing CI-MPR, sortilin as well as CD-MPR and VPS26 (data not shown; Dr Muriel Mari). The same cargo was also found on a new type of carrier, the ETCs. Previously, the tubular sorting endosomes/tubular-endosomal network (TSE/TEN) had been characterized as tubule-based sorting from early endosomes (Bonifacino and Rojas, 2006): these structures form extensive, branched networks and that transport a variety of cargo (ASPGRs, TfRs, Lamp-1, and the CI-MPR) to distinct destinations (plasma membrane, late endosomes/lysosomes and the TGN). In contrast to ETCs, buds off the TSE/TEN tubules were found to be decorated with 'classical' clathrin-coat and adaptor proteins, including AP1, AP-3 and clathrin (Tooze and Hollinshead, 1991; Stoorvogel et al., 1996; Futter et al., 1998). Apart from CI-MPR, none of the aforementioned proteins were found on ETCs, while they most likely derive from the same vacuole. This also puts into perspective other machinery involved in TGN-retrieval of the CI-MPR: as Rab9 and TIP47 are both proteins present on late endosomes (Aivazian et al., 2006), it is unlikely that ETCs are involved in this 'late' retrieval step. The two stretches in the cytoplasmic tail of the CI-MPR that contain the binding-site for TIP47 (Orsel et al., 2000) overlap with the two stretches containing the proposed binding sites for VPS35 (Arighi et al., 2004), maybe indicating 'successive options' to ensure efficient retrieval. Besides the already mentioned components, AP-1 and PACS-1 (Crump et al., 2001) have also been implicated in CI-MPR

retrieval. And while AP-1 is present on TSE/TEN but not ETCs, and given that (minor) amounts of CI-MPR have indeed previously been found in the TSE/TEN of HepG2 cells (Peden et al., 2004), this might suggests that AP-1/PACS-1-mediated sorting of the CI-MPR occurs from the TSE/TEN. Interestingly, neither TIP47 nor PACS-1 have homologues in yeast, and it remains to be established whether - or to which extent - Rab9, TIP47, PACS-1, as well as VPS35 are involved in sortilin recycling to the TGN, or whether this represent a CI-MPR-specific retrieval-machinery.

It is conceivable, although hypothetical, that as TSE/TEN also contains recycling cargo, transport to the TGN occurs first via the plasma membrane, while ETCs are a direct route: circumstantial evidence comes from the finding that sortilin and CI-MPR plasma membrane-levels are slightly enhanced in SNX1-suppressed HepG2 cells, and $VPS^{-/-}26$ ES (Seaman, 2004). It will remain to be established to which extend the TSE/TEN is frequented under retromer-depleted conditions.

Chapter 4 – Role of Retromer in Retrograde Toxin Transport

4.1. Preface

Much of the work described was carried out in the Bristol laboratory during the second and third year of my PhD, while the biochemical characterisation of retrograde toxin transport was made possible through collaboration with Dr Ludger Johannes at the *Institut Curie*, Paris, France. During two stays in his laboratory, I was able to learn the relevant techniques and carry out the described biochemical trafficking analysis. I would like to thank Mr Vincent Popoff at the Institut Curie for demonstrating the STxB-sulfation technique, and providing the VPS26 siRNA. I also would like to acknowledge the receipt of an EMBO Short Term Fellowship to assist financially in this undertaking. Lastly, sincere thanks again to my boss, Prof Pete Cullen, to fully endorse this project, and for the moral and additional financial support in order to accomplish this 'mission'.

4.2. Introduction

This chapter describes the work investigating the role of retromer, in particular SNX1, but also SNX2 and VPS26, in retrograde transport of the two bacterial toxins, Shiga toxin and cholera toxin. Both proteins have been extensively used as 'tools' in cell biology to study intracellular pathways; in fact, the existence of retrograde trafficking from the cell surface to the Golgi complex and ER was demonstrated for the first time using Shiga toxin (Sandvig et al., 1992).

Currently, it is not clear whether, or how, these toxins are sorted into TGN-bound carriers on endosomes. Here, I asked the precise question whether the retromer components SNX1, SNX2 and VPS26 were involved in this retrograde transport step of the non-toxic, receptor-binding B subunits of Shiga and cholera toxin –STxB and CTxB, respectively.

4.2.1. Shiga and Cholera Toxin – An Overview

Retrograde transport pathways and machinery do not only allow for endosome-to-TGN transport of endogenous proteins, but are also utilized by exogenous 'cargos' like toxins and viruses that are 'hitching a ride' to reach their intracellular destination [see (Bonifacino and Rojas, 2006; Gruenberg and van der Goot, 2006)]. The bacterial exotoxins of *Shigella dysenteriae*, Shiga toxin (STx), and *Vibrio cholerae*, cholera toxin (CTx), both belong to the family of AB_5-type toxins, comprised of a single catalytically active A subunit that confers the cytotoxicity and a pentameric B subunit that governs the association of the toxin with the cell surface (reviewed in (Sandvig and van Deurs, 2005). The B subunits assemble non-covalently with the A subunit, which consists of two domains: the A2-chain serves as tethering factor for the A and B subunits, while the cleavable A1-chain confers the enzymatic activity [review in (Lencer and Saslowsky, 2005)]. In spite very little sequence homology of the B subunits of STx and CTx, they are structurally highly similar and both bind to glycosphingolipids (Smith et al., 2004). The B subunit of Shiga toxin associates with globotriaosylceramide (Gb3) (Jacewicz et al., 1986), whereas the B subunit of cholera toxin binds to the ganglioside GM1 with high affinity (Fishman et al., 1976). Association of the B subunit with their receptors leads to subsequent internalisation, with the exact mechanisms behind the toxin-induced uptake largely unknown. The toxins are at least partially delivered to endosomes (see **par 4.2.2**), then on to the TGN, and from there to the ER. From the ER, the cleaved A1-chains are retro-translocated into the cytosol, where they exert their cytotoxic action: in case of cholera toxin, the A1 acts as an ADP-

ribosyltransferase that transfers ADP-ribose from NAD to the Gs_{α} subunit to activate adenylate cyclase [(Spangler, 1992) and references therein]. Hence, increased cAMP production directly affects intestinal chloride secretion, causing the substantial secretory diarrhoea seen in cholera. The A1 chain of STx acts as an rRNA *N*-glucosidase that interferes with ribosomal activity, thus inhibiting protein biosynthesis leading to cell death. As cells adjacent to one of the target tissues (the proximal nephron) are rich in Gb3, STx infection can lead to acute renal failure seen in haemolytic uremic syndrome [(O'Brien et al., 1992) and references therein].

4.2.2. Endosome-to-TGN transport of Shiga and cholera toxin

For both toxins, STx and CTx, several mechanisms of cell entry, including clathrin-dependent and –independent mechanisms have been proposed. [see (Sandvig and van Deurs, 2002; de Haan and Hirst, 2004; Sandvig and van Deurs, 2005) for review; see also Chapter 1]. In spite of the many proposed entry mechanisms, toxins internalized by clathrin-dependent and –independent mechanisms may end up in the same endosomal compartments after uptake (Tran et al., 1987; Hansen et al., 1993). This suggests that at least partially convergent mechanisms for the different forms of entry exist.

Transport to the TGN has been suggested to occur from early endosomes, rather than late endocytic compartments (Mallard et al., 1998; Mallard et al., 2002) and, at least in the case of CTxB, appears to bypass the endocytic recycling compartment (Sugimoto et al., 2001). A multitude of structural components and coats appears to be involved (see Table 4.1). Intriguingly, while there is data to suggest that STxB and CI-MPR require similar machinery for transport from early endosomes to the TGN (clathrin, epsinR, dynamin), there is also data suggesting subtle differences. While STxB endocytosis is not critically dependent on clathrin, its endosome transport to the TGN was shown to require clathrin, like it is the case for the CI-MPR. Similarly, transport of both, CI-MPR and STxB appears to depend on the clathrin adaptor epsinR (Saint-Pol et al., 2004). It is however of note that another study using an siRNA approach rather than overexpression (Saint-Pol et al., 2004) found that CI-MPR localization was unaffected when epsinR expression was suppressed (Hirst et al., 2003).

Interfering with AP1-function has been shown to re-localise the CI-MPR from the TGN to EE/ERC (Meyer et al., 2000; Crump et al., 2001), while suppression of this clathrin adaptor does not appear to affect STxB transport to the TGN (Saint-Pol et al., 2004). Which role the AP-1-binding protein PACS-1 plays in STxB transport is not clear; PACS-

1 interacts with the CI-MPR (Wan et al., 1998) as well as with AP-1, and this interaction is crucial for mediating CI-MPR sorting (Crump et al., 2001). Further still, while STxB is absent from late endocytic compartments (Mallard et al., 1998), a retrieval machinery for the CI-MPR exists from late endosomal compartment, including the GTPase Rab9 and the coat component TIP47 (Lombardi et al., 1993; Diaz and Pfeffer, 1998; Carroll et al., 2001).

Unlike for STx, the molecular machinery involved in endosome-to-TGN delivery of CTx is less well understood. While it has been shown that both toxins can enter the Golgi via the same 'raft'/GPI-transport intermediates (Nichols et al., 2001), it not known whether both toxins use the same endosome-to-TGN carriers. The finding that overexpression of Rab7 as well as Rab9 in Niemann-Pick type C (NP-C) fibroblasts is capable of restoring the correct Golgi targeting of CTxB (Choudhury et al., 2002) suggests that CTxB can utilise pathways that differ from STxB but are similar to CI-MPR to reach the TGN. In these sphingolipid storage disease cells, glycosphingolipids (GSL) accumulate in endocytic structures, and Rab7, which mediates early to late endosome transport/conversion as well as Rab9, involved in late endosome to Golgi transport, can alleviate accumulation of GLS by promoting transport to the TGN.

	Shiga Toxin	Cholera Toxin	Ricin	CI-MPR
Rab6a'	Yes[1,2]	?	Yes[3]	
Rab6a	No[2]	?	Yes* [3]	
Rab7	?	Yes[5]	No[6]	Yes[13]
Rab9	No* [6]	Yes[5]	No[7]	Yes[4]
Rab11	Yes [12]	No[5]	No[7]	
Dyna-min	Yes[8]	No[14]	Yes[9]	Yes[9,10]

Literature

1(Mallard et al., 2002)
2(Del Nery et al., 2006)
3(Utskarpen et al., 2006)
4(Lombardi et al., 1993)
5(Choudhury et al., 2002)
6 (Sandvig et al., 2002)
7 (Iversen et al., 2001)
9(Llorente et al., 1998)
10(Nicoziani et al., 2000)
11(Lu et al., 2004)
12 (Wilcke et al., 2000)
13 (Press et al., 1998)
14(Massol et al., 2004)

* only when suppression levels are between 40 – 75%; ** documented, but not confirmed

	Shiga Toxin	Cholera Toxin	Ricin	CI-MPR
clathrin	Yes[1,2]		No[5]	Yes[2]
AP-1	No[1]			Yes[3,4] *
epsinR	Yes[1]			Yes[1] ** No[6] ***

Literature

1(Saint-Pol et al., 2004)
2(Lauvrak et al., 2004)
3(Crump et al., 2001)
4(Meyer et al., 2000)
5 (Iversen et al., 2001)
6(Hirst et al., 2004)

* possibly at both sites (endosome ↔ TGN); ** affected under conditions of epsinR overexpression
*** localization of CI-MPR unaffected by epsinR suppression

Table 4. 1 Rabs and adaptors involved at the endosome/TGN interface

Listed are (selected) Rab GTPases and clathrin-coat machinery implicated in endosome-to-TGN transport of Shiga, cholera toxin, ricin (an AB-type plant toxin) and the CI-MPR.

4.3. Materials and Methods

For general materials and methods, buffer and media compositions, and suppliers, one is referred to Chapter 2. Here, methods specific to the investigation of retrograde transport of STxB and CTxB are described. If not stated otherwise, reagents were obtained from SigmaAldrich or Invitrogen.

The VPS26-specific siRNA (sequence #3 AAC TCC TGT AAC CCT TGA GdTdT) was designed by Mr Vincent Popoff, *Institut Curie*, Paris, France, and obtained from Sigma-Proligo (SigmaAldrich); for the transfection protocol see **para. 2.3.19**)

4.3.1. Sulfation Assays

Material

Sulphate-free DMEM	custom-made (INVITROGEN)
$Na_2[^{35}S]O_4$	(GE HEALTHCARE)
Radio-Immuno-Precipitation Assay buffer (RIPA)	1x PBS, 0.5% sodium deoxycholate 0.1% SDS pH 7.4, stored at 4°C
protease inhibitor cocktail (PIC)	stock 1000x 1mg/ml aprotinin, leupeptine, pepstatin,
antipain	1M benzamidine, 40 mg/ml PMSF in DMSO stored at -20°C
Tris Tricine gels	
Solution A	30% (w/v) acrylamide, 1.935% (w/v) bis-acrylamide
Solution B	30% (w/v) acrylamide, 0.938% (w/v) bis-acrylamide
Gel buffer	3 M Tris, pH 8.45, 0.3% (w/v) SDS
100% glycerol	
TEMED, 10% APS (stock)	(as described in Chapter 2, par 2.1.11)
Resolving gel	(all v/v), in sH_2O 0.32% solution A, 0.32% gel buffer, 0.13%
glycerol,	0.032 ‰ TEMED, 3.2‰ APS (stock)
Stacking gel	(all v/v), in sH_2O 0.08% solution B, 0.25% gel buffer, 0.8 ‰ TEMED, 8‰ APS (stock)
Electrophoresis buffer (anode)	0.2 M Tris, pH 8.9
Electrophoresis buffer (cathode)	0.1 M Tris, pH 8.25, 0.1 M Tricine, 0.1% SDS

Sample buffer (Tris Tricine)	187.5 mM TrisHCl, pH 6.8, 6% (w/v) SDS, 30% (v/v) glycerol, 0.03% (w/v) phenol red
Streptavidin beads	(PIERCE)
ImmunoPure Immobilized Protein G	(PIERCE)
B-($Sulf_2$) protein	Dr Ludger Johannes, Institut Curie, Paris, France (Mallard et al., 1998)
Anti-*Shiga* toxin (13C4)	(Johannes et al 1997)
CTxB-$Sulf_2$-biotin	(Amessou et al., 2007)
Gel fixing solution	40% (v/v) EtOH, 10% acetic acid
GF/C glass fibre filters	(WHATMAN)
Scintillation liquid (UltimaGold)	(PERKIN ELMER)
Scintillation Counter	(LKB Wallac)

Sulfation Assay - Methodology

The sulfation assays made either use of a modified STxB subunit (B-$Sulf_2$) genetically engineered to contain a tandem tyrosine sulfation site (Mallard et al., 1998), or a modified CTxB subunit (CTxB-$Sulf_2$-biotin), containing a sulfation site as well as a biotin-tag (Amessou et al., 2007). For these assays, HeLa cells were treated with siRNA as described in Chapter 2 (**par 2.3.19**) and after 60 hours, cells were reseeded to ensure same cell numbers, either at a density of 120.000 cells per well of a 24-well plate (STxB), or $1x10^6$ cells per well of a 6-well plate (CTxB). The next day (72 hours after treatment), cells were starved for 2 hours in sulphate-free medium before 1 μM of a modified B-($Sulf_2$) toxin subunit (per 120.000 cells) or 1 μM of the CTxB-$Sulf_2$-biotin construct (per $1x10^6$ cells) was surface-bound to cells at 4°C. After extensive washes with sulphate-free medium, toxin uptake was performed using media containing 0.5 mCi/ml radioactively labelled $Na_2[^{35}S]O_4$ for 20 minutes in case of STxB, or 40 minutes in the case of CTxB-$Sulf_2$-biotin. Cells were then lysed in either RIPA+PIC-buffer for STxB, or in the case of CTxB, in 1% Triton X-100 (in PBS) containing a protease inhibitor cocktail before the toxin subunits were immunoprecipitated using either a STxB-specific 13C4-antibody and protein G-sepharose in RIPA, or using immobilized streptavidin for the CTxB-$Sulf_2$-biotin construct. The supernatants were kept for further analysis of endogenous protein sulfation (**para. 4.3.2**). The precipitates were washed using Tris-HCl pH 6.8, then dried and resuspended in sample buffer, and heated to 95°C for 5 minutes, then centrifuged. The samples were subjected to gel electrophoresis using Tris-Tricine gels (25 – 30 mA/gel for 1 hour). The gel was incubated in fixing solution for 20 minutes, then dried using a BIORAD 583 gel dryer (ramp mode, 75°C, 90 minutes) and put on an erased phosphorimager film (GE

Healthcare) for at least one night before being analysed using a STORM phosphorimager (GE Healthcare) and appropriate software (ImageQuant, GE Healthcare), determining B-subunit-specific sulfation as intensity per area.

4.3.2. TCA Precipitation of Immunoprecipitation Supernatants

In parallel with B-subunit-specific sulfation, global sulfation of cellular components was assessed. Therefore, trichloroacetic acid was added to a final volume of 10% to immunoprecipitation supernatants. The samples were vigorously mixed, and incubated at 4°C for at least 30 minutes. A vacuum pump-connected filtration unit (Millipore) was used to transfer precipitated proteins onto glass fibre filters (Whatman). Therefore, filters that had been wet in 5% TCA were placed onto the unit, acid-precipitated proteins were added to filters, and washed with 1 ml of 5% TCA. Filters were subsequently transferred into scintillation vials, 3 ml scintillation fluid was added, and tubes were vigorously mixed. After 30 minutes incubation, samples were analysed by gamma counting (as counts per minute, cpm) using a liquid scintillation counter (LKB Wallac). The obtained values (cpm) were used to normalize the data obtained by autoradiography (area) as follows:

$$CTL = [Area\ (B\text{-subunit-specific sulfation})_{CTL} \times cpm_{CTL}]/cpm_{CTL}$$

$$EXP = [Area\ (B\text{-subunit-specific sulfation})_{EXP} \times cpm_{EXP}]/cpm_{CTL}$$

4.3.3. Fluorescently-labelled Toxin Uptake-Assays

Cells were plated onto coverslips and treated with siRNA as described. Coverslips were then transferred to ice-cold DHB medium for 15 minutes. After incubation with the respective toxin subunit for 30 min at 4°C (Alexa555-CTxB (Invitrogen): 0.5 µg/coverslip; FITC-STxB (Johannes et al., 1997): 1 µg/coverslip in DHB), cells were washed extensively to remove any unbound toxin. Subsequently, cells were either incubated at 19.5°C for 1 hour or at 37°C and 5% CO_2 for indicated periods to chase the toxin into the cells. Cells were then fixed using 4% paraformaldehyde and processed for immunofluorescence analysis as described previously (Chapter 2, **para. 2.4.21**).

4.3.4. Live Cell Imaging

Cells plated onto coverslips transiently transfected with RFP-SNX1 for 22 hours (refer to Chapter 2, para. 2.3.18) were transferred to ice-cold DHB-medium for 15 minutes. After incubation with 1 µg/100 µl FITC-STxB in DHB for 30 minutes (to allow surface-

binding) excess toxin was removed and cells were transferred to 19.5°C for at least 1 hour before being imaged live using a PerkinElmer Ultra*VIEW* LCI system (refer to Chapter 2, **para. 2.4.23**). For post-processing, live cell data for the recorded channels was exported from PerkinElmer Ultra*VIEW* as uncompressed movies. Where necessary, using ImageJ (NIH public domain software), background correction was performed using the 'rolling ball' option (set to 50). The contrast was enhanced by setting the maximum of allowed saturated pixels to 0.5% and normalizing it for all frames. All post-processing was performed on entire images only. An RGB merge was performed to yield an overlay of the channels. Typically, movies were exported as QuickTime movies or .avi files at a rate of 10 frames per second.

4.3.5. Co-localization Analysis

To quantify the toxin distribution in control and SNX-suppressed cells after either 30 minutes of FITC-STxB uptake or 40 minutes Alexa555-CTxB uptake (as described in **para. 4.4.3**), cells were additionally immuno-labelled with TGN46 or giantin, and imaged under identical conditions using confocal microscopy, taking 8 - 10 optical slices per visual field. For several visual fields, yielding at least 50 cells per sample (if not stated otherwise), co-localization was analysed using MetaMorph software (Molecular Devices). Co-localization was determined for every optical section individually for one visual field at a time. From these values, the mean was calculated; the standard deviation gives the deviation between individual visual fields. The co-localization of STxB and SNX1 was performed using the co-localization plug-in in ImageJ producing a co-localization composite image. Enumeration of vesicles was done using the Colony Counter tool of ImageQuant TL software (GE Healthcare) on individual channels and the co-localization composite image obtained through ImageJ-aided analysis.

4.4. Results

4.4.1. Analysis of Shiga toxin B-subunit transport through SNX1-positive compartments

Given that there is evidence that CI-MPR and STxB partially employ the same transport machinery from early endosomes, and given the role for SNX1 in endosome-to-TGN transport, I sought to scrutinize the relationship between STxB and SNX1 in more detail. To initially examine whether endocytosed Shiga toxin B-subunit was transported through SNX1-decorated early endosomes *en route* to the TGN, I performed a series of fluorescent toxin-uptake assays, combined with an immuno-labelling approach. In these assays, HeLa cells were incubated with FITC-conjugated Shiga toxin B subunit (FITC-STxB) at 4°C for 30 minutes to allow surface-binding of the subunit. Unbound FITC-STxB was removed by extensive washes prior to warming the cells to 37°C for various time points to internalize FITC-STxB. After fixation at 37°C cells were labelled with an anti-SNX1 antibody, followed by fluorescently-labelled secondary antibody to examine co-localization of the two proteins.

Inspection of samples for the different time points by confocal microscopy revealed that the FITC-STxB initially labelled the cell surface (**Figure 4. 1 A**) but was rapidly internalised as after 10 minutes incubation it was found on intracellular vesicular structures (**Figure 4. 1 B**). These FITC-STxB-positive punctae co-localized well with endogenous SNX1 on vesicular and tubular profiles in the cell periphery, but co-localization was most prominent in the juxtanuclear area (**Figure 4. 1 B**). Co-localization was not complete however. When performing a quantitative analysis scoring all SNX1-positive structures for the presence or absence of FITC-STxB [and *vice versa* for STxB (see **para. 4.2.6.** for details)], it was found that 481 out of 696 SNX1-positive vesicles (for the representative experiment shown) were positive for FITC-STxB (69.1%), while only 481 out of 1445 of all FITC-STxB punctae were SNX1-positive (33.3%).

A similar partial co-localization of STxB with endosomal markers has been observed before (Mallard et al., 1998). When co-internalizing EGF and STxB for 1 hour at 19.5°C, it was observed that they display a 'juxtaposed' distribution, and not all EGR structures were positive for STxB, while Tf and STxB were observed to co-localize almost perfectly under the same conditions and all Tf structures were positive for STxB (Mallard et al., 1998). This scenario suggest that STxB is delivered 'non-selectively' to the entire endosome

population, but that SNX1 and EGFR are probably only localized to a distinct subset (compare also (Lakadamyali et al., 2006) for CME-ligands).

The distribution of the two proteins furthermore appeared juxtaposed or polarized, and the 'comet-like tails' emerging from FITC-STxB punctae were in most, but not all cases SNX1-negative (arrowheads, **Figure 4. 1 B, C**). Thus, while it appeared that the toxin was delivered to the same endosome, it showed a differential distribution already perceivable at LM level (which given the achievable resolution was rather surprising). This tubular partitioning appears temperature-sensitive and incubation at 19.5°C still allows for internalisation of the toxin, but it subsequently fails to accumulate at the TGN (Mallard et al., 1998). To relate our findings to these results, FITC-STxB-surface-labelled cells were incubated at 19.5°C for 1 hour, which resulted in an accumulation of STxB in SNX1-positive structures (851 out of 2100 FITC-STxB-decorated structures positive for SNX1, 40.0%), and residual labelling at the plasma membrane, as inspection of single confocal z-sections revealed. So while not all STxB was internalised at this temperature, STxB was also not delivered from endosomes/SNX1-positive structures to the TGN.

Given the generally low overlap between SNX1 and STxB, it was possible that transit through SNX1-positive endosomes was a rapid event. Thus, in a fixed-cell 'snapshot' scenario', one would detect STxB prior, during or after passing through the 'SNX1 endosome'. I thus sought for ways to examine STxB flux through the endosomal system using live cell analyses. Therefore, using LCI (**para. 4.3.4**), I examined FITC-STxB transport in cells that were transiently transfected with RFP-SNX1. As discussed previously, incubation at low temperature can render GFP-SNX1 cytosolic (Chapter 3, **para. 3.3**), while the probe was associated with membranes at 19.5°C. With the observation that at this temperature STxB was delivered to SNX1-postive endosomes but also still found at the plasma membrane, it allowed me study the early stages of toxin uptake into SNX1-positive endosomes in live cells.

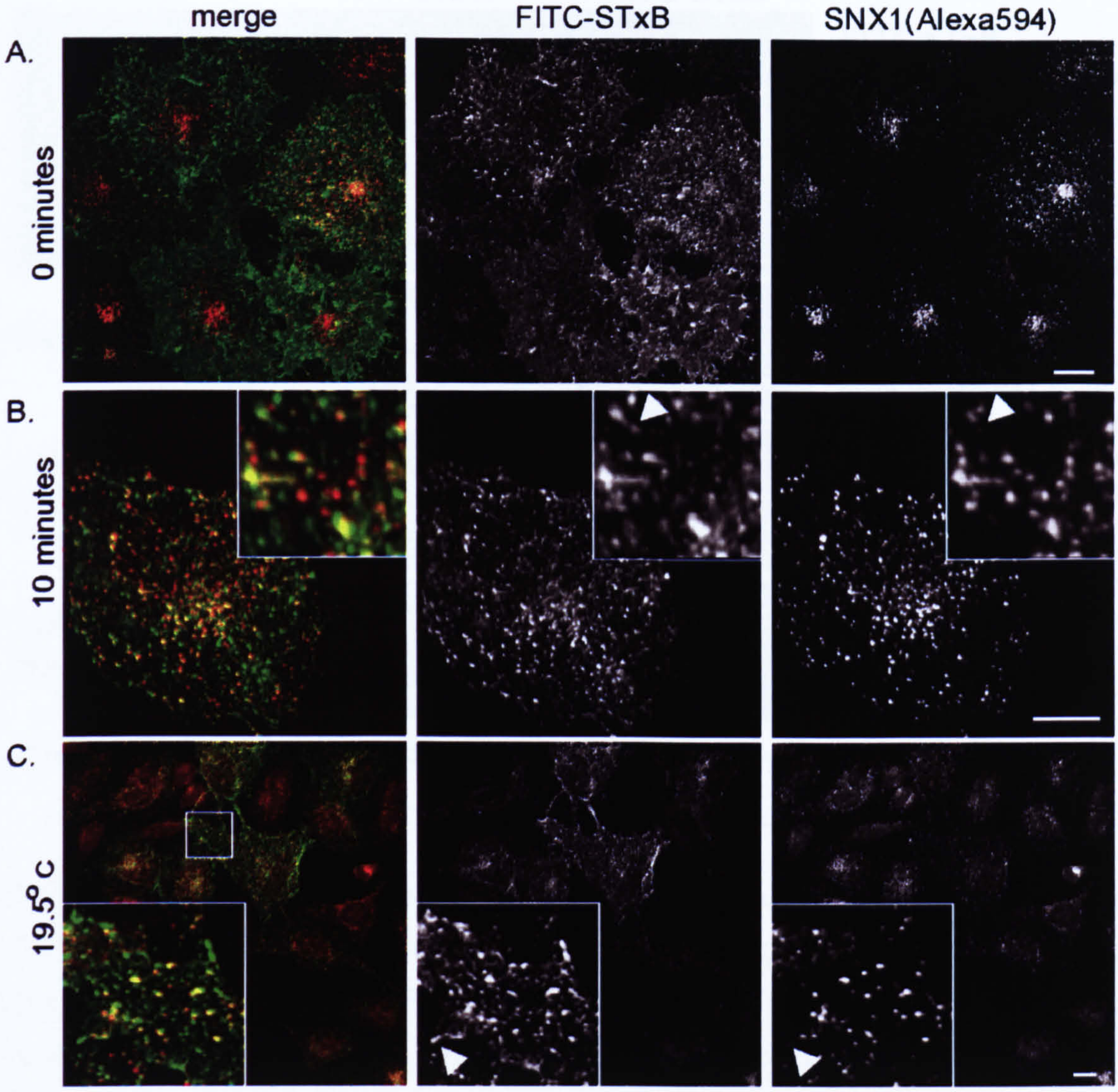

Figure 4. 1 Shiga Toxin B subunit localizes to SNX1-positive endosomes.

Fluorescently-labelled Shiga toxin B-subunit (FITC-STxB, green channel) was surface-bound to HeLa cells at 4°C. Excess toxin was removed before cells were transferred to 37°C or 19.5°C for indicated times to allow for FITC-STxB internalization. Cells were fixed, immuno-labelled with an anti-SNX1 antibody (Alexa594, red channel) and subsequently imaged using a confocal microscope. Maximum projections of 8 - 10 optical z-slices (480 nm z-separation) are shown. (A) Cells were fixed without incubation at 37°C (0 minutes). (B) After 10 minutes, the toxin displayed extensive co-localization with the SNX1-positive endosomal structures, as indicated by the yellow colour in the merged images. Note the subset of FITC-STxB tubules that were negative for SNX1 (arrowheads in B and C). (C) The toxin could be 'trapped' in SNX1-positive endosomes when incubated at 19.5°C for 1 hour. Scale bar is 10μm.

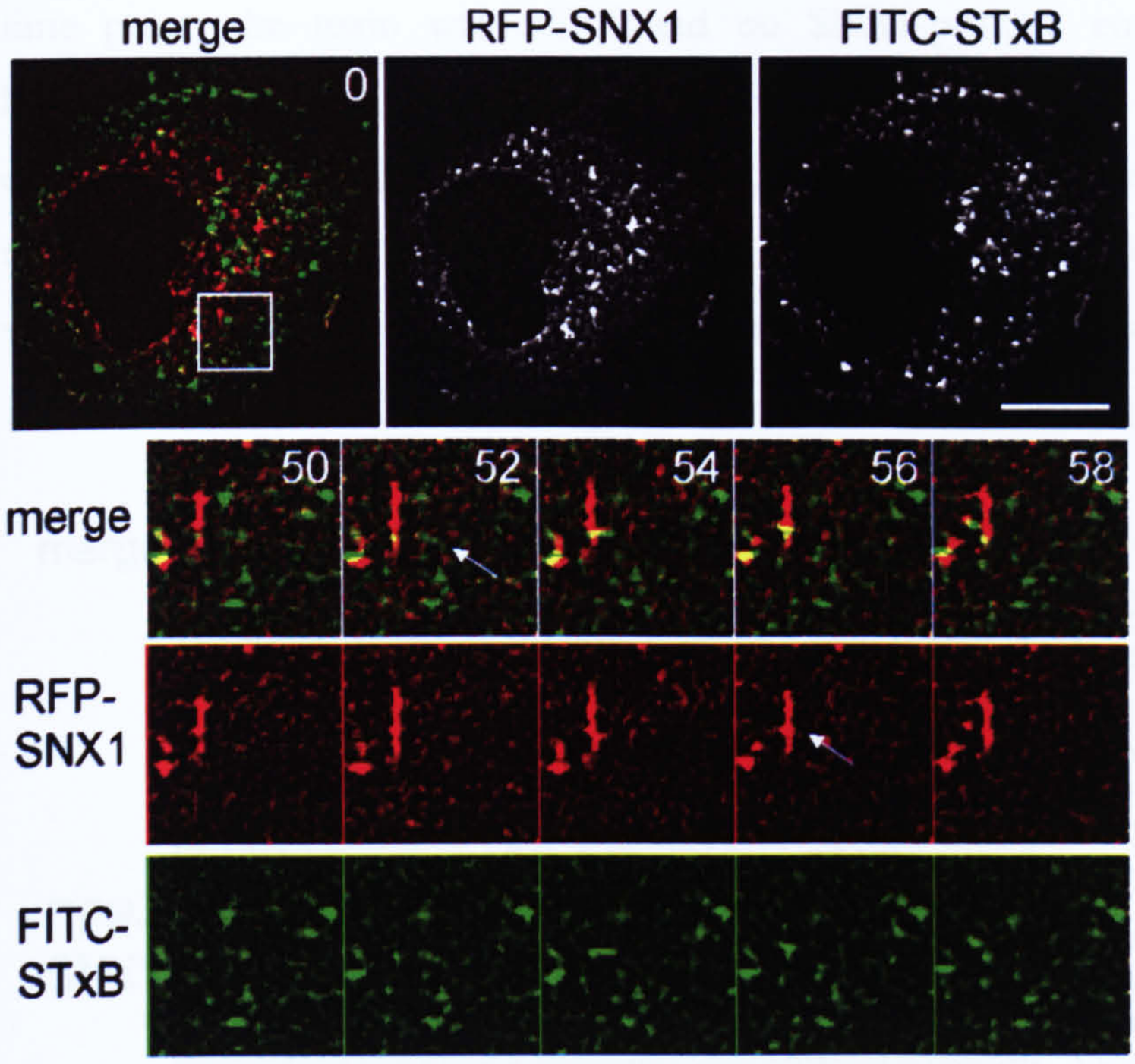

FITC-STxB is delivered to tubulo-vesicular SNX1-positive compartments.

HeLa cells transiently transfected with RFP-SNX1 were surface-labelled with FITC-STxB at 4°C for 30 minutes and, after removing any unbound toxin, transferred to 19.5°C for 1 hour. Cells were then transferred onto a heated stage and uptake of toxin was imaged live in one optical z-section. Selected images of the movie (see also Movies 4.1) are shown. Time is given in seconds. Scale bar is 10 μm.

Figure 4. 2 FITC-STxB is delivered to tubulo-vesicular SNX1-positive compartments.

Live cell confocal analysis of a single median z-section revealed that FITC-STxB was not only localized to static and motile SNX1-positive vesicles (**Movie 4.1.1**), it furthermore showed that on these vesicles, FITC-STxB and RFP-SNX1 moved together in rapid and burst-like motions of vectorial nature (a total of $n > 13$ coverslips were examined). In addition, it appeared that FITC-STxB was indeed delivered to SNX1-positive structures and then progressing intracellularly in, or with, SNX1-decorated vesicles (**Figure 4. 2**, arrows, **Movie 4.1.2**). Nevertheless, I also observed that more static FITC-STxB structures did not co-distribute with SNX1. In addition, I noted that STxB was not only delivered to SNX1-positive structures and tubules, but that structures appeared to fuse and exchange the fluorescent probe (**Figure 4. 4,** arrows). Sometimes, distribution of the two components appeared polarized. It is however likely that this behaviour represents an artefact of the spatio-temporal resolution. The observation that FITC-STxB was delivered to and transported 'within' SNX1-positive endosomes made it pertinent to examine whether this co-localization was preserved at later time points, and to which extent SNX1 was involved in the delivery step of endosomal STxB to the TGN. Here, I found that after 30 minutes, FITC-STxB became progressively enriched in the juxtanuclear area, where it co-localized extensively with TGN46 (**Figure 4. 4 A; Figure 4. 5**). Additionally, at this

time point, the toxin was still found on SNX1-positive endosomes. After 1 hour, localization to vesicles had almost completely ceased with FITC-STxB now being almost exclusively localized to the TGN (**Figure 4. 4 B**). It was furthermore apparent that at this time point, SNX1 displayed predominantly a juxtanuclear distribution in immediate vicinity to the STxB-decorated TGN ribbons (**Figure 4. 6**, arrows).

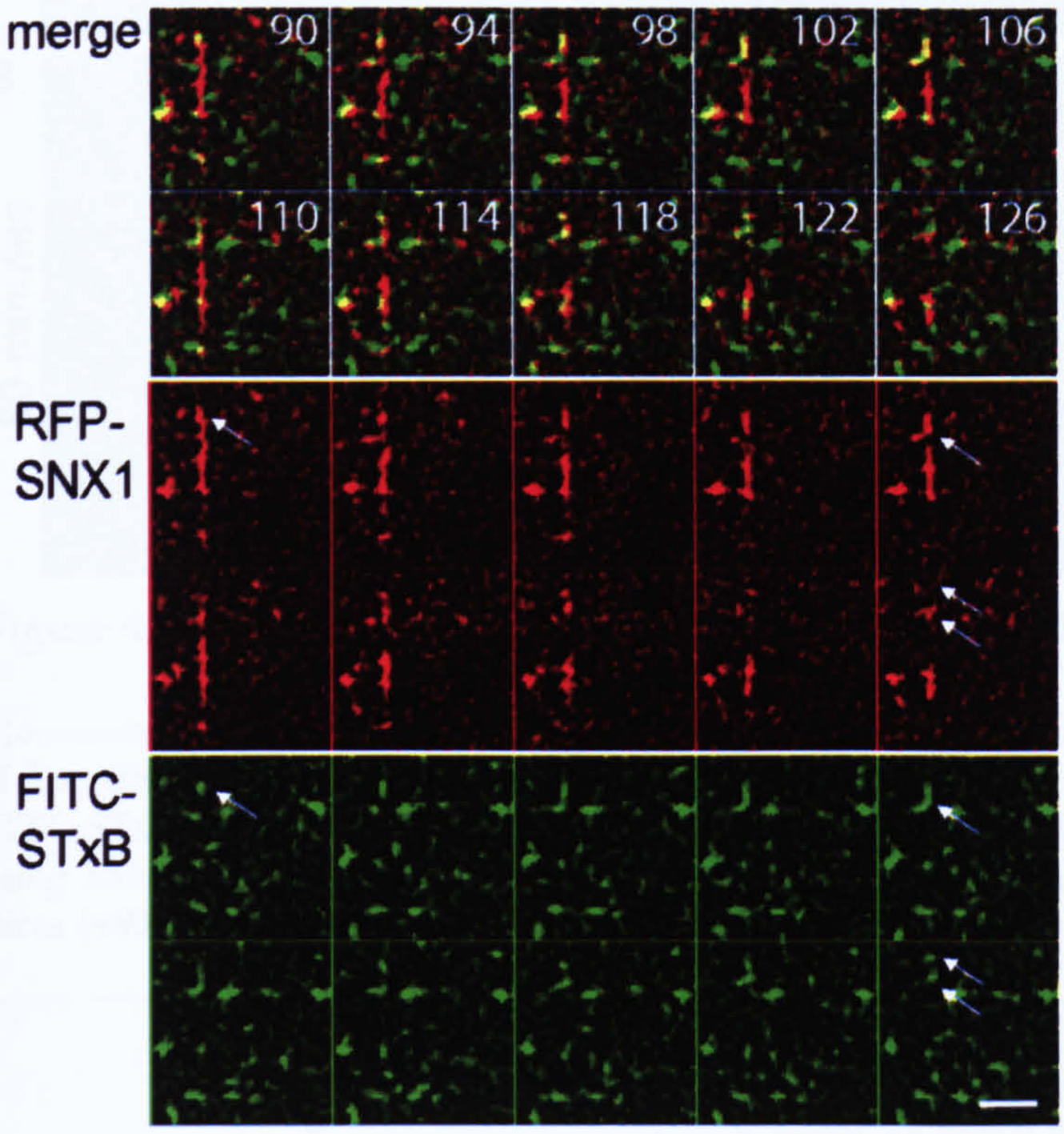

FITC-STxB punctae and SNX1-positive structures fuse and segregate.

Shown is the same region of interest as in **Figure 4. 2**.

HeLa cells transiently transfected with RFP-SNX1 were surface-labelled with FITC-STxB at 4°C for 30 minutes and, after washing off any unbound toxin, transferred to 19.5°C for 1 hour. Cells were then transferred onto a heated stage and uptake of toxin was imaged live in one optical z-section. Selected images of the movie (see also Movies **4.1.1 - .2**) are shown. Time is given in seconds. Scale bar is 10 μm.

Figure 4. 3 FITC-STxB punctae and SNX1-positive structures fuse and segregate.

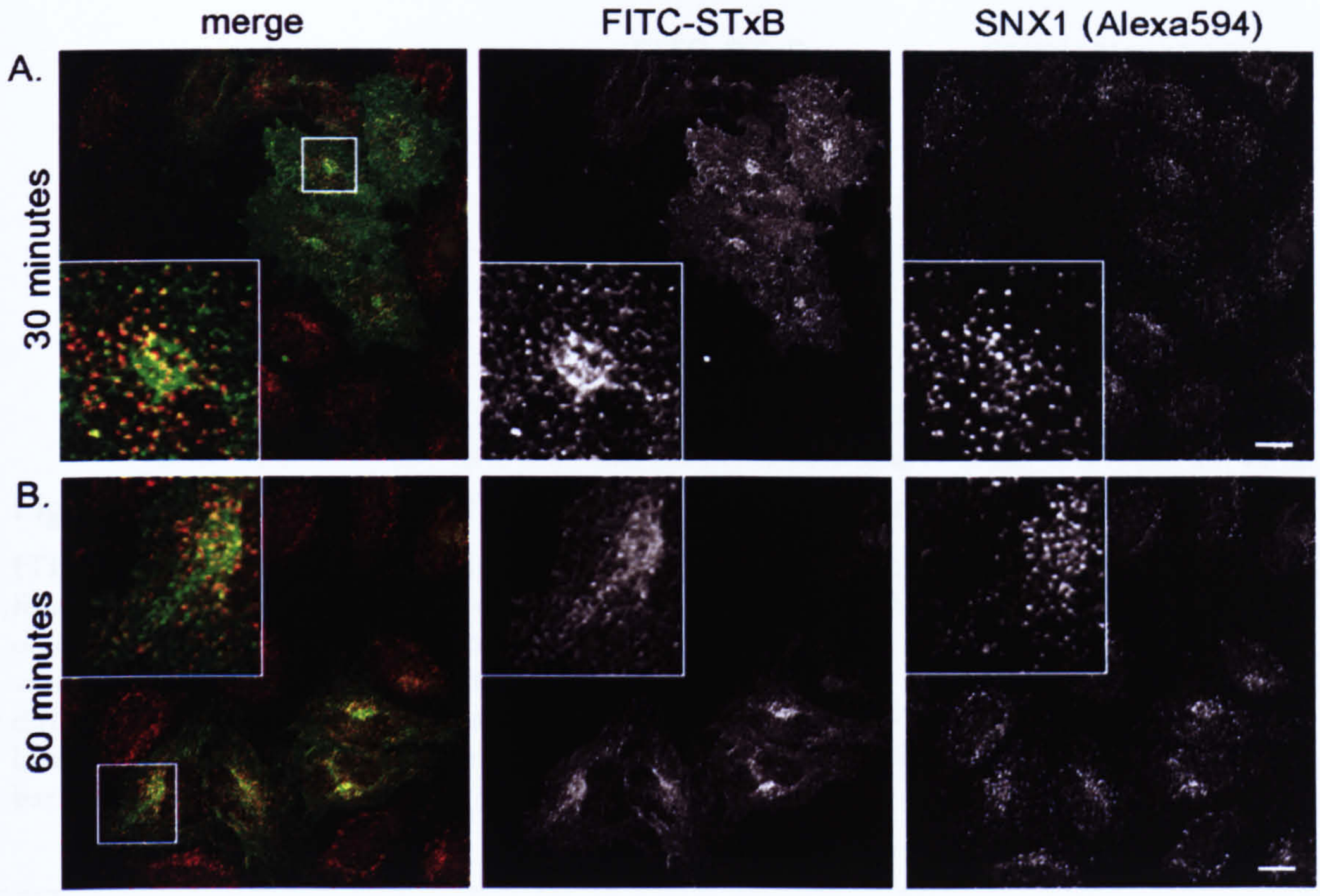

Figure 4. 4 From SNX1-positive structures, FITC-STxB is delivered to the perinuclear area.

Fluorescently labelled Shiga toxin B-subunit (FITC-STxB, green channel) was surface-bound to HeLa cells at 4°C. Excess toxin was removed before cells were transferred to 37°C to internalize FITC-STxB. At indicated times cells were fixed and processed for immunofluorescence labelling using anti-SNX1 antibodies (Alexa594, red channel). Maximum projections of 8 - 10 optical z-slices (480 nm z-separation) are shown. Scale bar is 10μm.

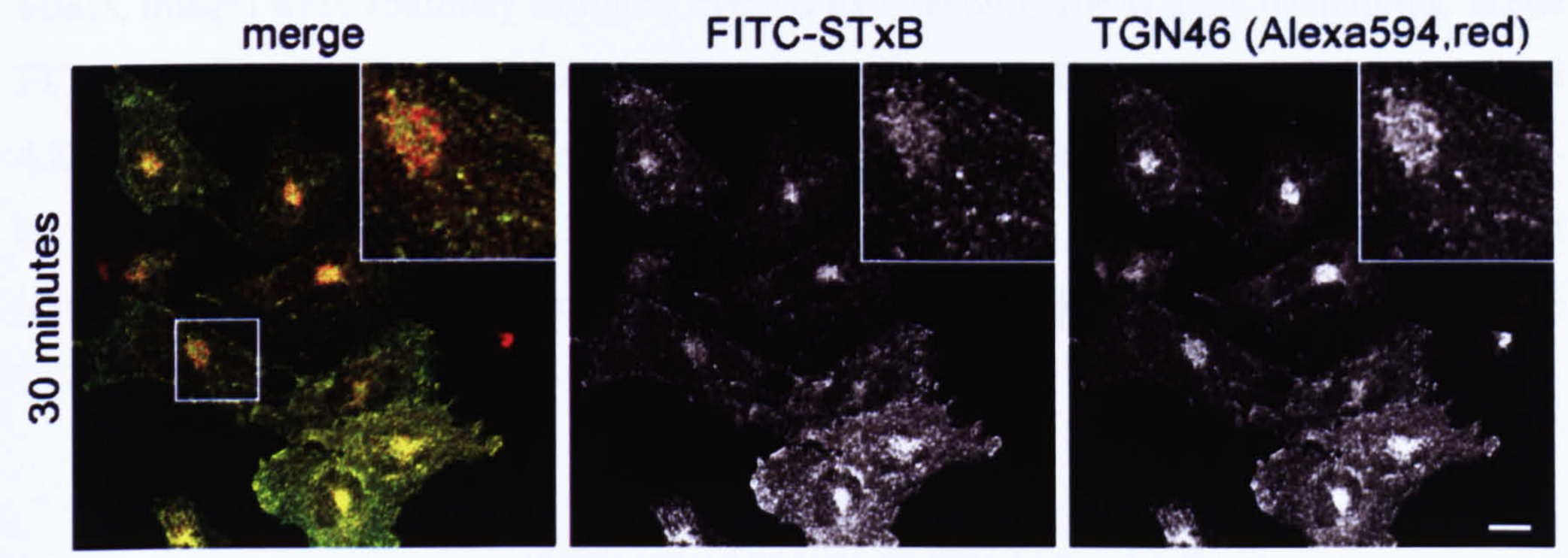

Figure 4. 5 FITC-STxB is delivered to the TGN46-labelled *trans*-Golgi network.

HeLa cells labelled with FITC were transferred to 37° for 30 minutes before being fixed and immuno-labelled with anti-TGN46 (Alexa594, red channel). Maximum projections of 8 - 10 optical z-slices (480 nm z-separation) are shown. Scale bar is 10μm.

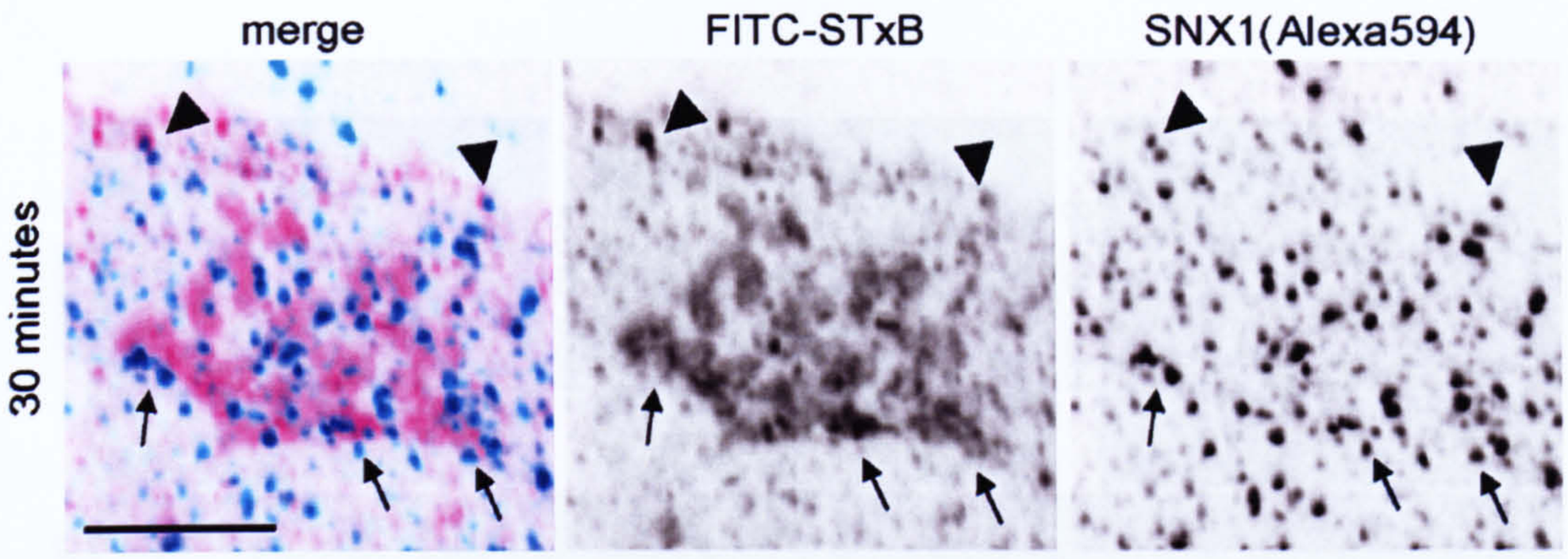

Figure 4. 6 Examination of juxtanuclear SNX1-enrichment in FITC-STxB.

FITC-STxB (pseudo-coloured in pink) was allowed to internalize for 30 minutes), before cells were fixed and immunolabelled with anti-SNX1 (pseudo-coloured in blue) and imaged using a 100x objective (The resulting images were colour-inverted using Adobe Illustrator). On SNX1-positive vesicles, the toxin appeared as punctae (arrowheads). In, or at, the TGN, the toxin appeared diffuse, while SNX1 retained its vesicular distribution that appeared juxtaposed to the FITC-STxB-labelled TGN (arrows). The adjacent cell at the top was not visibly labelled with FITC-STxB. Scale bar is 5 μm.

Thus, from these results it was feasible to speculate that STxB was directly delivered from SNX1-positive structures to the TGN. To further test this hypothesis, I again used a live cell imaging approach. In these assays, to overcome problems associated with long-time imaging, such as phototoxicity and bleaching of the RFP-SNX1 probe, I allowed the toxin to be pre-internalised for up to 30 minutes before starting the imaging process[9]. In these assays, images were routinely captured every 6 to 7 seconds for at least 10 minutes. While FITC-STxB was first seen as compact punctae with RFP-SNX1-positive vesicles (**Movies 4.2**, **Figure 4.7**), it was then seen to be 'handed over' to the more diffuse FITC-STxB-labelling at (presumably) the TGN. Thus, it appears that the SNX1-labelled compartment is both, a transit and a transporting compartment for FITX-STxB to on its itinerary to the TGN.

[9] After surface-labelling and transfer to 19.5°C for 1 hour, coverslips were mounted onto a heated stage before the imaging procedure was started 30 minutes later.

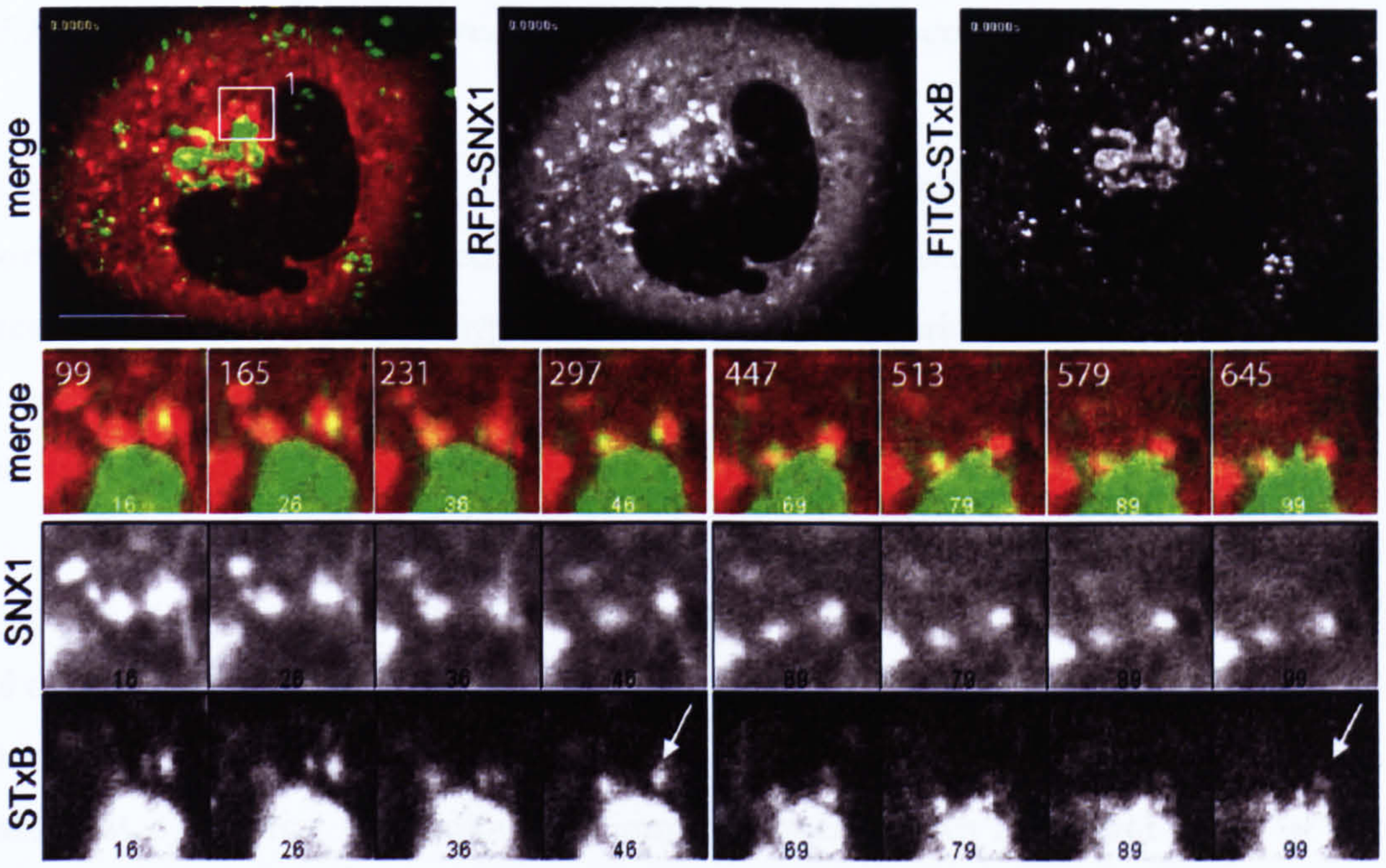

Figure 4.7 Vesicular FITC-STXB reaches the TGN area in SNX1-positive carriers.

FITC-STxB (green) was surface-bound to RFP-SNX1-transfected HeLa cells. After extensive washes and incubation at 19.5°C for 1 hour, cells were transferred to a heated stage and toxin was pre-internalized for 10 minutes, before the imaging process was started (see also **Movies 5.2.1 – 5.2.6**). Shown are separate and merged frames of the ROI, time of the set is given in seconds (white numbers, top left). Note the FITC-STxB delivered to (presumably) the TGN (arrow). Scale bar is 10 μm.

4.5. Functional Characterization

4.5.1. Effect of SNX1 suppression on immunofluorescence-based toxin traffic assays

To examine whether delivery of STxB to SNX1-positive endosomes was required for transport to the TGN, I employed an RNA interference-based strategy combined with fluorescent-toxin uptake assay. I hypothesized that in a scenario paralleled to retrieval of the CI-MPR and sortilin, this procedure could block, or at least reduce the transport of toxin to the TGN, if SNX1 was critically involved in this transport step.

Routinely, in these assays HeLa cells were treated with either the previously described control or SNX1-specific siRNAs for 72 hours and were surface-labelled with FITC-STxB for 30 minutes at 4°C. Then cells were either fixed directly or the toxin subunit was internalised at 37°C prior to fixation and immuno-labelling. An important result of the early time point analysis was that STxB appeared to label the surface in SNX1-suppressed cells to the same extent as in control cells, as analysed by confocal microscopy (**Figure 4. 8 A**). This indicated that the siRNA treatment did not affect trafficking of the toxin receptor. I then embarked upon a detailed kinetic analysis of FITC-STxB endosome-to-TGN transport in SNX1-suppressed cells. As described for untreated cells, in control siRNA-treated cells the TGN accumulation became discernible as early as 8 – 10 minutes after temperature shift, and was robustly developed after 30 minutes, for which an example is shown in **Figure 4. 8 B**. In striking contrast to the control, in SNX1-suppressed cells FITC-STxB remained predominantly associated with peripheral structures after internalisation for 30 minutes (**Figure 4. 8 B**). I thus extended the study examining the toxin localization at later time points (**Figure 4. 8 C,D**). In these assays, the difference became even more evident, as in controls the toxin displayed a compact juxtanuclear accumulation at the TGN. In comparison, in SNX1-suppressed cells even after 120 minutes, only few cells showed slight perinuclear toxin enrichment, while the majority still exhibited a dispersed peripheral localization (**Figure 4. 8 C,D**; asterisk).

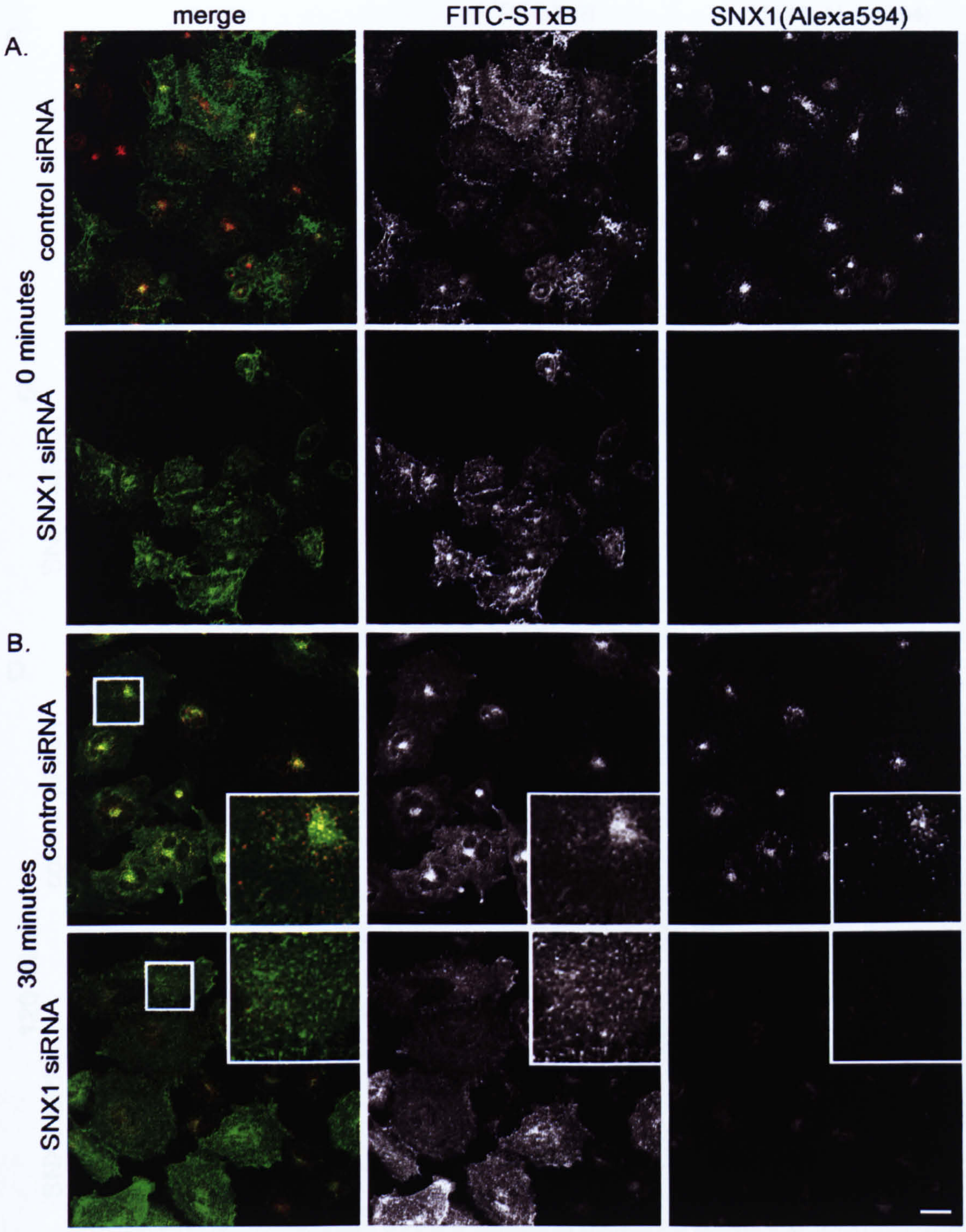

Figure 4. 8 In SNX1-suppressed cells, endosome-to-TGN transport of STxB is perturbed.

HeLa cells treated with indicated siRNAs were subjected to FITC-STxB uptake assays, fixed at indicated times and immuno-labelled for SNX1 (Alexa594, red channel). In cells treated with SNX1-specific siRNA, the immunofluorescence signal was markedly reduced. (A) Surface labelling was comparable in control and SNX1-suppressed conditions. (B) After 30 minutes internalization, the toxin showed juxtanuclear enrichment in control siRNA-treated cells, but remained associated with peripheral structures in SNX1-suppressed cells. Scale bar is 20 μm. (Fig. cont. overleaf)

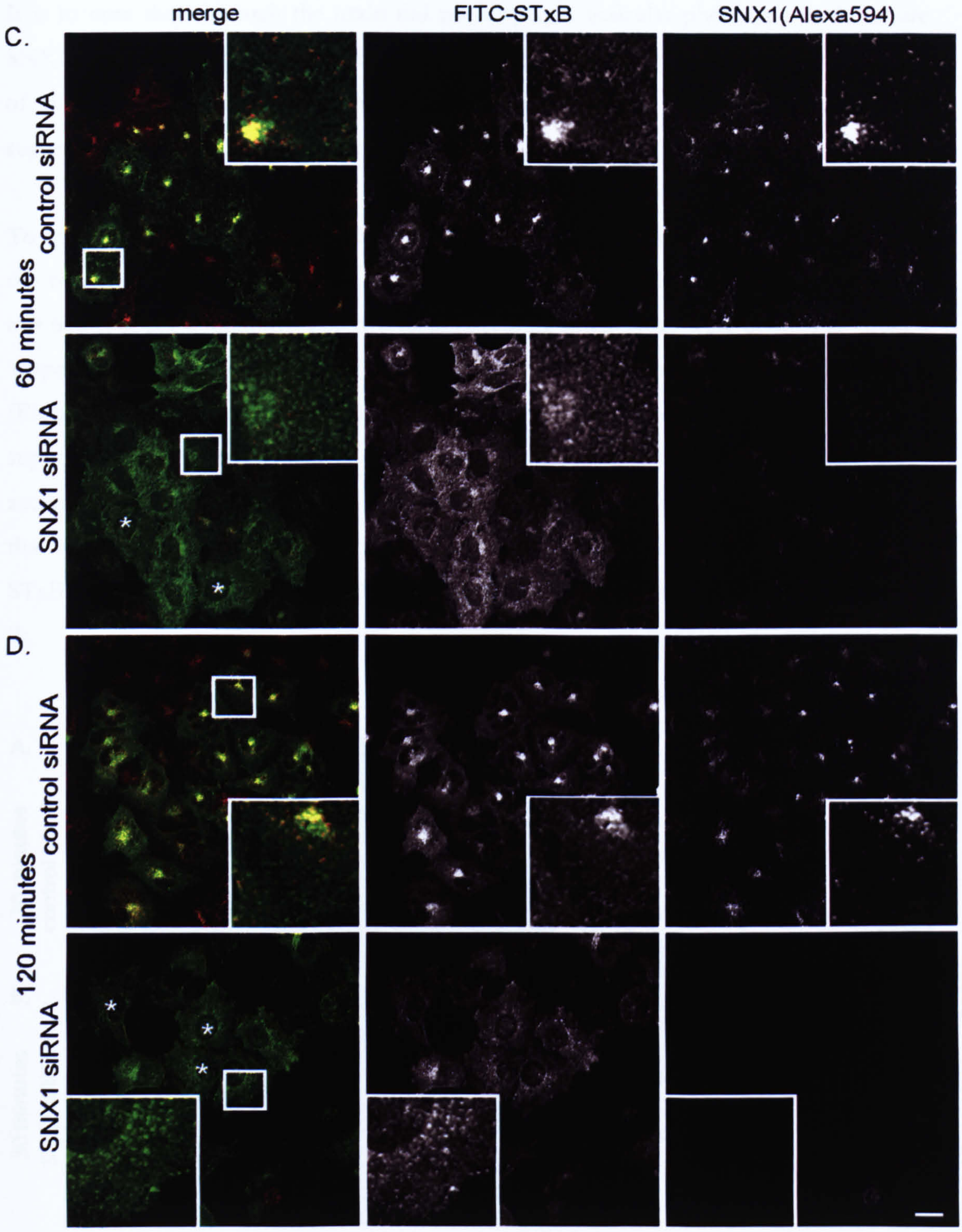

Figure 4.8 (Cont.) **In SNX1-suppressed cells, endosome-to-TGN transport of STxB is perturbed.**

HeLa cells treated with indicated siRNAs were subjected to FITC-STxB uptake assays, fixed at indicated times and immuno-labelled for SNX1 (Alexa594, red channel). Compared to control cells, in SNX1-suppressed cells, only moderate amounts of FITC-STxB had accumulated at the TGN after 60 min (C) and 120 min (D) and the majority still displayed a punctate distribution (asterisks). Scale bar is 20 μm.

It is to note that although the toxin did not display a vesicular phenotype in the entire SNX1-suppressed population, it was evident that cells displaying a perinuclear enrichment of the toxin also possessed a comparably high proportion of vesicular STxB. This suggested that also in those cells, transport kinetics were partially altered.

To quantify this effect, I scored the frequency with which I observed the appearance of the two distinct morphologies at single-cell level using epifluorescence microscopy (for n > 600 cells per condition). The two distinct scoring phenotypes were defined as either a 'dispersed' appearance (**Figure 4. 9,** asterisk), or a tight juxtanuclear toxin enrichment (**Figure 4. 9,** marked with an x). A rigid scoring criterion was applied; even SNX1-suppressed cells with remaining perinuclear enrichment but more prominent TGN accumulation were assigned to the latter category. This type of 'analogue analysis' revealed that after 30 minutes, 55% of control cells showed a clear TGN-like enrichment of the STxB, whereas only 33% of SNX1-suppressed cells displayed this phenotype (**Figure** 4. 9).

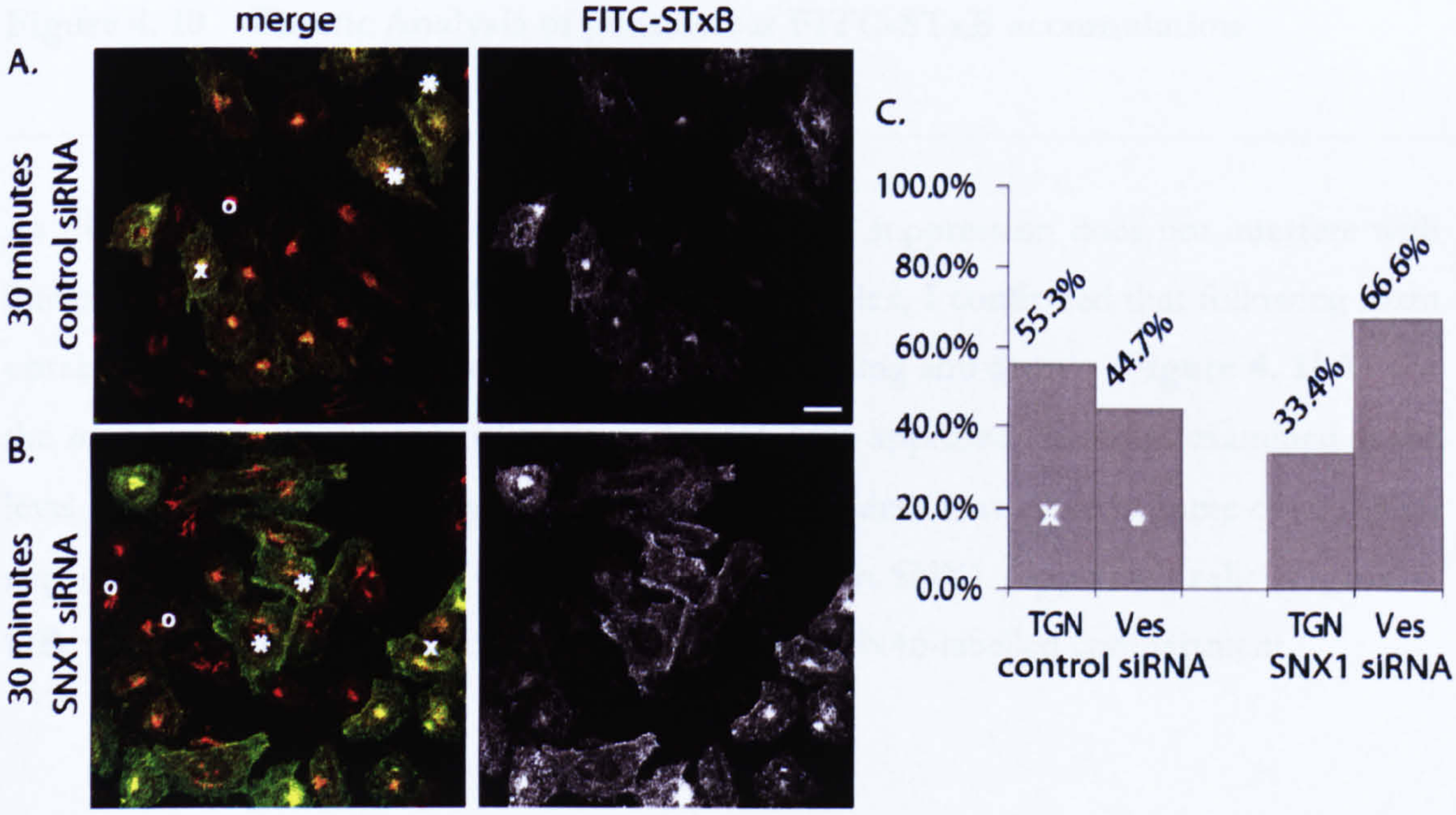

Figure 4. 9 Quantification of the reduced endosome-to-TGN transport of FITC-STxB in SNX1-suppressed cells.

Toxin uptake assays were performed in control and SNX1-suppressed HeLa cells as described. After fixation, samples were inspected by epifluorescence microscopy and scored 'blindly' for either a TGN-like enrichment (x) or a vesicular appearance (*). Cells marked with (o) were not scored because of low toxin levels. To clarify, not all scored cells are labelled. (A) and (B) illustrate the scoring phenotypes; with FITC-STxB in the green channel and TGN46 (Alexa594) in the red channel for control and SNX1-suppressed cells after 30 minutes uptake. (C) Representative data for a set of control and SNX1-suppressed cells (n > 600) after 30 minutes toxin uptake.

This type of analogue analysis allowed me to define the kinetics of endosome-to-TGN transport of STxB by scoring the FITC-STxB distribution in both, control and SNX1-suppressed cells for different time points (**Figure 4. 10**).

It was apparent from these assays that over the course of 2 hours the percentage of cells with a perinuclear enrichment did not change notably, indicating that in a subset of cells STxB transport to the TGN was stalled.

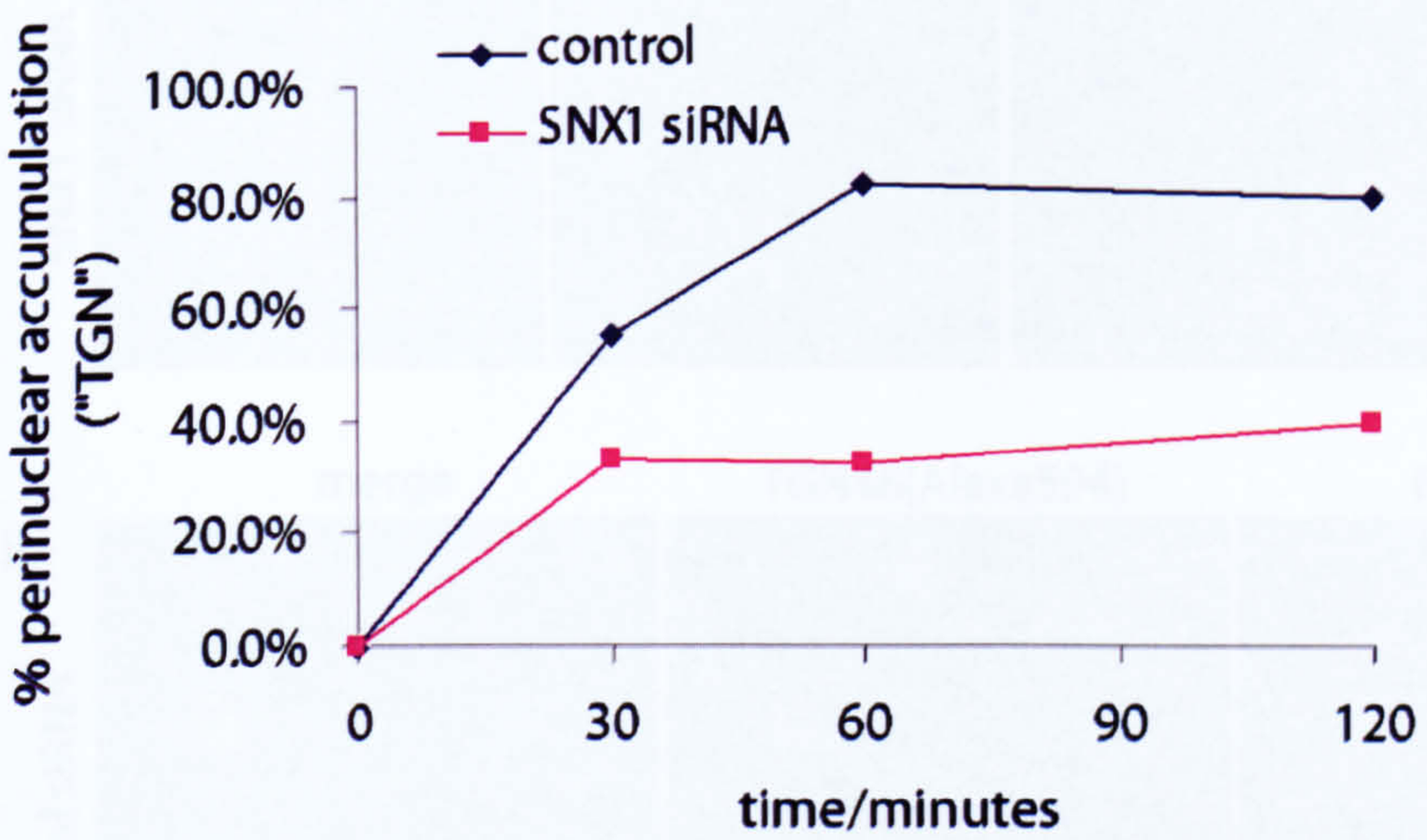

Kinetic Analysis of perinuclear FITC-STxB transport
Using epifluorescence microscopy, FITC-STxB accumulation in the perinuclear area was scored in control and SNX1-suppressed cells after 30, 60, 120 min uptake (n > 600 for each time point).

Figure 4. 10 Kinetic Analysis of perinuclear FITC-STxB accumulation

As this assay is based on the assumption that SNX1 suppression does not interfere with integrity of the target organelle, *id est* the Golgi complex, I confirmed that following toxin uptake, neither the *cis*- and *medial*-Golgi as labelled using anti-giantin (**Figure 4. 11 A**) nor the *trans*-Golgi network as labelled using anti-TGN46 appeared altered as examined at the level of light microscopy (**Figure** 4. 11 **B**). It was evident that while in some cases, STxB appeared co-localized with TGN46 to some extent in SNX1-suppressed cells (**Figure 4. 11B, inset**), the majority not co-localized with the TGN46-labelled compartment.

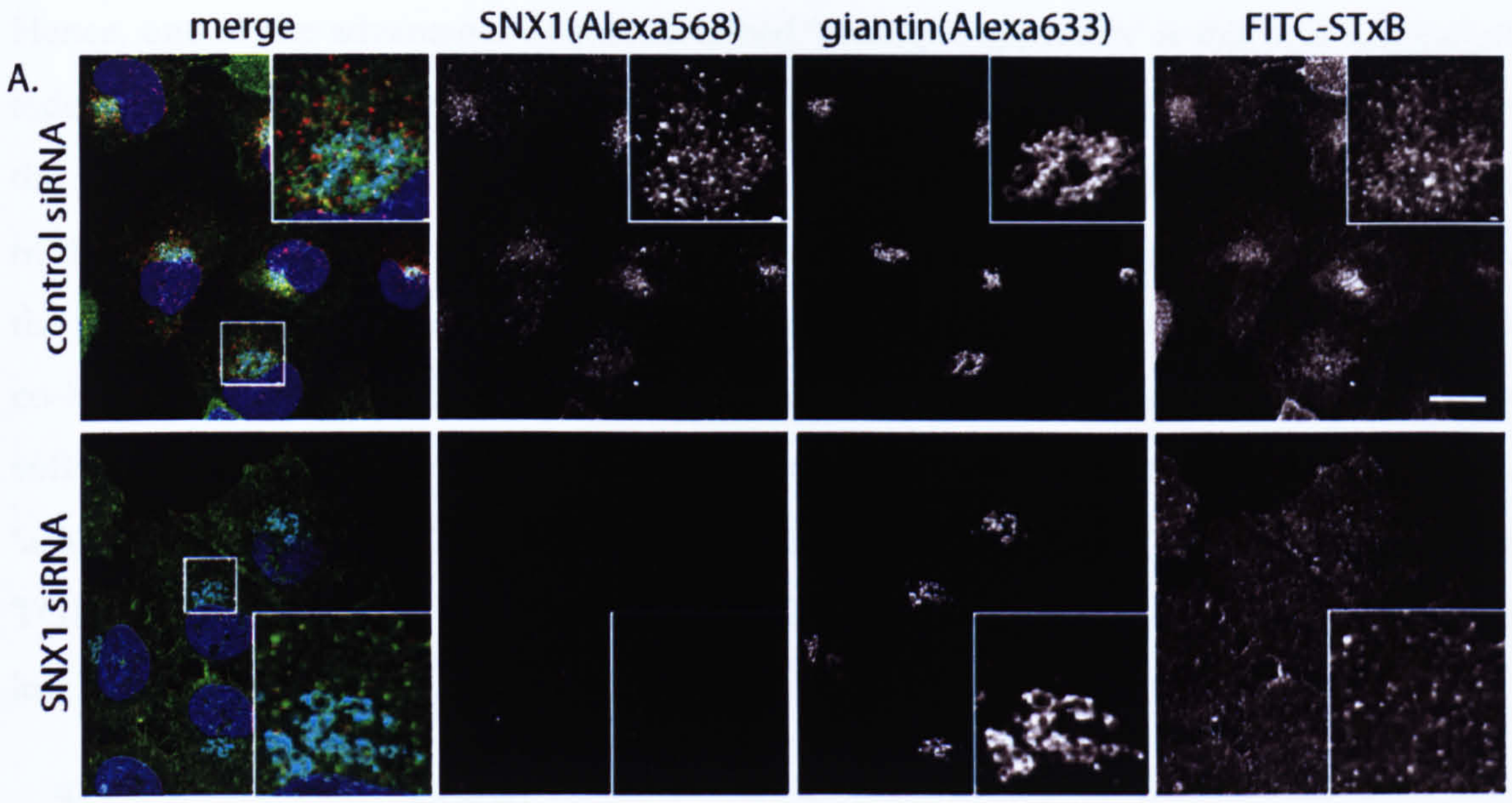

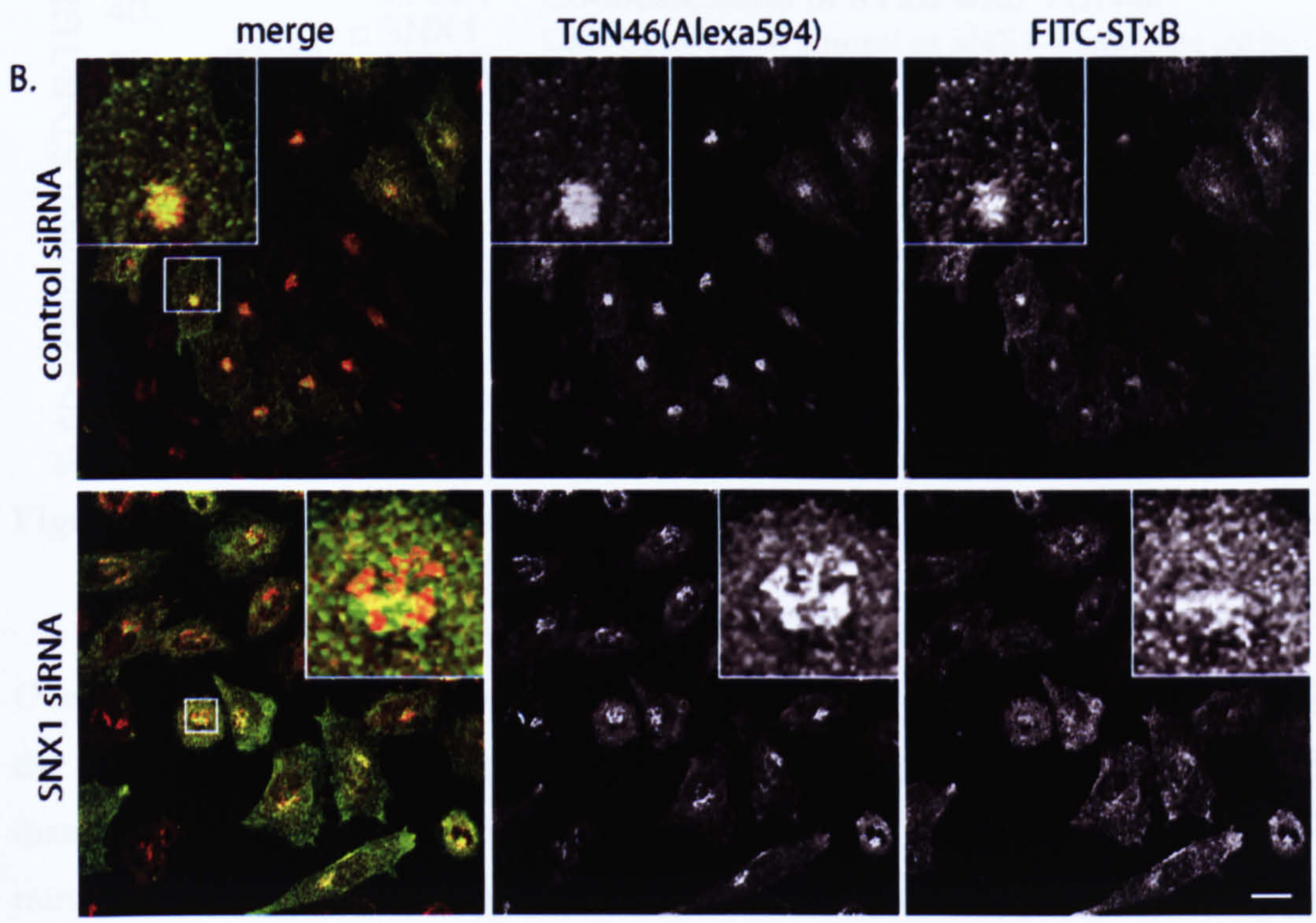

Figure 4. 11 SNX1-suppression does not grossly perturb Golgi/TGN appearance. Control and SNX1-suppressed cells were subjected to a toxin uptake assay with FITC-STxB (green channel) for 30 minutes and then fixed. (A) Cells were immuno-labelled for SNX1 (Alexa594) and giantin (Alexa633, cyan channel), a marker of the *cis*- and *medial*-Golgi complex. (B) Cells were immuno-labelled for TGN46 (Alexa633, red channel). Scale bar is 20 μm.

Hence, one of the advantages of the described 'analogue approach' is that it is somewhat independent of marker proteins, in contrast to a digital co-localization approach that uses the marker as a reference point. On the other hand one could interject that the definition of the two phenotypes is somewhat arbitrary, although I took great care to carefully define the phenotypes. Thus, I additionally thought to substantiate these findings by analysing the co-localization STxB with TGN46 using a digital imaging analysis approach (MetaMorph software, Molecular Devices). This method confirmed the results from the 'analogue 'analysis, showing that 12% ± 1% (s.d.) of internalized FITC-STxB co-localized with TGN46 after 30 minutes of internalization in SNX1-suppressed cells, which was markedly less than in control cells (37% ± 0.4% s.d.).

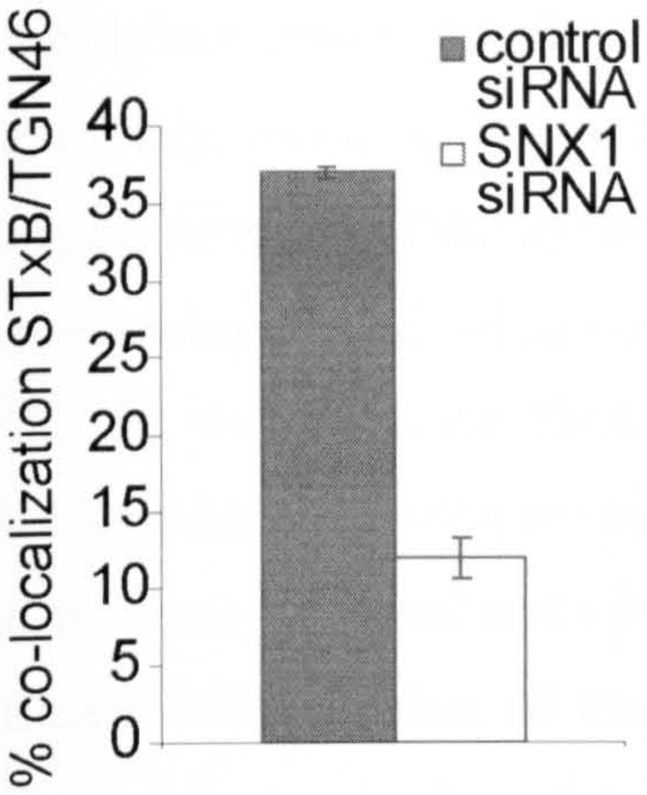

Co-localization of STxB with TGN46
Cells treated with control or SNX1-suppressed siRNA were subjected to FITC-STxB uptake assays, fixed after 30 minutes and immuno-labelled with anti-TGN46. To quantify co-localization, 8 - 10 confocal sections of several visual fields were analysed using MetaMorph software, determining co-localization per individual z-section. In control cells, 37% ± 0.4% (s.d.) STxB co-localized with TGN46; SNX1-suppressed cells showed 12% ± 1% (s.d.) co-localization (s.d. determined from mean for individual visual fields for a total of n > 50 cells).

Figure 4. 12 Co-localization of STxB with TGN46 is markedly reduced in SNX1-suppressed cells

Overall, these data are therefore consistent with a model in which SNX1 is required for the efficient transport of Shiga toxin between the early endosome and the TGN, in a manner that under conditions of SNX1-suppression the rate of endosome-to-TGN transport of the toxin is markedly reduced. These assays do however not provide a functional evidence for delivery to the TGN. These issues were tackled in **para. 4.4.3** using a biochemical approach.

4.5.2. Functional analysis of the role of sorting nexins in STxB transport to the TGN

To further examine whether delivery to the TGN was dependent on SNX1, I employed a methodology that couples the arrival of the toxin B subunit at the TGN to a biochemical reaction, which can subsequently be quantified, and hence give an indirect measure for the amount of toxin at the organelle.

For these assays, a modified Shiga toxin B subunit was used (B-Sulf$_2$) which has been genetically engineered to contain a tandem tyrosine sulfation site (Mallard et al., 1998). Since protein sulfation specifically occurs at the level of the TGN (Baeuerle and Huttner, 1987; Niehrs and Huttner, 1990), the degree of sulfation, measured as incorporation of [35S]sulphate provides a direct read-out for the amount of B subunit at the organelle. Importantly, insertion of a sulfation site into the B subunit does not appear to alter its transport properties (Mallard et al., 1998).

In these assays, I decided not only to examine sulfation in SNX1-suppressed cells, but also SNX2, as well as jointly SNX1- and SNX2-suppressed cells. The day before the assay, siRNA treated cells were re-seeded to ensure identical cell numbers for all conditions, but also to obtain identical wells for paralleled duplicate analysis (see **para. 4.3.1**). To ensure sufficient incorporation of the radioactively labelled [35S]-sulphate, siRNA-treated cells had to be depleted of non-labelled sulphate by incubating them in sulphate-free medium (see also **para. 4.3.1**). Then, B-(Sulf$_2$) was allowed to bind to the cell surface. After extensive washes to remove unbound toxin subunit, cells were transferred into pre-warmed medium (37°C) containing [35S]-sulphate for 20 minutes, which allows for measuring initial arrival of the toxin at the TGN (as determined by IF analysis). Cells were subsequently lysed and radioactively labelled B-(Sulf$_2$) was captured by performing an immunoprecipitation (IP) using STxB-specific antibodies. Ultimately, following SDS-PAGE, the incorporated radioactivity was determined from autoradiographs by volume integration (see also **Figure 4.** 13 B; inset). Importantly, I also determined the levels of endogenous sulfation under these conditions: sulphated proteins were acid-precipitated from the IP supernatants, then retained on glass fibre filters and radioactivity was measured by scintillation counting. This serves as an internal control of the experiment as well as it allows normalization of the sulfation data (compare **para. 4.3.2** for details).

For all assays performed, I routinely determined achieved protein suppression levels of cells treated with the respective siRNAs by Western blotting, confirming successful

suppression of protein expression in the entire cell population (**Figure 4. 13 A**). Cells from the same siRNA-treated batches were subsequently used for the sulfation assay.

To aid clarity, I chose to present the results for the respective siRNAs in consecutive order, starting with SNX1- (**para. 4.4.2.1**), followed by SNX2- (**para. 4.4.2.2**) and lastly, jointly SNX1- and SNX2-suppressed cells (**para. 4.4.2.3**). Some of the figures contain the pooled data for all conditions, as I felt it aids direct comparison and limits recapitulation of data.

4.5.2.1. Effect of a SNX1-specific siRNA on STxB sulfation

In these assays, I regularly observed a clear decrease in sulfation in SNX1-suppressed cells (**Figure 4. 13 B**). Band intensities of autoradiographs obtained from six independent assays, all in duplicates, were quantified using densitometry. The obtained values were normalized to overall protein sulfation (**para. 4.3.2**) and normalized to control values being deemed 100% (**Figure 4. 13 B**). Compared to these, the degree of sulfation was clearly reduced [57% ± 24.4% (s.d.)] in SNX1-suppressed cells, indicating that endosome-to-TGN transport was effectively, but not completely, blocked in these cells. Nonetheless, in some instances, I observed that even comparably high levels of SNX1 suppression did not result in a marked inhibition of STxB sulfation. This prompted me to determine to which extend the level of SNX1 suppression influences the retrograde transport. Hence, in an attempt to correlate suppression efficiency with B-($Sulf_2$) sulfation state, I compared achieved levels of siRNA-mediated suppression of each experimental set (x-axis) with the corresponding levels of B-($Sulf_2$) sulfation for the respective experiments (**Figure 4. 13 C**). From these experiments, I concluded that only suppression levels greater than 92% lead to marked sulfation inhibition, whereas suppression levels lower than 89% did not lead to a clear sulfation. Hence, without these 'ineffective' levels, sulfation in the four sets (in duplicate) with suppression levels greater than 92% is reduced to 46.3% ± 13.05% (s.d.) (**Figure 4. 13 C,** pink closed triangles). These results further supported the model of a critical but minimal threshold level of SNX1 to maintain efficient endosome-to-TGN transport.

4.5.2.2. Effect of a SNX2-specific siRNA on STxB sulfation

When I embarked on the toxin traffic project described in this chapter, a role for SNX2 in intracellular sorting was still elusive. As described in Chapter 3, SNX2 appeared to play only a minor role in promoting endosome-to-TGN transport of the CI-MPR. Thus I hoped to get further insights into SNX2 function using this quantitative biochemical assay. When I carefully quantified the levels of SNX2 suppression using densitometry (**Figure** 4. 13 **A**), I found a reduction of cellular SNX2 to 81.3% ± 6.64% (s.d., n = 6) of control cells. This marked reduction resulted in a sulfation inhibition of B-($Sulf_2$) of 78% ± 26.7% (s.d., n = 6 in duplicate), which was considerably less compared to the effect of SNX1 suppression on toxin sulfation (**Figure 4. 13 B**). Looking at the experimental sets individually, in 10 out of 12 individual data sets, the levels of B-(Sulf2) sulfation exceeded the levels observed under SNX1-suppressed conditions, after normalisation for global sulfation. Notably, even when suppression was greater than 91%, sulfation was not further inhibited, as it was observed for SNX1. From these biochemical assays, it thus appeared that SNX2 slightly, and less robustly (compare s.d.) affected endosome-to-TGN transport of STxB.

One problem I noticed early on, and have already discussed in Chapter 3, was that cell batches treated with SNX2 siRNA had lower cell counts after 72 hours. As lower cell numbers would affect the biochemical readout, I tried to compensate the effect by re-seeding equal cell numbers for all conditions the night before the assay. Unfortunately, there is no direct 'input' control to normalize the sulfation signal against. It is pertinent to note that the levels of sulfation of endogenous proteins were also slightly reduced. Thus, I was concerned that the reduction in sulfation was also attributable to reduced cell numbers. This prompted me to further investigate the effect of SNX2-suppression on STxB transport using microscopy techniques.

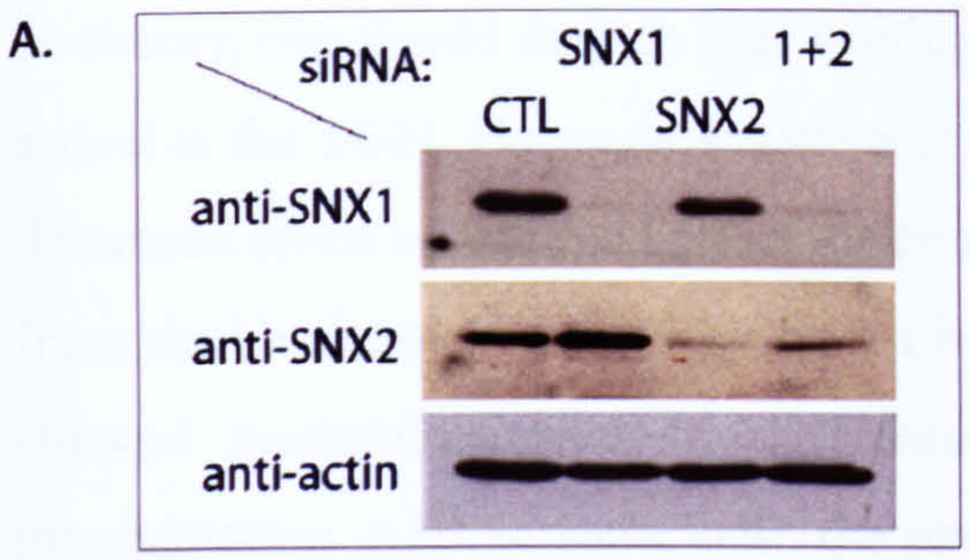

siRNA	SNX1	SNX2	SNX1+SNX2	
average	91.4	81.3	93.2	58.2
STDEV	4.23	6.64	6.80	11.61

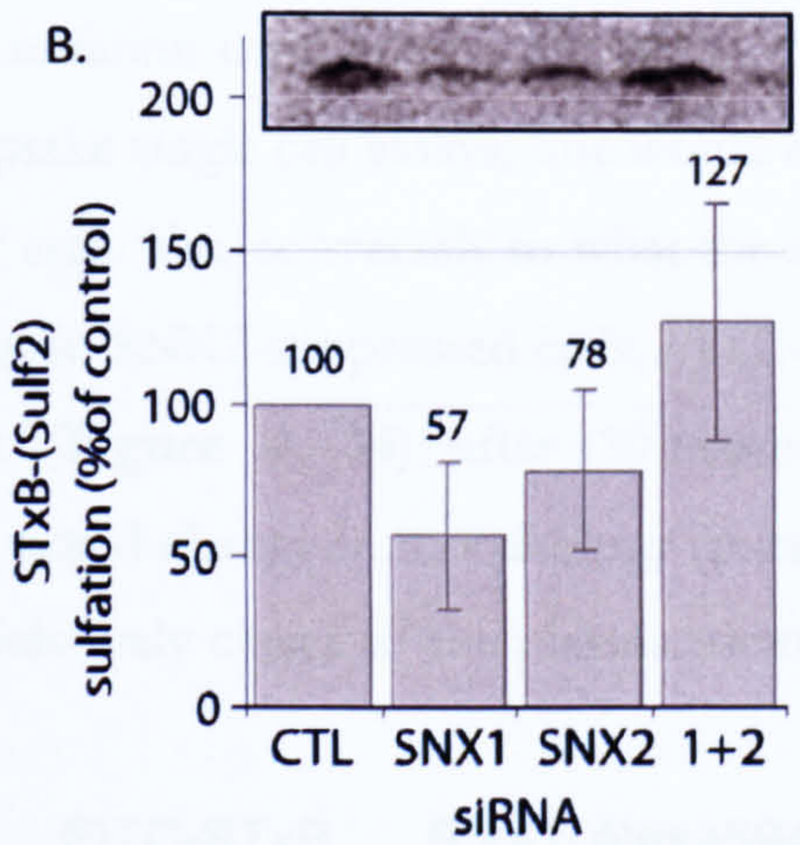

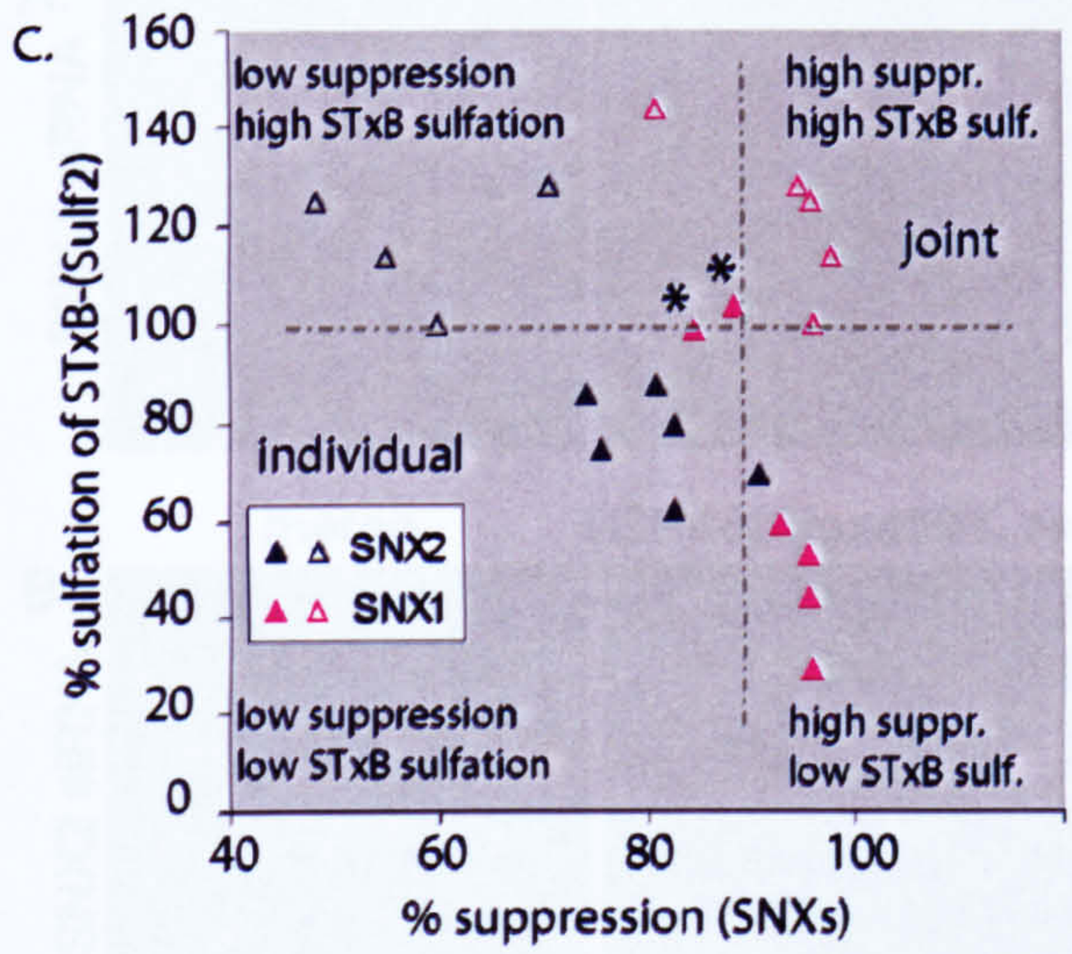

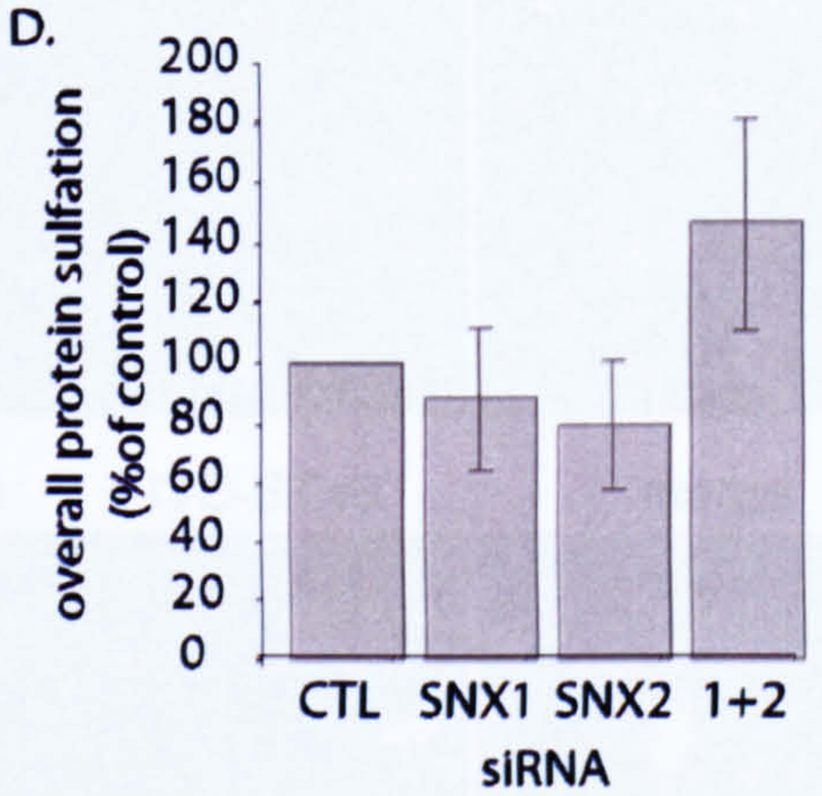

Figure 4. 13 Analysis of STxB sulfation in SNX1- and SNX2-suppressed cells.

(A) Representative Western blots showing levels of siRNA-mediated protein suppression. The table summarizes achieved levels of suppression quantified using ImageQuant from $n \geq 4$ assays ($n = 6$ for SNX1 and SNX2 individually). **(B)** The autoradiograph (inset) shows a typical result of a sulfation experiment using the B-($Sulf_2$) construct. The graph below summarizes results from $n = 6$ for SNX1 and SNX2, $n = 4$ for SNX1+SNX2 (each in duplicate) as percentage of control. Autoradiographs were quantified by densitometry and normalized to overall levels of protein sulfation. In SNX1-suppressed cells, sulfation was reduced by 43% ± 24.4% (s.d.) compared to control cells, whereas in SNX2-suppressed cells sulfation was reduced by 22% ± 26.7% (s.d.). In contrast, sulfation of STxB in jointly suppressed cells was increased to 127% ± 39.2% (s.d.). **(C)** Levels of siRNA-mediated suppression as determined by Western blotting and quantified by densitometry were plotted against the levels of STxB sulfation (each data point represents mean from duplicates, normalized to global sulfation) for six experimental sets (pink triangles: SNX1 siRNA , blue triangles: SNX2 siRNA; solid for individual, open for joint suppression). Lower levels of SNX1-suppression (< 90%) do not result in reduced sulfation (marked with asterisks). The regions were determined using the highest suppression level for SNX1 (x-axis) that was found not to induce a reduction in STxB sulfation (100%, y-axis). **(D)** Graph shows mean levels (± s.d.) of overall protein sulfation for the different siRNA conditions from at least five different experiments (in duplicates).

In theory, one would deduce that a reduction in sulfation correlates with a reduced toxin arrival at the TGN. Hence, in fluorescent toxin-uptake single cell assays, one would expect decreased levels of FITC-STxB in the perinuclear area. Yet, conversely to what the results from the biochemical assay suggested, I found that in SNX2-suppressed cells, FITC-STxB showed predominantly perinuclear enrichment (**Figure 4. 14**) after 30 minutes of internalisation. And, in some cells, the previously noted change in morphology (**para. 3.5**) was noted to result in the TGN being localized relatively closer to the plasma membrane (Figure 4. 14 B, ROI2).

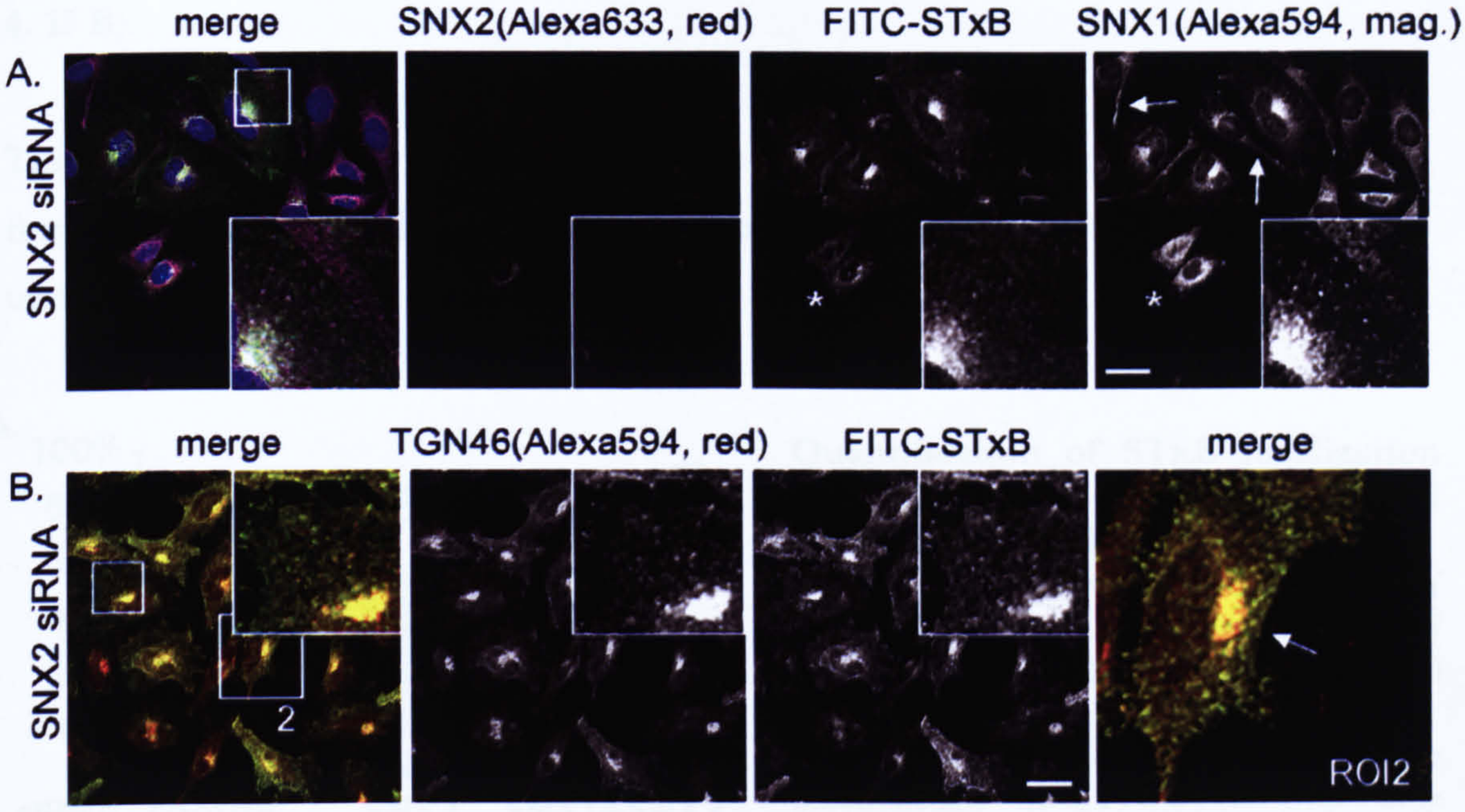

In cells treated with SNX2-specific siRNA, FITC-STxB is localized to the TGN.

Surface-bound FITC-STxB (green) was internalized into SNX2-suppressed cells for 30 min (see **para. 4.3.3**). Cells were fixed and immuno-labelled using (A) anti-SNX2 (Alexa633, red) and anti-SNX1 (Alexa594, pseudo-coloured in magenta), or (B) using anti-TGN46 (Alexa594, red). SNX2 was successfully suppressed as indicated by the absence of signal. In these cells, STxB showed enrichment at the TGN, as indicated by the co-localization with TGN46. Arrow in ROI2 highlights closeness of TGN to plasma membrane. (C) Co-localization with TGN46 in confocal images from n > 50 cells was quantified using MetaMorph. For each cell, co-localization in 8 - 10 z-sections was analysed, s.d. was determined from mean for individual visual fields. See also **Figure 4. 12.**

Figure 4. 14 In cells treated with SNX2-specific siRNA, FITC-STxB is localised to the TGN.

Indeed, when I analysed the co-localization between internalized FITC-STxB and TGN46, I found that in control cell, 37% ± 0.4% (s.d.) of STxB co-localized with the TGN marker (see also **Figure 4. 12**), while in SNX2-suppressed cells 40% ± 8% (s.d.) did. Consistently, in these cells, I failed to observe a marked vesicular distribution of the toxin; when I scored the frequency with which I observed the previously characterised morphologies (being either a TGN-like enrichment or vesicular) I could not distinguish between control and SNX2-suppressed samples (**Figure 4. 15 A**). Further still, the kinetics of FITC-STxB transport to the TGN were indistinguishable for the two samples (**Figure 4. 15 B**).

Taken together, the data obtained from single-cell immunofluorescence analysis suggests that SNX2 suppression does not markedly alter retrograde transport of STxB, at least not under these experimental conditions.

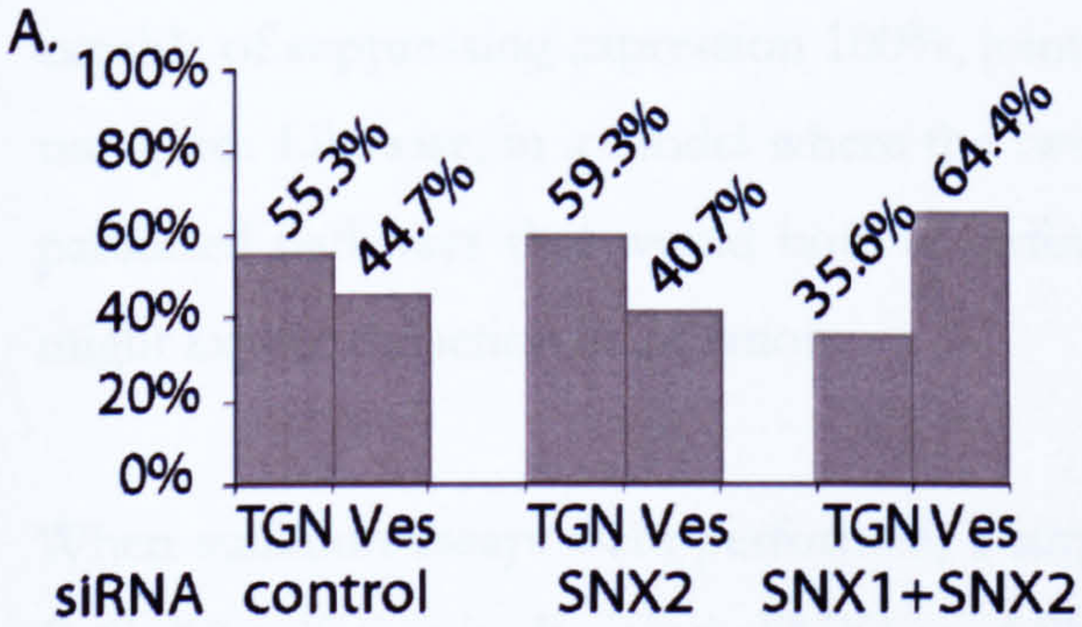

Quantification of STxB localization in SNX2- and jointly SNX1- and SNX2-suppressed cells.
(A) The TGN- or vesicular appearance of FITC-STxB was scored in siRNA-treated cells described in **Figure 4. 9** for n > 600 cells after 30 min toxin uptake.
(B) Representative data set for TGN-like accumulation of FITC-STxB over time (n > 600 for each sample; scored for 30, 60 and 120 minutes) for control cells and, individually and jointly, SNX1- (compare to **Figure 4. 10**) and SNX2-suppressed cells.

Figure 4. 15 Quantification of STxB localization in SNX2- and jointly SNX1- and SNX2- suppressed cells.

4.5.2.3. Effect of joint treatment with SNX1- and SNX2-specific siRNA on STxB sulfation

As discussed in Chapter 3, joint suppression of SNX1 and SNX2 lead to a marked redistribution of the CI-MPR and reduced endosome-to-TGN transport kinetics. Regarding retrograde transport of STxB, through results obtained by sulfation assays and immunofluorescence-based analysis, I concluded that STxB retrograde transport was notably dependent upon SNX1 expression but was less reliant on SNX2. Hence, it was tempting to investigate the effect of joint suppression on the retrograde transport of STxB transport: if the two proteins do not serve the same route, and differ in their function, one would at least expect the sulfation reduction observed for SNX1 suppression. Assuming that SNX1 and SNX2 interacted as complex on exactly the same pathway [as suggested from the 'retromer model' (Seaman, 2005; Pfeffer, 2001)], one may expect to see no further reduction in retrograde transport, assuming that both proteins acted 'unidirectionally' in a 'genetic null scenario'. As siRNA suppression was however not capable of suppressing expression 100%, joint suppression could further reduce retrograde transport. Likewise, in a model where the two sorting nexins were to act on different but paralleled pathways that would both contribute towards retrograde STxB transport, one might expect reduction in sulfation.

When sulfation assays were performed, I surprisingly observed a striking upregulation of B-($Sulf_2$) sulfation in the jointly SNX1- and SNX2-suppressed cells (**Figure 4. 13 B,C**).
In the course of these experiments, several other observations were made: when I quantified the suppression efficiency in these cells, I noticed that SNX2 suppression was even less prominent in the SNX1/SNX2 siRNA-treated cells, despite the same transfection protocol (**Figure 4. 13 A**). This gave rise to the question whether SNX2 expression was upregulated in SNX1-suppressed cells. Indeed, with the protocol used in this study, I found that SNX2 expression was slightly upregulated in SNX1-suppressed cells, but this effect was rather variable (median 123.8%, n = 4). Disappointingly, this apparent difference to previous findings (Carlton et al., 2004; Carlton et al., 2005b) can not be explained satisfactorily at this point; I suggest that it might be attributable to the different siRNA concentrations used in these studies[10]. This would imply that the transfection conditions and reagents used in this particular case would not compensate the

[10] NB: These findings are also at odds with the recent study from Rojas and colleagues (Rojas et al., 2007), which, obviously, for different protocols, can not be directly compared with the data presented here.

additionally produced protein. Nevertheless, from the proposed role for SNX2, it is not immediately evident how the weaker suppression of SNX2 in jointly suppressed cells may lead to an increase in sulfation; even more so in the light that in the jointly SNX1- and SNX2-suppressed cells I found SNX1 suppression to be greater than 90% (**Figure** 4. 13 **A,C**). Here, I did not observe an upregulation of SNX1 expression in SNX2-suppressed cells (96.6% of control (median); n = 6). Interestingly, in the majority of cases, levels of SNX1 suppression in the jointly suppressed cells even exceeded the levels achieved with SNX1 siRNA treatment alone (**Figure 4. 13 C**). Despite these high levels though, I failed to observe an effect on STxB sulfation (**Figure 4. 13 B**); accordingly, when I plotted achieved levels of suppression against the level of sulfation after correction for global sulfation, values were always greater than 100% despite the higher suppression levels for SNX1 (**Figure** 4. 13 **C**; open pink triangles = SNX1, open blue triangles = SNX2). Importantly, when I scrutinised the levels of endogenous sulfation, I noticed that joint SNX1 and SNX2 suppression lead to a substantial increase in global protein sulfation of cellular molecules to 147.7% ± 35.36% (n = 5 in duplicates) **(Figure 4. 13 D**). As mentioned, the data shown in **Figure 4. 13** (B) and (C) are already corrected for global sulfation. Hence, it is crucial to point out that even without this correction B-($Sulf_2$) sulfation values exceeded 100% in 9 out of 10 cases (87%).

Taken together, the augmented sulfation of B-($Sulf_2$) and endogenous proteins could be indicative for an enhanced delivery to the TGN under the jointly SNX1- and SNX2-suppressed conditions. As this data was not easy to reconcile with the results from the individual suppressions, I sought to examine the toxin localization under jointly suppressed conditions by microscopy using fluorescent toxin-uptake assays. I reasoned that if delivery was enhanced, I would see an increase in FITC-STxB at the TGN in these assays. However, when I examined jointly SNX1- and SNX2-suppressed cells after 30 minutes uptake of FITC-STxB, I failed to observe an increased TGN accumulation. In samples with joint SNX1 and SNX2 suppression, the toxin predominantly displayed a vesicular distribution (**Figure 4. 15 A)**, which was indistinguishable to the localization observed in SNX1-supressed cells (**Figure 4. 9 C**). Likewise, when I analysed the kinetics of toxin transport scoring the frequency of the previously characterized two distinct morphologies (**Figure 4. 9 A,B**), I could not discriminate between the jointly SNX1- and SNX2-suppressed cells and only SNX1-suppressed samples (**Figure 4. 15 B**).

From the results of the immunofluorescence analysis, it furthermore appears that SNX1-suppression is causative for the vesicular localization of STxB. Concordantly, in cells in which SNX1 is suppressed, SNX2 appears more dispersed compared to control cells after 30 minutes of FITC-STxB uptake (**Figure** 4. 16). In contrast, SNX1 displayed an equally compact juxtanuclear enrichment in control and SNX2-suppressed cells (**Figure 4. 14 A**).

One interpretation of the obtained results that would reconcile the predominantly vesicular distribution observed in single cell assays and the increase in sulfation (of both, B-($Sulf_2$) and endogenous proteins) is to propose that the sulfation machinery was mis-localised to endosomes in the jointly suppressed cells. Unfortunately, our attempts to confirm proper targeting of the tyrosylprotein sulfotransferases TPST1 and TPST2 by immunofluorescence analysis proved unsuccessful, as all commercially available antibodies were unsuited. Earlier attempts by the Johannes Lab to use a cDNA approach were hampered by the finding that ectopically expressed TPST1 was mis-localised to the ER (personal communication). Hence, at this moment in time confirmation of the correct

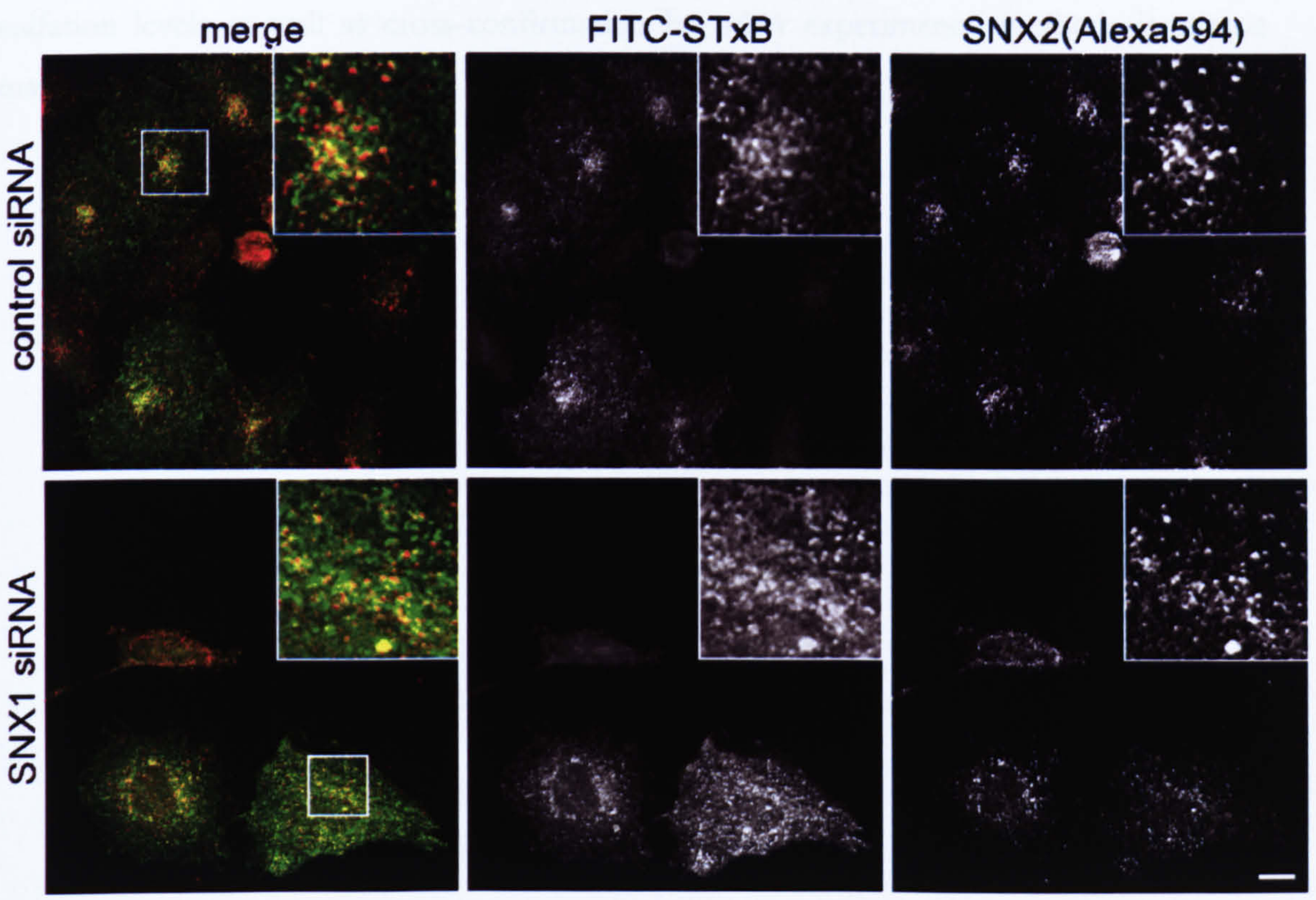

Figure 4. 16 Analysis of SNX2 localization after FITC-STxB uptake in cells treated with SNX1-siRNA

Control and SNX1-suppressed cell were subjected to a FITC-STxB uptake assay. The toxin was surface-bound at 4°C, then internalized at 37°C for 30 minutes. Fixed cells were immuno-labelled with anti-SNX2 (Alexa633, red channel). Scale bar is 10 μm.

localization of the sulfotransferases is not possible. Interestingly, the finding that downmodulation of certain proteins can affect endogenous sulfation levels has been observed before (Ludger Johannes, personal communication). Further still, a very recent study showed that in HEK 293 cells, SNX1 suppression altered level of sulfation of endogenous proteins in a similar assay investigating retrograde transport the plant cytotoxin ricin (Skanland et al., 2007). Importantly, in HeLa cells, I only observed an upregulation of overall protein sulfation in the jointly suppressed cells.

Overall, the data presented here is consistent with the conclusion that SNX1 is required for transport of STxB as its suppression led to a marked reduction in the transport of STxB to the TGN, and the retention of the toxin in vesicular structures. SNX2 appears to be less important in promoting the endosome-to-TGN 'retrograde' step of STxB, at least under the experimental conditions of this study.

These data furthermore illustrates that one has to take care when analysing data obtained by only one type of analysis; while the biochemical assay provides an elegant way to assess TGN delivery at the functional level, it shows that carefully monitoring the endogenous sulfation levels as well as cross-confirmation by other experimental methods is almost mandatory.

4.6. Investigations into the Role of VPS26 in Retrograde STxB Transport

I have not analysed the role of VPS26 in this process in detail; these assays were intended as further confirmation that the observed defect in endosome-to-TGN transport was specific and to see whether the process was retromer-dependent, as opposed to dependent only on SNX1.

In an analogous approach to the previous analyses (**para. 4.2.1 – 4.2.3**), cells were treated with VPS26-specific siRNA and subjected to both, fluorescent toxin-uptake assays using FITC-STxB and sulfation assays utilizing the B-($Sulf_2$) toxin subunit. The siRNAs were originally designed and characterized by Mr Vincent Popoff, *Institut Curie*, Paris, France.

As **Figure 4. 17 A** shows, in cells treated with control siRNA, VPS26 displayed a punctate pattern, and partially co-localized with FITC-STxB on vesicular structures in the perinuclear area. After 30 minutes uptake of FITC-STxB, most of the toxin was found juxtanuclearly displaying a TGN-like enrichment. In cells treated with the VPS26 siRNA, protein expression of VPS26 was successful as the absence of signal shows[11]. In these cells, FITC-STxB displayed clearly a vesicular pattern, reminiscent of the phenotype observed under SNX1-suppressed conditions. Like for SNX1, these vesicles partially co-localized with EEA1 (indicating the endosomal nature of these vesicles, data not shown). To quantify this effect, sulfation assays were performed. I found that B-$Sulf_2$ sulfation was markedly reduced to 38% ± 11.1% (s.d., n = 4 in duplicates) compared to control cells (**Figure 4. 17 B**). Examining the levels of endogenous sulfation, I noticed that sulfation of cellular components was reduced to 69% ± 31.4% (s.d., n = 4 in duplicates) (**Figure** 4. 17 **C**). This was a comparably high - but variable – degree. I suggest that this could in part be due to the previously observed fragmentation of the Golgi, including TGN under VPS26 suppressed conditions, as indicated by labelling using anti-TGN46 and GM130 (Seaman, 2004). While in these cells, a CD8-CI-MPR construct was still targeted to the TGN fragments (Seaman, 2004), indicating correct 'targeting', one could surmise that this might interfere with TPST function, which, for the outlined reasons (**para. 4.4.2.3**), I was unable to address.

---

11 Suppression was regularly confirmed by SDS-PAGE/Western blot analysis from whole-cell lysates and confirmed the reduction in VPS26 protein levels.

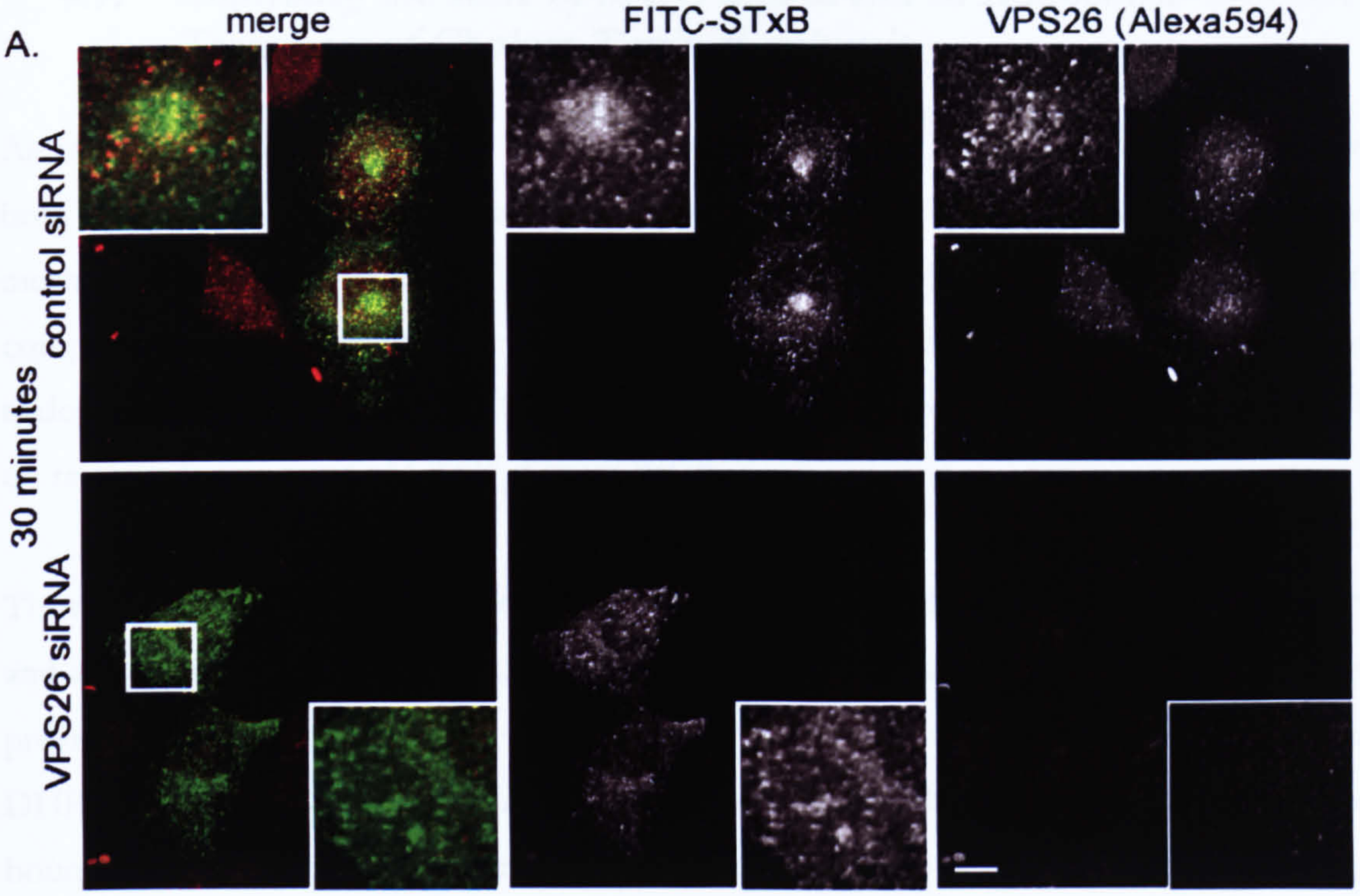

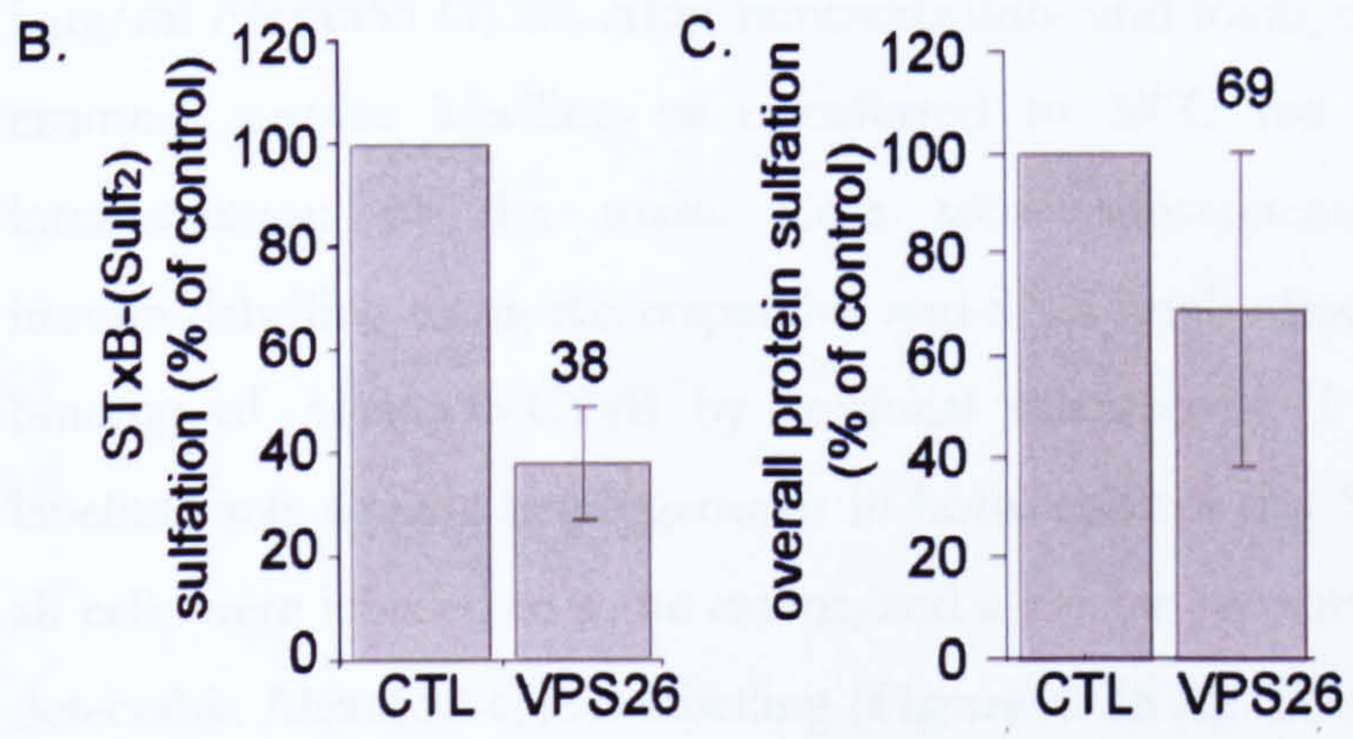

Figure 4. 17 Suppression of VPS26 perturbs endosome-to-TGN transport of STxB

(A) Cells treated with either control or VPS26-specific siRNA were subjected to a FITC-STxB uptake assay. After 30 min, cells were fixed and labelled with anti-VPS26 (Alexa594, red). VPS26 expression was successful, as indicated by the absence of signal in VPS26-suppressed cells, where FITC-STxB displays a vesicular distribution. Scale bar is 10 μm. (B) Control and VPS6-suppressed cells were subjected to a sulfation assay using the modified B-($Sulf_2$) subunit. Graph shows average from n = 4 assays (in duplicate) adjusted for overall sulfation of endogenous proteins and normalized to control (± s.d.). (C) Global sulfation under control and VPS26-suppressed conditions from n = 4 assays (in duplicate, ± s.d).

4.7. Analysing the Role of SNX1 and SNX2 in Endosome-to-TGN Transport of Cholera Toxin B-subunit

As outlined in the introduction of this chapter (**para. 4.1**), Shiga and cholera toxin are both AB_5-toxins, and have been proposed o enter the TGN via "indistinguishable mechanisms" (Nichols et al., 2001) regarding GPI-positive intermediates. However, compared to Shiga toxin, not much is known about the mechanisms involved in endosome-to-TGN transport of CTxB. This prompted me to examine the effect of SNX1 on retrograde transport of CTxB in more detail.

Thus, I adapted the previously described STxB assays to study retrograde CTxB transport and a fluorescent toxin-uptake assay using Alexa555-CTxB (Invitrogen) was developed. As previously, cell treated with the respective siRNA for 72 hours were incubated in cold DHB medium on ice to stop intracellular transport. The fluorescent toxin subunit was bound to the cell surface for 30 minutes by incubating in ice-cold DHB media containing 1 μg/ml Alexa555-CTxB. After removing unbound toxin, cells were either fixed directly to examine surface labelling or transferred to 37°C for the indicated times to allow internalization of the toxin. Cells were subsequently fixed and processed for immunolabelling using the respective anti-SNX antibodies. When I examined the surface binding of Alexa555-CTxB by confocal microscopy, I noticed that Alexa555-CTxB-labelling was equally heterogeneous in both, control and SNX1-suppressed samples. Not all cells were labelled to same extent, and a similar proportion displayed no or less readily detectable Alexa555-CTxB labelling (**Figure 4. 18 A**). This most likely reflects the cell-to-cell variability of plasma membrane content of the CTxB receptor GM1 (Pang et al., 2004). Importantly though, examining the cells visibly labelled with Alexa555-CTxB, I could not distinguish between plasma membrane-labelling of Alexa555-CTxB in control and SNX1-suppressed samples (**Figure 4. 18 A**). I concluded that SNX1 suppression did not affect GM1 levels at the plasma membrane.

After internalizing Alexa555-CTxB for 15 minutes, the subunit showed extensive co-localization with SNX1-positive structures in control cells, with a slight enrichment in the perinuclear area. This distribution of Alexa555-CTxB was not markedly different in SNX1-suppressed cells (**Figure 4. 18 B**).

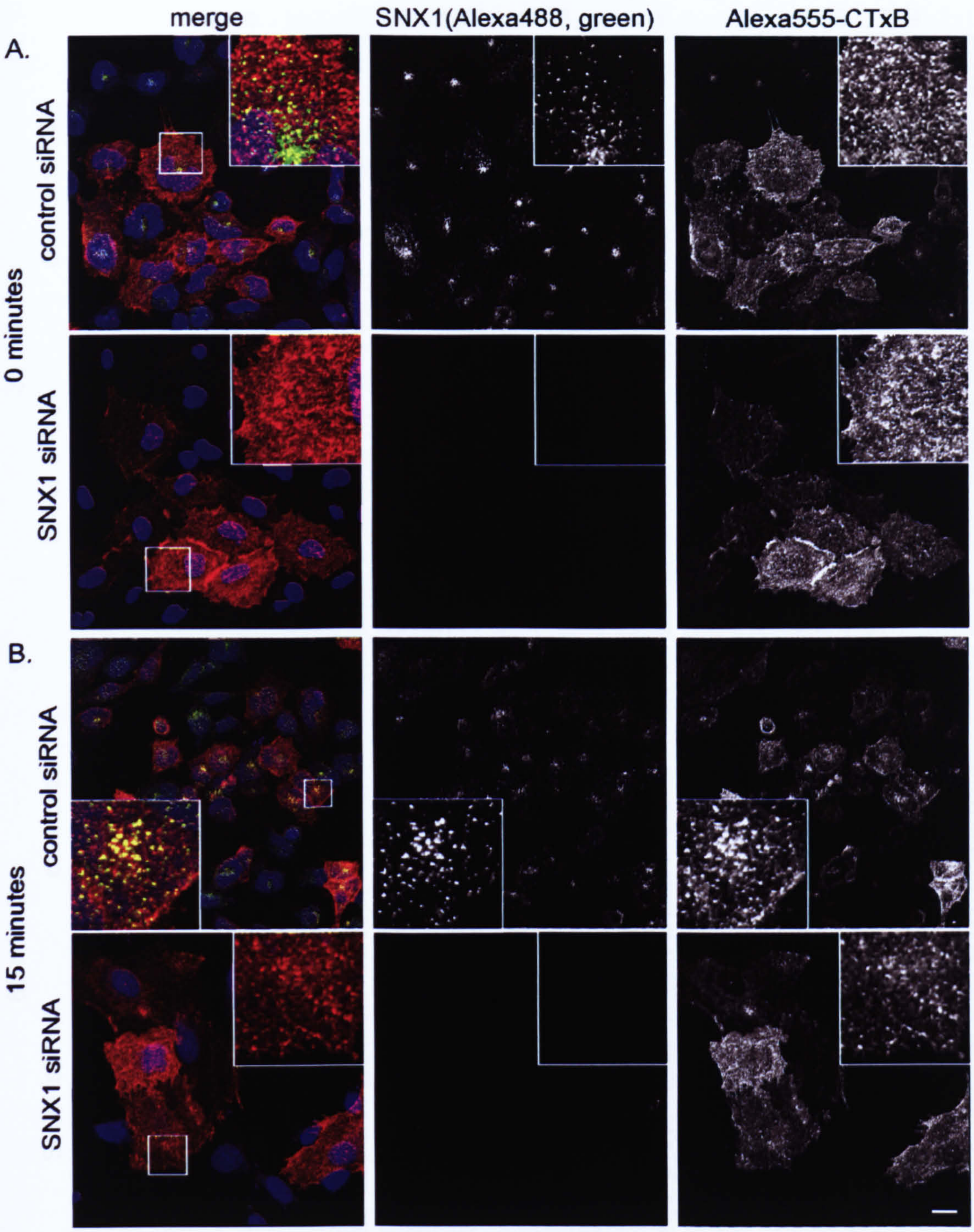

Figure 4. 18 Retrograde transport of CTxB appears to be unaffected by SNX1 suppression

Control and SNX1-suppressed cell were subjected to an Alexa555-CTxB uptake assay. The toxin subunit was surface-bound at 4°C, then cells were either fixed directly (A), or after internalization of Alexa555-CTxB at 37°C for 15 min (B). Fixed cells were immuno-labelled with anti-SNX1 (Alexa488, green channel) and imaged using confocal microscopy. Scale bar is 20 μm.

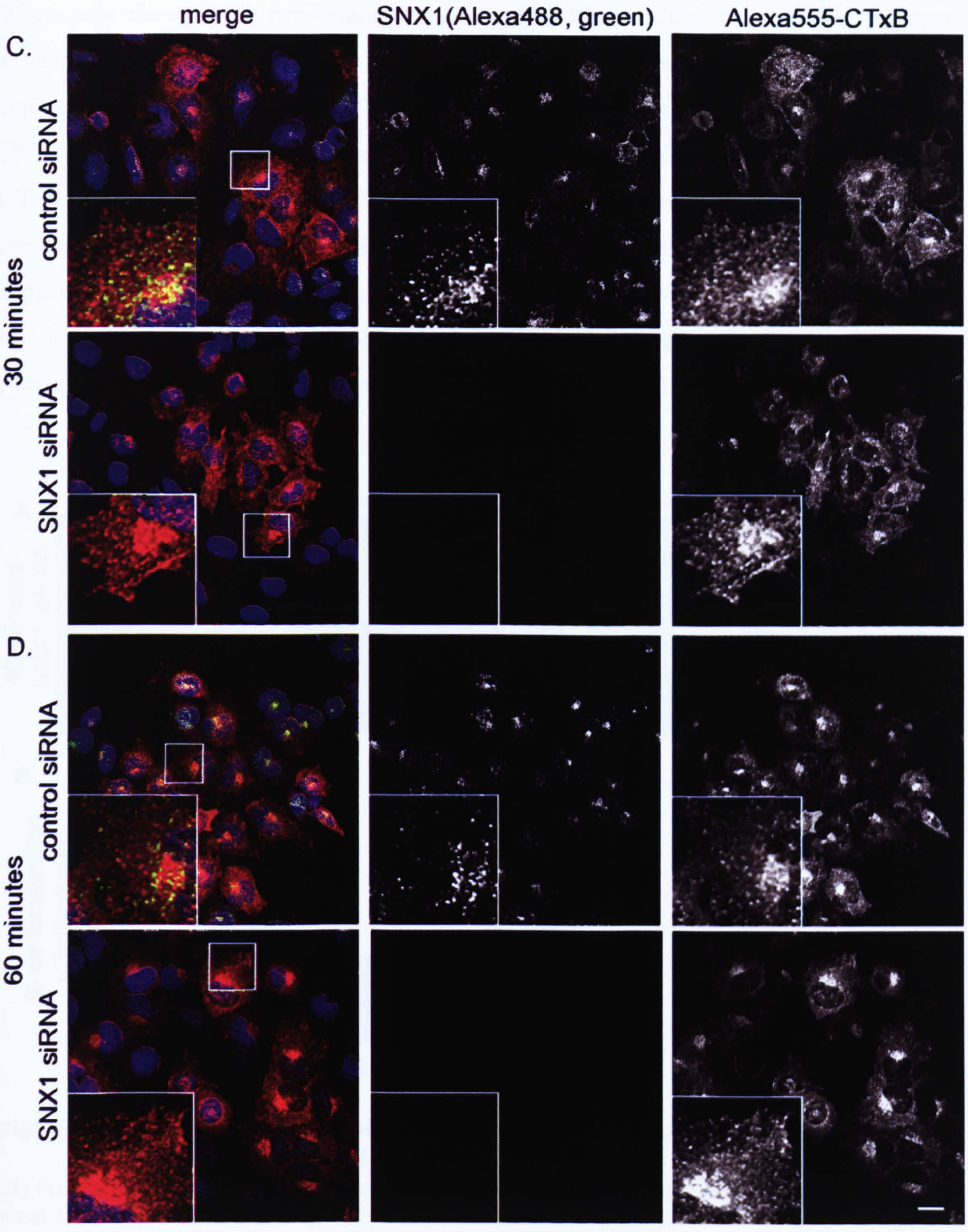

Figure 4.18 (cont'd) Retrograde transport of CTxB appears to be unaffected by SNX1 suppression

Control and SNX1-suppressed cell were subjected to an Alexa555-CTxB uptake assay (red channel). The toxin subunit was surface-bound at 4°C, then internalized of Alexa555-CTxB at 37°C for either 30 min (C) or 60 min (D). Fixed cells were immuno-labelled with anti-SNX1 (Alexa488, green channel). Scale bar is 20 μm.

When cells where fixed after longer periods of internalisation, the toxin subunit displayed similar degrees of enrichment in the perinuclear area in control compared to SNX1-suppressed cell (**Figure 4. 18 B,C**). This finding suggested that unlike the case for STxB, SNX1-suppression did not markedly perturb endosome-to-TGN transport of Alexa555-CTxB. I confirmed that the perinuclear enrichment of toxin corresponded to the Golgi complex by immuno-labelling with anti-giantin (following 40 min toxin uptake in SNX1-suppressed cells; **Figure 4. 19 A**). This type of experiments also allowed me to quantify the degree of co-localization of Alexa555-CTxB with the Golgi marker giantin using two previously described approaches (**para. 4.3.5**; **Figure 4. 9 A,B**).

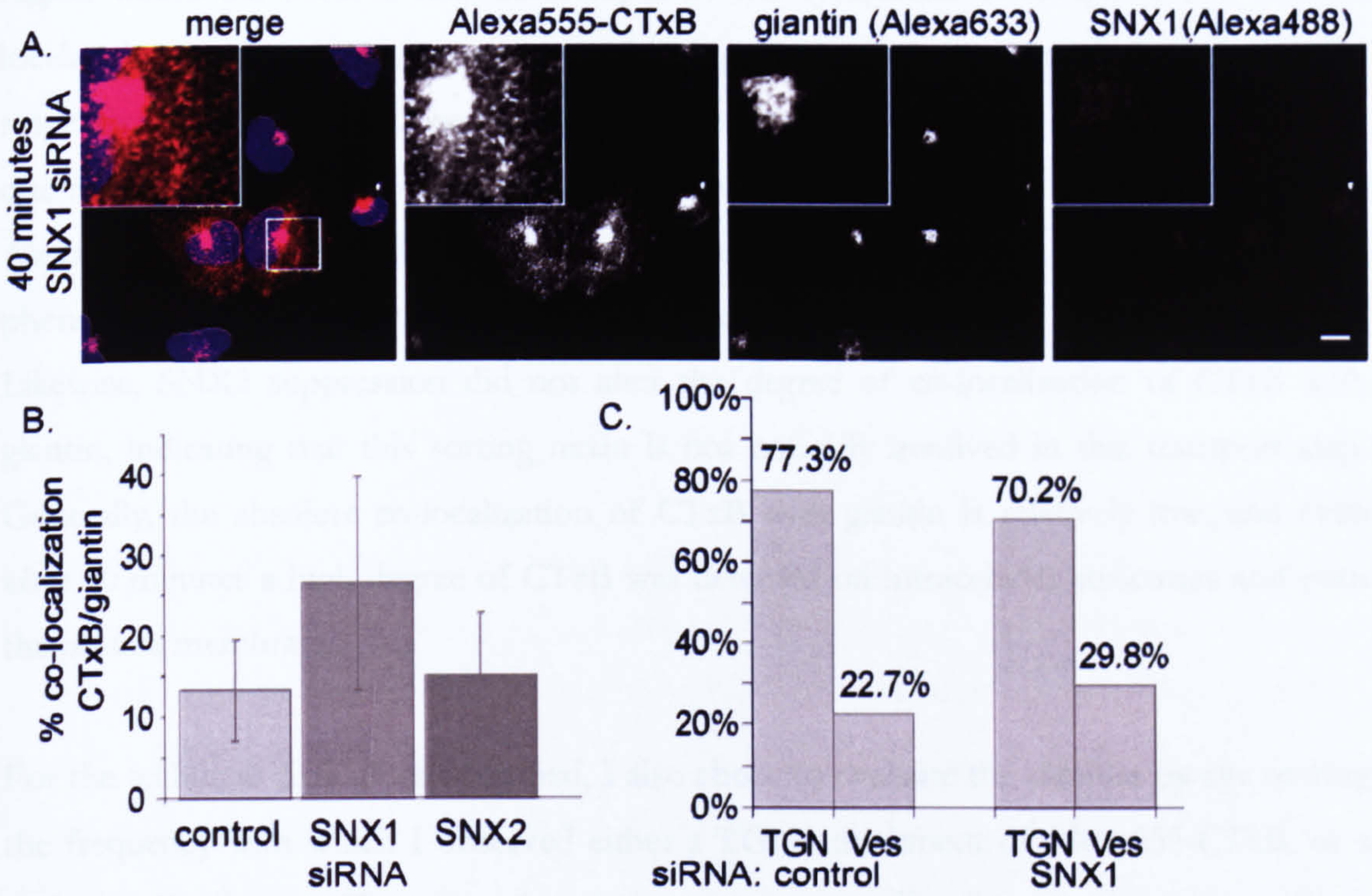

Figure 4. 19 Co-localization of CTxB with giantin is not markedly reduced in SNX1-suppressed cells

(A) Surface-bound Alexa555-CTxB was internalized into SNX1-suppressed cells for 40 min. Cells were fixed and immuno-labelled with anti-SNX1 (Alexa48, green) and the Golgi-marker giantin (Alexa633, magenta). In these cells, Alexa555-CTxB showed a clear Golgi enrichment. (B) Co-localization between Alexa555-CTxB and giantin after 40 min uptake was quantified using MetaMorph software (Molecular Devices). Co-localization was not reduced in SNX1-suppressed cells (27% ± 13% s.d.; 94 of 200 cells with detectable Alexa555-CTxB label) compared to control (13% ± 6% s.d; 71 of 149 cells with label) or SNX2-suppressed cells (15% ± 8% s.d.; 21 of 43 cells); s.d. determined from mean of visual fields (see para. **4.3.5** for details). (C) Quantification of proportion of TGN-like enrichment or vesicular appearance of Alexa555-CTxB after 60 min uptake in control and SNX1-suppressed cells ('analogous approach' n > 650 cells). Scale bar is 20 μm.

When employing the digital co-localization analysis approach using MetaMorph software, I found that co-localization between Alexa555-CTxB and giantin was not reduced in SNX1-suppressed cells (**Figure 4. 19 B**). Quite the contrary, from these results it appears that co-localization was increased under SNX1-suppressed conditions. However, when interpreting the results from the digital quantification of CTxB and giantin co-localization, one has to bear in mind that the cells displayed heterogeneity for levels of Alexa555-CTxB uptake, probably owing to the heterogeneous levels of GM1 in HeLa cells (Pang et al., 2004). The analysis algorithm is based on spatial overlap of pixels, and identical threshold levels had to be applied to all images from the different treatment conditions; for a cell that takes up less toxin relatively more pixels will fall below threshold level, especially in region where the toxin is less clustered, *id est* the cytoplasm. Consequently, as the co-localization is computed as spatially overlapping pixels over the sum of all pixels for the respective channel, this will be manifested as increased co-localization with giantin. Thus, due to the heterogeneity of label, this approach does not provide an absolute measure of Alexa555-CTxB at the TGN. The relatively large error bar is also indicative for this phenomenon. Importantly however, the co-localization is not lower than in control cells. Likewise, SNX2 suppression did not alter the degree of co-localization of CTxB with giantin, indicating that this sorting nexin is not critically involved in this transport step. Generally, the absolute co-localization of CTxB with giantin is relatively low, and even after 60 minutes a high degree of CTxB was detected on intracellular structures and even the plasma membrane.

For the technical difficulties described, I also chose to evaluate the samples by eye scoring the frequency with which I observed either a TGN enrichment of Alexa555-CTxB, or a vesicular distribution. This type of analysis scoring over 650 cells per treatment condition confirmed that Golgi localization was observed with similar frequencies in cells where SNX1 was suppressed (70.2%) compared to control cells (77.3%) (**Figure 4. 19 C**). Importantly, the 'analogue' approach evaluated cells of all intensities in which Alexa555-CTxB was readily detectable by eye. It furthermore appeared that transport kinetics of Alexa555-CTxB in controls are faster than FITC-STxB comparing the frequencies of TGN-localization (**Figure 4. 8**). I was however unable to examine this in a directly comparative study (see **para. 4.8**).

4.8. Attempts of a Comparative STxB and CTxB Analysis

It would have been desirable to further confirm the findings for CTxB using a biochemical assay. When these studies commenced, the Johannes Lab had just developed a tool to study retrograde transport of CTxB biochemically by using a sulfation approach with a genetically engineered CTxB-biotin subunit mutant. Despite several attempts however, I was unable to detect a strong enough signal by autoradiography. This is most likely due to the low GM1 levels in the cell line used in this study; quantification showed that 47% - 49% of all cells exhibited readily detectable levels of Alexa555-CTxB when examined by epifluorescence microscopy, in line with the previously reported "significant differences" in GM1 levels in HeLa cells (Pang et al., 2004).

Similarly, it would have been desirable to directly compare CTxB and STxB in the same cell using fluorescent toxin-uptake assays. These assays gave however inconsistent results. Firstly, the CTxB-label was generally low (compare **para. 4.6**), and secondly, in 70% - 80% of all cases cells were found to be positive for either one or the other toxin (**Figure 4. 20**). This is not surprising given that it has been shown that the labelling pattern of the two toxins is strongly cell cycle-dependent and almost complementary (Majoul et al., 2002). In the few instances where co-labelling was observed, STxB was generally of very low intensity. In the very few instances, where cells were labelled with both toxins at acceptable intensities, the toxins were often found clustered in unusually enlarged structures, with suspiciously 'perfect overlap'[12] (**Figure 4. 21**). These were not observed when incubating the cells individually with the probes. Moreover, unlike observations for the individual probes, these structures did not notably co-localize with SNX1; I chose not to evaluate these data further, as I suggest that this might at least in part represent toxin 'co-clusters' attributable to receptor aggregates [the pentameric B subunit of cholera toxin can bind up to five gangliosides at once (Sixma et al., 1992; Merritt et al., 1994; Merritt et al., 1998). For Shiga toxin, the B subunit may dispose of as many as 15 binding sites for Gb3 (Ling et al., 1998)].

12 (Given that at lower levels, the two probes did not exhibit this behaviour.)

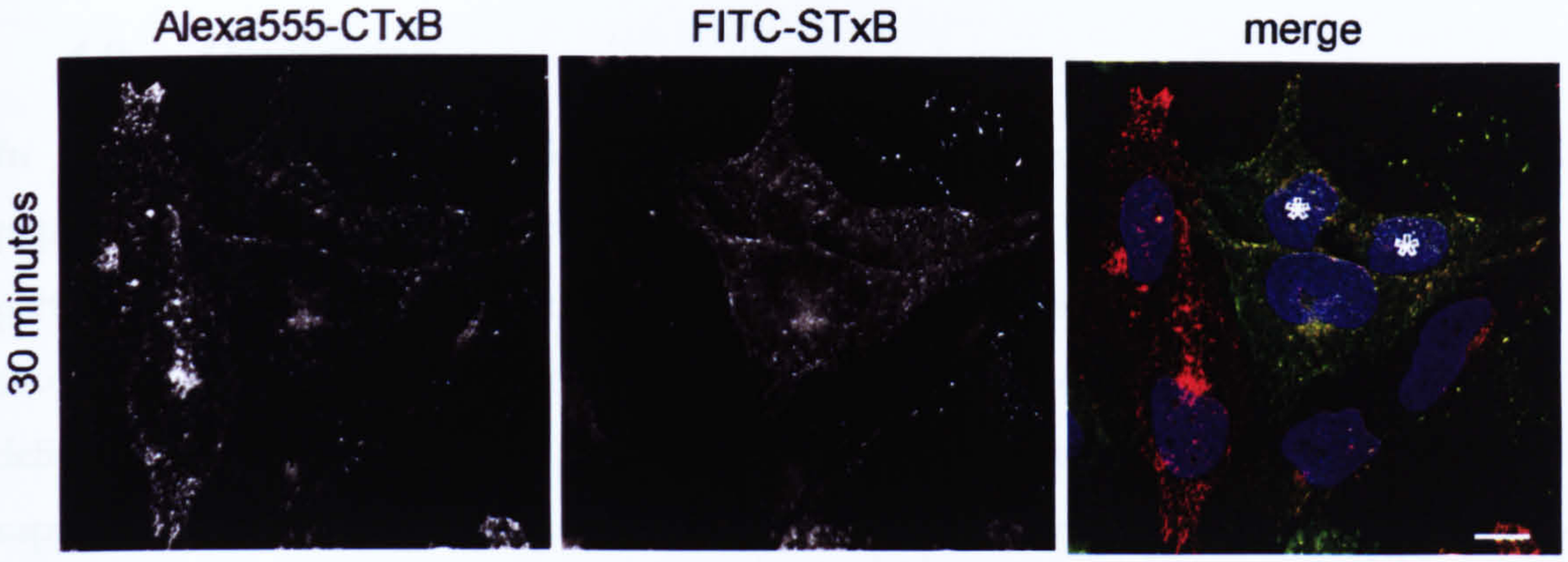

Figure 4. 20 Analysis of joint labelling with Alexa555-CTxB and FITC-STxB

Cells were surface-labelled with a mixture of FITC-STxB (green) and Alexa555-CTxB in DHB medium, rinsed, transferred to 37°C for 30 minutes before being fixed. The merge illustrates preferential labelling for either STxB or CTxB. Generally labelling was very low in cells positive for both toxins, while it was furthermore noted that in these cells the toxin did not exhibit the (expected) juxtanuclear enrichment (asterisks) Scale bar is 10 μm.

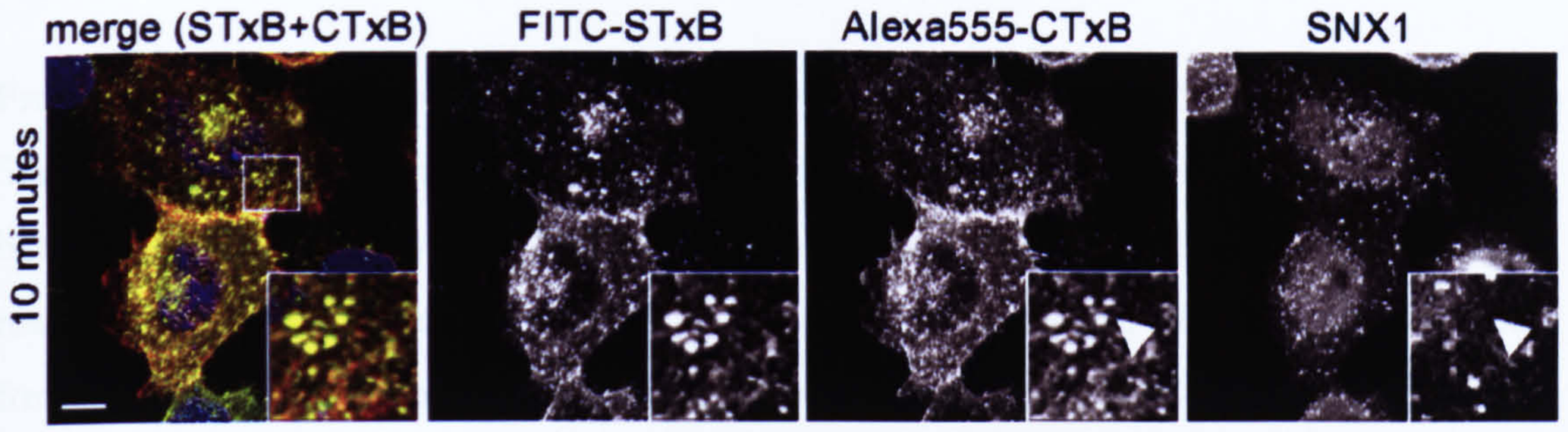

Figure 4. 21 Examining the co-localization in jointly FITC-STxB- and Alexa555-CTxB-labelled structures.

Cells were surface-labelled with a mixture of FITC-STxB (green) and Alexa555-CTxB in DHB medium, rinsed, transferred to 37°C for 10 minutes before being fixed and immunolabelled with anti-SNX1 (Alexa633, magenta). The merge shows both, STxB and CTxB but SNX1 was omitted for clarity. Joint labelling with FITC-STxB and CTxB can lead to formation of enlarged punctate structures that rarely co-localize with SNX1 (arrowheads, inset). Scale bar is 20 μm.

4.9. Discussion

In this study, combining single-cell fluorescent toxin uptake assays and biochemical population-based analyses, I show that RNAi-mediated silencing of SNX1 markedly perturbs retrograde endosome-to-TGN transport of Shiga toxin B subunit. I furthermore show that in contrast to SNX1, the closely related SNX2 does not markedly alter the delivery of STxB to the TGN. Alongside with the data presented that RNAi-mediated suppression of VPS26 also perturbs retrograde STxB transport, this establishes that retrograde early endosome-to-TGN transport of Shiga toxin B subunit occurs, at least in part, *via* a SNX1-and retromer-regulated mechanism. The observed endosomal arrest of STxB under SNX1-suppressed conditions was highly reminiscent of the redistribution of CI-MPR/sortilin under the same conditions; in the following paragraphs I will discuss aspects arising from comparing results of Chapters 3 and 4 (see also **Figure 4. 22** for a model).

From analysis of the role of SNX1 (Chapter 3) as well as VPS26 (Arighi et al., 2004; Seaman, 2004) in retrograde transport – on one hand of CI-MPR and sortilin, on the other hand of STxB - it is evident that at least some components of the retromer transport machinery must be shared between these two components/steps. Likewise, a requirement for clathrin and dynamin (Saint-Pol et al., 2004; Lauvrak et al., 2004), as well as lipid rafts (Falguieres, et al., 2001; Carroll et al., 2001) are common features of both, endosome-to-TGN transport of CI-MPR and Shiga toxin transport

Possible relation of clathrin and the retromer?

Although I have not investigated this aspect in detail, there is coincidental evidence to suggest that clathrin and the retromer may operate in a successive manner. The EM data presented here (Chapter 3) and previously (Carlton et al., 2004) show that SNX1-/CI-MPR-positive tubular profiles originate from a portion of early endosomal limiting membrane that does not possess a recognizable electron-dense clathrin coat. Likewise, SNX1 is not found ETCs, but STxB can be found on small vesicles highly reminiscent of ETCs where it co-localized with CD-MPR (Mallard et al., 1998).

Conversely, VPS26 not only localizes to endosome-associated tubules and ETCs (Muriel Mari, personal communication), but also localizes to some extent to the bilayered clathrin coat (Arighi et al., 2004). From a very recent study, it furthermore appears that clathrin and

the retromer component VPS26 do not only co-localize on STxB-positive endosomes at EM level but upon their suppression, STxB appeared to be trapped in these distinct endosomal subdomains (Ludger Johannes, personal communication)[13]. These findings corroborate a model in which clathrin and the different retromer components could act at distinct stages on the same transport pathway. LCI and EM analysis furthermore showed that STxB exits the endosomal vacuole *via* distinct tubules, compared to Tf (Ludger Johannes, personal communication)[13]. Similarly, sortilin and CI-MPR were found on distinct tubules, compared to Tf (Chapter 3). Strikingly, upon clathrin suppression, Tf and STxB appear on the same tubule (Ludger Johannes, personal communication)[13], further illustrating the role of clathrin in the sorting/cargo-separation process.

Again, a 'no-role' for SNX2?

The finding that SNX2 only plays a minor role in promoting STxB retrograde transport to the TGN ties in with the lack of an effect of SNX1 suppression on CI-MPR retrieval to the TGN. Unlike the situation for SNX1, I was not able to establish a critical threshold level for SNX2-suppression with regard to B-($Sulf_2$) sulfation, meaning that even given comparably high levels of suppression, sulfation appeared slightly but not markedly altered compared to SNX1. The biochemical data must also be interpreted in the light of the effect on cell proliferation and morphological changes under SNX2-suppressed conditions, which I have not further characterized in this study. In assays less susceptible to potential effects of SNX2 suppression on proliferation rate, which furthermore allowed monitoring of suppression levels of individual cells, the toxin clearly accumulated at the TGN, which argues against a major role of this SNX in endosomal retention of the toxin and is in line with previous findings for the CI-MPR (Chapter 3 and Rojas et al., 2007)[14]. The unexpected finding that joint suppression produced a vesicular phenotype comparable to SNX1 but led to increased sulfation further complicates the interpretation. One constant finding is that inclusion of SNX1-specific siRNA results in peripheral, endosomal localization of CI-MPR, sortilin as well as STxB.

Interestingly, while preparing this thesis, Skanland et al. reported that SNX2, but not SNX1, is important in retrograde transport of the plant toxin ricin (Skanland et al., 2007), which, like Shiga and cholera toxin, is an ER-trafficking toxin [see (Sandvig and VanDeurs,

---

13 V. Popoff, G. A. Mardones, D. Tenza, R. Rojas, C. Lamaze, J.S. Bonifacino, G. Raposo, and L. Johannes (2007) The Retromer complex and clathrin define an early endosomal exit site. *J Cell Sci* (in press)

14 NB: Rojas et al. do not see an effect when suppressing SNX2 alone.

1996) for review]. This is particularly exciting in the view that it provides furthers our argument that SNX2 and SNX1 might (also) have independent properties: with regards to toxin traffic (Skanland et al., 2007 and this study), but also with respect to receptor sorting (see discussion in Chapter 3; Gullapalli et al., 2004 and 2006). So it could be possible that SNX2 either mediates transport out of the sorting endosome *via* SNX1-independent tubules (given the data presented here on SNX2 function and the finding that SNX1 suppression did not affect ricin sulfation). Additionally, clathrin appears not to be important for ricin delivery to the TGN (Iversen et al., 2001), which further suggest that sorting into 'ricin retrograde carriers' is different from sorting into 'STxB retrograde carriers'.

Interestingly, after uptake, only a small fraction of the toxin reaches the Golgi (van Deurs et al., 1986; van Deurs et al., 1988), while a large fraction of ricin is recycled back to the cell surface (Sandvig and Olsnes, 1979), and maybe even to lysosomes (Sandvig and Olsnes, 1979), although this has been questioned more recently (Moisenovich et al., 2004). The finding that most of the internalized ricin is recycled is particularly exciting given that besides SNX2, SNX4 was found to be important in the transport step of ricin to the TGN. Our lab has recently shown that SNX4 is involved in mediating early endosome-to-ERC transport, as shown, *inter alia*, by the finding that upon its suppression, the TfR is mis-sorted to lysosomes[15]. In this context, the finding of Skanland and colleagues that suppressing SNX2 and SNX4 together had a somewhat additive effect on ricin transport suggests that they might function at slightly different steps (see below; and compare **Figure 4.22** overleaf). So while SNX4 regulates transport of ricin to the ERC, it is not clear how it would be transported from here to the TGN. It might be recycled to the plasma membrane, or, if delivered to the TGN, this occurs in a manner independently of Rab11 (Iversen et al., 2001).

So what about the 'residual' STxB that reaches the TGN under SNX1-suppressed conditions? Although the correlation between sulfation level and suppression level is clear, it seems likely that other pathways contribute to STxB retrograde sorting: in a rough estimation, this would otherwise mean that the remaining 5 – 10% of SNX1 would account for as much as 40 – 60% of retrograde toxin transport. In contrast, VPS26

---

[15] C.J. Traer, A.C. Rutherford, K.J. Palmer, T. Wassmer, J. Oakley, N. Attar, J.G. Carlton, J.Kremerskothen, D. J. Stephens, and P.J. Cullen (2007) Sorting nexin-4 co-ordinates endosomal sorting of transferrin receptor with dynein-mediated transport into the endocytic recycling compartment. *Nat Cell Biol* (under revision)

suppression appeared much more efficient, although there are provisos that this might at (least in part) result from TGN fragmentation. Besides these technical issues, there is indication that STxB might take another route: the toxin has been shown to use a pathway taken by TGN38/TGN46 (Mallard et al., 1998), which is probably Rab11-dependent as overexpression of Rab11 affects both, STxB as well as TGN38/46 transport to the TGN (Wilcke et al., 2000).

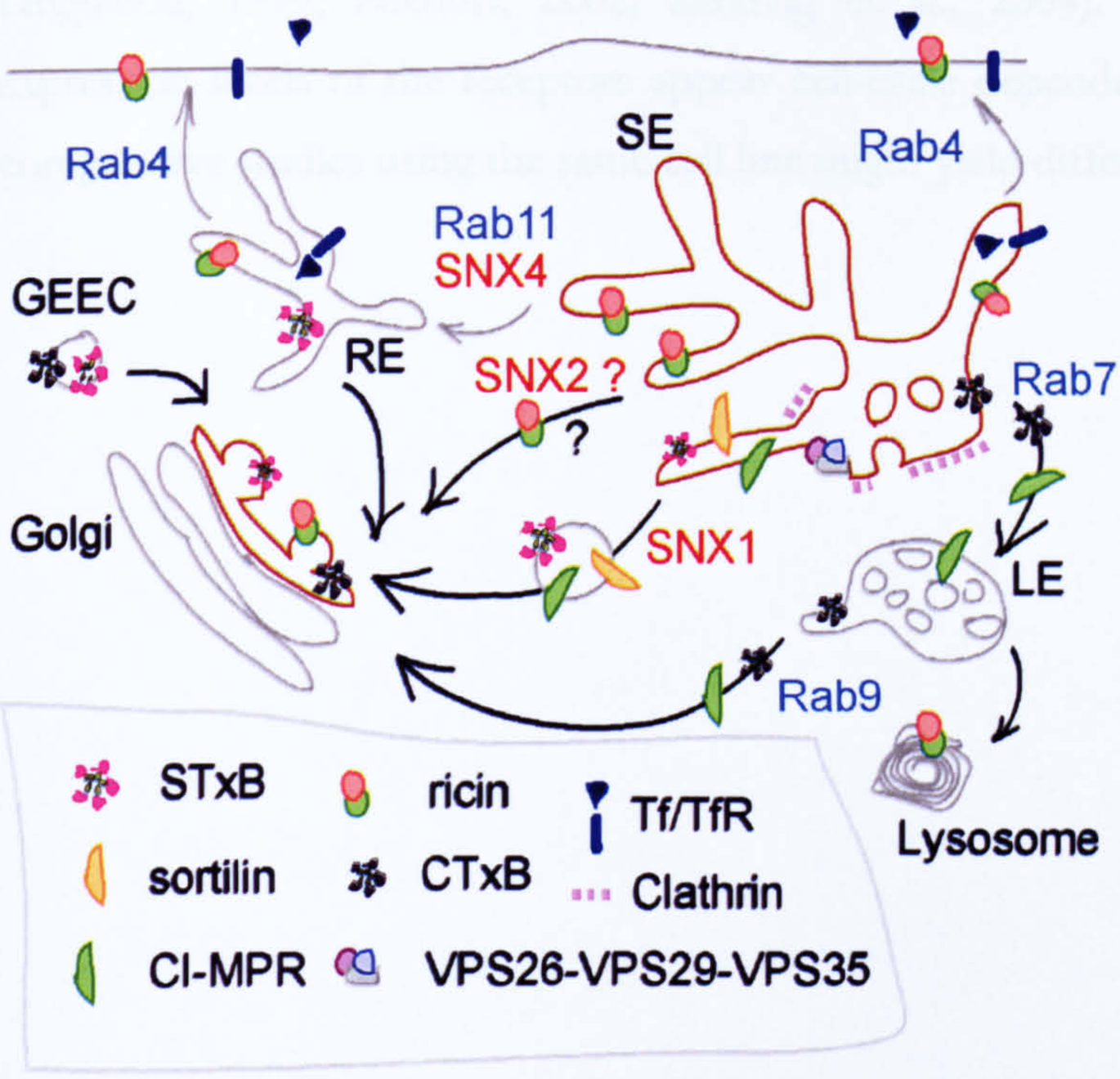

Simplified schematic for endosome-to-TGN transport for the cargo and coats discussed (see also text for details).
SE = sorting endosome;
RE = recycling endosome; GEEC = GPI-AP enriched early endosomal compartment;
LE = late endosome.

Figure 4. 22 Working model of endosomal transport to the TGN for the cargo and components discussed

Likewise, differences between STxB to CI-MPR transport arise when one considers the role of Rab9, which provides a retrieval pathway for the CI-MPR from late endosomes back to the Golgi complex (Diaz and Pfeffer, 1998; Carroll et al., 2001; Barbero et al., 2002). In contrast, it has been proposed (documented but not confirmed) that Rab9 is not required for STxB retrieval (Sandvig et al., 2002). This is interesting in the light that I have also presented data (based on fluorescent toxin-uptake assays) that SNX1-suppression does not appear to markedly reduce endosome-to-TGN transport of cholera toxin B-subunit. Taken together with the finding that Rab9 overexpression is capable of restoring correct Golgi targeting CTxB in NPC cells (Choudhury et al., 2002), this might suggest

that CTxB endosome-to-TGN transport occurs at least in part from late endosomes. (Hence, one would expect CTxB to be absent from ETCs.)

On a more general note, uptake of Shiga toxin is a prime example to study variance of endocytic pathways used in different cell types. Like for CTx regarding requirement for caveolin (see Chapter 1, **par 1.3.4**), the fraction of toxin internalized by clathrin-dependent, as opposed to clathrin–independent mechanisms, seems to depend on the cell line used and on the conditions under which the cells are grown (Schapiro et al., 1998; Lingwood, 1999; Nichols, 2002; Sandvig et al., 2004). Especially in the light that expression levels of the receptors appear cell-cycle dependent (Majoul et al., 2002), even comparative studies using the same cell line might yield different results.[16]

[16] (cell cycle progress dependent on 'batch age', starvation protocols, etc)

Chapter 5 – Role of Sorting Nexins in *Salmonella* Invasion

5.1. Preface

The work described in this chapter was initially started when developing and overseeing the final year undergraduate projects of Ms Emily de Looze and Ms Frances Mulvany. While Ms Emily de Looze was involved in all initial SNX1-related fixed-cell and live-cell imaging, Ms Frances Mulvany was involved in work relating to SNXs other than SNX1.

I am immensely grateful to Dr Mark Jepson, for help and advice with this project, and acknowledge the help of Ms Charlotte Perett with initial fixed cell assays, and advice on evaluation of invasion/adherence assays, and am grateful to Alan Leard for help with live cell imaging.

5.2. Introduction

Bacteria may be considered true 'cell biology experts', as pathogens like *Salmonella Typhimurium* (*S. Typhimurium*), the leading cause of food-borne gastroenteritis, have developed sophisticated ways to gain access to host cells and to utilise intracellular machinery and resources to replicate within them. This includes very refined mechanisms to stimulate uptake into non-phagocytic cells by influencing actin dynamics and involves extensive interactions with the host cells' endocytic machinery, as well as downmodulation of stimulatory effects on the cytoskeleton in order to allow for cell recovery. The mechanisms of orchestrating these effects must be highly regulated, and in many cases, the details and the degree of bacterial interactions with host cell organelles are still poorly understood. As these bacteria hijack and mimic cell function, studying the life cycle of this pathogen from a cell's perspective and analyzing the cellular targets and machinery exploited has thus the potential to provide information about both, bacteria and the cell itself. Here, I explored the role of sorting nexins in bacterial entry.

5.2.1. Salmonella Typhimurium – Type III secretion

A group of bacterial pathogens including the enterobacterium *S. Typhimurium* is capable of invading non-phagocytic cells by actively inducing, or *triggering*, their own uptake (Alonso and Portillo, 2004). Invasion of epithelial not only allows the pathogen to escape immune response but also enables replication within the host, as it establishes its replicative niche within its cells [(Knodler and Steele-Mortimer, 2003; Patel and Galan, 2005) for review]. In order to colonize and replicate within the host, S*almonellae* employ a multitude of virulence factors, including two Type III secretion systems (TTSS) (Groisman and Ochman, 1997; Buttner and Bonas, 2002). These secretion systems translocate bacterial effector proteins into the host cell, which specifically interact with a variety of cellular targets. While the *Salmonella* pathogenicity island (SPI)-2 encoded TTSS plays no role in invasion, but is only induced after successful entry and is required for intracellular survival [(Waterman and Holden, 2003) for review], the SPI-1 system is already activated extracellularly and essential for invasion of non-phagocytic cells (Lostroh and Lee, 2001). On one hand, this gene locus encodes components of a multi-protein needle complex that acts as a 'molecular syringe' (Kimbrough and Miller, 2002). On the other hand, it also encodes for the proteins injected through this 'needle' into the cytoplasm of the host [(Ehrbar and Hardt, 2005) for review]. Through 'functional mimicry', these effectors influence the cellular cytoskeleton

and interfere with host signalling function to achieve uptake in a mechanism resembling macropinocytosis. At early time points of infection, the proteins transferred into the host include the *Salmonella* invasion protein SipA (also known as SspA)[17], the *Salmonella* outer proteins SopE and SopE2 and the product of the *Salmonella* invasion gene SigD (also known as SopB). In brief, SipA binds actin, and has the capacity to catalyse actin polymerization and to bundle actin filaments (Zhou et al., 1999a; Zhou et al., 1999b; Galkin et al., 2002). SopE and SopE2 act as guanine-nucleotide exchange factors (GEFs) on different host cell Rho GTPases (Rudolph et al., 1999; Stender et al., 2000; Friebel et al., 2001), thus influencing cytoskeletal rearrangements (Hardt et al., 1998), while another SPI-1 effector, the *Salmonella* protein tyrosine phosphatase SptP acts as GTPase-activating protein (GAP) for Cdc42 and Rac1 (Fu and Galan, 1999; Zhou and Galan, 2001), thus reverting the effects evoked by SopE and SopE2.

Of particular interest for this study is the SPI-1-encoded SopB. This bacterial virulence protein is a phosphatase presenting broad substrate specificity, hydrolyzing various phosphatidylinositol polyphosphates and inositol polyphosphates (Norris et al., 1998; Terebiznik et al., 2002; Hernandez et al., 2004; Mason et al., 2007) . This includes turnover of PtdIns(4,5)P_2 (Terebiznik et al., 2002) yielding PtdIns5P (Mason et al., 2007), and additionally, as shown in *in vitro* assays the hydrolysis of 5-phosphates from PtdIns(3,5)P_2 and PtdIns(3,4,5)P_3 (Marcus et al., 2001). Further still, generation of Ins(1,4,5,6)P_4 from Ins(1,3,4,5,6)P_5 in i*n vitro* and *in vivo* assays has been demonstrated (Zhou et al., 2001). Due to the conflicting results regarding its enzymatic specificity, the exact molecular function and its *in vivo* targets are still matter of debate. However, it is clear that PPIn and the active subversion of the phosphoinositide metabolism by the bacteria play an important role in the invasion process of this pathogens (Pizarro-Cerda and Cossart, 2004).

[17] Ssp: *Salmonella* secreted protein

5.2.2. Bacterial invasion and interactions with the host cell's endosomal system

Through concerted action of the translocated SPI-1 effector proteins, *S. Typhimurium* first induces changes in the actin cytoskeleton leading to extensive ruffling. Upon closure of membrane tips, extracellular-liquid filled macropinosomes are produced, which can be empty or contain bacteria. These *Salmonella*-containing vacuoles, or SCVs, are thus initially derived from plasma membrane but quickly resemble early endosomes [see (Knodler and Steele-Mortimer, 2003) for review]. Kinetic studies have shown that within 5 minutes after infection, early SCVs become enriched in PtdIns3*P* (Pattni et al., 2001), and hence recruit PtdIns3*P*-ligands and their respective interacting proteins, like EEA1 (Steele-Mortimer et al., 1999) and Rab5 (Scott et al., 2002). At these early time points SCVs also acquire components of the endocytic recycling system, like Rab4 (Smith et al., 2005), and transferrin receptors (Steele-Mortimer et al., 1999). Akin to endosomes, early SCVs are thought to gradually mature into 'late SCVs' (Gorvel and Meresse, 2001): they acidify (Rathman et al., 1996; Drecktrah et al., 2007) and acquire late endosomal proteins, such as Rab7 (Meresse et al., 1999), and lysosomal glycoproteins including Lamp-1 (Steele-Mortimer et al., 1999). The virtual absence of the CI-MPR on SCVs (Garcia-del Portillo and Finlay, 1995) has long been interpreted as indicator for limited, or selective, interaction with late endosomes. It was shown that acquisition of cathepsin D and cathepsin L is markedly delayed, indicating that the maturation kinetics are slowed down in SCV biogenesis compared to endosomal maturation (Garcia-del Portillo and Finlay, 1995; Steele-Mortimer et al., 1999).

Besides acquisition of endosomal proteins, SCVs also employ intracellular transport machinery and interact with molecular motors, as they become progressively enriched in the perinuclear area with time, and are eventually positioned in close proximity to the TGN (see (Henry et al., 2006) for review). It is thought that maintaining the correct positioning enables the bacteria to escape lysosomal degradation and to establish a replication niche near the TGN (Beuzon et al., 2000; Salcedo and Holden, 2003; Abrahams et al., 2006; Deiwick et al., 2006). Here, interactions with the host are mediated by a set of 'late' effector proteins, encoded by SPI-2.

Given the capacity of SNX1 to bind to PtdIns3*P* and, moreover, its function as an important regulator of sorting processes between endosomes and the TGN, I sought to explore the role of SNX1 in SCV biogenesis.

5.3. Materials and Methods

For general materials and methods, buffer and media compositions, suppliers and equipment, one is referred to Chapter 2. If not stated otherwise, reagents were obtained from SigmaAldrich or Invitrogen.

5.3.3. Bacterial Strains

In this study, the wild type strain SL1344 (Hoiseth and Stocker, 1981), an isogenic SL1344-ΔsigD deletion mutant (ΔsigD) and as control, a SL1344-ΔsigD strain complemented with a plasmid encoding for SigD and its chaperone SigE (SL1344-ΔsigD-pSigD-pSigE) were used (generously provided by Dr O. Steele-Mortimer, NIAID/NIH, Hamilton, MT, USA). For all experiments, 100 µl of an overnight culture were diluted in 10 ml LB broth and grown to mid-log phase. For live cell imaging and colony forming unit assays, a multiplicity of infection (m.o.i.) of approximately 50 in 1 ml of Krebs buffer or imaging buffer (see **para. 5.3.3**) was used; for fixed cell imaging, the m.o.i. was 50 or 150. The m.o.i. was calculated as follows:

m.o.i. = N° bacteria/N° cells, while number of bacteria was determined spectrophotometrically using 1 ml of the bacterial culture and determining the OD_{600} (while 1 OD_{600} corresponds to $1x10^9$ colony forming units (cfu) per ml), and by having determined the number of cells when seeding the night before the assay using an improved-NEUBAUER hemocytometer (Marienfeld).

5.3.4. Cloning of pmRFP-2xFYVE

The pEGFP-C1-2xFYVE vector was a kind gift from Prof George Banting, University of Bristol, Bristol, UK (Pattni et al., 2001). In this vector, using the AgeI and BsrGI restriction sites the GFP-coding sequence was excised, and replaced with the sequence coding for mRFP, excised from pmRFP (see Chapter 2, **para. 2.1.5.**) using the same restriction endonucleases (see also **Appendix II.3**), and ligated into the vector (see **par 2.3.6**).

5.3.5. Infection Assays – Fixed Cell Analysis

Cells (untreated, siRNA transfected or DNA transfected) were washed twice with pre-warmed (37°C) modified Krebs buffer (137 mM NaCl, 5.4 mM KCl, 1 mM $MgSO_4$, 0.3 mM KH_2PO_4, 0.3 mM NaH_2PO_4, 2.4 mM $CaCl_2$, 10 mM glucose and 10 mM Tris base, adjusted to pH 7.4 at 37°C with HCl). Infection was carried out at the respective m.o.i. for 15 min in modified Krebs buffer at 37°C. Bacteria were removed and cells were washed extensively with PBS, supplemented with 0.9 mM $CaCl_2$ and 0.5 mM $MgCl_2$

(PBS++). Where appropriate, cells were incubated in PBS++ for further 15 min before being transferred into PBS++ supplemented with 16 µg/ml gentamicin (Sigma) to prevent furher infection and then fixed using 2% PFA for 45 min at 4°C, or 4% PFA for 15 min at 37°C to improve tubule preservation. Cells were then processed for immuno-labelling as described elsewhere (Chapter 2, **para. 2.4.21**), mounted on microscope slides using either Mowiol or Vectashield containing DAPI (Vector Laboratories). Imaging was performed as described (**para. 2.4.23**), and obtained images were merged using Leica confocal software (Leica Microsystems). Vol*ocity* software V4.0.1 (Impro*vision*) was used for compiling and compressing movies, deconvolution of data sets and 3D image volume rendering. Where applicable, contrast and brightness adjustments were made using Adobe Photoshop® 6.0 (Adobe Systems Inc.). If not stated otherwise, time points are given from the start of experiment, thus before infection.

5.3.6. Infection Assays – Live Cell Imaging

Transfected cells were washed twice with modified Krebs buffer and coverslips were transferred into pre-warmed (37°C) coverslip holders together with approximately 1 ml imaging buffer (125 mM NaCl, 42 mM HEPES, pH 7.4, 18 mM glucose, 5.4 mM KCl, 3 mM $NaHCO_3$, 1.6 mM $MgCl_2$ and 1.3 mM EGTA). For image capturing, a wide-field system in an environmental control chamber was used [inverted Leica DMIRB microscope equipped with a Hamamatsu C4742-95 cooled CCD camera, controlled with Openlab4 software (Improvision)]. Three focal depths were captured at 20-second intervals; bacteria were added at the indicated m.o.i. **(para. 5.3.3)** and cells were imaged for 25 to 30 minutes.

5.3.7. Quantification of Bacterial Adherence and Invasion

Cells were treated with control or SNX1-specific siRNA **(par 2.4.19)** and invasion assays were performed as described (**para. 5.3.5**). After fixation, bacteria were immuno-labelled with an anti-*Salmonella* primary antibody omitting any detergent, followed by a FITC-coupled secondary antibody. Cells were then permeabilized using 0.1% TritonX-100 in PBS. Subsequently, all bacteria (inside and adhered) were labelled with the same primary, but a TRITC-coupled secondary antibody and mounted onto slides using Vectashield mounting medium containing DAPI (Vector Labs). Slides were analysed under epifluorescence counting total numbers of bacteria (TRITC-labelled) and number of adhered bacteria (FITC-labelled), the difference between the two yielded number of invaded bacteria.

5.3.8. Colony Forming Unit Assay (Gentamicin protection assay)

HeLa cells were treated with siRNA for 60 hours as described, and then trypsinized and several wells of 120.000 cells per condition were prepared. The next day (totalling 72 hours of siRNA treatment) cells were washed twice with pre-warmed (37°C) modified Krebs buffer and three wells per siRNA condition were simultaneously infected with bacteria at the indicated m.o.i. for 15 minutes at 37°C. Bacteria were removed and cells were washed three times with PBS++, incubated in modified Krebs buffer for a further 15 minutes at 37°C and subsequently, transferred to DMEM (+ 10% FCS) containing 50 µg/ml gentamicin to prevent further infection. After further 30 minutes at 37°C, cells were washed into DMEM (+ 10% FCS) containing 16 µg/ml gentamicin and kept at 37°C until lysed. At indicated times (from start of experiments), cells were washed once with PBS++, lysed (1% TritonX-100, 0.1% SDS in PBS) and a serial dilution of lysates in PBS++ was plated in replicates onto LB-agar plates. After incubation for 16 hours at 37°C, the number of colonies was determined. For evaluation, the mean of the replicate plating was taken, separately for each assay (3 wells per condition). The mean of all 3 wells was then calculated, and the result was deemed one experimental set.

5.3.9. Distance Analysis

Maximum z-stack projections of images from bacterial infection and immuno-labelling experiments (carried out as described in **para. 5.3.5**) in control and SNX1-suppressed cells were evaluated. The distance covered from the plasma membrane by each bacterium/bacterial cluster was determined. As the exact point of entry can not be determined at the chosen time point (180 min p.i.), I assumed that bacterial entry occurred at α_z=0° in all cases (i.e. not taking into account entry from top of cell but only in the plane; copmpare also **Figure 5. 19**). For single bacteria, the shortest distance from the cell edge in a straight line toward the cell centre (DAPI-labelled nucleus) was measured. For a bacterial cluster, a straight line (the base) was constructed running through the centre of the cluster and from here an isosceles triangle toward the plasma membrane was constructed (the vertex representing the projected entry point). From this point, the distance covered for the fraction of the slowest and fastest bacteria was measured (see also model in **Figure 5. 19**). Intracellular progress of at least six clusters from greater than three cells was analysed per condition. The error gives standard deviation from mean; significance was assessed with Student's t-test.

5.3.10. Analysis of Vacuolar Shrinking in GFP-SNX1 transfected cells

Movies of real time infection assays using GFP-SNX1 transfected MDCK cells and infected with wild type SL1344 bacteria were used for this analysis. Using single frames of one focal depth (phase contrast, 1322x1024 pixels), shrinkage of vesicles was analysed as difference in area over individual frames [18]. Area in pixels was determined using ImageJ (NIH Image). It was chosen to analyse the largest, rounded vesicles (indicative for sealing), which also had visibly ceased interacting with other SCVs. The frame where the area of the vesicle in question was observed to be largest was deemed t(start); the end point was determined either by virtual disappearance of the vacuole or, when the end of the image sequence was reached, the area was measured again at this time point. Speed of shrinkage was determined as the difference in area ΔA(end-start), expressed in pixels over time (expressed in frames); these units were chosen to mirror the somewhat qualitative character.

[18] In an ideal case scenario, one would choose to analyse change in volume; with the set-up used in this study this was however not possible.

5.4. Analysis of SNX1 recruitment to Salmonella-containing vacuoles

5.4.1. Fixed cell analysis

Given the ability of the SNX1-PX domain to bind to PtdIns3*P*, as shown in liposome-based assays (Cozier et al., 2002), I wished to examine whether SNX1 was recruited to *Salmonella*-containing vacuoles (SCVs). Therefore, infection assays using the *Salmonella* strain SL1344 were performed [modified from (Steele-Mortimer et al., 1999)]. In these assays, HeLa cells were challenged with bacteria for 15 minutes, after which time the cells were washed extensively to remove excess bacteria. The cells were then either fixed directly, or further incubated for up to 6 hours before being fixed and processed for immunofluorescence labelling to analyse recruitment dynamics (**Figure 5.1 A**). Cells were additionally treated with DAPI (which strongly binds to bacterial and cellular DNA) and TRITC-phalloidin (which binds to F-actin). These treatments enabled me to visualize the bacteria and the rearrangements of the actin cytoskeleton, respectively.

Compared to uninfected controls, a striking shift in the subcellular distribution of SNX1 was observed; within 15 minutes post infection (p.i.), most of the cellular SNX1 was redistributed and appeared as 'globular accumulations' at the site of infection (**Figure 5.1 B**). At this time point, the cells exhibited dramatic actin rearrangements at sites of infection, and SNX1 appeared accumulated directly adjacent to, or underneath, these membrane ruffles. Analysis of later time points showed that this association was prolonged, as even 60 min p.i., SNX1 was still found to be associated with the SCVs[19]. At this time point, the ruffling had ceased and the bacteria had progressed towards the perinuclear area (**Figure 5.1 C**). At the later time points (**Figure 5.1 D** and data not shown), SNX1 was no longer associated with SCVs, and instead had resumed a distribution similar to the pattern observed prior to infection.

To analyse the kinetics of SNX1 acquisition in HeLa cells, SCVs were scored for the absence or presence of SNX1 at different times p.i., which showed that the recruitment of SNX1 to the SCV was rapid and transient (**Figure 5.1 D**). This prolonged association was also observed for a second epithelial cell line (MDCK cells), a cell line that later was used for live cell analysis.

---

19 Term used synonymously with 'bacteria' = DAPI-positive structures

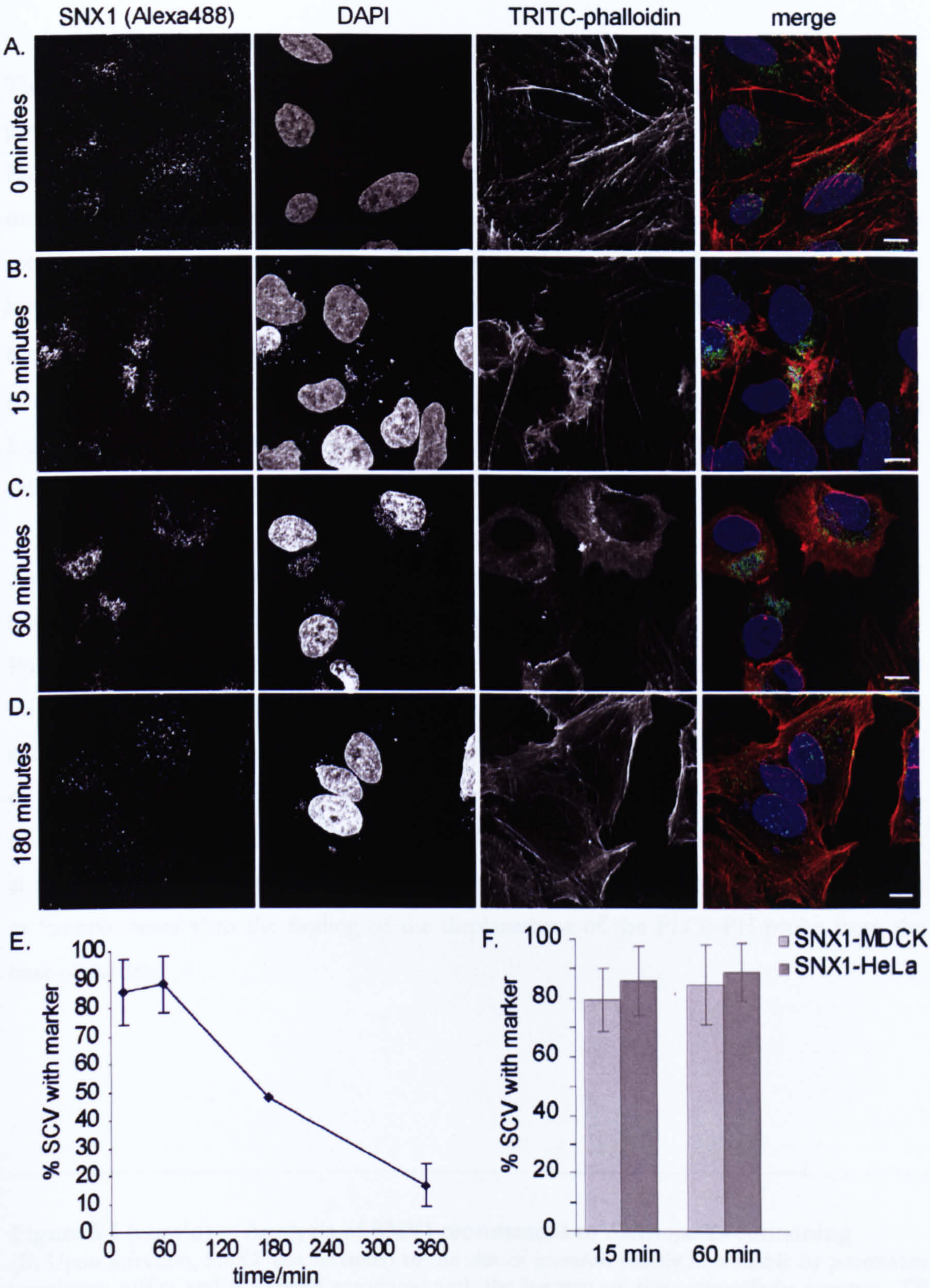

Figure 5. 1 Analysis of SNX1 recruitment to Salmonella-containing vacuoles

HeLa cells were either fixed directly (uninfected) for 45 minutes in 2% PFA at 4°C, or were infected with SL1344 for 15 minutes, then gentamicin-washed prior to fixation at indicated time points. Cells were immuno-labelled for endogenous SNX1 (Alexa488, green) and stained with TRITC-phalloidin to visualize actin (red) and DAPI to label bacterial and cellular DNA (blue). (A) In uninfected cells, SNX1 displayed a vesicular distribution with perinuclear enrichment. **→p.t.o.**

5.4.2. Further analysis of the plasma membrane-recruitment of SNX1

The observed localization of GFP-SNX1 to (or very close to) the plasma membrane prompted me to investigate this recruitment in more detail. It is well established that PtdIns(4,5)P_2 plays a central role recruiting actin-associated proteins to the plasma membrane (Sechi and Wehland, 2000). However, PtdIns(4,5)P_2 and actin also confer to membrane rigidity (Sheetz, 2001), which one would assume to be detrimental to the invasion process. It has been shown that invaginating areas at the S. *Typhimurium*-induced membrane ruffles are largely devoid a phospholipase C-δ_1 PH domain-probe (PLCδ-PH) (Hernandez et al., 2004). PLCδ_1 ligates PtdIns(4,5)P_2 with high affinity (Garcia et al., 1995; Lemmon et al., 1995); hence, these observations suggested that that PtdIns(4,5)P_2 was selectively depleted from the base of the ruffle.

As in the infection process 'plasma membrane' identity appears to be rapidly converted into 'endosome/SCV' identity, it prompted me to closer investigate the recruitment of the PtdIns3*P*-ligating endosomal protein SNX1 to the plasma membrane in this context. To be able to analyse the ruffles in detail, optical z-sections of images taken were deconvolved and subsequently 3D-rendered and animated to allow a '360° view' of the ruffles. This type of analysis showed that the protein not only clearly accumulated around the bacteria in a non-uniform fashion (**Figure 5. 2** top inset, **Movie 5.1**), but that SNX1 is directly present at the base of the TRITC-phalloidin labelled ruffle. Thus, coincidentally this data appears as 'complementary' to the finding of the displacement of the PLCδ-PH-probe from the base of ruffles.

Figure 5.1 (cont'd) Analysis of SNX1 recruitment to *Salmonella*-containing (B) Upon infection, SNX1 was recruited to the site of invasion readily identifiable by prominent membrane ruffles and (C) stayed associated with the bacteria on their intracellular itinerary. (D) After 180 minutes, SNX1 had resumed its original distribution. (E) For the kinetic analysis of SNX1 association with SCVs over 6 hours p.i., between 50 - 150 SCVs were scored per assay for the absence or presence of SNX1 ($n \geq 6$ for 15 min and 60 min ± standard deviation, s.d.; $n = 2$ for 180 min and 360 min, error ± min/max). (F) SNX1 recruitment to SCVs is comparable in MDCK ($n = 4$, ± s.d., 50 – 150 SCVs scored per assay) and HeLa cells ($n > 3$, ± s.d. 50 – 150 SCVs scored per assay) after a 15-minute bacterial 'pulse' or further 45 minutes incubation. Scale bar is 10 μm.

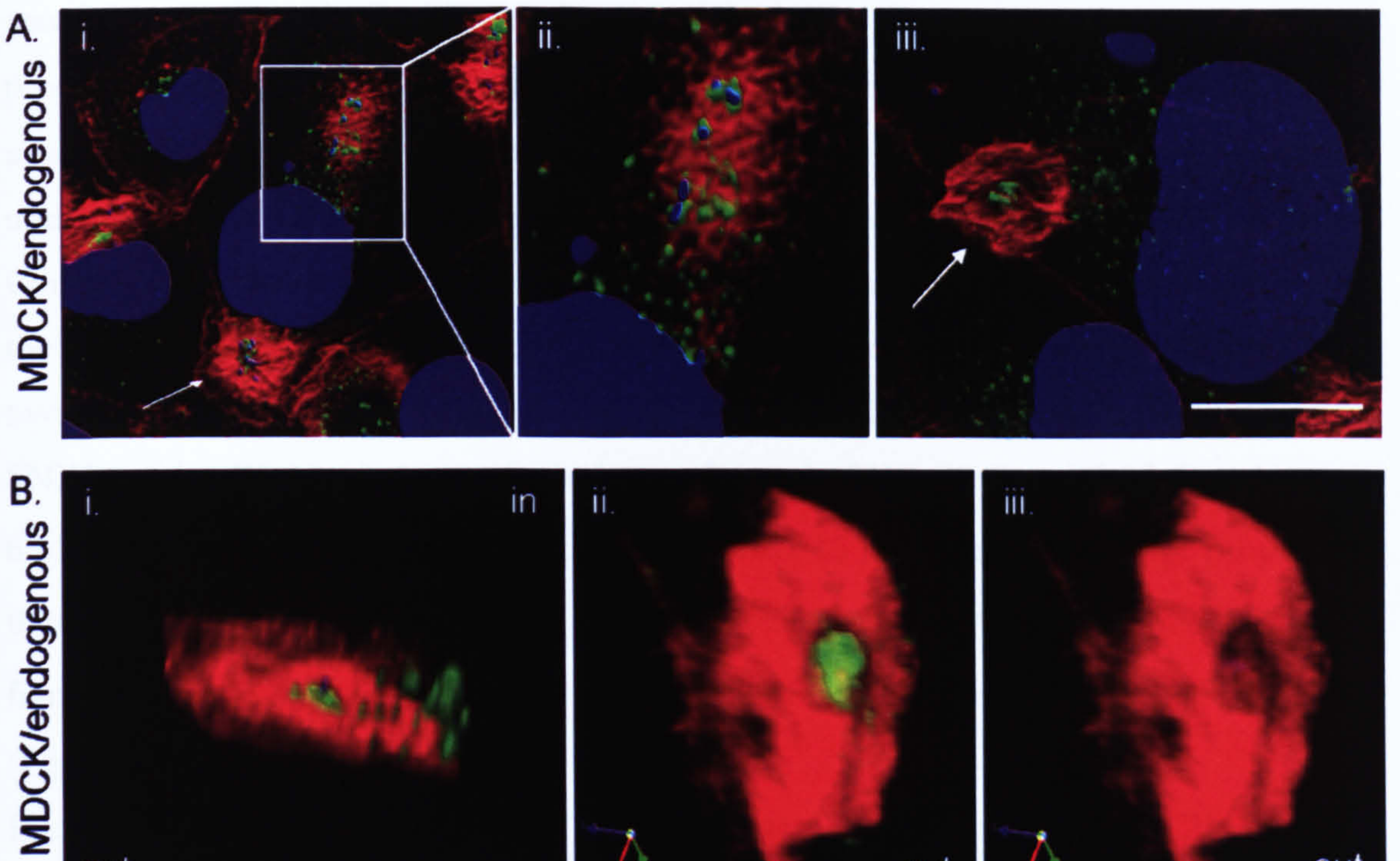

Figure 5. 2 Analysis of SNX1-recruitment to ruffles at the plasma membrane. MDCK cells were infected with the SL1344 strain for 15 minutes. Cells were fixed, immuno-labelled and optical z-slices were acquired using a Leica SP2 AOBS system, deconvolved and 3D image volume rendered using Volo*city* software (Improvision); see also **Movie 5.1** (Ai.-iii.) SNX1 (green) clearly accumulates at membrane ruffles (arrows) and around bacteria (boxed area in Ai., and magnification in Aii.). Scale bar is 10 μm. (B) Magnification of the membrane ruffle shown in (Aiii.), with the green (SNX1-) channel omitted in (Biii.). (C) One single optical z-section of the membrane ruffle shown in (Aiii.) and (B), respectively, is displayed with insets on the left and on top of the image providing the respective YZ- and XZ-view. Note that SNX1 is localized as a ring around the bacterium.

The observed globular or meshwork-like manifestation of protein at the site of infection was furthermore markedly different from the appearance of the FYVE-domain containing protein EEA1 (**Figure 5. 3**), or the appearance of a GFP-2xFYVE probe at the site of infection (data not shown, but compare **Figure 5. 9**). These proteins were rarely clustered underneath the ruffle and exhibited a discrete vesicular appearance (**Figure 5. 3 A**). Compared to the recruitment of the 'pure' PtdIns3*P*-ligand, SNX1 stayed associated with the bacteria for a prolonged time (**Figure 5. 3 B, C**). When the recruitment patterns of the two proteins were analysed comparatively by scoring only bacteria that were positive for SNX1 and/or EEA1 (the sum of which was deemed 100%), it was noticed that although 68.1% ± 6.86% were positive for both markers after 15 min, there was a large proportion that was exclusively positive for SNX1 (31.2% ± 0.65%). After 60 min, this SNX1-positive fraction increased to 63.7% ± 0.72% whereas only few SCVs were still labelled for EEA1 (**Figure 5. 3 B, C**).

Hence, one can conclude that SNX1 is not only associated with 'nascent' SCVs but with the 'maturing' SCVs as characterized by its intracellular progress to the perinuclear area. That these SCVs are indeed 'maturing' was furthermore confirmed by co-labelling with Lamp-1 antisera (**Figure 5. 3 D**), which starts to accumulate on SCVs 20 – 30 minutes p.i. (Steele-Mortimer et al., 1999; and data not shown).

These initial studies showed two important things: first, SNX1 is indeed recruited to the site of infection in a unique manifestation pattern[20], and second this recruitment is transient and prolonged. Numerous previous studies have analysed the recruitment of EEA1 (Steele-Mortimer et al., 1999; Scott et al., 2002; Deiwick et al., 2006), PtdIns3*P*-reporter constructs like the described 2xFYVE (Pattni et al., 2001; Scott et al., 2002), as well as using the PX domain of the 40-kD subunit of NADPH, p40PX (Hernandez et al., 2004), which binds PtdIns3*P* (Kanai et al., 2001). In spite of the different PtdIns3*P*-ligands used, these studies find marked association of the different probes with SCVs maximally up to 20 – 30 minutes. This difference is unlikely to be due to their respective affinities for PtdIn3*P*, as the K_D for PtdIns3*P* of the SNX1-PX domain (micromolar range) is considerably higher than the K_D of EEA1 (nanomolar range), although no immediate comparative study exists (Gaullier et al., 2000; Cozier et al., 2002; Zhong et al., 2002). Given the ability of SNX1 to additionally ligate PtdIns(3,5)P_2 (Carlton et al., 2004), it appears feasible to suggest that this binding-specificity of the SNX1-PX domain might

[20] compared to FYVE-ligating proteins and probes

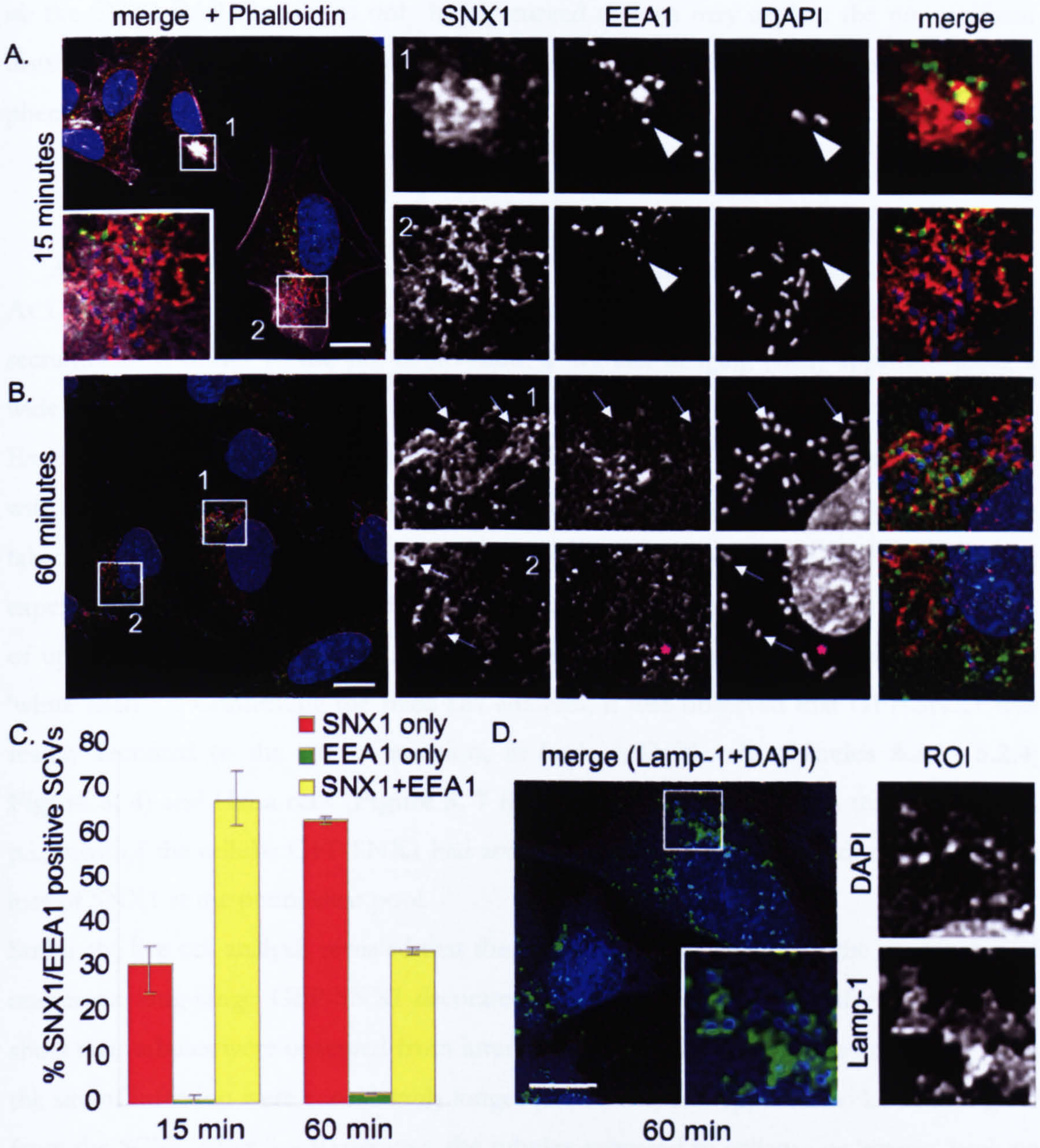

Figure 5. 3 Analysis of EEA1-recruitment to the site of bacterial invasion.
HeLa cells infected with SL1344 for 15 min were either fixed directly (A) or after further 45 minutes (B) before being labelled with anti-SNX1 (Alexa594, red), EEA1 (Alexa488, green), DAPI (blue) and TRITC-phalloidin (magenta, 15-minute time point only). (A) Two regions of interest show the globular or tubular manifestation of SNX1 at the site of infection, whereas EEA1 displays a punctuate distribution (arrowheads). (B) After 60 min, most bacteria show exclusive enrichment for SNX1 (arrows), while few are EEA1-positive (asterisk). (C) Quantification of marker enrichment scoring between 40 - 100 bacteria for enrichment of the respective marker in individual z-sections expressed as percentage of the sum of all SNX1- and/or EEA1-positive bacteria (n = 3 for 15 min, n = 2 for 60 min, error ± min/max). (D) HeLa cells infected with SL1344 for 15 min were fixed after 60 min and labelled anti-Lamp-1 (Alexa488) and DAPI (blue). Scale bar is 10 μm.

be involved in mediating the prolonged association. In this light, potentially, the targeting *via* the SNX1-BAR domain to only highly curved regions may explain the non-uniform distribution of SNX1 on vacuoles and globular appearance (compare overexpression phenotype)[21].

5.4.3. Live cell analysis: Recruitment of GFP-SNX1 triggers tubule formation

As I wished to further investigate the dynamics of the rapid and prolonged yet transient recruitment of SNX1 to the site of invasion, a live cell imaging (LCI) approach using a wide-field set up was chosen.

Experiments were performed using either HeLa or MDCK cells transiently transfected with a vector encoding for a GFP-SNX1 fusion protein for 22 hours and great care was taken to select cells displaying low to moderate GFP-SNX1 expression levels for infection experiments (see **par 5.3.6** for details). Images were taken every 20 seconds over a period of up to 30 minutes[22]. The time point of addition of bacteria is readily recognisable as a 'white flash' [23]. Confirming the fixed cell analyses, it was observed that GFP-SNX1 was readily recruited to the site of invasion, in both, MDCK cells (**Movies 5.2.1 – 5.2.4**; **Figure 5. 4**) and HeLa cells (**Figure 5. 7** for fixed-cell analysis). In less than 15 minutes p.i., most of the cellular GFP-SNX1 had accumulated at the site of infection resulting in a loss of SNX1 at the perinuclear pool.

Strikingly, live cell analysis revealed that the recruitment coincided with the appearance of numerous long-range GFP-SNX1-decorated tubules, while prior to infection only few short rage tubules were observed from internal SNX1 pools. The tubules emanating from the site of infection were considerably longer (see below) and appeared to be shooting off from the SCVs. After 5 – 10 minutes, the tubules appeared to collapse or 'retract' back on to the site of infection, and the protein stayed accumulated around the SCVs. In some cases, tubules were observed to make contact with cytoplasmic[24], vesicular pools of SNX1 (boxed area, **Figure 5. 4 C**). The GFP-SNX1 recruitment and tubulation was most evident and pronounced at large vacuolar structures, being a multiple of the size of a bacterium in diameter (**Movies 5.1.1 – 5.1.4; Figure 5. 4**, asterisks).

---

[21] Indeed, neither the K214R PX domain mutant (incapable of binding to PPIn), nor the KKR-EEE BAR domain mutant are recruited to infection sites, but remain cytosolic (data not shown).

[22] Movies are replayed at 10 frames per second.

[23] Bacteria are added as aliquots in LB medium during the 20-second interval between image capturing; due to its composition, LB medium will naturally have different optical 'properties' than imaging buffer.

[24] as opposed to infection site

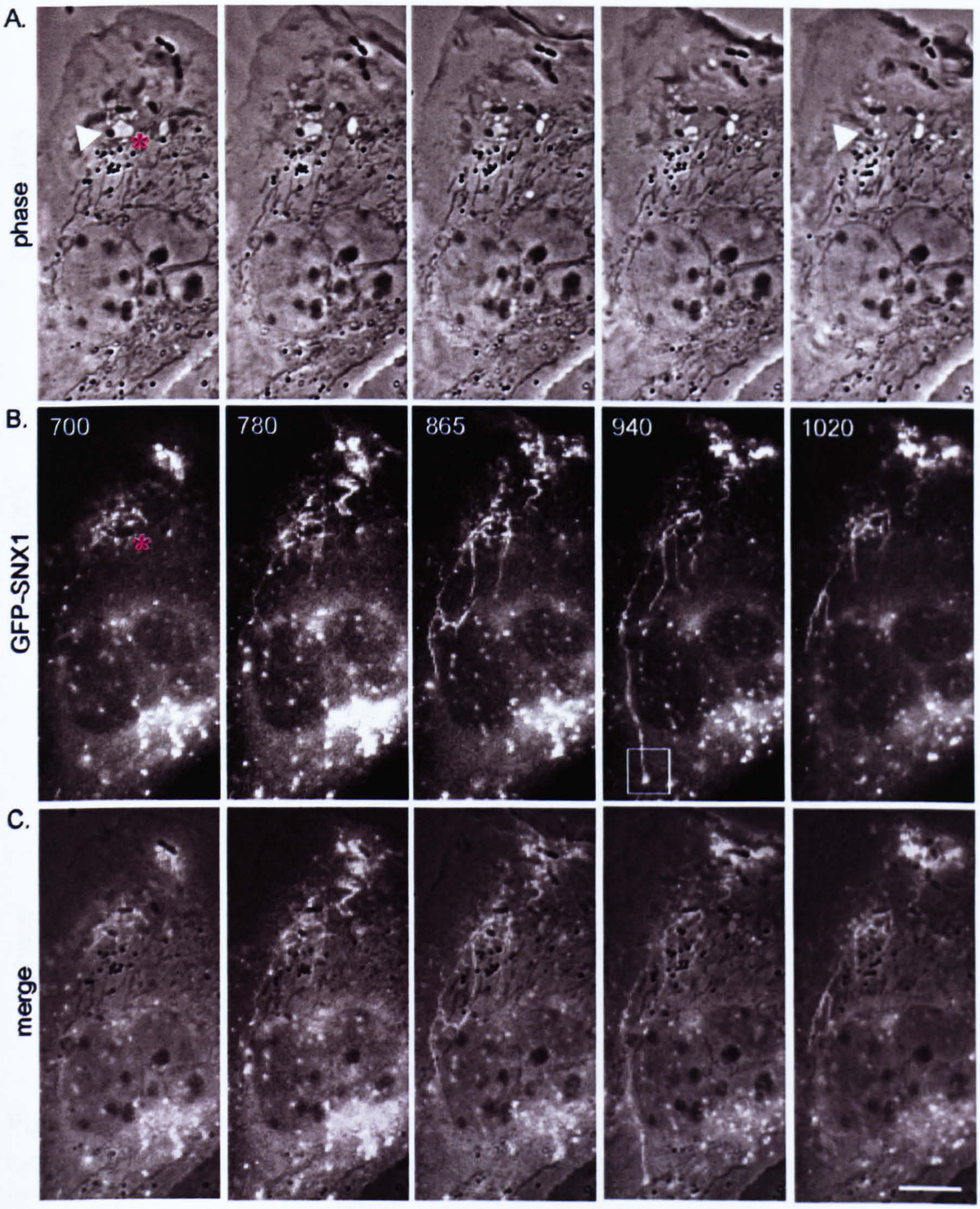

Figure 5. 4 Live cell imaging shows that recruitment of SNX1 induces highly dynamic long-range tubules.

MDCK cells were transiently transfected with GFP-SNX1, then infected with SL1344 and imaged live (see also **Movies 5.2.1 – 5.2.4**). Selected frames of movies are shown (time is in seconds). (A) Phase contrast. Note size reduction of vacuoles (asterisk) with bacteria (arrowhead). (B) Fluorescent channel. GFP-SNX1 is recruited to bacteria and spacious SCVs. The protein labelled long-rage tubules that were occasionally observed to make contact with vesicular SNX1-positive structures (boxed area). (C) Merge of phase contrast and fluorescent channel at 50% opacity. Scale bar 10μm.

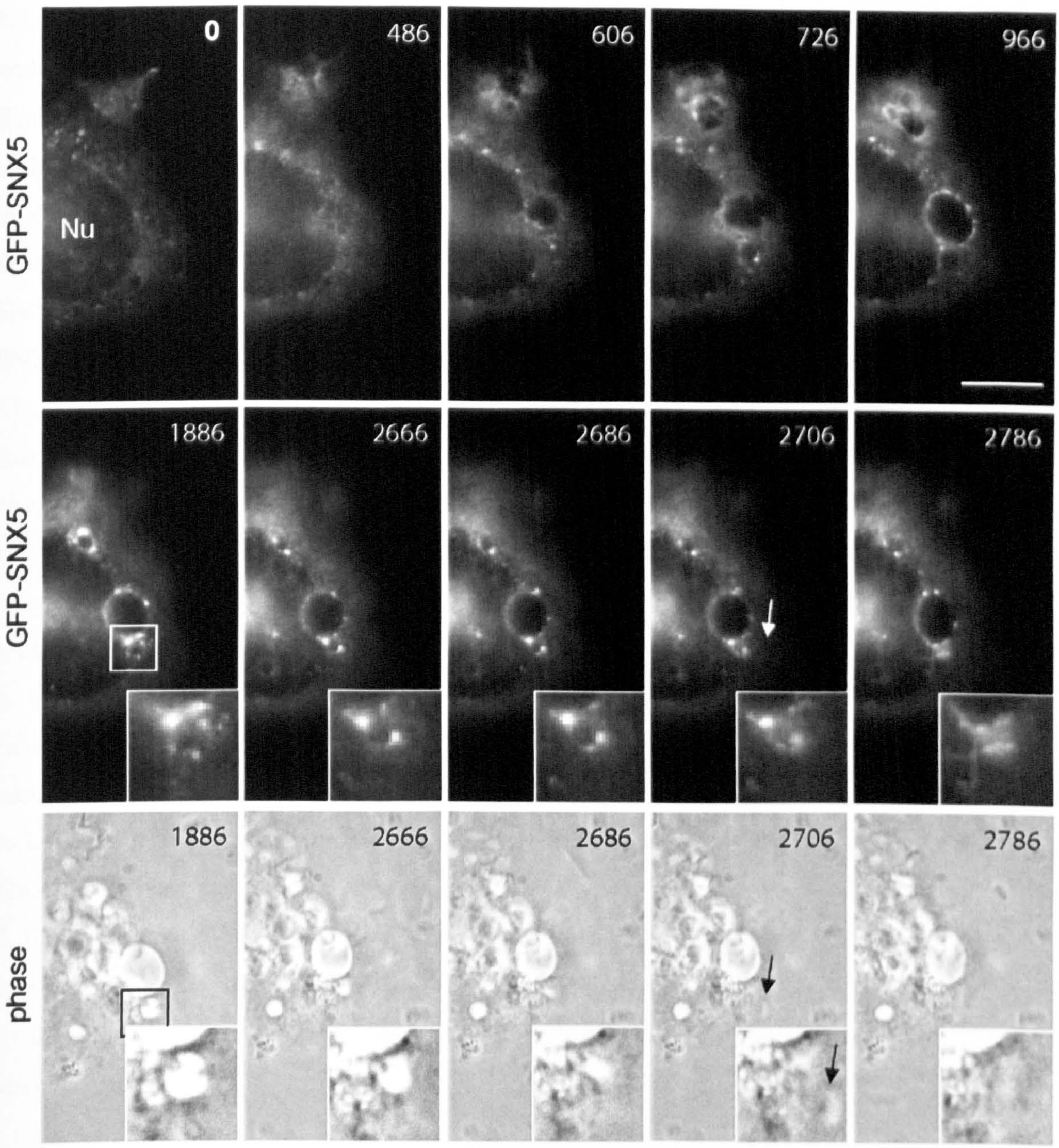

Figure 5. 5 Analysis of SNX5 recruitment of the SCV.

Cells transfected with GFP-SNX5 were infected with wild type SL1344 and infection was imaged in real time (see also **Movies 5.3.1 – 5.3.2**); stills from these movies are shown ('Nu' denotes nucleus), time is in seconds. Tubulation observed upon SNX5 recruitment is markedly less prominent; note the release of SCV content into the extracellular space toward the end of the movie from one of the SCVs (arrows). Scale bar 10μm.

When analysing phase contrast images, it was noted that these spacious structures underwent rapid size-reduction concomitant with the appearance of SNX1-tubules in the fluorescent channel. This data is representative for over n = 3 independent experiment for each cell type (HeLa or MDCK cells) with over 10 cells imaged. Tubulation was observed in all cases but to a variable extent and generally it was observed to be most prominently developed in MDCK cells. In no case comparable tubulation was observed using other SNX/BAR proteins, such as SNX5 (compare **Figure 5. 5**; **Movies 5.3.1 – 5.3.2**), or SNX2, SNX4, or SNX8 (data not shown).

The finding that GFP-SNX1 was less readily detected on smaller vacuoles could suggest that the observed recruitment and tubulation is a size- and/or concentration-dependent phenomenon. In a simple logic one would suggest that increased ruffling leads to larger vacuoles, hence more membrane, which in turn is converted to relatively higher PtdIns3*P*-levels that subsequently recruit (by avidity) more SNX1, which –indirectly or directly – leads to pronounced tubulation.

A quantitative characterization of the correlation between vacuolar size and degree of tubulation is not trivial, considering the poor control over the parameters, the stochastic nature of the process and overlap with endogenous processes. Nonetheless, in an attempt to estimate of the speed of the process, I analysed the shrinking of large vacuoles in GFP-SNX1-expressing cells *versus* non-transfected cells present in the same visual field (**Figure 5. 6**; see also **para. 5.3.10**). Here, the difference in the area of light-lucent large vacuoles was measured over time (in frames), and it appears that cells visibly recruiting GFP-SNX1 to the vacuoles, shrank approximately 2.5 times faster than non-transfected cells in the analysed sample.

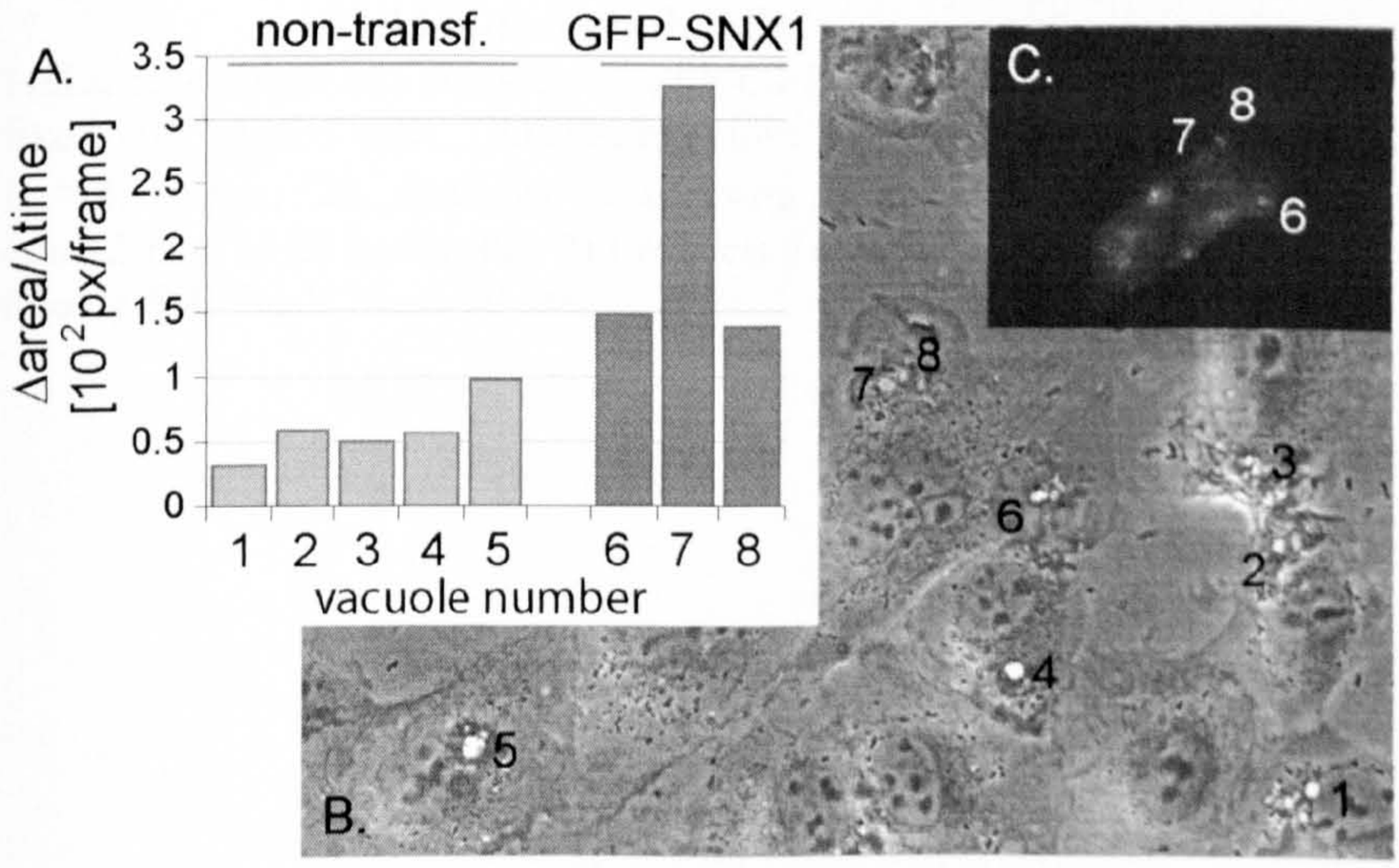

Change of vesicle area (in pixels) per frame of one focal depth of LCI infection assays (see par 5.3.6) was analysed, examining randomly chosen large light-lucent vesicles (see B.) in cells expressing GFP-SNX1 (vesicles 6 – 8, compare C.) or non-transfected cells (1 -5).

Figure 5. 6 Analysing vacuolar shrinking in GFP-SNX1-expressing cells.

To better document the observed tubular nature of SNX1 at the site of infection, I decided to fix the GFP-SNX1 transfected (and bacterially infected) cells. Acquired confocal images were subjected to iterative deconvolution and 3D image volume rendering, animated and exported as movies, which allowed to fully appreciate the extent of tubulation (**Movie 5.4**; **Figure 5. 7**). The results show that bacteria, as labelled by DAPI, were partially 'covered' with GFP-SNX1 or had an extensive tubular network associated with them. Bacteria often appeared as clustered but even at lower bacterial numbers (bottom **Movie 5.4** or **Movies 5.2.1 – 5.2.4**) extensive SNX1 accumulation was observed.

Given the precedent of artefacts related to SNX1 overexpression, these findings also raised concerns to which extent the observed phenotype was related to the procedure (Chapter 3, **para. 3.3**). Hence, it became pertinent to closer examine the infection sites at endogenous SNX1 levels for (potential) tubulation.

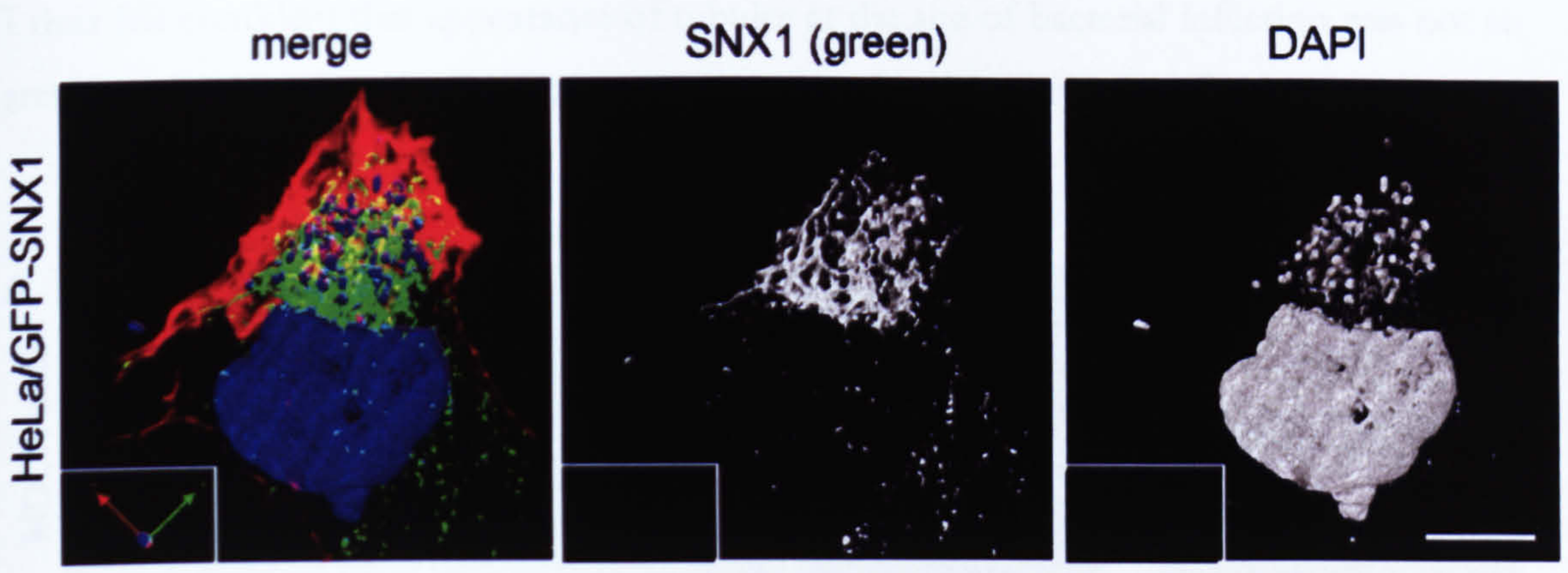

Figure 5. 7 Deconvolution analysis of tubular SNX1-decorated structures in SL1344-infected cells.

HeLa cells transiently transfected with GFP-SNX1 were infected with SL1344 for 15 minutes, then fixed and treated with TRITC-phalloidin (red) and DAPI (blue). Optical z-slices were acquired (z = 4.76 µm, 29 sections) and, using Volo*city* V4.0.1, data sets were deconvolved (98% confidence, or 20 iterations), 3D-rendered and animated, and sequence was exported as movie (see **Movie 5.4**). Scale bar is 10 µm.

5.4.4. Optimized fixation conditions allow for tubule preservation.

To verify that these tubules were not an artefact of overexpressing the GFP-SNX1 fusion protein, I sought for ways to visualize possible tubulation of previously undetected endogenous SNX1 (compare **Figures 5.1, 5.2, 5.3**). As discussed, it was noted that prolonged exposure to low temperature can affect the intracellular membrane morphology and render GFP-SNX1 cytosolic (Chapter 3, **para. 3.3**), so attempts were made to optimize the fixation protocol aiming to keep conditions as 'physiological' as possible: in these experiments it was found that fixing the cells in 4% PFA (diluted in DMEM rather than PBS) at 37°C resulted in successful preservation of SNX1-decorated tubules, in both, HeLa and MDCK cells (**Figure 5. 8 A,B**). With this procedure, it was possible to preserve tubules decorated with endogenous SNX1 as contiguous 'filaments' that were exclusively observed in direct proximity of bacteria, preserved up to a length of 25 μm in length in MDCK cells (**Figure 5. 13 A**).

I thus felt confident that appearance of tubules at the site of bacterial infection was not an artefact of overexpressing SNX1, but merely a question of appropriate fixation conditions.

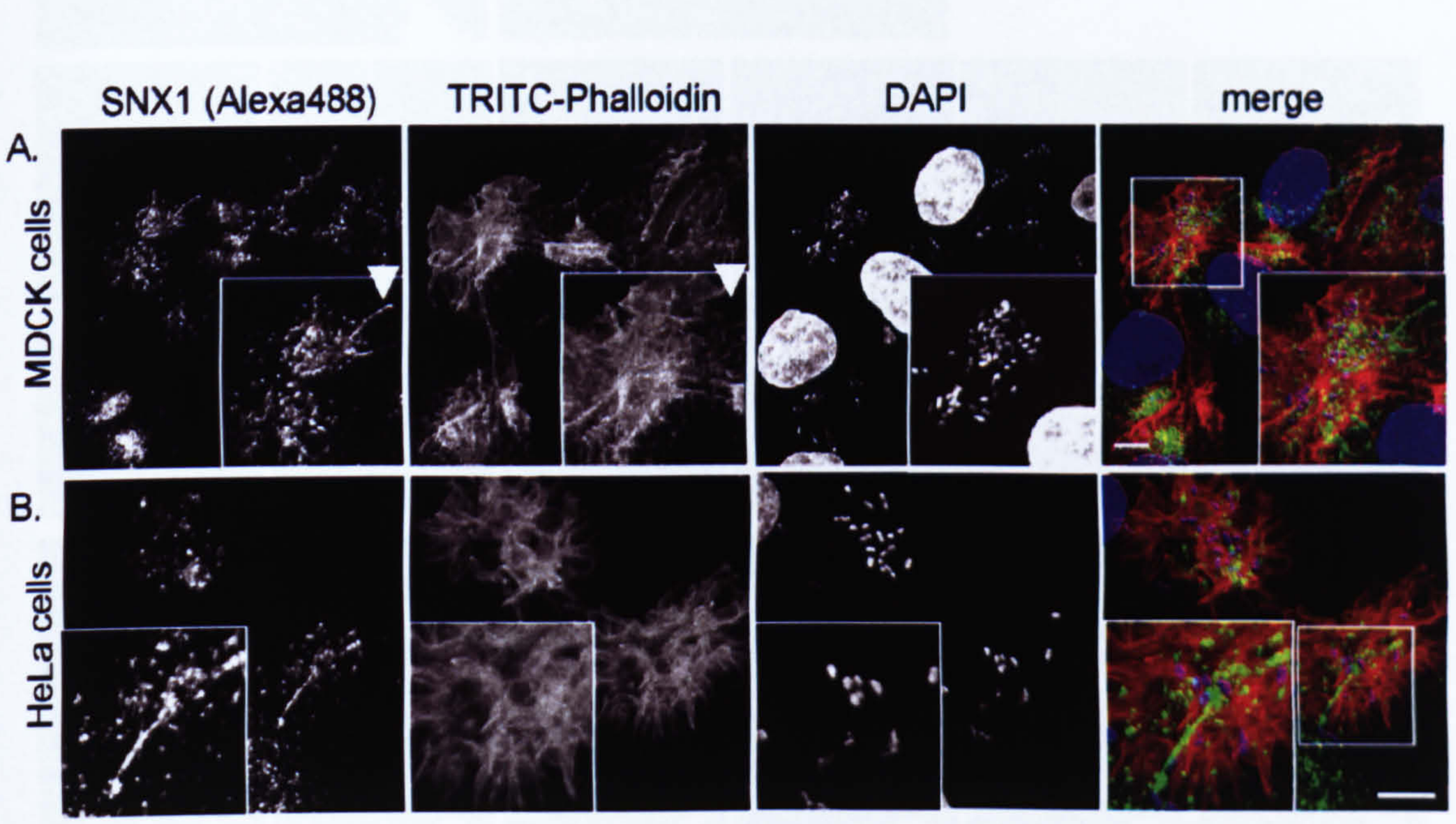

Figure 5. 8 Optimized fixation conditions allow for tubule preservation.
MDCK cells (A) and HeLa cells (B) were infected with the SL1344 strain for 15 minutes, then fixed using 4% paraformaldehyde at 37°C for 15 minutes. Subsequently, cells were immuno-labelled with anti-SNX1 antibodies (Alexa488, green) and incubated with TRITC-phalloidin (red) and DAPI (blue) to visualize bacteria. Tubules (arrowhead) are emanating from bacterial clusters sites of infection Scale bar is 10 μm.

5.4.5. Investigations into the differential recruitment of a 2xFYVE probe and SNX1

One big challenge was to further characterize the observed SNX1-decorated tubules (as opposed to vacuoles), as these structures were highly dynamic, short-lived and displayed high variance in extent of tubulation and scale.

Initial attempts were aimed at better correlating the SNX1-structures to other SCV-recruited probes. As shown, EEA1 did not appear to label these structures in fixed cell assays. Likewise, when infection was recorded in real time in cells transfected with a GFP-2xFYVE probe, the appearance of the probe at the site of infection was markedly different from a SNX1 probe, whether on apparently empty 'macropinosomes' (**Figure 5. 9**; **Movies 5.5**) or on tight fitting SCVs (**Figure 5. 10**; **Movie 5.6**).

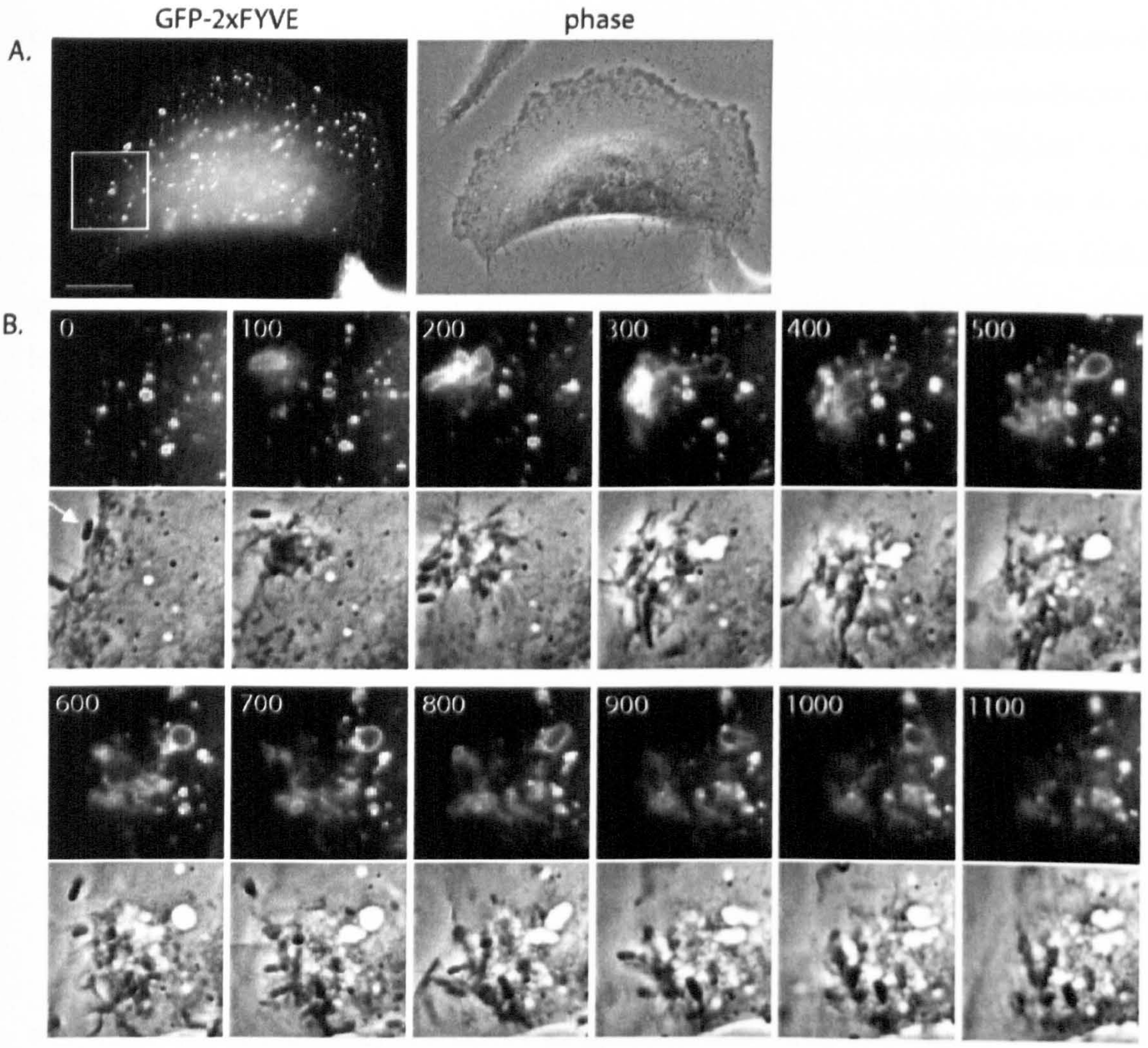

Figure 5. 9 Recruitment of a GFP-2xFYVE probe to the site of bacterial infection.

HeLa cells were transfected with a GFP-2xFYVE probe and, after 22 hours, infected with SL1344. Time (in seconds) is given from first discernible contact of bacterium (arrow). See also **Movies 5.5.1 and 5.5.2** Scale bar is 10 μm.

In the course of these analyses, I also attempted real-time infection analyses when co-expressing an RFP-2xFYVE probe and GFP-SNX1 to better monitor and dissect the different recruitment patterns in HeLa cells. It is to be said that these experiments are very challenging in the regard that first, cells co-expressing both proteins at acceptable levels[25] were rarely encountered and second, cells targeted by bacteria can only be poorly predicted .

The results obtained were however very interesting as they revealed a marked difference in the initial recruitment steps of the two proteins: while the RFP-2xFYVE probe localized around the entering pathogen, SNX1 appeared to be recruited to, or very close to, the plasma membrane at an 'angle' to the entering pathogen (**Movie 5.6; Figure 5. 10**)[26]. In contrast to SNX1, the fluorescent 2xFYVE probe was evenly distributed on the vacuolar membrane. As previously observed in MDCK cells (Pattni et al., 2001), the association of the 2xFYVE probe around the SCV was often transient and appeared as 'flashes' as the probe repeatedly re-associated with the same tight fitting SCVs. Strikingly, in the shown example, marked tubulation of the SNX1-probe was not observed. At first this finding appears at odds with the previous studies, but it correlates with the absence of markedly large vacuoles. The absence of large vacuoles correlates with the absence of marked ruffling; and ruffling in HeLa cells was generally found to be less pronounced than in MDCK cells. So in conclusion, regardless of the 'vacuole size', SNX1 is recruited to the site of infection, but pronounced tubulation was not always observable at LM level.

---

[25] Defined as relatively low levels of SNX1 for the discussed reasons, while generally, the 2xFYVE probe was found very highly expressed, hence resulting in markedly different exposure times, which is highly undesirable when attempting to visualize dynamic events in a directly comparative study.

[26] The accompanying movie starts with an overlay of all three channels (phase, RFP-2xFYVE in red, GFP-SNX1 in green), then a merge of the fluorescent channels (RFP-2xFYVE and GFP-SNX1), followed by RFP-2xFYVE, then GFP-SNX1.

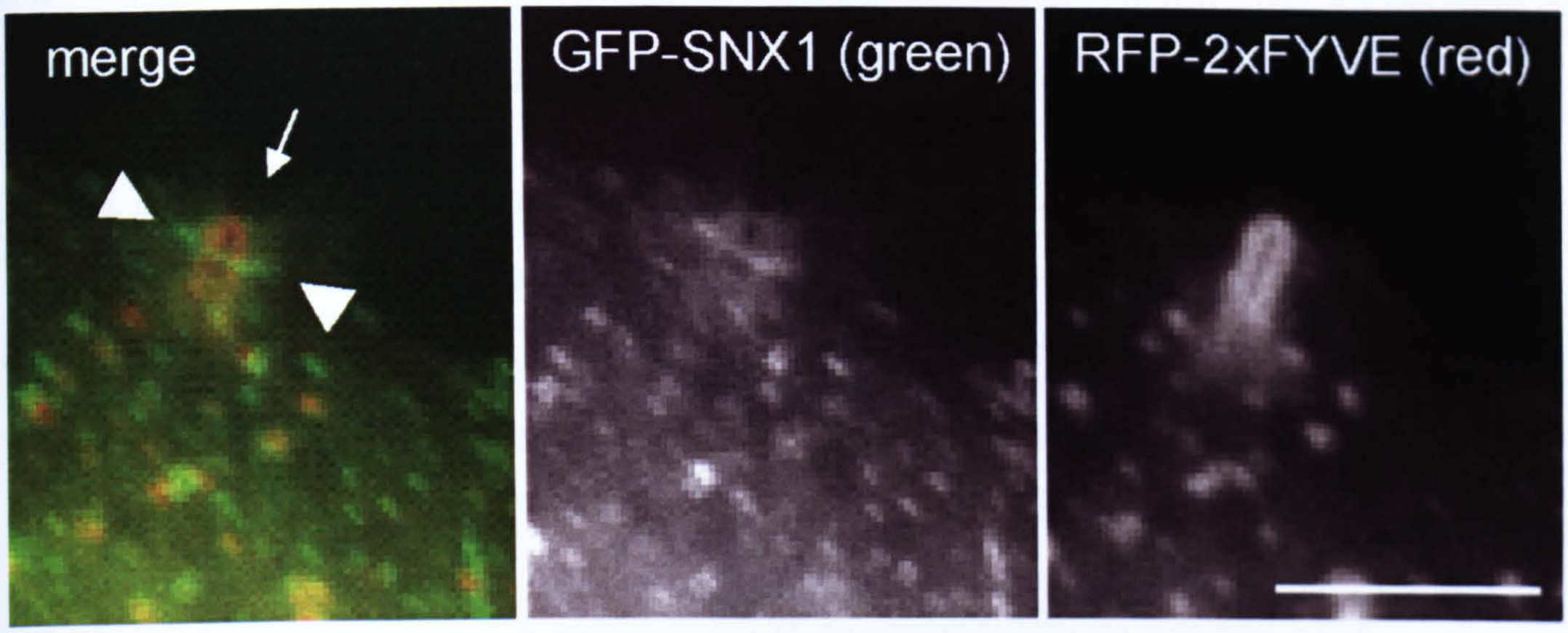

Figure 5. 10 Infection of cells co-expressing fluorescently labelled 2xFYVE and SNX1 shows differential recruitment of both probes to SCVs.

HeLa cells were transfected with RFP-2xFYVE and GFP-SNX1 and after 22 hours, infection was imaged live for approximately 30 minutes (see also **Movie 5.6**). Whereas the 2xFYVE-probe uniformly labelled vesicular structures and the SCV (arrow), SNX1 was found on vesicles and at the plasma membrane (arrowheads). Scale bar is 5 μm.

5.5. Characterization of infections using a ΔsigD mutant

5.5.1. Fixed and live cell analysis of SNX1 recruitment to sites of infection using a SL1344-ΔsigD strain

The size of the vacuoles is linked to the ruffling induced by the bacterium, which is therefore not sufficiently controllable. So I chose to make use of a SL1344 mutant (SL1344-ΔsigD) to carry out infection assays. One reasoning behind utilizing this mutant stemmed from the previous finding that infection of Henle-407 cells with a ΔsigD strain resulted in formation of only small vacuoles that additionally rarely fused with one another (Hernandez et al., 2004). Likewise, ectopic overexpression of SigD in mammalian cells has been shown to induce formation of large vacuoles (Terebiznik et al., 2002; Mason et al., 2007). Thus, it appears that SigD is somehow involved in size regulation.

Additionally, given the binding preferences of the SNX1-PX domain, my interest in investigating this mutant in more detail was sparked by the fact that SigD is a PPIn phosphatase: as discussed, at current state the literature is somewhat divergent about the substrate specificity, and - *inter alia* - PtdIns(4,5)P_2 (Terebiznik et al., 2002; Mason et al., 2007), but excitingly, also PtdIns(3,5)P_2 and PtdIns(3,4,5)P_3 (Marcus et al., 2001) have been proposed as substrates from *in vitro* studies.

So if in the cellular context, dephosphorylation of PtdIns(3,5)P_2 would considerably contribute to SCV-PtdIns3*P* levels, one might hypothesize that in absence of SigD, PtdIns3*P* is not sufficiently generated at the infection site. This would appear to be a legitimate conclusion from the observed absence of a PtdIns3*P*-ligating p40PX-contruct when infecting with a ΔsigD strain (Hernandez et al., 2004). Furthermore, analysis of the PPIn species in infected cells using electrospray ionization mass spectrometry (ESI-MS) has suggested that cellular PtdIns*P* [sic][27] levels are increased upon wild type-strain but not ΔsigD-strain infection (Hernandez et al., 2004). Following this logic, it implies that PtdIns(3,5)P_2 levels are elevated on the SCV in the absence of SigD, as had been suggested, but not shown (Hernandez et al., 2004).

To investigate this hypothesis, I chose to analyse recruitment of SNX1 to sites of infection when using the ΔsigD mutant by LCI analysis. In these assays, HeLa cells were first transiently transfected with GFP-SNX1 and after 22 hours infected with a SL1344-ΔsigD

---

[27] This ESI-MS set-up is capable to discriminate between mono- and bis-phosphorylation (Wenk et al., 2003)

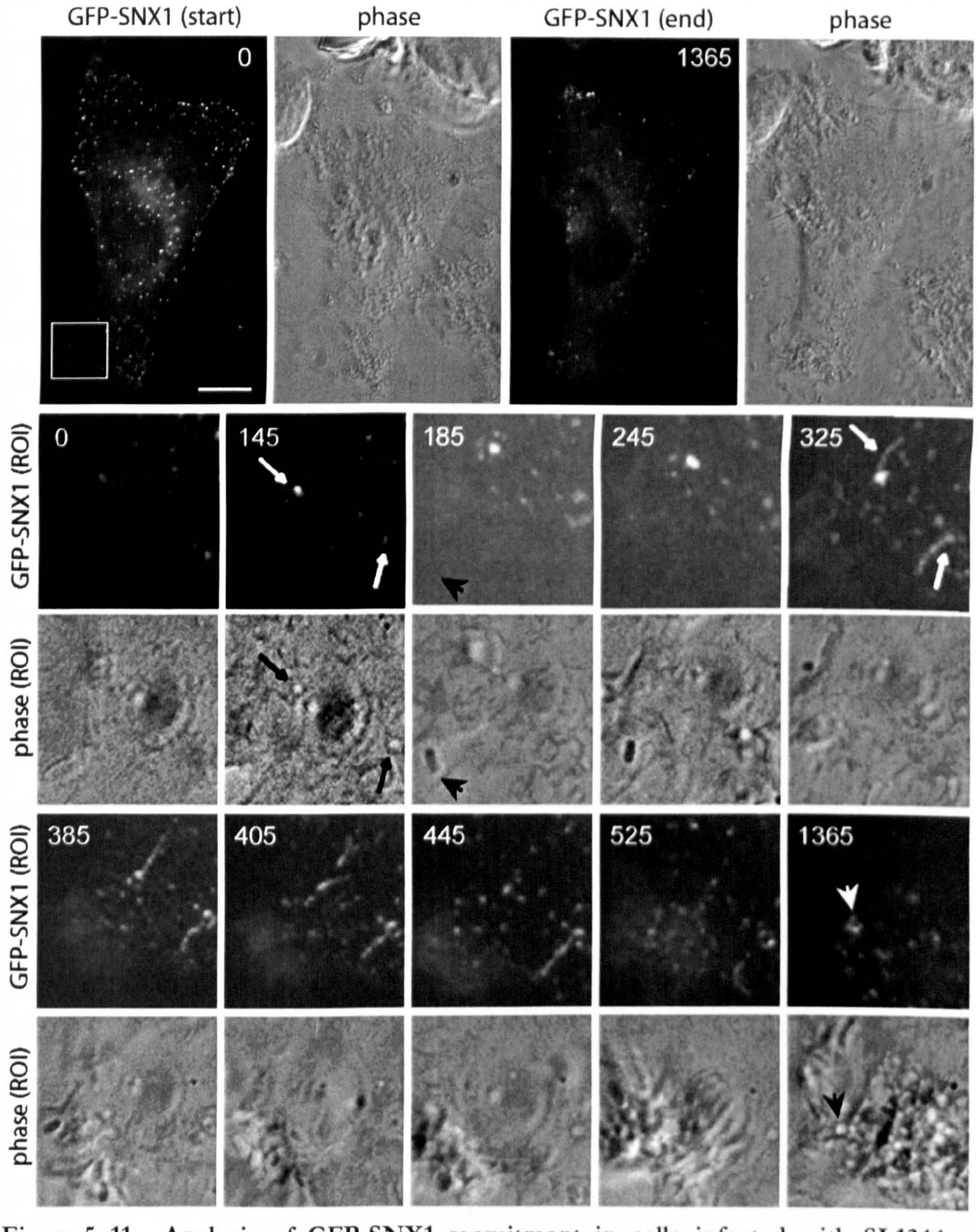

Figure 5. 11 Analysis of GFP-SNX1 recruitment in cells infected with SL1344-ΔsigD

HeLa cells were transfected with GFP-SNX1 for 22 hours, then infected with a SL1344 strain lacking SigD (ΔsigD). Infection was imaged live (see also **Movies 5.7.1 -5.7.2**); stills and a region of interest (ROI) from the movies are shown, time is in seconds from the start of experiment. Although SNX1-positive tubules emanating from endosomal structures were observed (arrows, black and white), there was no pronounced enrichment of GFP-SNX1 at the site of infection (arrowheads, black and white). Data is representative for three independent experiments with over 10 cells imaged Scale bar is 10 μm.

strain (**Movies 5.7.1– 5.7.2; Figure 5. 11**). Several observations were made: in these assays, I indeed failed to observe generation of spacious vacuolar structures upon infection with ΔsigD, as evidenced by the lack of large light-lucent structures in the phase contrast images (**Figure 5. 11; Movie 5.7.2**). More over, in these cells accumulation of GFP-SNX1 at the site of infection was not observed (**Figure 5. 11**, arrowheads). While short-range tubules from endosomal compartments were evident (**Figure 5. 11**, arrows), tubulation from SCVs was not detected, as the probe failed to accumulate. In a control experiment, using a SL1344-ΔsigD mutant complemented with a plasmid encoding for SigD and its chaperone SigE, recruitment of GFP-SNX1 was restored (**Figure 5. 12; Movies 5.8.1– 5.8.2**). To further confirm these findings, I also chose to analyse the recruitment in MDCK cells at overexpressed (data not shown) and endogenous SNX1-levels (**Figure** 5. 13). In no case, long-range tubules were observed upon infection with the ΔsigD-strain, although in some exceptional cases (when large vacuoles were produced) SNX1 was indeed recruited. The generation of spacious vacuoles when infecting cells using the ΔsigD mutant was however a rare event. A correlation of the lack of tubules and/or recruitment with bacterial numbers appeared also unlikely as in wild type-infected cells continuous tubules of up to 25 μm (**Figure 5. 13 A**, arrows)[28] emanated from infection sites with seven bacteria or less, while clusters of 10 - 20 ΔsigD bacteria were not seen with associated tubules (**Figure 5. 13 B**)[29].

Given that SNX1 is not recruited to the SCV or site of infection in spite its documented ability to bind to PtdIns(3,5)P_2 (Cozier et al., 2002), I consider it unlikely that PtdIns(3,5)P_2 levels are elevated on SCVs in absence of SigD. This is supported by the finding the basal PtdIns(3,5)P_2 levels and PtdIns(3,5)P_2 levels after infection with a ΔsigD are equally low (Mason et al., 2007).

So it appears that the absence of SigD could simply lead to persistence of PtdIns(4,5)P_2 (Terebiznik et al., 2002). Very recently, another study convincingly showed that ectopic expression of SigD dephosphorylates PtdIns(4,5)P_2 as its main substrate and in doing so, alters epithelial structure and function (Mason et al., 2007). Although not shown in an infection model, one would extrapolate from the findings by Mason and colleagues that in

---

[28] As measured from one confocal z-section

[29] Number of bacteria was analysed from co-labelling DNA with DAPI (channel omitted in **Figure 5.13**).

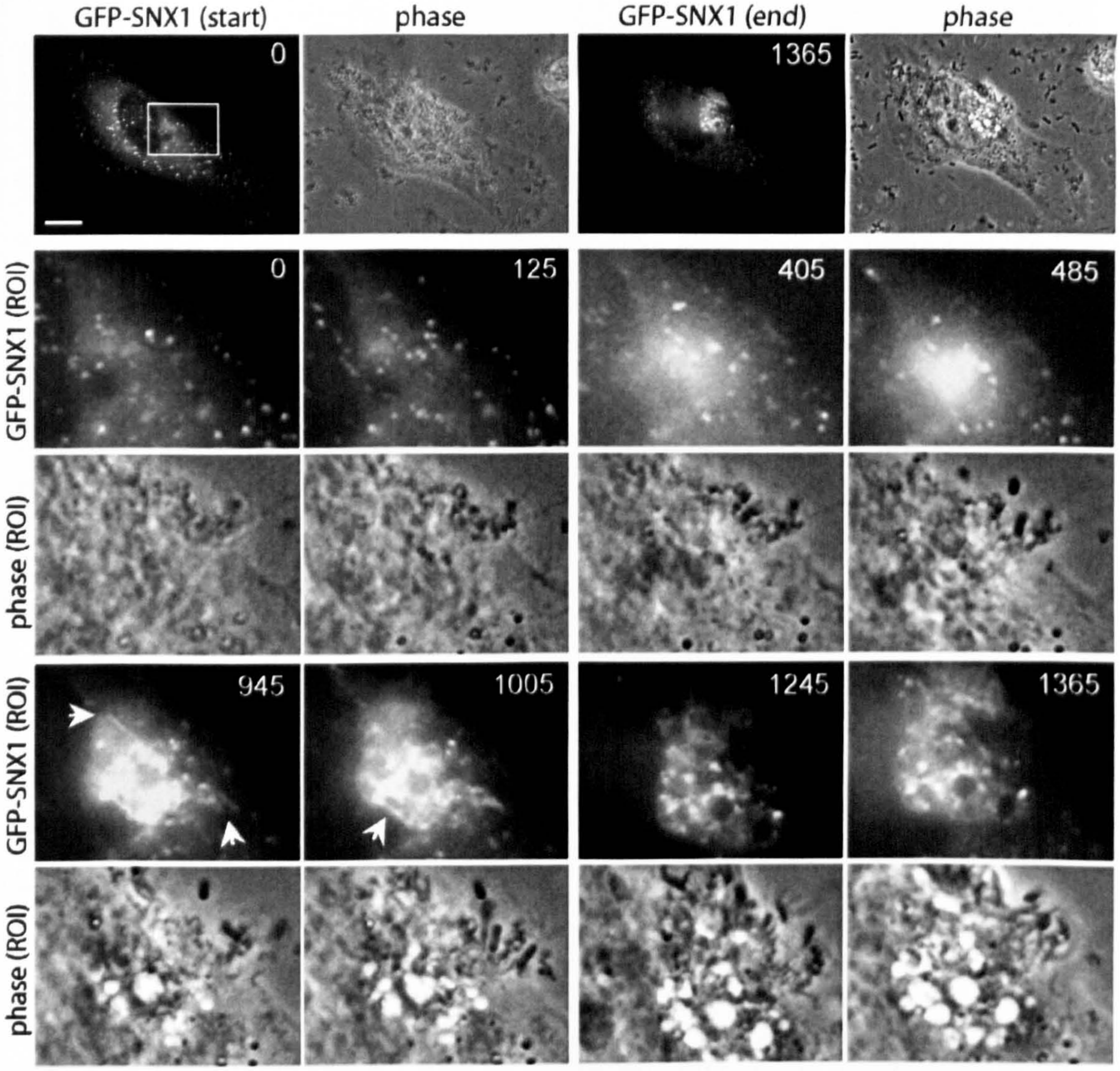

Figure 5. 12 Recruitment of GFP-SNX1 is restored using SL1344-ΔsigD bacteria complemented with SigD encoded for on a plasmid

HeLa cells transfected with GFP-SNX1 were infected with a SL1344-ΔsigD mutant that additionally carried plasmids encoding for SigD and SigE (SL1344-ΔsigD-pSigD-pSigE), and infection was imaged live. Stills from these movies (**Movies 5.8.1** and **5.8.2**) and a region of interest (ROI) are shown. Time is in seconds from start of experiment. Scale bar is 10 μm.

cells infected using a ΔsigD strain, PtdIns(4,5)P_2 might not be appropriately converted and hence, given the binding specificity of the SNX1-PX domain, there is no appropriate 'cue' for SNX1 to be targeted to. This hypothesis was further supported by results from the analysis of the relation between actin-loss and SNX1 enrichment in cells infected with the ΔsigD strain (see following paragraph).

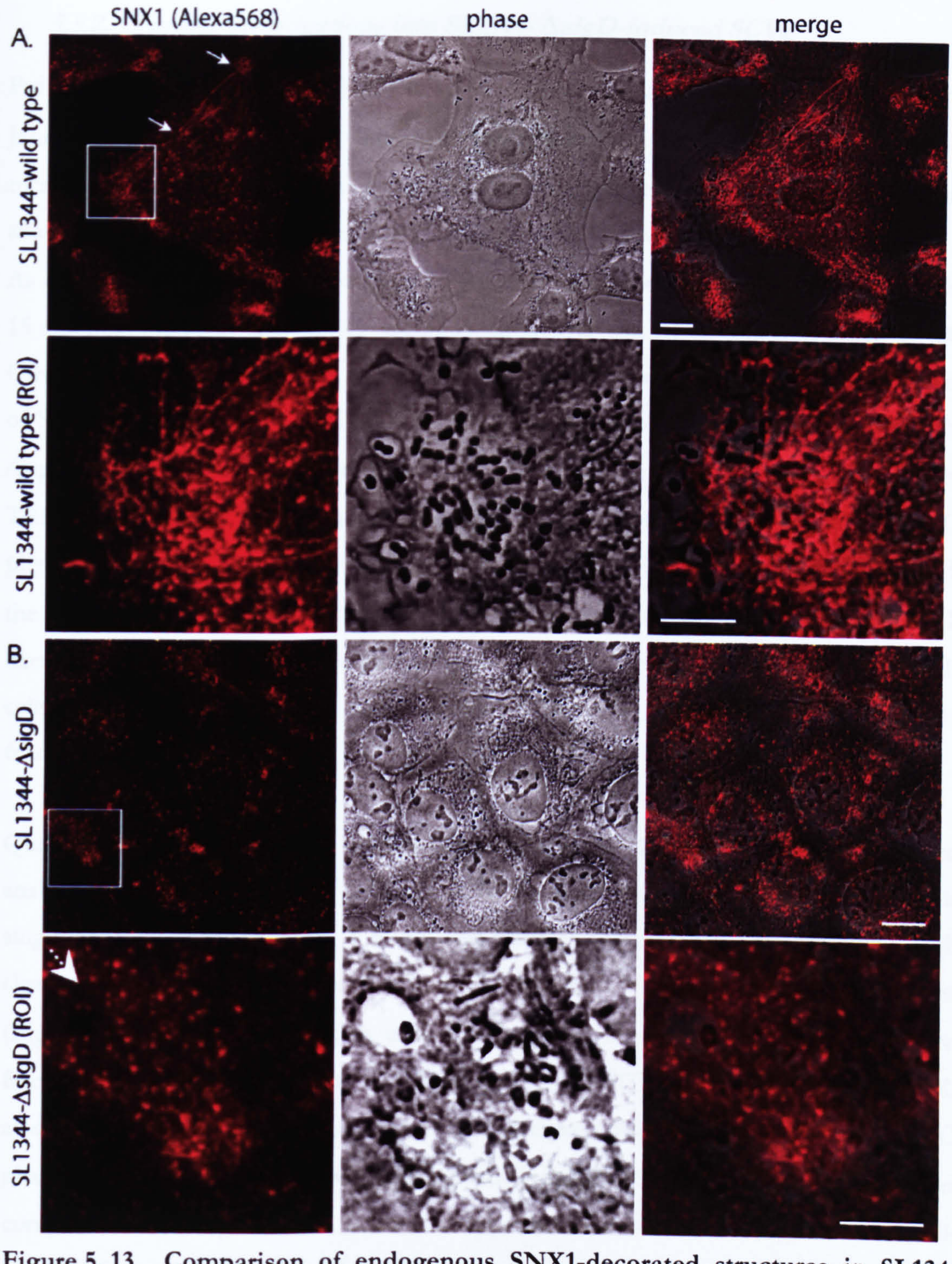

Figure 5. 13 Comparison of endogenous SNX1-decorated structures in SL1344 wild type SL1344- or SL1344ΔsigD-infected MDCK cells.

MDCK cells were infected a with wild type SL1344 or with a SL1344-ΔsigD strain for 15 minutes, then fixed and labelled for endogenous SNX1 (Alexa568, red). Maximum projections of two z-sections (at 488 nm z-separation) are shown. Tubules up to 25 μm could be preserved in control cells (arrows). In SL1344-ΔsigD-infected cells, SNX1 is mainly vesicular with no pronounced recruitment to bacteria or even unusual large vacuoles (arrowhead). Scale bar is 10 μm.

5.5.2. Further investigations into SL1344- ΔsigD-induced SCVs

PtdIns(4,5)P_2 has an established role in cytoskeleton–plasma membrane linkage [(Yin and Janmey, 2003) for review], so to investigate the effect of ΔsigD strain-infections on SNX1 recruitment and the actin cytoskeleton simultaneously, I performed a series of fixed cell analyses monitoring endogenous SNX1 levels and F-actin levels using TRIC-phalloidin.

As expected, compared to the wild type strain, in cells infected with the ΔsigD strain for 15 minutes, markedly less SNX1 accumulated at the site of infection (**Figure 5. 14**). Careful inspection showed that while in cells infected with wild type SL1344, the majority of SCVs were observed to be SNX1-positive (**Figure 5. 14 A,E**), in cells infected with the ΔsigD strain, bacteria appeared mostly 'trapped' in actin-rich structures as visualized by the TRITC-phalloidin stain: here, no marked 'shift' in the association of SCVs with TRITC-phalloidin and SNX1 was observed (**Figure 5. 14 C,D,E**). Even after 60 minutes, when in the control, bacteria rarely co-localized with phalloidin-positive structures, most ΔsigD bacteria were still enclosed by tight-fitting phalloidin-positive SCVs (**Figure 5. 14 D**). In cells infected with wild type strain I only occasionally observed 'entrapment' after 60 minutes (**Figure 5. 14 B**).

Quantification of the kinetics of actin-loss versus SNX1-enrichment was performed, analysing the co-distribution of actin and SNX1 at or in immediate vicinity of bacteria in single confocal sections. Here, I found that bacteria infected with the wild type strain clearly changed from actin to exclusive SNX1 enrichment over the course of one hour (**Figure 5. 14 E**). In contrast, in cells infected with the ΔsigD strain, the respective fractions of SCVs positive for TRITC-phalloidin, TRITC-phalloidin+SNX1 or SNX1 alone remained largely unaltered. Further still, the percentage of doubly labelled TRITC-phalloidin+SNX1 structures on ΔsigD-strain induced SCVs was markedly increased compared to wild type-induced SCVs. The apparent high level of co-distribution of actin and SNX1 was surprising but I feel that it is in the first instance a result of the method of analysis: while exclusively SNX1-labelled SCVs are readily identifiable due to the globular, clustered appearance of the protein at these sites (arrowheads, **Figure 5. 14 B,D**), the SNX1 distribution at, or close to, SCVs that are also positive for actin is markedly different (arrows, **Figure 5. 14 B,D**). Although single confocal z-sections were evaluated, it is not always immediately evident, whether the marker is 'on' the SCV or just very close by as endosomal SNX1 will also be detected. Especially in large-size clusters, this might

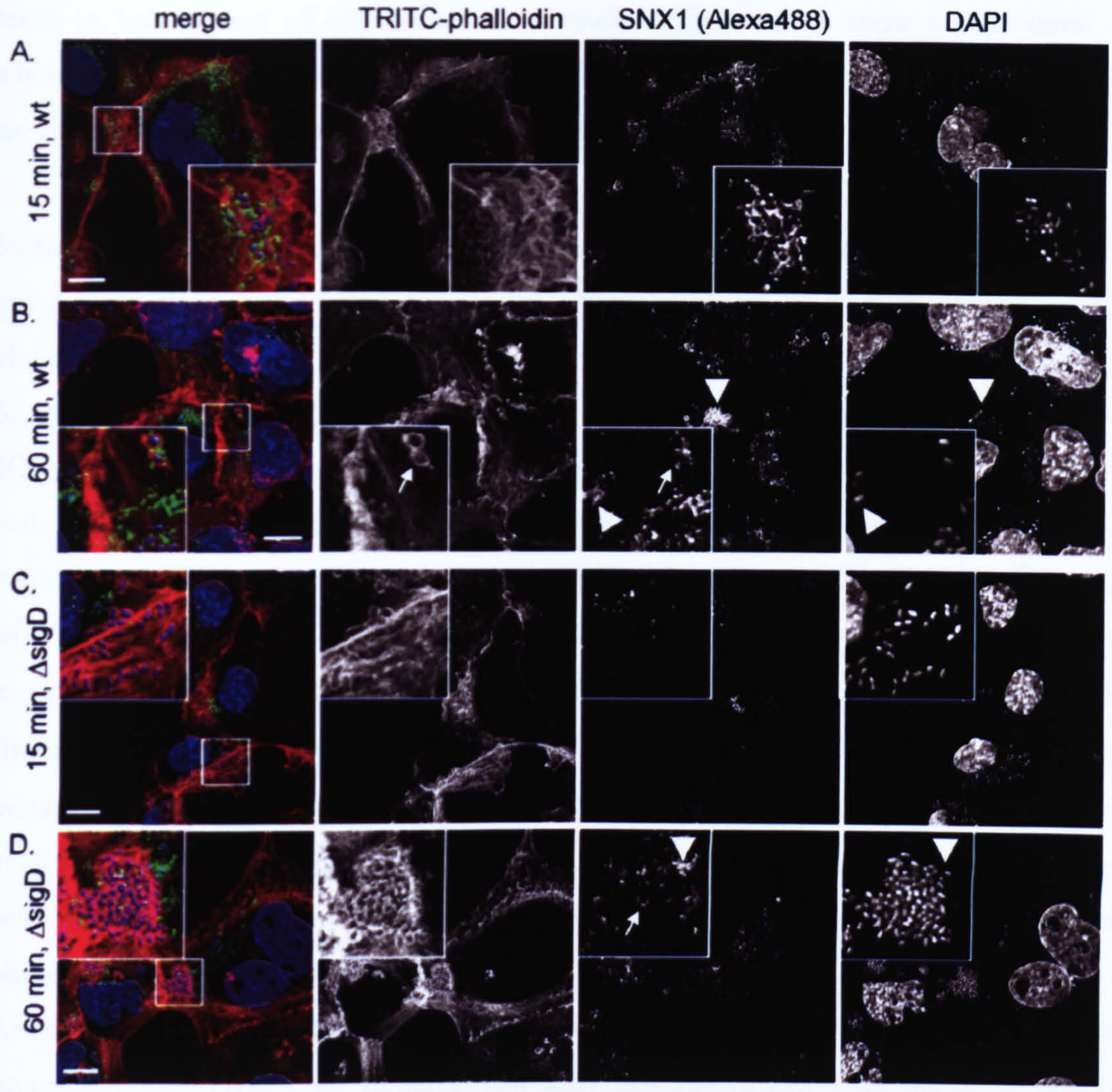

Figure 5. 14 Kinetic analysis of actin- and SNX1-enrichment on wild type or ΔsigD SL1344 SCVs.

Cells infected with wild type or the ΔsigD mutant strain for 15 minutes were either fixed directly or after further 45 minutes, and were then immuno-labelled with anti-SNX1 (Alexa488, green) and treated with TRITC-phalloidin (red) to visualize F-actin, and DAPI (blue) to visualize DNA. (A-D) Three merged confocal z-slices, z(total) = 1 µm, are shown. Arrows point out unusual SNX1 manifestation on or near actin-positive structures; arrowheads highlight SNX1 accumulation as usually observed on SCVs. (E) Co-localization of bacteria with the respective marker was analysed for individual z-slices in the entire stack (10 - 12 z-slices at 480nm z-separation) and more than 100 SCVs per set (n = 2, error gives minimum and maximum). Scale bar is 10 µm.

result in 'entrapment' of endosomes. Nevertheless, these assays show a clear trend and while it might overestimate the degree of the jointly actin- and SNX1-labelled SCVs, 'actin-only' and 'SNX1-only' SCVs were readily distinguished.

So this data suggests that in cells infected with ΔsigD mutant, the SCV conversion from 'plasma membrane, PtdIns(4,5)P_2 enriched identity' to 'endosomal, PtdIns3P enriched identity' is stalled.

So how does this stalling affect the bacterial life cycle in the host cell? As discussed, the SCVs undergo a maturation process and it appears that the processes associated with this maturation and intracellular progress are crucial for optimal replication: acidification for induction of SPI-2, as well as tethering to the TGN to (potentially) branch off nutrients and 'anchoring' to the TGN to maintain correct positioning. Nonetheless, earlier studies investigating the replication of a strain lacking SigD in T84 colonic epithelial cells (Bertelsen et al., 2004) after 10 hours did not detect an defect in replication for a ΔsigD mutant. Likewise, studies using a RAW 264.7 macrophage cell line found no replication defect after 15 hours (Drecktrah et al., 2005). It is to be said, that generally, in epithelial cells replication is initiated after a lag period of 4 – 6 hours, while in macrophages this phase is thought to take between 8 – 10 hours (Knodler and Steele-Mortimer, 2003).
Although preliminary data (n = 1), I have also investigated the effect of the ΔsigD mutant on replication in HeLa cells. In agreement with the cited studies, I did not detect a defect in replication when infecting cells with the ΔsigD mutant after 12 hours, compared to cells infected with wild type SL1344 (**Figure 5. 15**). Interestingly, when I examined earlier time points (6 hours p.i.), *id est* at the proposed onset of replication, I found a marked difference though: while in control cells bacteria had already started replicating, numbers of ΔsigD bacteria were found to be unchanged. While it would be desirable to further confirm these findings, they are in line with a model in which SCVs are stalled but will eventually start to replicate.

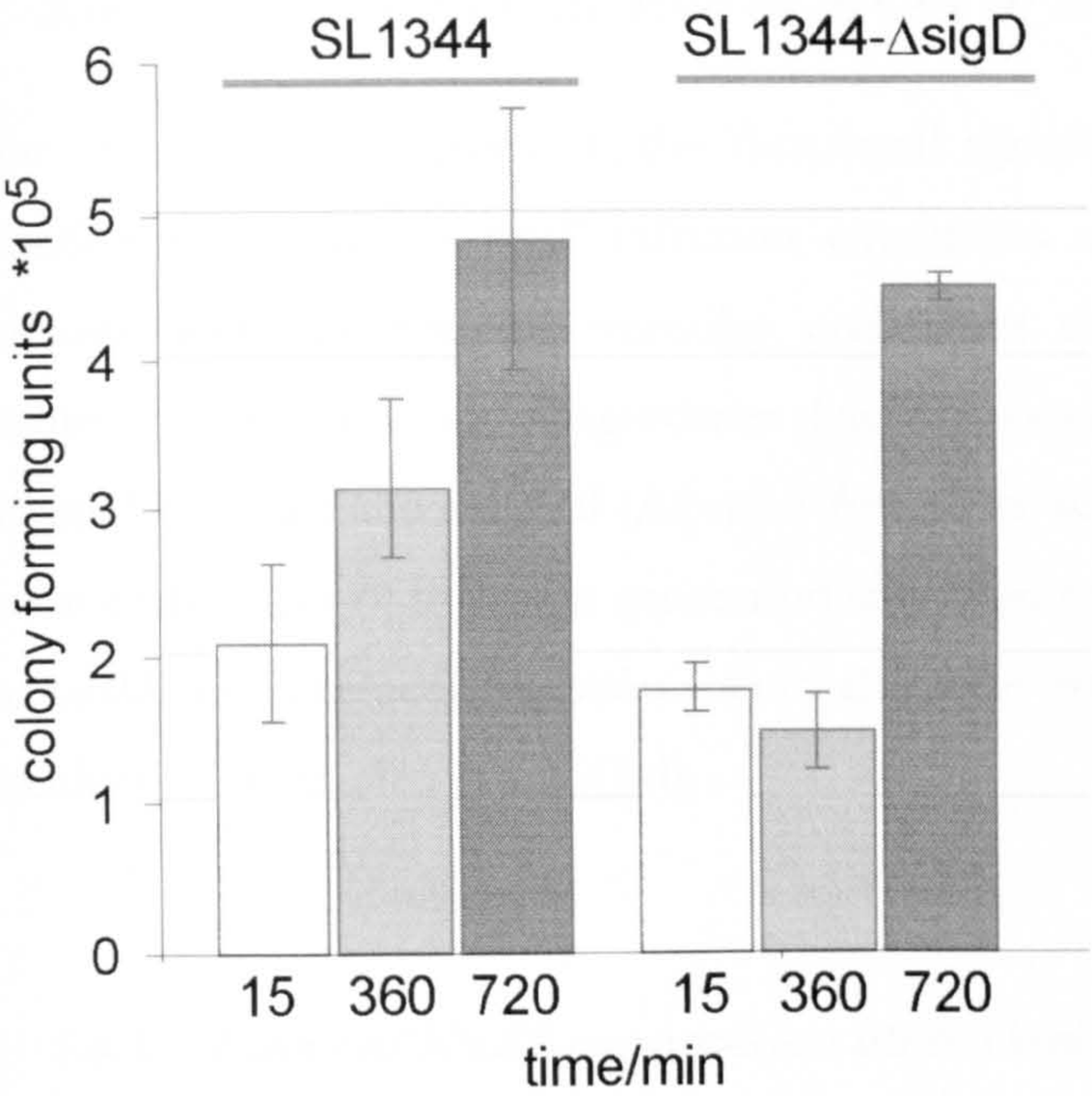

Colony forming unit assay

To analyse kinetics of bacterial replication (see **para. 5.3.8**) cells were infected with either wild type SL1344 or SL1344-ΔsigD for 15 minutes, then cells were either lysed directly or after incubation for indicated times. Lysates were plated onto LB plates (in duplicate) and incubated for 16 hours, before number of bacterial colonies was determined. NB: Data was obtained from triplicate analysis in replicate plating for control (error is min/max for triplicate), while data for SL1344-ΔsigD is from one experimental set in replicate plating (error is min/max for replica).

Figure 5. 15 Analysis of bacterial replication: SL1344 wild type and SL1344-ΔsigD strains

5.6. Studies into the role of SNX1 in Salmonella infection

One other question related to the functional significance of SNX1 recruitment to the infection site under 'normal' infection conditions using the SL1344 wild type, where spacious bacteria-containing vacuoles underwent size-reduction. In macrophages, the maintenance of spacious phagosomes has previously been suggested to contribute to bacterial virulence and survival (Alpuche-Aranda et al., 1994) and it has been hypothesized that at early stages of infection generation and maintenance of large vesicles may provide a favourable environment for *Salmonella* to allow for transition to the SPI-2 encoded TTSS machinery (Hernandez et al., 2004).

5.6.1. Effect of SNX1-suppression ob bacterial infection

To dissect the role of SNX1 in the infection process, an RNA interference approach targeting SNX1 expression was chosen using the previously characterised siRNA (Chapter 3, **para. 3.5**). When analysing SNX1-suppressed cells after SL1344-infection assays followed by immunofluorescence detection, several observations were made (see also following paragraphs): first, the CI-MPR was enriched at the site of infection, which in control cells was virtually absent from SCVs (**Figure 5. 16**). Second, bacteria appeared in most cases less clustered in SNX1-suppressed cells (**Figure 5. 17**). Third, I observed - to a variable degree - TRITC-phalloidin positive vacuoles in SNX1-suppressed but not in control cells (**Figure 5. 18**).

5.6.2. CI-MPR recruitment to sites of infection in SNX1-suppressed cells

The observation that certain proteins appear to be absent or undetectable on SCVs, most prominently the CI-MPR (Garcia-del Portillo and Finlay, 1995), has led to the general 'paradigm' that SCVs only selectively interact with endosomes, and actively segregate from the degradative route. This view has however been scrutinised recently (Drecktrah et al., 2007) uncovering an unprecedented degree of interactions of SCVs with the endo-lysosomal system, when assessing transfer of pre-loaded and newly incoming endocytic bulk-phase material to the SCV.

Generally, we would argue that the CI-MPR is only a moderately appropriate marker for late endosomes, as a negligible amount of the CI-MPR is localized endosomally or at the plasma membrane at steady state (Waguri et al., Lin et al..; see also Chapter 3). Likewise, the receptor rarely traffics through late endosomes or pre-lysosomal compartments (Hirst et al., 1998; Lin et al., 2004). Given that at steady state the vast majority of the receptor is localized to the TGN, I would predict that detection on SCVs at LM level would be challenging unless it would, by some means, become enriched on SCVs during the infection process.

In accordance with this, when I assessed CI-MPR levels on SCVs, I could not detect notable labelling at LM level (**Figure 5. 16**). Yet, in SNX1-suppressed cells, the receptor was found localized to the site of infection. Given that treatment with SNX1-specific siRNA leads to accumulation of the CI-MPR in endosomes, it appears plausible that upon infection, these 'pre-loaded' endosomes are recruited to plasma membrane.

The finding that under infection conditions, SNX1 is localized to SCVs might also help to consolidate the discrepancy that hydrolases delivered by the CI-MPR, but not the receptor itself is found on SCVs (Garcia-del Portillo and Finlay, 1995). I would postulate that recruitment of SNX1 to macropinosomes and vacuoles could allow for efficient elimination of these receptors under control ('wild-type') conditions.

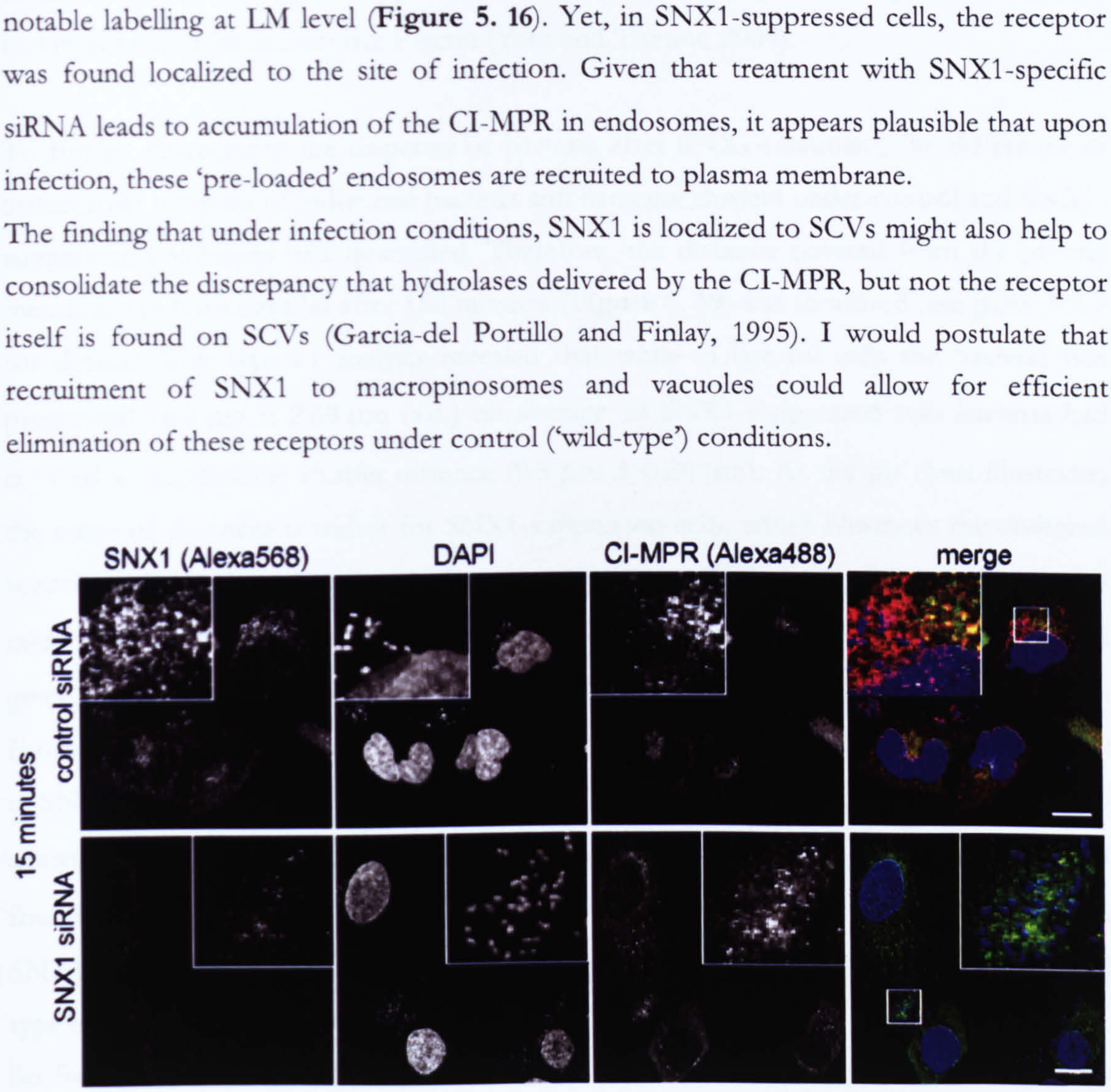

Figure 5. 16 Analysis of CI-MPR-enrichment at the site of infection in SNX1-suppressed cells.

Control and SNX1-suppressed cells were infected for 15 minutes with SL1344, washed and fixed as described and immuno-labelled with anti-SNX1 (Alexa568, red), anti-CI-MPR (Alexa488) and treated with DAPI (blue). While the CI-MPR was largely absent from sites of infection in control cells, it co-localized with DAPI stained bacteria in SNX1-suppressed cells. Scale bar is 10 μm.

5.6.3. Role of SNX1 in clustering bacteria

One observation made is that in 60 – 70% of all cases in SNX1-suppressed cells infected with SL1344, the resulting bacterial clusters appeared less tight than in control cells and were often stalled close to the plasma membrane (**Figure 5. 17**). It was also observed that in some cases, cells treated with the SNX1-specific siRNA contained, to a variable extent, TRITC-phalloidin-positive vacuoles (**Figure 5. 18**), while under control conditions at 1 hour p.i., F-actin was virtually absent from SNX1-positive SCVs. One possible explanation is that in SNX1-suppresssed cells, vacuoles are not efficiently reduced in size, and might therefore accumulate F-actin (Yam and Theriot, 2004).

To further characterize the dispersal of bacteria after SNX1-treatment, the difference in intracellular progress of individual bacteria and bacterial clusters under control and SNX1-suppressed conditions was quantified. Therefore, the distance covered from the plasma membrane in both samples after 180 minutes (**Figure 5. 19**) was measured (see **para. 5.3.9** for details). This type of analysis revealed that while in control cells the bacteria had progressed 16.8 µm ± 2.69 µm (s.d.) on average, in SNX1-suppressed cells bacteria had covered a significantly shorter distance (9.5 µm ± 6.26 µm). As the pie chart illustrates, the range of distances is widest for SNX1-suppressed cells, which illustrates the observed scattering. While one fraction of bacteria appeared stalled at or close to the plasma membrane (blue quarter), the largest fraction showed progress between 10 to 15 µm (light green); this variance also explains the relatively large standard deviation (**Figure 5. 19**). From these results, it appears that overall, intracellular progress of bacteria is less efficient in SNX1-depleted cells. Furthermore, as part of the analysis of intracellular progress I also analysed behaviour of the SL1344-ΔsigD mutant (ΔsigD) in SNX1-supressed cells. Here, I found a mean progress of 12.2 µm ± 3.27 µm, which is farther than wild type bacteria in SNX1-depleted cells, although not significantly. It is however significantly less than wild type bacteria in control cells (**Figure 5. 19**).

So from this data I concluded that both factors, cellular SNX1 and bacterial SigD, are required for optimal perinuclear transport of SCVs. It furthermore appeared that in SNX1-suppressed cells, the ΔsigD mutant 'alleviated' the stalling: strikingly, in cells infected with the ΔsigD-mutant, specifically the plasma membrane-stalled fraction (0 –

5 μm), as observed for wild type, was conspicuously absent. I thus wished to examine the 'stalling effect' of effect of SNX1 in more detail.

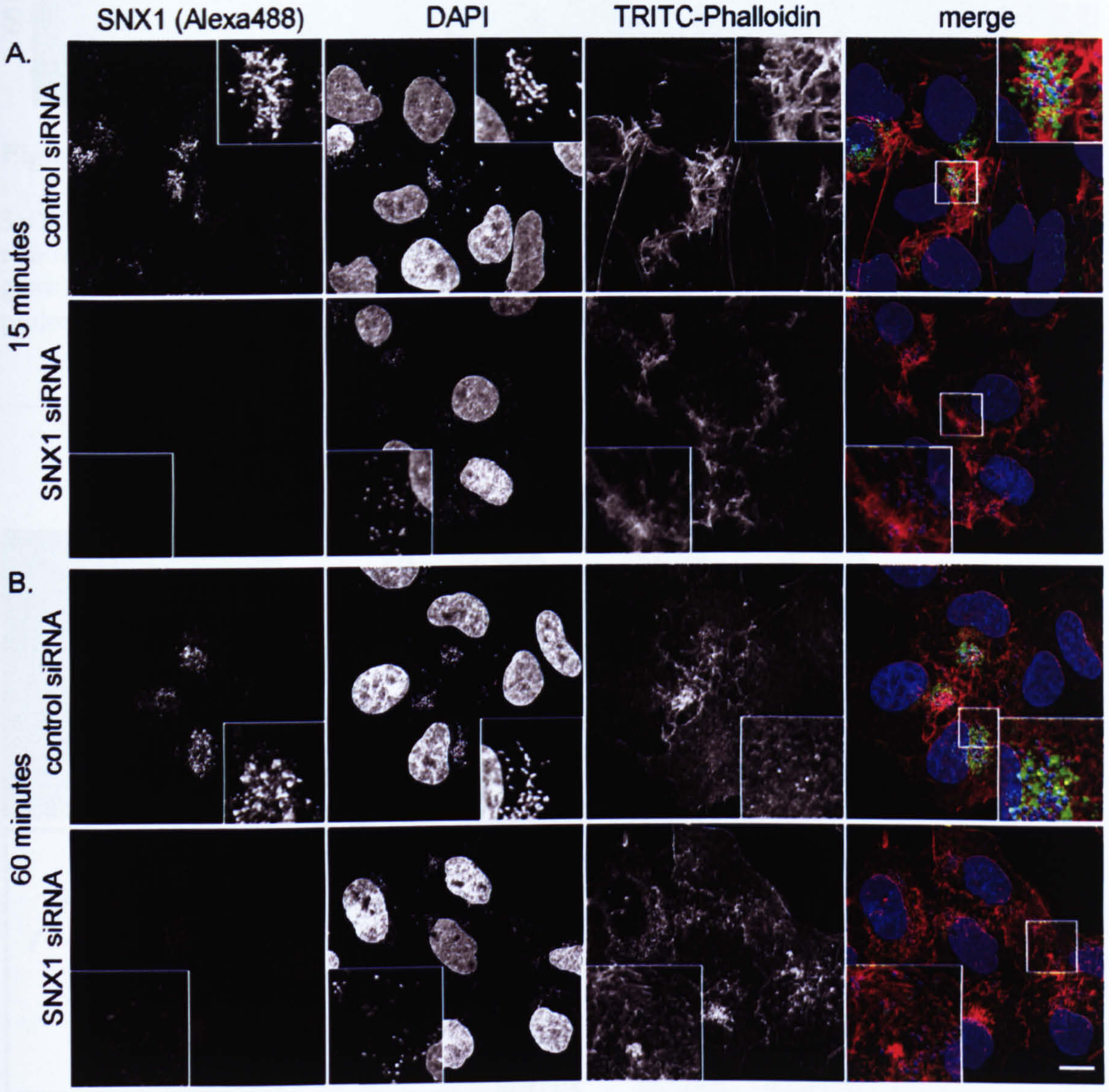

Figure 5. 17 In SNX1-suppressed cells, *S.* Typhimurium displays reduced clustering.

Control and SNX1-suppressed cells were infected for 15 minutes with SL1344. After removing bacteria, cells were either fixed directly (A) or after further 45 minutes (B), and subsequently immuno-labelled with anti-SNX1 (Alexa568, green) and treated with TRITC-phalloidin (red) and DAPI (blue). Scale bar is 10 μm.

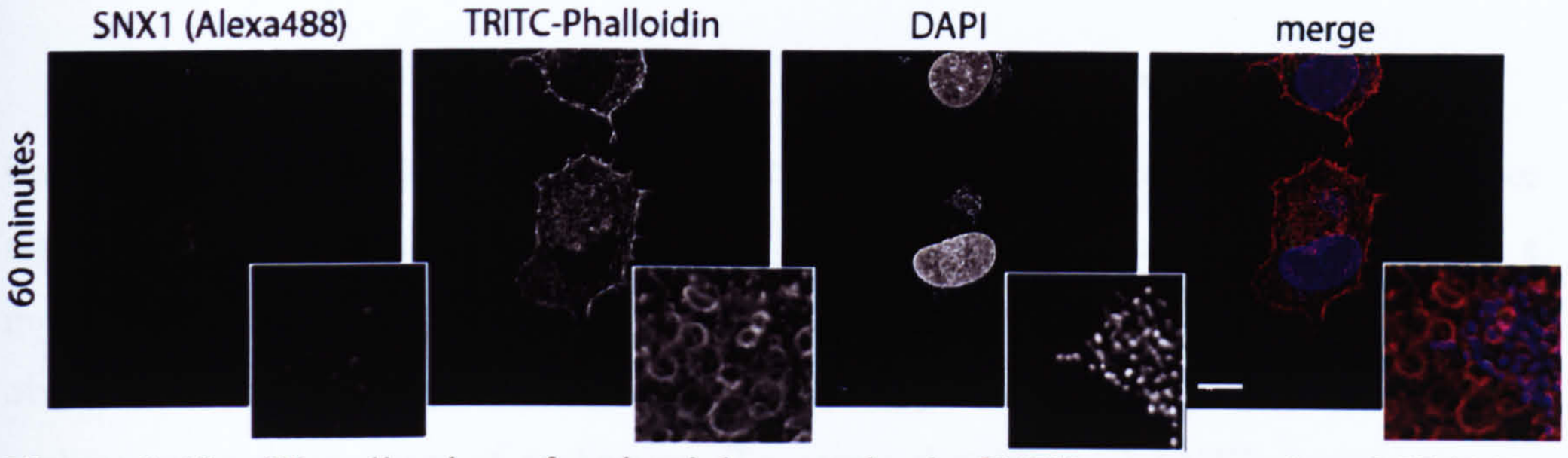

Figure 5. 18 Visualization of actin-rich vacuoles in SNX1-suppressed and SL1344-infected cells.

SNX1-suppressed cells were infected with wild type SL1344 for 15 minutes. Bacteria were removed and after 45 minutes cells were fixed and immuno-labelled using anti-SNX1 (Alexa488, green) and treated with TRITC-phalloidin (red) to visualize F-actin and DAPI (blue). Maximum projection of three z-sections (480 nm z-separation) is shown. Scale bar is 10 µm.

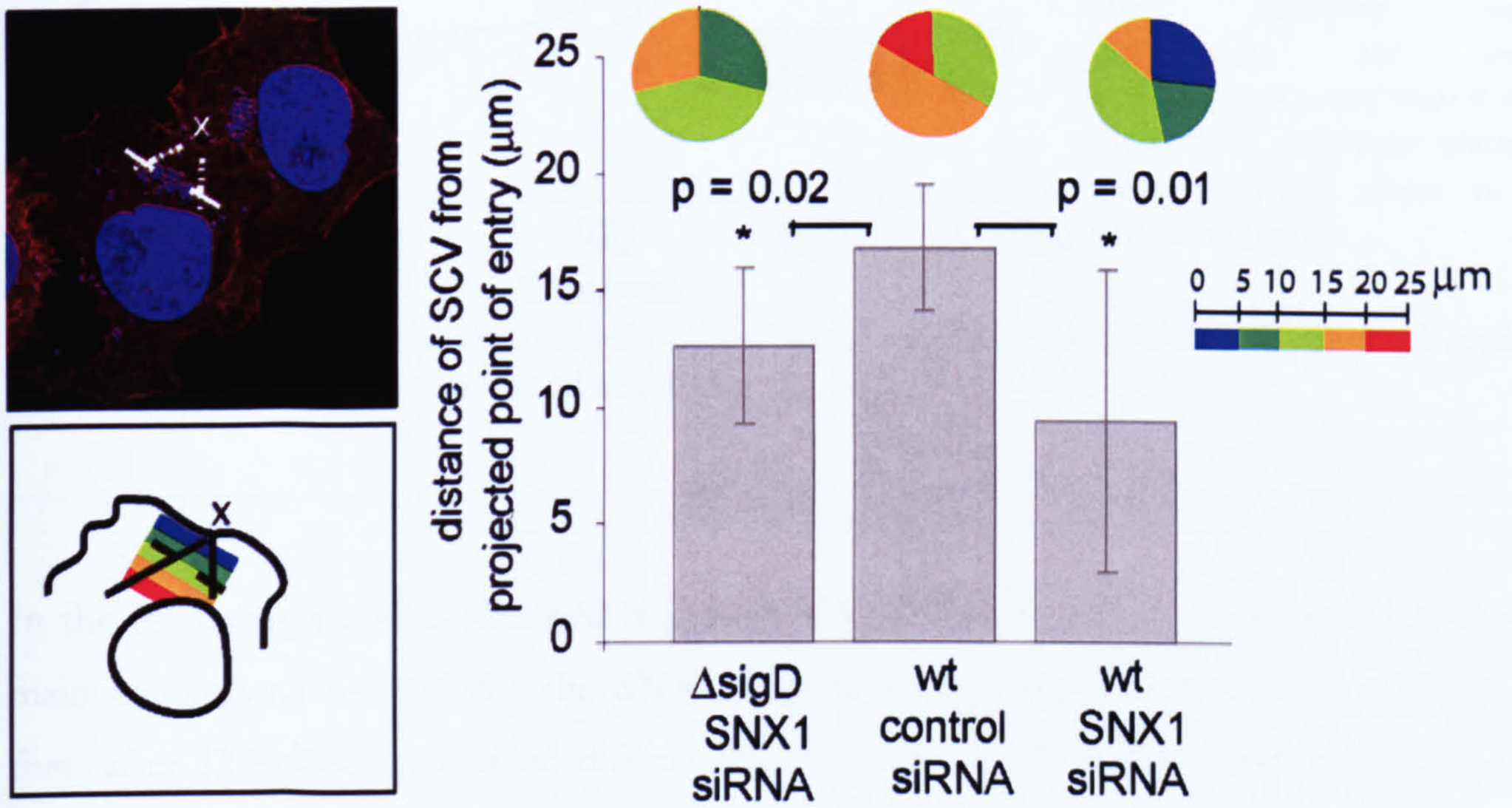

Figure 5. 19 Analysis of intracellular progression of wild type and ΔsigD bacteria in control and SNX-suppressed cells.

Cells treated with control or SNX1-specific siRNA were infected with either wild type (for control) or ΔsigD bacteria (for control and SNX1-suppressed cells) for 15 minutes. Bacteria were removed and cells were fixed after a total of 180 minutes. After appropriate labelling, cells were imaged and distance covered by bacteria/bacterial clusters was measured for at least six clusters (s.d.) in n = 3 cells, calculating the distance covered from the plasma membrane (**para. 5.3.9**).

5.6.4. Investigating the effect of SNX1 suppression on bacterial replication

Positioning in close proximity to the perinuclear/TGN area appears to directly influence replication (Beuzon et al., 2000; Salcedo and Holden, 2003; Abrahams et al., 2006), and a more distal localization may result in attenuated replication (Brawn et al., 2007). Given the observed stalling, I hypothesized that SNX1-suppression could markedly decrease replication or delay onset of replication. To assess the effect of SNX1 suppression on replication, a technique combining RNA interference and the previously mentioned population-based replication assays (c.f.u. assays, see **para. 5.2.3**) was developed.

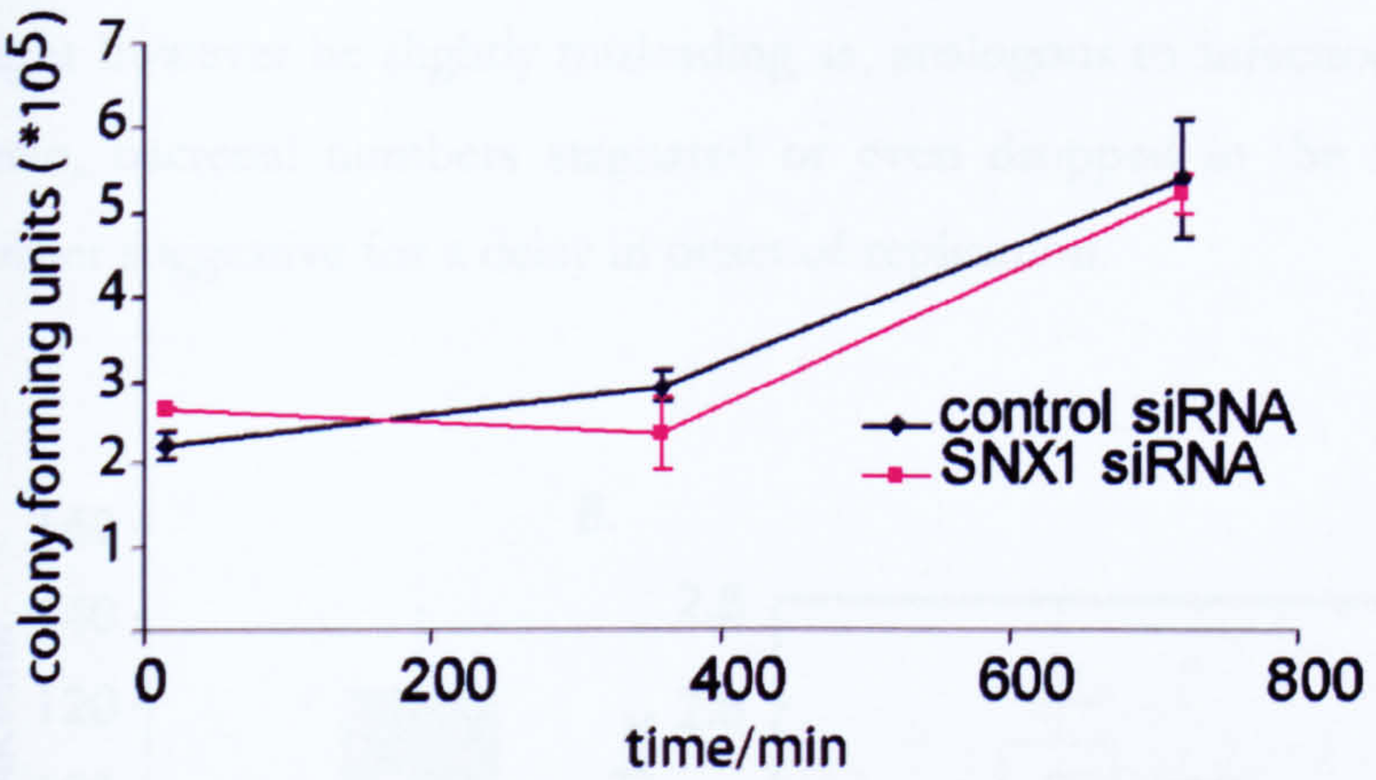

To analyse kinetics of bacterial replication (see **para. 5.3.7**) in control and SNX1-suppressed cells, bacterial colonies obtained after a 15-min infection pulse and subsequent incubation for time indicated were determined; for each condition, two sets with n = 3 each (with replicate plating) were analysed; error is ± min/max per set.

Figure 5. 20 Comparative analysis of bacterial replication kinetics in control and SNX1-suppressed cells

---

In the following, the data obtained is presented in different ways to better illustrate the main conclusions reached for the SNX1-suppressed conditions compared to controls: first, after 12 hours, no marked difference in absolute numbers was observed; second, onset of replication appeared delayed; third, invasion appeared increased.

As can be seen in **Figure 5. 20**, there appears to be no marked difference in absolute numbers of bacteria at the late time points for SNX1-suppressed cells, indicating that bacterial replication is not defective (n = 2, in triplicates)[30]. Nevertheless, for SNX1-suppressed cells, higher bacterial counts for the 15-minute time point were observed. A clearer representation of the data obtained from n = 3 assays (in triplicate with replicative plating) is shown in **Figure 5. 21** (**A**) demonstrating an increase of bacteria in SNX1-

suppressed cells to 123.3% of the control value. That these bacteria had indeed successfully invaded was verified by an independent assay. In this assay, adhered bacteria and total numbers (adhered + invaded) were differentially labelled using *Salmonella*-specific antibodies, and the total numbers of bacteria invaded bacteria could be calculated (**para. 5.2.7**). These assays confirmed that invaded bacteria were shifted to higher numbers in SNX1-suppressed cells (compare **Figure 5. 22**). Thus, it appears that despite increased bacterial numbers, these higher numbers are not maintained over the time course.

Hence, the 'replication index' (ratio of bacteria obtained after 16 hours compared to numbers after 1 hour) is lower for bacteria in SNX1-supressed cells (**Figure 5. 21**). This might however be slightly misleading as, analogous to infections using the ΔsigD-mutant strain, bacterial numbers stagnated or even dropped in the first 6 hours p.i., which is further suggestive for a delay in onset of replication.

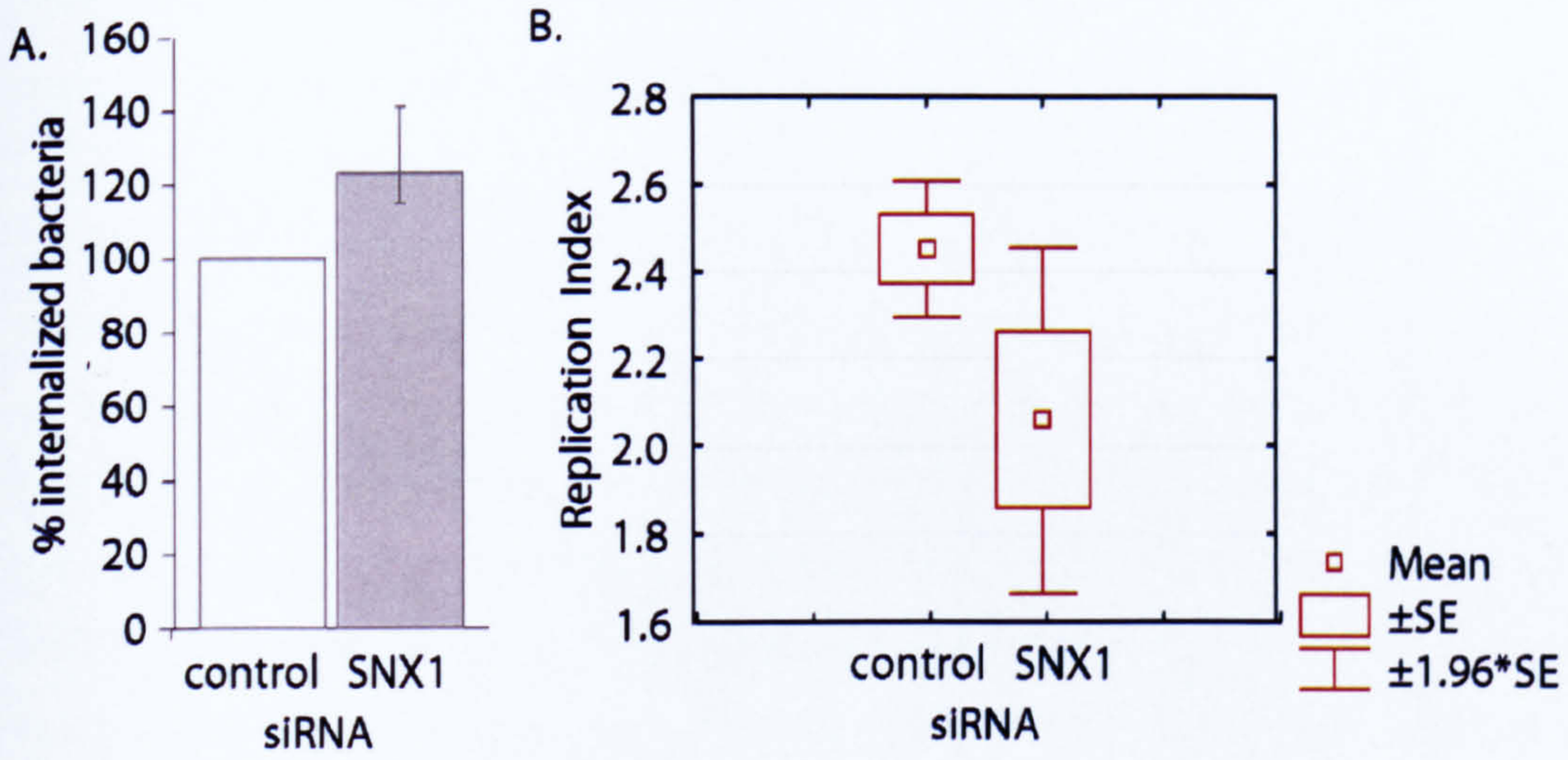

Figure 5. 21 Analysis of bacterial invasion in control and SNX1-suppressed cells
(A) Bacterial colonies retrieved from c.f.u. assays in SNX1-suppressed cells (see **para. 5.3.8**) after an infection pulse for 15 min and 45-minute incubation (in gentamicin-supplemented medium) were normalized to control siRNA-treated cells (mean from n = 3 experiments, in triplicates with replicative plating, error: minimal and maximal deviation from mean). (B) Box and Whiskers-plot to analyse replication in control versus SNX1-suppressed cells. Replication Index was determined by dividing number of colonies obtained after 1 hour by numbers obtained after 12 hours (separately for each set, *id est* 2 x 3 data sets (mean of replica) for each siRNA-treatment, SE = standard error).

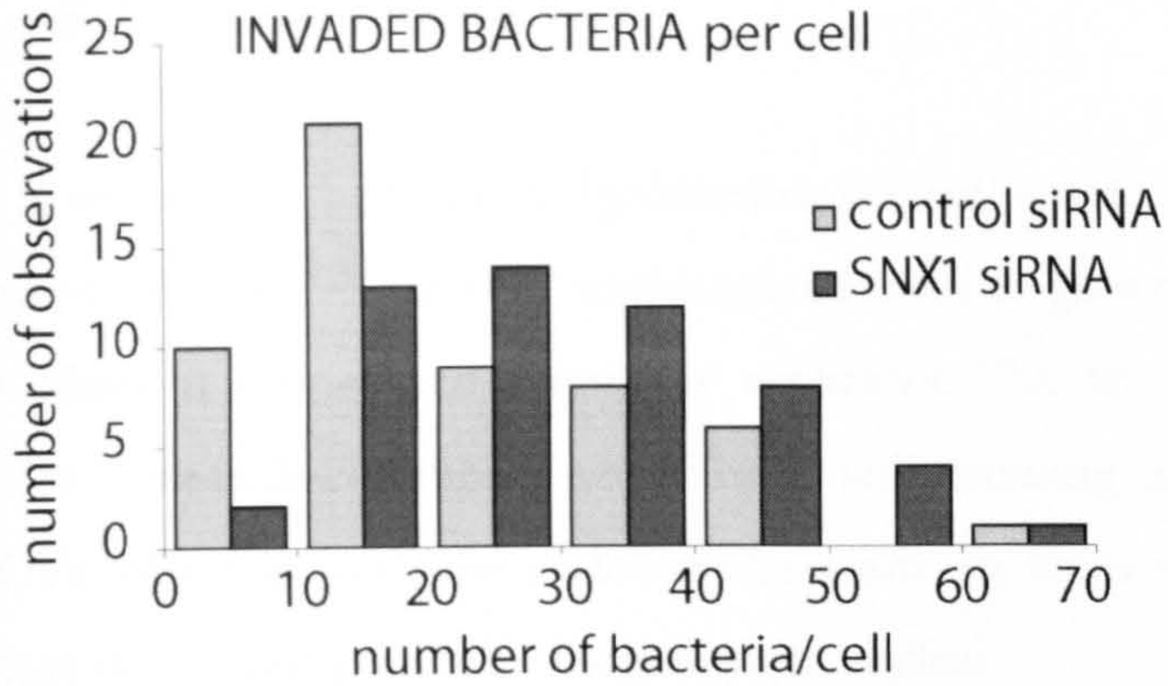

To analyse internalization at single cell level, bacteria were differentially immuno-labelled. Adhered and total (adhered + invaded) was determined, and invaded bacteria were calculated as Δ(total-adhered); a representative data set for n = 55 cells is shown (total of n = 3 yielding same trend).

Figure 5. 22 Analysing number of successfully invaded bacteria.

5.7. Discussion

It is well established that *S. Typhimurium* can influence the endocytic uptake and endosomal system of host cells in very sophisticated ways to generate a unique vacuolar compartment in which it resides and eventually replicates. The list of endosomal proteins targeted to these *Salmonella*-containing vacuoles is still growing and this shows how seamlessly the SCVs 'blend in' with the endosomal system. In many cases, the functional significance of these interactions for SCV biogenesis is unclear.

This study suggests that SNX1 is critically involved in remodelling early *Salmonella*-containing vacuoles and empty macropinosomes. While previously interactions of the SCV with the endosomal/lysosomal system have been thought of as selective or limited, this work also proffers the idea that recruitment of appropriate sorting machinery could allow for removal of cellular proteins from the SCV. More specifically, the CI-MPR and other receptors could be effectively removed in the process, and hence not be readily detected. These data fit in with the recent finding that *Salmonellae* extensively interact with compartments delivering late endosome- and lysosome-content (Drecktrah et al., 2007).

Several lines of evidence suggest that SNX1 is involved in the remodelling, and hence possibly the maturation process - of SCVs: SNX1 affects the SCV morphology, influences intracellular SCV progress, and stalls replication. How is this mechanistically achieved? Besides the points discussed, one model can be deduced from a recent study investigating the role of sorting nexins in macropinocytosis (Kerr et al., 2006). This study investigated SNX5 recruitment to nascent macropinosomes upon EGF stimulation, observing similar tubulation effects. This tubulation was not only microtubule-dependent but moreover, critically depended on the presence of SNX1, as tubulation was abolished in cells lacking SNX1. This interconnectivity becomes more comprehensible when taking into account that SNX1 and SNX5 do physically interact (Kerr et al., 2006; Wassmer et al., 2007), and that protein stability of SNX1 is critically dependent on the presence of SNX5 (Wassmer et al., 2007). Intriguingly, besides PtdIns3*P*, the PX domain of SNX5 additionally binds to PtdIns(3,4)P_2 (Merino-Trigo et al., 2004), a phosphoinositide that is found at the cytosolic face of the plasma membrane (Gray et al., 1999; Oatey et al., 1999), that can be derived from PtdIns(3,4,5)P_2, a potential substrate of SigD (Marcus et al., 2001). Indeed, an Akt-PH reporter construct has been shown to localize to membrane ruffles (Steele-Mortimer et al., 2000) but not membrane invaginations (Terebiznik et al., 2002). Corollary, SNX5 is

recruited to *Salmonella*-induced vacuoles and could therefore act as a bridging molecule recruiting SNX1 to the plasma membrane. Nevertheless, it is interesting to note that unlike SNX5, SNX1 is not recruited to the plasma membrane upon stimulation with EGF (Cozier et al., 2002; Merino-Trigo et al., 2004) but found on sealed macropinosomes (Kerr et al., 2006). Further still, although serum starved cells shows membrane ruffling upon EGF treatment, they fail to recruit a 2xFYVE (Pattni et al., 2001). Thus, these results highlight that the extent of local PtdIns3*P* enrichment at the plasma membrane is specific to the infection process and allow for a model in which recruitment of SNX1 occurs independently of SNX5.

The PPIn-binding specificity might also be important in the sense that through the ability of SNX1 to ligate PtdIns(3,5)P_2 (Carlton et al., 2004), it might be implicated in the maturation, as this PPIn has extensively been associated with endosomal maturation processes (Michell et al., 2006). In the 'cell context', PtdIns(3,5)P_2 can be generated by direct phosphorylation of PtdIns3*P* through the 5'-phoshoinositide kinase PIKfyve, which is indeed recruited to nascent macropinosomes/SCVs (data not shown). Interestingly, the lack of PIKfyve has been associated with dramatically enlarged vacuoles in numerous organisms (Shisheva, 2001; Efe et al., 2005; Nicot et al., 2006; Rusten et al., 2006; Rutherford et al., 2006), suggesting an important role of PIKfyve, and PtdIns(3,5)P_2 (Michell et al., 2006), in vacuolar size regulation and membrane homeostasis. SNX1 in turn appears to (directly or indirectly) reduce the macropinosome's size.

Why would size reduction be important for optimal infection? In macrophages, it has long been known that phagosomes gradually contract *en route* to the perinuclear area (Racoosin and Swanson, 1993). Regarding *S. Typhimurium* infection however, the maintenance of spacious vacuoles appears to play an important role for optimal virulence in macrophages (Alpuche-Aranda et al., 1994). Accordingly, bacterial mutants defective in generating or maintaining large SCVs are attenuated in replication and survival (Alpuche-Aranda et al., 1994; Hernandez et al., 2004). The data presented here indicates that size reduction might nonetheless be a necessary process for optimal multiplication. Suppression of SNX1 results in persistence of actin-positive vacuoles and in stagnating numbers of bacteria in the first 6 hours after infection. There appear to be several possible ways in which size regulation could affect the invasion and infection process. Firstly, one would assume that the larger size might physically hamper intracellular centrifugal transport (Luby-Phelps,

2000). Positioning of SCVs close to the TGN and tethering to this organelle is however critical for bacterial replication (Beuzon et al., 2000; Salcedo and Holden, 2003; Abrahams et al., 2006; Deiwick et al., 2006). Centripetal progress and juxtanuclear positioning might also be important to avoid back-fusion with the plasma membrane. Naturally, the rapid conversion of the nascent SCV from plasma membrane-derived components to endosomal identity would allow for swift integration into the intracellular machinery. Furthers still, intracellular progress and maturation is associated with acidification of the SCV. Although acidification of SCVs is thought to be actively delayed *Salmonella*, it is nevertheless believed to be a key stimulus to activate TTSS2 activity (Coombes et al., 2004).

Mechanistically, SNX1 appears to be a good candidate protein to aid size reduction of SCVs, as it possesses a BAR domain, a domain that has been implicated in membrane tubulation (Peter et al., 2004; Zimmerberg and McLaughlin, 2004). *In vitro* studies have shown that the SNX1-BAR domain is capable to induce, or stabilize, tubulation of liposomes in a concentration-dependent fashion (Carlton et al., 2004). Thus, the data presented here on overexpressed as well as endogenous protein is in line with a model in which SNX1 participates in SCV tubulation and hence, in membrane removal from the vacuole body. It is however to be noted that compared to other BAR domains, the tubulation capacity of the SNX1-BAR domain (as determined in *in vitro* studies) is only poorly developed. In these *in vivo* studies however, I observed highly dynamic tubulation events, which makes it likely that additional, unidentified components are crucially involved in this process. The role of microtubules and microtubule-dependent motors at early stages of SCV biogenesis has however only been poorly studied.

A note on tubules on SCVs: microtubule-dependent tubules emerging from SCVs have been described before. These structures termed *Salmonella*-induced filaments (Sifs) are dependent on the balanced interplay both, kinesins and dynein/dynactin (Guignot et al., 2004). Sifs are rather stable structures and depend on expression of the (late) bacterial SPI-2 effector SifA (Stein et al., 1996). Although the function of Sifs is not entirely clear, they appear to play a role replication and probably SCV 'dilation' [reviewed in (Guignot et al., 2004; Henry et al., 2006)]. Mechanistically, bacteria that lack SifA fail to recruit the SifA kinesin interacting protein (SKIP) to SCVs, a host cell kinesin inhibitor, which prevents acquisition of kinesin mediating centrifugal transport (Boucrot et al., 2005). At the same

time, Rab7-interacting lysosomal protein (RILP) recruits minus-end dynein-dynactin motor complexes to SCVs (Marsman et al., 2004). So SifA might also be required to uncouple RILP/dynein from Rab7 (Harrison et al., 2004).

So in this context, SNX1-decorated tubules have rather opposed characteristics: they are 'fragile' and very transient; rather than leading to dilation of the SCV, these tubules coincide with size reduction, rather than preventing centripetal transport, they appear to facilitate centripetal SCV transport. The role of an bacterial effector in promoting SNX1-tubules is probably more indirect, as these tubules also arise in the normal context, but SigD is certainly involved in the sense that it provides an appropriate 'recruitment cue'.

Assuming that SCV maturation occurred similarly to endosome maturation, fusion but also fission, with concurrent removal of membrane and cargo are characteristics of the process. These findings may be interpreted in the light of the model proposed be Zerial and colleagues (Rink et al., 2005), and may propose a more general model for endosomal maturation: individual early endosomes are proposed to form a 'network in time', and through repeated fusion and fission events, these structures are continually regenerated and renewed in the cell periphery. Enrichment of degradative cargo is achieved through repetitive fusion events in progressively fewer and larger endosomes, which are rapidly removed from the early-endosomal network in the cell centre. This maturation is characterized by the loss of Rab5 and the concomitant acquisition of Rab7 – while interestingly, SNX1 tubulation appears to occur concomitantly with this conversion step (Kerr et al., 2006). Hence, under SNX1-suppressed conditions, like the case with PIKfyve suppression, the reduction in retrograde fission from the early endosome would thereby result in a progressive swelling of endosomal structures. Given the data presented here that SNX1 recruitment coincides with size reduction of large vacuoles in a concentration-dependent manner, while enlargement of vacuoles correlates with PIKfyve suppression levels, it is tantalizing to speculate PtdIns(3,5)P_2 might the direct key for membrane removal 'out' of the vacuole.

Chapter 6 – Conclusions and Outlook

As the data contained within each chapter of this thesis has been discussed *ibidem*, the following paragraphs are aimed at putting the conclusions reached into the wider context of endosomal trafficking and will provide an outlook on potential further research.

Since the identification of SNX1 in 1996 (Kurten et al., 1996), huge progress has been made in recent years uncovering the roles of mammalian sorting nexins in endosomal sorting processes; specifically, the evidence that SNXs have important roles in cargo retrieval rather than pro-degradative transport is increasing - for SNX1 (see this thesis; Carlton et al., 2004; Rojas et al., 2007), as well as for SNX4 (Traer et al. 2007)[31] and as recently shown for SNX5 and SNX6 (Wassmer et al., 2006). In its regard, SNX1 plays an evolutionary conserved role as part of the retromer retrieval complex, and like its yeast counterpart, it also appears that the mammalian retromer complex functions to sort multiple cargos.

One of the interesting remaining questions is how this retrieval is mechanistically achieved. Our findings strongly suggest that SNX1 is crucially involved in the generation of retrieval transport carriers. While the endosomal tubules appear 'pre-formed' independently of SNX1 (compare EM studies), the scission step appears to require SNX1 – so how is this achieved? Coincidental evidence for a role of dynamin in the fission step comes from studies showing that efficient STxB- (Lauvrak et al., 2004) as well as CI-MPR- (Nicoziani et al., 2000) retrograde transport require this large GTPase. Whether SNX1 can directly bind to dynamin is not known. It is however intriguing that numerous studies have linked SNX-BAR proteins to other N- or F-BAR proteins, and thus indirectly to dynamin. F-BAR proteins are cytosolic proteins that tubulate and deform membranes, probably by inducing membrane curvature (Dawson et al., 2006). Interestingly, expression of F-BAR proteins leads to membrane tubulation but when co-expressed with dynamin, tubules are vesiculated, presumably courtesy to the pinchase activity of dynamin. So far, all F-BAR proteins have been linked to plasma membrane events and actin dynamics (Itoh et al., 2005). Regarding the relation of SNXs and other BAR proteins, the BAR protein SNX2 is an interaction partner for the F-BAR protein forming-binding protein 17, FBP17 (Fuchs et

---

[31] [31] C.J. Traer, A.C. Rutherford, K.J. Palmer, T. Wassmer, J. Oakley, N. Attar, J.G. Carlton, J.Kremerskothen, D. J. Stephens, and P.J. Cullen (2007) Sorting nexin-4 co-ordinates endosomal sorting of transferrin receptor with dynein-mediated transport into the endocytic recycling compartment. *Nat Cell Biol* (under revision)

al., 2001), which in turn can bind to dynamin 1 – 3 (Kamioka et al., 2004). The BAR protein SNX4, which localises to early and recycling endosomes, can heterodimerize with amphiphysin 2 (Leprince et al., 2003); amphiphysin in turn can directly bind to dynamin (David et al., 1996; Takei et al., 1999). SNX9 has been shown to directly bind to dynamin 1 and dynamin 2 via its N-terminal SH3 domain (Soulet et al., 2005); it might further be classified 'inverse F-BAR' protein, given its N-terminal SH3 and C-terminal BAR domain and its recently identified inducible binding to WASp (Badour et al., 2007). Recruitment of dynamin may ultimately be required for vesicles fission, and given the PtdIns3*P*-binding capacities and subcellular localization of SNX2 and SNX4, this might even occur from endosomes.

Another aspect that has only poorly been studied is, in a sense, the PX domain of sorting nexins: while most studies have concentrated on the phosphoinositide-binding abilities of this domain, it is not to forget that it also contains a PxxP motif that, at least potentially, may serve as binding site for SH3 domains. This has been described for $p47^{phox}$, which intramolecularly, interacts with its C-terminal SH3 domain, hence providing an regulatory mechanism for membrane association (Karathanassis et al., 2002). Likewise, a recent genome-wide two-hybrid screen and *in vitro* binding approach has generated a protein-protein interaction map of yeast PX domains (Vollert and Uetz, 2004), showing that this motif indeed serves as protein-binding module. A precedent for SNXs, is the recent finding that SNX9 uses its PX domain to interact with the PI3-kinase regulatory subunit p85 as well as its product, PtdIns(3,4,5)P_3 (Badour et al., 2007). This raises the distinct possibility that membrane association of sorting nexins might be regulated by phosphorylation status or accessory proteins binding to its PX domain.

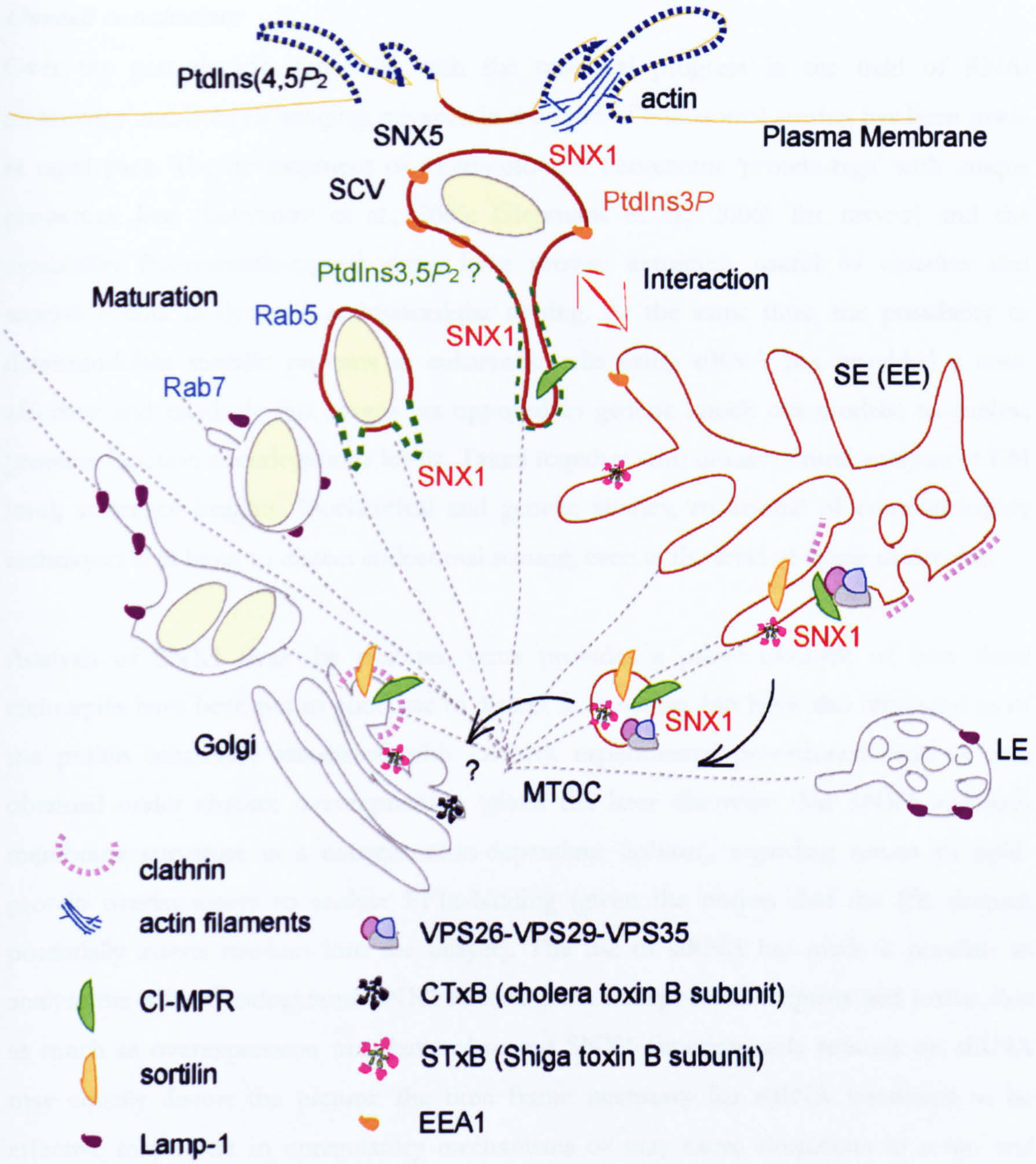

Figure 6. 1 Overview over results presented in this thesis

SNX1 is a peripheral membrane protein that (through coincidence detection by means of its PX domain and BAR domain) is targeted to PtdIns3*P*-/PtdIns(3,5)P_2-enriched, highly curved membranes of sorting endosomes. From here, it regulates endosome-to-TGN retrieval of a variety of cargo, probably as part of a pentameric sorting complex, termed the retromer (consisting of the cargo-selective VPS complex, and a sorting nexin 'coat' complex). Owing to its BAR domain it is thought to stabilize membrane curvature, and it appears that SNX1 is critically involved in formation of the endosome-to-TGN transport carriers (ETCs). Its role in regulating membrane transport and fission processes is also illustrated by the ability of SNX1 to remodel SCVs and macropinosomes (*Salmonellae* shown as light-yellow ovals). It appears that upon infection, SNX1 is directly recruited to the plasma membrane, probably owed to the ability of *Salmonella* effector proteins to subvert plasma membrane PPIn to 3-phosphoinositides. Generally speaking, SNX1 promotes centripetal membrane and protein transport processes.

Abbreviations: SCV = *Salmonella*-containing vacuole (SCV); SE (EE) = sorting endosome (part of the early endosome); LE = late endosome; ETC = endosome-to-TGN transport carrier; MTOC = microtubule-organizing centre.

Overall conclusion:

Over the past decade, especially with the technical progress in the field of RNAi technology and live cell imaging, advance in the field of endosomal sorting has been made at rapid pace. The development of multi-coloured fluorescent 'protein-tags' with unique properties [see (Lukyanov et al., 2005; Giepmans et al., 2006) for review] and the availability fluorescently-tagged cargo have proven extremely useful to visualize and analyse events as dynamic as intracellular sorting. At the same time, the possibility to downmodulate specific proteins in eukaryotic cells using siRNA has provided a cost-effective and relatively fast means (as opposed to genetic knock out models) to analyse proteins function at endogenous levels. Taken together with ultrastructural analyses at EM level, structural insights, biochemical and genetic studies, an arsenal of complementary techniques is at hand to dissect endosomal sorting, even at the level of single molecules.

Analysis of SNX1 over the past ten years provides a prime example of how these techniques have been put to good use to dissect its function, but have also reminded us of the pitfalls inherently associated with invasive experimental procedures: such as data obtained under chronic overexpression (given the later discovery that SNX1 stabilizes membrane curvature in a concentration-dependent fashion), regarding results of lipid-protein overlay-assays to analyse PPIn-binding (given the notion that the PX domain potentially inserts residues into the bilayer). The use of siRNA has made it possible to analyse the role of endogenous SNX1 in retrograde transport of receptors and toxins, but as much as overexpression may have obscured SNX1 function, sole reliance on siRNA may equally distort the picture: the time frame necessary for siRNA treatment to be effective may result in upregulatory mechanisms or may cause alterations in cargo and membrane flux. The (nominally) same technique already produced divergent results (Carlton et al., 2004; Carlton et al., 2005b; Rojas et al., 2007). Through synergistic use of techniques, with a growing understanding of the nature and function of the protein and its context, we will be able to refine the methodologies and further define protein function. Nonetheless, it must be borne in mind that given the inherent properties of networks, it will be somewhat impossible to define a unique functional role. – so it might therefore be more worthwhile to look at the 'concepts' that have already emerged from analysing sorting nexins (take PX-BAR coincidence detection) to extrapolate and further predict functional relations.

MVB, May 2007.

References

Abdul-Ghani, M., Hartman, K. L. and Ngsee, J. K. (2005). Abstrakt interacts with and regulates the expression of sorting Nexin-2. *Journal of Cellular Physiology* **204**, 210-218.

Abrahams, G. L., Muller, P. and Hensel, M. (2006). Functional Dissection of SseF, a Type III Effector Protein Involved in Positioning the Salmonella-Containing Vacuole. *Traffic* **7**, 950-965.

Abramoff, M.D., Magelhaes, P.J., Ram, S.J. (2004) Image Processing with ImageJ. Biophotonics International, volume 11, issue 7, pp. 36-42, 2004.

Aivazian, D., Serrano, R. L. and Pfeffer, S. (2006). TIP47 is a key effector for Rab9 localization. *J. Cell Biol.* **173**, 917-926.

Alonso, A. and Portillo, F. G.-d. (2004). Hijacking of eukaryotic functions by intracellular bacterial pathogens. *Int Microbiol.* **3**, 181-91.

Alpuche-Aranda, C. M., Racoosin, E. L., Swanson, J. A. and Miller, S. I. (1994). Salmonella stimulate macrophage macropinocytosis and persist within spacious phagosomes. *J. Exp. Med.* **179**, 601-608.

Amessou, M., Fradagrada, A., Falguieres, T., Lord, J. M., Smith, D. C., Roberts, L. M., Lamaze, C. and Johannes, L. (2007). Syntaxin 16 and syntaxin 5 are required for efficient retrograde transport of several exogenous and endogenous cargo proteins. *J Cell Sci* **120**, 1457-1468.

Anderson, R. G. (1998). The caveolae membrane system. *Annu Rev Biochem* **67**, 199-225.

Arighi, C. N., Hartnell, L. M., Aguilar, R. C., Haft, C. R. and Bonifacino, J. S. (2004). Role of the mammalian retromer in sorting of the cation-independent mannose 6-phosphate receptor. *J Cell Biol* **165**, 123-33.

Badour, K., McGavin, M. K. H., Zhang, J. Y., Freeman, S., Vieira, C., Filipp, D., Julius, M., Mills, G. B. and Siminovitch, K. A. (2007). Interaction of the Wiskott-Aldrich syndrome protein with sorting nexin 9 is required for CD28 endocytosis and cosignaling in T cells. *Proceedings of the National Academy of Sciences of the United States of America* **104**, 1593-1598.

Baeuerle, P. A. and Huttner, W. B. (1987). Tyrosine sulfation is a trans-Golgi-specific protein modification. *J. Cell Biol.* **105**, 2655-2664.

Baranski, T. J., Faust, P. L. and Kornfeld, S. (1990). Generation of a Lysosomal-Enzyme Targeting Signal in the Secretory Protein Pepsinogen. *Cell* **63**, 281-291.

Baranski, T. J., Koelsch, G., Hartsuck, J. A. and Kornfeld, S. (1991). Mapping and Molecular Modeling of a Recognition Domain for Lysosomal-Enzyme Targeting. *Journal of Biological Chemistry* **266**, 23365-23372.

Barr, V. A., Phillips, S. A., Taylor, S. I. and Haft, C. R. (2000). Overexpression of a novel sorting nexin, SNX15, affects endosome morphology and protein trafficking. *Traffic* **1**, 904-16.

Behnia, R. and Munro, S. (2005). Organelle identity and the signposts for membrane traffic. *Nature* **438**, 597-604.

Bertelsen, L. S., Paesold, G., Marcus, S. L., Finlay, B. B., Eckmann, L. and Barrett, K. E. (2004). Modulation of chloride secretory responses and barrier function of intestinal epithelial cells by the Salmonella effector protein SigD. *Am J Physiol Cell Physiol* **287**, C939-948.

Beuzon, C. R., Meresse, S., Unsworth, K. E., Ruiz-Albert, J., Garvis, S., Waterman, S. R., Ryder, T. A., Boucrot, E. and Holden, D. W. (2000). Salmonella maintains the integrity of its intracellular vacuole through the action of SifA. *Embo Journal* **19**, 3235-3249.

Bigay, J., Gounon, P., Robineau, S. and Antonny, B. (2003). Lipid packing sensed by ArfGAP1 couples COPI coat disassembly to membrane bilayer curvature. *Nature* **426**, 563-6.

Bigay J, Casella JF, Drin G, Mesmin B, Antonny B. (2005) ArfGAP1 responds to membrane curvature through the folding of a lipid packing sensor motif. *EMBO J.* **24**(13):2244-53.

Birkeland, H. C. G. and Stenmark, H. (2004). Protein targeting to endosomes and phagosomes via FYVE and PX domains. In *Phosphoinositides in Subcellular Targeting and Enzyme Activation*, vol. 282, pp. 89-115.

Bonifacino, J. S. and Rojas, R. (2006). Retrograde transport from endosomes to the trans-Golgi network. *Nat Rev Mol Cell Biol* **7**, 568-579.

Boucrot, E., Henry, T., Borg, J. P., Gorvel, J. P. and Meresse, S. (2005). The intracellular fate of Salmonella depends on the recruitment of kinesin. *Science* **308**, 1174-1178.

Brawn, L. C., Hayward, R. D. and Koronakis, V. (2007). Salmonella SPI1 Effector SipA Persists after Entry and Cooperates with a SPI2 Effector to Regulate Phagosome Maturation and Intracellular Replication. *Cell Host and Microbe* **1**, 63-75.

Brazil, D. P. and Hemmings, B. A. (2001). Ten years of protein kinase B signalling: a hard Akt to follow. *Trends Biochem Sci* **26**, 657-64.

Brodsky, F. M., Chen, C. Y., Knuehl, C., Towler, M. C. and Wakeham, D. E. (2001). Biological basket weaving: formation and function of clathrin-coated vesicles. *Annu Rev Cell Dev Biol.* **15**.

Brown, D. A. and London, E. (1998). Functions of lipid rafts in biological membranes. *Annu Rev Cell Dev Biol.* **14**.

Brown, D. A. and Rose, J. K. (1992). Sorting of GPI-anchored proteins to glycolipid-enriched membrane subdomains during transport to the apical cell surface. *Cell* **68**, 533-544.

Burden, J. J., Sun, X. M., Garcia, A. B. and Soutar, A. K. (2004). Sorting motifs in the intracellular domain of the low density lipoprotein receptor interact with a novel domain of sorting nexin-17. *J Biol Chem.* **279**, 16237-45.

Buttner, D. and Bonas, U. (2002). Port of entry - the type III secretion translocon. *Trends in Microbiology* **10**, 186-192.

Campbell, R. E., Tour, O., Palmer, A. E., Steinbach, P. A., Baird, G. S., Zacharias, D. A. and Tsien, R. Y. (2002). A monomeric red fluorescent protein. *PNAS* **99**, 7877-7882.

Campellone, K. G., Robbins, D. and Leong, J. M. (2004). EspFU Is a Translocated EHEC Effector that Interacts with Tir and N-WASP and Promotes Nck-Independent Actin Assembly. *Developmental Cell* **7**, 217-228.

Carlton, J., Bujny, M., Peter, B. J., Oorschot, V. M. J., Rutherford, A., Mellor, H., Klumperman, J., McMahon, H. T. and Cullen, P. J. (2004). Sorting nexin-1 mediates tubular endosome-to-TGN transport through coincidence sensing of high-curvature membranes and 3-phosphoinositides. *Current Biology* **14**, 1791-1800.

Carlton, J., Bujny, M., Rutherford, A. and Cullen, P. (2005a). Sorting nexins - Unifying trends and new perspectives. *Traffic* **6**, 75-82.

Carlton, J. G., Bujny, M. V., Peter, B. J., Oorschot, V. M. J., Rutherford, A., Arkell, R. S., Klumperman, J., McMahon, H. T. and Cullen, P. J. (2005b). Sorting nexin-2 is associated with tubular elements of the early endosome, but is not essential for retromer-mediated endosome-to-TGN transport. *J Cell Sci* **118**, 4527-4539.

Carroll, K. S., Hanna, J., Simon, I., Krise, J., Barbero, P. and Pfeffer, S. R. (2001). Role of Rab9 GTPase in facilitating receptor recruitment by TIP47. *Science* **292**, 1373-6.

Chidambaram, S., Mullers, N., Wiederhold, K., Haucke, V. and von Mollard, G. F. (2004). Specific interaction between SNAREs and epsin N-terminal homology (ENTH) domains of epsin-related proteins in trans-Golgi network to endosome transport. *J Biol Chem* **279**, 4175-9.

Chin, L. S., Raynor, M. C., Wei, X., Chen, H. Q. and Li, L. (2001). Hrs interacts with sorting nexin 1 and regulates degradation of epidermal growth factor receptor. *Journal of Biological Chemistry* **276**, 7069-78.

Choi, J. H., Hong, W. P., Kim, M. J., Kim, J. H., Ryu, S. H. and Suh, P. G. (2004). Sorting nexin 16 regulates EGF receptor trafficking by phosphatidylinositol-3-phosphate interaction with the Phox domain. *J Cell Sci* **117**, 4209-18.

Choudhury, A., Dominguez, M., Puri, V., Sharma, D. K., Narita, K., Wheatley, C. L., Marks, D. L. and Pagano, R. E. (2002). Rab proteins mediate Golgi transport of caveola-internalized glycosphingolipids and correct lipid trafficking in Niemann-Pick C cells. *Journal of Clinical Investigation* **109**, 1541-1550.

Christoforidis, S., Miaczynska, M., Ashman, K., Wilm, M., Zhao, L., Yip, S. C., Waterfield, M. D., Backer, J. M. and Zerial, M. (1999). Phosphatidylinositol-3-OH kinases are Rab5 effectors. *Nat Cell Biol* **1**, 249-52.

Cooke, F. T. (2002). Phosphatidylinositol 3,5-bisphosphate: metabolism and function. *Arch Biochem Biophys* **407**, 143-51.

Coombes, B. K., Brown, N. F., Valdez, Y., Brumell, J. H. and Finlay, B. B. (2004). Expression and Secretion of Salmonella Pathogenicity Island-2 Virulence Genes in Response to Acidification Exhibit Differential Requirements of a Functional Type III Secretion Apparatus and SsaL. *J. Biol. Chem.* **279**, 49804-49815.

Cooper, A. A. and Stevens, T. H. (1996). Vps10p cycles between the late-Golgi and prevacuolar compartments in its function as the sorting receptor for multiple yeast vacuolar hydrolases. *J Cell Biol* **133**, 529-41.

Cozier, G. E., Carlton, J., McGregor, A. H., Gleeson, P. A., Teasdale, R. D., Mellor, H. and Cullen, P. J. (2002). The phox homology (PX) domain-dependent, 3-phosphoinositide-mediated association of sorting nexin-1 with an early sorting endosomal compartment is required for its ability to regulate epidermal growth factor receptor degradation. *J Biol Chem* **277**, 48730-6.

Crump, C. M., Xiang, Y., Thomas, L., Gu, F., Austin, C., Tooze, S. A. and Thomas, G. (2001). PACS-1 binding to adaptors is required for acidic cluster motif-mediated protein traffic. *Embo J* **20**, 2191-201.

Cullen, P. J., Cozier, G. E., Banting, G. and Mellor, H. (2001). Modular phosphoinositide-binding domains--their role in signalling and membrane trafficking. *Curr Biol* **11**, R882-93.

Czubayko, M., Knauth, P., Schluter, T., Florian, V. and Bohnensack, R. (2006). Sorting nexin 17, a non-self-assembling and a PtdIns(3)P high class affinity protein, interacts with the cerebral cavernous malformation related protein KRIT1. *Biochem Biophys Res Commun.* **345**, 1264-72.

Dahms, N. M., Lobel, P. and Kornfeld, S. (1989). Mannose 6-phosphate receptors and lysosomal enzyme targeting. *J Biol Chem* **264**, 12115-8.

David, C., McPherson, P. S., Mundigl, O. and De Camilli, P. (1996). A role of amphiphysin in synaptic vesicle endocytosis suggested by its binding to dynamin in nerve terminals. *PNAS* **93**, 331-335.

Dawson, J. C., Legg, J. A. and Machesky, L. M. (2006). Bar domain proteins: a role in tubulation, scission and actin assembly in clathrin-mediated endocytosis. *Trends in Cell Biology* **16**, 493-498.

de Haan, L. and Hirst, T. R. (2004). Cholera toxin: a paradigm for multi-functional engagement of cellular mechanisms (Review). *Molecular Membrane Biology* **21**, 77-92.

De Matteis, M. A. and Godi, A. (2004). PI-loting membrane traffic. *Nat Cell Biol.* **6**, 487-92.

de Renzis, S., Sonnichsen, B. and Zerial, M. (2002). Divalent Rab effectors regulate the sub-compartmental organization and sorting of early endosomes. *Nat Cell Biol* **4**, 124-33.

Degroote, S., Wolthoorn, J. and van Meer, G. (2004). The cell biology of glycosphingolipids. *Seminars in Cell & Developmental Biology* **15**, 375-387.

Deiwick, J., Salcedo, S. P., Boucrot, E., Gilliland, S. M., Henry, T., Petermann, N., Waterman, S. R., Gorvel, J.-P., Holden, D. W. and Meresse, S. (2006). The Translocated Salmonella Effector Proteins SseF and SseG Interact and Are Required To Establish an Intracellular Replication Niche. *Infect. Immun.* **74**, 6965-6972.

Del Nery, E., Miserey-Lenkei, S., Falguieres, T., Nizak, C., Johannes, L., Perez, F. and Goud, B. (2006). Rab6A and Rab6A' GTPases Play Non-overlapping Roles in Membrane Trafficking. *Traffic* **7**, 394-407.

Deretic, V. (2005). Ay, there's the Rab: organelle maturation by Rab conversion. *Dev Cell.* **9**, 446-8.

Desjardins, M. (2003). ER-MEDIATED PHAGOCYTOSIS: A NEW MEMBRANE FOR NEW FUNCTIONS. *Nature Reviews Immunology* **3**, 280-291.

Desjardins, M., Houde, M. and Gagnon, E. (2005). Phagocytosis: the convoluted way from nutrition to adaptive immunity. *Immunol Rev.* **207**.

Di Paolo, G. and De Camilli, P. (2006). Phosphoinositides in cell regulation and membrane dynamics. *Nature* **443**, 651-657.

Diaz, E. and Pfeffer, S. R. (1998). TIP47: a cargo selection device for mannose 6-phosphate receptor trafficking. *Cell* **93**, 433-43.

Doray, B., Ghosh, P., Griffith, J., Geuze, H. J. and Kornfeld, S. (2002). Cooperation of GGAs and AP-1 in packaging MPRs at the trans-Golgi network. *Science* **297**, 1700-3.

Dove, S. K., Piper, R. C., McEwen, R. K., Yu, J. W., King, M. C., Hughes, D. C., Thuring, J., Holmes, A. B., Cooke, F. T., Michell, R. H. et al. (2004). Svp1p defines a family of phosphatidylinositol 3,5-bisphosphate effectors. *Embo J* **23**, 1922-33.

Dowler, S., Currie, R. A., Downes, C. P. and Alessi, D. R. (1999). DAPP1: a dual adaptor for phosphotyrosine and 3-phosphoinositides. *Biochem J* **342 (Pt 1)**, 7-12.

Drecktrah, D., Knodler, L. A., Galbraith, K. and Steele-Mortimer, O. (2005). The Salmonella SPI1 effector SopB stimulates nitric oxide production long after invasion. *Cellular Microbiology* **7**, 105-113.

Drecktrah, D., Knodler, L. A., Howe, D. and Steele-Mortimer, O. (2007). Salmonella Trafficking is Defined by Continuous Dynamic Interactions with the Endolysosomal System. *Traffic* **8**, 212-225.

Dumas, J. J., Merithew, E., Sudharshan, E., Rajamani, D., Hayes, S., Lawe, D., Corvera, S. and Lambright, D. G. (2001). Multivalent endosome targeting by homodimeric EEA1. *Mol Cell* **8**, 947-58.

Dunn, K. W. and Maxfield, F. R. (1992). Delivery of ligands from sorting endosomes to late endosomes occurs by maturation of sorting endosomes. *J Cell Biol* **117**, 301-10.

Dunn, K. W., McGraw, T. E. and Maxfield, F. R. (1989). Iterative fractionation of recycling receptors from lysosomally destined ligands in an early sorting endosome. *J Cell Biol* **109**, 3303-14.

Edgar, A. J. and Polak, J. M. (2000). Human homologues of yeast vacuolar protein sorting 29 and 35. *Biochem Biophys Res Commun* **277**, 622-30.

Efe, J. A., Botelho, R. J. and Emr, S. D. (2005). The Fab1 phosphatidylinositol kinase pathway in the regulation of vacuole morphology. *Current Opinion in Cell Biology* **17**, 402-408.

Ehrbar, K. and Hardt, W.-D. (2005). Bacteriophage-encoded type III effectors in Salmonella enterica subspecies 1 serovar Typhimurium. *Infection, Genetics and Evolution* **5**, 1-9.

Ehrenfried, J. A., Zhou, Z., Thompson, J. C. and Evers, B. M. (1994). Expression of the Neurotensin Gene in Fetal Human Liver and Fibrolamellar Carcinoma. *Annals of Surgery* **220**, 484-491.

Ekena, K. and Stevens, T. H. (1995). The Saccharomyces cerevisiae MVP1 gene interacts with VPS1 and is required for vacuolar protein sorting. *Mol Cell Biol* **15**, 1671-8.

Elbashir, S. M., Harborth, J., Lendeckel, W., Yalcin, A., Weber, K. and Tuschl, T. (2001). Duplexes of 21-nucleotide RNAs mediate RNA interference in cultured mammalian cells. *Nature* **411**, 494-8.

Eugster, A., Pecheur, E. I., Michel, F., Winsor, B., Letourneur, F. and Friant, S. (2004). Ent5p is required with Ent3p and Vps27p for ubiquitin-dependent protein sorting into the multivesicular body. *Mol Biol Cell.*

Evers, B. M., Rajaraman, S., Chung, D. H., Townsend, C. M., Wang, X., Graves, K. and Thompson, J. C. (1993). Developmental Expression of the Neurotensin Gene in the Rat-Liver. *Annals of Surgery* **218**, 183-188.

Farsad, K. and De Camilli, P. (2003). Mechanisms of membrane deformation. *Curr Opin Cell Biol* **15**, 372-81.

Ferguson, K. M., Kavran, J. M., Sankaran, V. G., Fournier, E., Isakoff, S. J., Skolnik, E. Y. and Lemmon, M. A. (2000). Structural basis for discrimination of 3-phosphoinositides by pleckstrin homology domains. *Mol Cell* **6**, 373-84.

Fishman, P. H., Moss, J. and Vaughan, M. (1976). Uptake and Metabolism of Gangliosides in Transformed Mouse Fibroblasts - Relationship of Ganglioside Structure to Choleragen Response. *Journal of Biological Chemistry* **251**, 4490-4494.

Florian, V., Schluter, T. and Bohnensack, R. (2001). **A new member of the sorting nexin family interacts with the C-terminus of P-selectin.** *Biochem Biophys Res Commun.* **281**, 1045-50.

Ford, M. G., Mills, I. G., Peter, B. J., Vallis, Y., Praefcke, G. J., Evans, P. R. and McMahon, H. T. (2002). Curvature of clathrin-coated pits driven by epsin. *Nature* **419**, 361-6.

Ford, M. G., Pearse, B. M., Higgins, M. K., Vallis, Y., Owen, D. J., Gibson, A., Hopkins, C. R., Evans, P. R. and McMahon, H. T. (2001). Simultaneous binding of PtdIns(4,5)P2 and clathrin by AP180 in the nucleation of clathrin lattices on membranes. *Science* **291**, 1051-5.

Frech, M., Andjelkovic, M., Ingley, E., Reddy, K. K., Falck, J. R. and Hemmings, B. A. (1997). High affinity binding of inositol phosphates and phosphoinositides to the pleckstrin homology domain of RAC/protein kinase B and their influence on kinase activity. *J Biol Chem* **272**, 8474-81.

Friant, S., Pecheur, E. I., Eugster, A., Michel, F., Lefkir, Y., Nourrisson, D. and Letourneur, F. (2003). Ent3p Is a PtdIns(3,5)P2 effector required for protein sorting to the multivesicular body. *Dev Cell* **5**, 499-511.

Frick M, Bright NA, Riento K, Bray A, Merrified C, Nichols BJ. (2007) Coassembly of flotillins induces formation of membrane microdomains, membrane curvature, and vesicle budding. *Curr Biol.* **17**(13):1151-6.

Friebel, A., Ilchmann, H., Aepfelbacher, M., Ehrbar, K., Machleidt, W. and Hardt, W.-D. (2001). SopE and SopE2 from Salmonella typhimurium Activate Different Sets of RhoGTPases of the Host Cell. *J. Biol. Chem.* **276**, 34035-34040.

Fu, Y. and Galan, J. E. (1999). A Salmonella protein antagonizes Rac-1 and Cdc42 to mediate host-cell recovery after bacterial invasion. *Nature* **401**, 293-297.

Fuchs, U., Rehkamp, G., Haas, O. A., Slany, R., Konig, M., Bojesen, S., Bohle, R. M., Damm-Welk, C., Ludwig, W. D., Harbott, J. et al. (2001). The human formin-binding protein 17 (FBP17) interacts with sorting nexin, SNX2, and is an MLL-fusion partner in acute myelogeneous leukemia. *Proc Natl Acad Sci U S A* **98**, 8756-61.

Futter, C. E., Gibson, A., Allchin, E. H., Maxwell, S., Ruddock, L. J., Odorizzi, G., Domingo, D., Trowbridge, I. S. and Hopkins, C. R. (1998). In polarized MDCK cells basolateral vesicles arise from clathrin-gamma-adaptin-coated domains on endosomal tubules. *J Cell Biol* **141**, 611-23.

Futter, C. E., Pearse, A., Hewlett, L. J. and Hopkins, C. R. (1996). Multivesicular endosomes containing internalized EGF-EGF receptor complexes mature and then fuse directly with lysosomes. *J Cell Biol* **132**, 1011-23.

Galkin, V. E., Orlova, A., VanLoock, M. S., Zhou, D. G., Galan, J. E. and Egelman, E. H. (2002). The bacterial protein SipA polymerizes G-actin and mimics muscle nebulin. *Nature Structural Biology* **9**, 518-521.

Garcia-del Portillo, F. and Finlay, B. B. (1995). Targeting of Salmonella typhimurium to vesicles containing lysosomal membrane glycoproteins bypasses compartments with mannose 6-phosphate receptors. *J. Cell Biol.* **129**, 81-97.

Garcia, P., Gupta, R., Shah, S., Morris, A. J., Rudge, S. A., Scarlata, S., Petrova, V., McLaughlin, S. and Rebecchi, M. J. (1995). The pleckstrin homology domain of phospholipase C-delta(1) binds with high affinity to phosphatidylinositol 4,5-bisphosphate in bilayer membranes. *Biochemistry* **34**, 16228-16234.

Garmendia, J., Phillips, A. D., Carlier, M.-F., Chong, Y., Schuller, S., Marches, O., Dahan, S., Oswald, E., Shaw, R. K., Knutton, S. et al. (2004). TccP is an enterohaemorrhagic Escherichia coli O157:H7 type III effector protein that couples Tir to the actin-cytoskeleton. *Cellular Microbiology* **6**, 1167-1183.

Gaullier, J.-M., Ronning, E., Gillooly, D. J. and Stenmark, H. (2000). Interaction of the EEA1 FYVE Finger with Phosphatidylinositol 3-Phosphate and Early Endosomes. ROLE OF CONSERVED RESIDUES. *J. Biol. Chem.* **275**, 24595-24600.

Gaullier, J. M., Simonsen, A., D'Arrigo, A., Bremnes, B., Stenmark, H. and Aasland, R. (1998). FYVE fingers bind PtdIns(3)P. *Nature* **394**, 432-3.

Gey, G. O., Coffman, W. D. and Kubicek, M. T. (1952). Tissue culture studies of the proliferative capacity of cervical carcinoma and normal epithelium. *Cancer Res.* **12**, 264-265.

Ghosh, P., Dahms, N. M. and Kornfeld, S. (2003). Mannose 6-phosphate receptors: new twists in the tale. *Nat Rev Mol Cell Biol* **4**, 202-12.

Giepmans, B. N. G., Adams, S. R., Ellisman, M. H. and Tsien, R. Y. (2006). Review - The fluorescent toolbox for assessing protein location and function. *Science* **312**, 217-224.

Gillooly, D. J., Morrow, I. C., Lindsay, M., Gould, R., Bryant, N. J., Gaullier, J. M., Parton, R. G. and Stenmark, H. (2000). Localization of phosphatidylinositol 3-phosphate in yeast and mammalian cells. *Embo J* **19**, 4577-88.

Glebov OO, Bright NA, Nichols BJ. (2006) Flotillin-1 defines a clathrin-independent endocytic pathway in mammalian cells. *Nat Cell Biol.* 8(1):46-54.

Godi, A., Di Campli, A., Konstantakopoulos, A., Di Tullio, G., Alessi, D. R., Kular, G. S., Daniele, T., Marra, P., Lucocq, J. M. and De Matteis, M. A. (2004). FAPPs control Golgi-to-cell-surface membrane traffic by binding to ARF and PtdIns(4)P. *Nat Cell Biol* **6**, 393-404.

Gorvel, J. P. and Meresse, S. (2001). Maturation steps of the Salmonella-containing vacuole. *Microbes and Infection* **3**, 1299-1303.

Gray, A., Van der Kaay, J. and Downes, C. P. (1999). The pleckstrin homology domains of protein kinase B and GRP1 (general receptor for phosphoinositides-1) are sensitive and selective probes for the cellular detection of phosphatidylinositol 3,4-bisphosphate and/or phosphatidylinositol 3,4,5-trisphosphate in vivo. *Biochemical Journal* **344**, 929-936.

Griffin, C. T., Trejo, J. and Magnuson, T. (2005). Genetic evidence for a mammalian retromer complex containing sorting nexins 1 and 2. *Proceedings of the National Academy of Sciences of the United States of America* **102**, 15173-15177.

Griffiths, G. and Gruenberg, J. (1991). The arguments for pre-existing early and late endosomes. *Trends Cell Biol* **1**, 5-9.

Groisman, E. A. and Ochman, H. (1997). How Salmonella became a pathogen. *Trends in Microbiology* **5**, 343-349.

Grosshans, B. L., Ortiz, D. and Novick, P. (2006). Rabs and their effectors: achieving specificity in membrane traffic. *Proc Natl Acad Sci U S A* **103**, 11821-7.

Gruenberg, J. (2001). The endocytic pathway: a mosaic of domains. *Nat Rev Mol Cell Biol.* **2**, 721-30.

Gruenberg, J. and Maxfield, F. R. (1995). Membrane transport in the endocytic pathway. *Curr Opin Cell Biol* **7**, 552-63.

Gruenberg, J. and Stenmark, H. (2004). The biogenesis of multivesicular endosomes. *Nat Rev Mol Cell Biol* **5**, 317-23.

Gruenberg, J. and van der Goot, F. G. (2006). Mechanisms of pathogen entry through the endosomal compartments. *Nat Rev Mol Cell Biol* **7**, 495-504.

Gu, F. and Gruenberg, J. (1999). Biogenesis of transport intermediates in the endocytic pathway. *FEBS Lett* **452**, 61-6.

Guignot, J., Caron, E., Beuzon, C., Bucci, C., Kagan, J., Roy, C. and Holden, D. W. (2004). Microtubule motors control membrane dynamics of Salmonella-containing vacuoles. *J Cell Sci* **117**, 1033-1045.

Gullapalli, A., Garrett, T. A., Paing, M. M., Griffin, C. T., Yang, Y. and Trejo, J. (2004). A role for sorting nexin 2 in epidermal growth factor receptor down-regulation: evidence for distinct functions of sorting nexin 1 and 2 in protein trafficking. *Mol Biol Cell* **15**, 2143-55.

Gullapalli, A., Wolfe, B. L., Griffin, C. T., Magnuson, T. and Trejo, J. A. (2006). An essential role for SNX1 in lysosomal sorting of protease-activated receptor-1: Evidence for retromer-, Hrs-, and Tsg101-independent functions of sorting nexins. *Molecular Biology of the Cell* **17**, 1228-1238.

Habermann, B. (2004). The BAR-domain family of proteins: a case of bending and binding? *EMBO Rep* **5**, 250-5.

Haft, C. R., de la Luz Sierra, M., Bafford, R., Lesniak, M. A., Barr, V. A. and Taylor, S. I. (2000). Human orthologs of yeast vacuolar protein sorting proteins Vps26, 29, and 35: assembly into multimeric complexes. *Mol Biol Cell* **11**, 4105-16.

Haft, C. R., de la Luz Sierra, M., Barr, V. A., Haft, D. H. and Taylor, S. I. (1998). Identification of a family of sorting nexin molecules and characterization of their association with receptors. *Molecular & Cellular Biology* **18**, 7278-87.

Han, J., Luby-Phelps, K., Das, B., Shu, X., Xia, Y., Mosteller, R. D., Krishna, U. M., Falck, J. R., White, M. A. and Broek, D. (1998). Role of substrates and products of PI 3-kinase in regulating activation of Rac-related guanosine triphosphatases by Vav. *Science* **279**, 558-60.

Hansen, S. H., Sandvig, K. and Vandeurs, B. (1993). Molecules Internalized by Clathrin-Independent Endocytosis Are Delivered to Endosomes Containing Transferrin Receptors. *Journal of Cell Biology* **123**, 89-97.

Hanson, B. J. and Hong, W. (2003). Evidence for a role of SNX16 in regulating traffic between the early and later endosomal compartments. *J Biol Chem* **278**, 34617-30.

Hardt, W.-D., Chen, L.-M., Schuebel, K. E., Bustelo, X. R. and Galan, J. E. (1998). S. typhimurium Encodes an Activator of Rho GTPases that Induces Membrane Ruffling and Nuclear Responses in Host Cells. *Cell* **93**, 815-826.

Harrison, R. E., Brumell J.H., Khandani A., Bucci C., Scott C.C., Jiang X., Finlay B.B. and S., G. (2004). Salmonella impairs RILP recruitment to Rab7 during maturation of invasion vacuoles. *Mol Biol Cell* **15**, 3146-54.

Hassan, A. J., Zeng, J., Ni, X. and Morales, C. R. (2004). The trafficking of prosaposin (SGP-1) and GM2AP to the lysosomes of TM4 sertoli cells is mediated by sortilin and monomeric adaptor proteins. *Molecular Reproduction and Development* **68**, 476-483.

Henry, T., Gorvel, J.-P. and Meresse, S. (2006). Molecular motors hijacking by intracellular pathogens. *Cellular Microbiology* **8**, 23-32.

Hernandez, L. D., Heuffer, K., Wenk, M. R. and Galan, J. E. (2004). Salmonella modulates vesicular traffic by altering phosphoinositide metabolism. *Science* **304**, 1805-1807.

Hettema, E. H., Lewis, M. J., Black, M. W. and Pelham, H. R. (2003). Retromer and the sorting nexins Snx4/41/42 mediate distinct retrieval pathways from yeast endosomes. *Embo J* **22**, 548-57.

Heydorn, A., Sondergaard, B. P., Hadrup, N., Holst, B., Haft, C. R. and Schwartz, T. W. (2004). Distinct in vitro interaction pattern of dopamine receptor subtypes with adaptor proteins involved in post-endocytotic receptor targeting. *FEBS Lett* **556**, 276-80.

Hickenbottom, S. J., Kimmel, A. R., Londos, C. and Hurley, J. H. (2004). Structure of a lipid droplet protein; the PAT family member TIP47. *Structure.* **12**, 1199-207.

Hille-Rehfeld, A. (1995). Mannose 6-phosphate receptors in sorting and transport of lysosomal enzymes. *Biochim Biophys Acta* **1241**, 177-94.

Hirst, J., Futter, C. E. and Hopkins, C. R. (1998). The kinetics of mannose 6-phosphate receptor trafficking in the endocytic pathway in HEp-2 cells: the receptor enters and rapidly leaves multivesicular endosomes without accumulating in a prelysosomal compartment. *Mol Biol Cell* **9**, 809-16.

Hirst, J., Miller, S. E., Taylor, M. J., von Mollard, G. F. and Robinson, M. S. (2004). EpsinR Is an Adaptor for the SNARE Protein Vti1b. *Mol Biol Cell* **15**, 5593-602.

Hirst, J., Motley, A., Harasaki, K., Peak Chew, S. Y. and Robinson, M. S. (2003). EpsinR: an ENTH domain-containing protein that interacts with AP-1. *Mol Biol Cell* **14**, 625-41.

Hoepfner, S., Severin, F., Cabezas, A., Habermann, B., Runge, A., Gillooly, D., Stenmark, H. and M., Z. (2005). Modulation of receptor recycling and degradation by the endosomal kinesin KIF16B. *Cell* **121**, 437-50.

Hoiseth, S. K. and Stocker, B. A. D. (1981). Aromatic-Dependent Salmonella-Typhimurium Are Non-Virulent and Effective as Live Vaccines. *Nature* **291**, 238-239.

Hopkins, C. R., Gibson, A., Shipman, M. and Miller, K. (1990). Movement of internalized ligand-receptor complexes along a continuous endosomal reticulum. *Nature* **346**, 335-9.

Hopkins, C. R., Gibson, A., Shipman, M., Strickland, D. K. and Trowbridge, I. S. (1994). In migrating fibroblasts, recycling receptors are concentrated in narrow tubules in the pericentriolar area, and then routed to the plasma membrane of the leading lamella. *J Cell Biol* **125**, 1265-74.

Horazdovsky, B. F., Davies, B. A., Seaman, M. N., McLaughlin, S. A., Yoon, S. and Emr, S. D. (1997). A sorting nexin-1 homologue, Vps5p, forms a complex with Vps17p and is required for recycling the vacuolar protein-sorting receptor. *Mol Biol Cell* **8**, 1529-41.

Howard, L., Nelson, K. K., Maciewicz, R. A. and Blobel, C. P. (1999). Interaction of the metalloprotease disintegrins MDC9 and MDC15 with two SH3 domain-containing proteins, endophilin I and SH3PX1. *J Biol Chem.* **274**, 31693-9.

Hughes WE, Cooke FT, Parker PJ. (2000) Sac phosphatase domain proteins. *Biochem J.* **350** Pt 2:337-52.

Ikonen, E. (2001). Roles of lipid rafts in membrane transport. *Curr Opin Cell Biol* **13**, 470-7.

Irion, U. and Leptin, M. (1999). Developmental and cell biological functions of the Drosophila DEAD-box protein Abstrakt. *Current Biology* **9**, 1373-1381.

Irion, U., Leptin, M., Siller, K., Fuerstenberg, S., Cai, Y., Doe, C. Q., Chia, W. and Yang, X. H. (2004). Abstrakt, a DEAD box protein, regulates Insc levels and asymmetric division of neural and mesodermal progenitors. *Current Biology* **14**, 138-144.

Ishibashi, Y., Maita, H., Yano, M., Koike, N., Tamai, K., Ariga, H. and Iguchi-Ariga, S. M. (2001). Pim-1 translocates sorting nexin 6/TRAF4-associated factor 2 from cytoplasm to nucleus. *FEBS Lett* **506**, 33-8.

Itoh, T., Erdmann, K. S., Roux, A., Habermann, B., Werner, H. and De Camilli, P. (2005). Dynamin and the actin cytoskeleton cooperatively regulate plasma membrane invagination by BAR and F-BAR proteins.
. *Dev Cell.* **9**, 791-804.

Itoh, T., Koshiba, S., Kigawa, T., Kikuchi, A., Yokoyama, S. and Takenawa, T. (2001). Role of the ENTH domain in phosphatidylinositol-4,5-bisphosphate binding and endocytosis. *Science* **291**, 1047-51.

Iversen, T. G., Skretting, G., Llorente, A., Nicoziani, P., van Deurs, B. and Sandvig, K. (2001). Endosome to Golgi transport of ricin is independent of clathrin and of the Rab9-and Rab11-GTPases. *Molecular Biology of the Cell* **12**, 2099-2107.

Jacewicz, M., Clausen, H., Nudelman, E., Donohuerolfe, A. and Keusch, G. T. (1986). Pathogenesis of Shigella Diarrhea .11. Isolation of a Shigella Toxin-Binding Glycolipid from Rabbit Jejunum and Hela-Cells and Its Identification as Globotriaosylceramide. *Journal of Experimental Medicine* **163**, 1391-1404.

Jacobson, K., Mouritsen, O. G. and Anderson, R. G. (2007). Lipid rafts: at a crossroad between cell biology and physics. *Nat Cell Biol.* **9**, 7-14.

Jaillais, Y., Fobis-Loisy, I., Miege, C., Rollin, C. and Gaude, T. (2006). AtSNX1 defines an endosome for auxin-carrier trafficking in Arabidopsis. *Nature* **443**, 106-9.

Jeffries, T. R., Dove, S. K., Michell, R. H. and Parker, P. J. (2004). PtdIns-specific MPR pathway association of a novel WD40 repeat protein, WIPI49. *Mol Biol Cell* **15**, 2652-63.

Johannes, L., Tenza, D., Antony, C. and Goud, B. (1997). Retrograde Transport of KDEL-bearing B-fragment of Shiga Toxin. *J. Biol. Chem.* **272**, 19554-19561.

Johnson, K. F. and Kornfeld, S. (1992). The cytoplasmic tail of the mannose 6-phosphate/insulin-like growth factor-II receptor has two signals for lysosomal enzyme sorting in the Golgi. *J Cell Biol* **119**, 249-57.

Kalia, M., Kumari, S., Chadda, R., Hill, M. M., Parton, R. G. and Mayor, S. (2006). Arf6-independent GPI-anchored protein-enriched early endosomal compartments fuse with sorting endosomes via a Rab5/phosphatidylinositol-3 '-kinase-dependent machinery. *Molecular Biology of the Cell* **17**, 3689-3704.

Kamioka, Y., Fukuhara, S., Sawa, H., Nagashima, K., Masuda, M., Matsuda, M. and Mochizuki, N. (2004). A Novel Dynamin-associating Molecule, Formin-binding Protein 17, Induces Tubular Membrane Invaginations and Participates in Endocytosis. *J. Biol. Chem.* **279**, 40091-40099.

Kanai, F., Liu, H., Field, S. J., Akbary, H., Matsuo, T., Brown, G. E., Cantley, L. C. and Yaffe, M. B. (2001). The PX domains of p47phox and p40phox bind to lipid products of PI(3)K. *Nat Cell Biol* **3**, 675-8.

Karathanassis, D., Stahelin, R. V., Bravo, J., Perisic, O., Pacold, C. M., Cho, W. and Williams, R. L. (2002). Binding of the PX domain of p47(phox) to phosphatidylinositol 3,4-bisphosphate and phosphatidic acid is masked by an intramolecular interaction. *Embo J* **21**, 5057-68.

Katzmann, D. J., Odorizzi, G. and Emr, S. D. (2002). Receptor downregulation and multivesicular-body sorting. *Nat Rev Mol Cell Biol* **3**, 893-905.

Kerr, M. C., Lindsay, M. R., Luetterforst, R., Hamilton, N., Simpson, F., Parton, R. G., Gleeson, P. A. and Teasdale, R. D. (2006). Visualisation of macropinosome maturation by the recruitment of sorting nexins. *J Cell Sci* **119**, 3967-3980.

Kimbrough, T. G. and Miller, S. I. (2002). Assembly of the type III secretion needle complex of Salmonella typhimurium. *Microbes and Infection* **4**, 75-82.

Kirkham, M., Fujita, A., Chadda, R., Nixon, S. J., Kurzchalia, T. V., Sharma, D. K., Pagano, R. E., Hancock, J. F., Mayor, S. and Parton, R. G. (2005). Ultrastructural identification of uncoated caveolin-independent early endocytic vehicles. *J. Cell Biol.* **168**, 465-476.

Klumperman, J., Hille, A., Veenendaal, T., Oorschot, V., Stoorvogel, W., von Figura, K. and Geuze, H. J. (1993). Differences in the endosomal distributions of the two mannose 6-phosphate receptors. *J Cell Biol* **121**, 997-1010.

Klumperman, J., Kuliawat, R., Griffith, J. M., Geuze, H. J. and Arvan, P. (1998). Mannose 6-phosphate receptors are sorted from immature secretory granules via adaptor protein AP-1, clathrin, and syntaxin 6-positive vesicles. *J Cell Biol* **141**, 359-71.

Knauth, P., Schluter, T., Czubayko, M., Kirsch, C., Florian, V., Schreckenberger, S., Hahn, H. and Bohnensack, R. (2005). Functions of sorting nexin 17 domains and recognition motif for P-selectin trafficking. *J Mol Biol.* **347**, 813-25.

Knodler, L. A. and Steele-Mortimer, O. (2003). Taking Possession: Biogenesis of the Salmonella-Containing Vacuole. *Traffic* **4**, 587-599.

Kornfeld, S. (1992). Structure and Function of the Mannose 6-Phosphate/Insulinlike Growth Factor II Receptors. *Annual Review of Biochemistry* **61**, 307-330.

Kurten, R. C., Cadena, D. L. and Gill, G. N. (1996). Enhanced degradation of EGF receptors by a sorting nexin, SNX1. *Science* **272**, 1008-10.

Kurten, R. C., Eddington, A. D., Chowdhury, P., Smith, R. D., Davidson, A. D. and Shank, B. B. (2001). Self-assembly and binding of a sorting nexin to sorting endosomes. *Journal of Cell Science* **114**, 1743-56.

Lakadamyali, M., Rust, M. J. and Zhuang, X. W. (2006). Ligands for clathrin-mediated endocytosis are differentially sorted into distinct populations of early endosomes. *Cell* **124**, 997-1009.

Lang, L., Reitman, M., Tang, J., Roberts, R. M. and Kornfeld, S. (1984). Lysosomal-Enzyme Phosphorylation - Recognition of a Protein-Dependent Determinant Allows Specific Phosphorylation of Oligosaccharides Present on Lysosomal-Enzymes. *Journal of Biological Chemistry* **259**, 4663-4671.

Lang DM, Lommel S, Jung M, Ankerhold R, Petrausch B, Laessing U, Wiechers MF, Plattner H, Stuermer CA. (1998) Identification of reggie-1 and reggie-2 as plasmamembrane-associated proteins which cocluster with activated GPI-anchored cell adhesion molecules in non-caveolar micropatches in neurons. *J Neurobiol.* **37**(4):502-23.

Lauvrak, S. U., Torgersen, M. L. and Sandvig, K. (2004). Efficient endosome-to-Golgi transport of Shiga toxin is dependent on dynamin and clathrin. *Journal of Cell Science* **117**, 2321-2331.

Lawe, D. C., Chawla, A., Merithew, E., Dumas, J., Carrington, W., Fogarty, K., Lifshitz, L., Tuft, R., Lambright, D. and Corvera, S. (2002). Sequential roles for phosphatidylinositol 3-phosphate and Rab5 in tethering and fusion of early endosomes via their interaction with EEA1. *J Biol Chem* **277**, 8611-7.

Lawe, D. C., Patki, V., Heller-Harrison, R., Lambright, D. and Corvera, S. (2000). The FYVE domain of early endosome antigen 1 is required for both phosphatidylinositol 3-phosphate and Rab5 binding. Critical role of this dual interaction for endosomal localization. *J Biol Chem* **275**, 3699-705.

Le Blanc, I., Luyet, P. P., Pons, V., Ferguson, C., Emans, N., Petiot, A., Mayran, N., Demaurex, N., Faure, J., Sadoul, R. et al. (2005). Endosome-to-cytosol transport of viral nucleocapsids. *Nat Cell Biol.* **7**, 653-64.

LeBorgne, R., Griffiths, G. and Hoflack, B. (1996). Mannose 6-phosphate receptors and ADP-ribosylation factors cooperate for high affinity interaction of the AP-1 Golgi assembly proteins with membranes. *Journal of Biological Chemistry* **271**, 2162-2170.

LeBorgne, R. and Hoflack, B. (1997). Mannose 6-phosphate receptors regulate the formation of clathrin-coated vesicles in the TGN. *Journal of Cell Biology* **137**, 335-345.

Lee, J. J., Radice, G., Perkins, C. P. and Costantini, F. (1992). Identification and characterization of a novel, evolutionarily conserved gene disrupted by the murine H beta 58 embryonic lethal transgene insertion. *Development* **115**, 277-88.

Lee, M. C. and Schekman, R. (2004). Cell biology. BAR domains go on a bender. *Science* **303**, 479-80.

Lefrancois, S., Zeng, J. B., Hassan, A. J., Canuel, M. and Morales, C. R. (2003). The lysosomal trafficking of sphingolipid activator proteins (SAPs) is mediated by sortilin. *Embo Journal* **22**, 6430-6437.

Lemmon, M. A. (2003). Phosphoinositide recognition domains. *Traffic* **4**, 201-13.

Lemmon, M. A., Ferguson, K. M., Obrien, R., Sigler, P. B. and Schlessinger, J. (1995). Specific and High-Affinity Binding of Inositol Phosphates to an Isolated Pleckstrin Homology Domain. *Proceedings of the National Academy of Sciences of the United States of America* **92**, 10472-10476.

Lencer, W. I. and Saslowsky, D. (2005). Raft trafficking of AB5 subunit bacterial toxins. *Biochimica et Biophysica Acta (BBA) - Molecular Cell Research* **1746**, 314-321.

Leprince, C., Le Scolan, E., Meunier, B., Fraisier, V., Brandon, N., De Gunzburg, J. and Camonis, J. (2003). Sorting nexin 4 and amphiphysin 2, a new partnership between endocytosis and intracellular trafficking. *J Cell Sci* **116**, 1937-48.

Lietzke, S. E., Bose, S., Cronin, T., Klarlund, J., Chawla, A., Czech, M. P. and Lambright, D. G. (2000). Structural basis of 3-phosphoinositide recognition by pleckstrin homology domains. *Mol Cell* **6**, 385-94.

Lin, Q., Lo, C. G., Cerione, R. A. and Yang, W. (2002). The Cdc42 target ACK2 interacts with sorting nexin 9 (SH3PX1) to regulate epidermal growth factor receptor degradation. *J Biol Chem.* **277**, 10134-8.

Lin, S. X., Mallet, W. G., Huang, A. Y. and Maxfield, F. R. (2004). Endocytosed cation-independent mannose 6-phosphate receptor traffics via the endocytic recycling compartment en route to the trans-Golgi network and a subpopulation of late endosomes. *Mol Biol Cell* **15**, 721-33.

Ling, H., Boodhoo, A., Hazes, B., Cummings, M. D., Armstrong, G. D., Brunton, J. L. and Read, R. J. (1998). Structure of the Shiga-like Toxin I B-Pentamer Complexed with an Analogue of Its Receptor Gb3. *Biochemistry* **37**, 1777-1788.

Lingwood, C. A. (1999). Glycolipid receptors for verotoxin and Helicobacter pylori: role in pathology. *Biochimica Et Biophysica Acta-Molecular Basis of Disease* **1455**, 375-386.

Linstedt, A. D. and Hauri, H. P. (1993). Giantin, a Novel Conserved Golgi Membrane-Protein Containing a Cytoplasmic Domain of at Least 350-Kda. *Molecular Biology of the Cell* **4**, 679-693.

Llorente, A., Rapak, A., Schmid, S. L., van Deurs, B. and Sandvig, K. (1998). Expression of Mutant Dynamin Inhibits Toxicity and Transport of Endocytosed Ricin to the Golgi Apparatus. *J. Cell Biol.* **140**, 553-563.

Lombardi, D., Soldati, T., Riederer, M. A., Goda, Y., Zerial, M. and Pfeffer, S. R. (1993). Rab9 functions in transport between late endosomes and the trans Golgi network. *Embo J* **12**, 677-82.

Lostroh, C. P. and Lee, C. A. (2001). The Salmonella pathogenicity island-1 type III secretion system. *Microbes and Infection* **3**, 1281-1291.

Lu, L., Tai, G. and Hong, W. (2004). Autoantigen Golgin-97, an effector of Arl1 GTPase, participates in traffic from the endosome to the TGN. *Molecular Biology of the Cell* **15**, 461A-461A.

Luby-Phelps, K. (2000). Cytoarchitecture and physical properties of cytoplasm: Volume, viscosity. diffusion, intracellular surface area. In *International Review of Cytology - a Survey of Cell Biology, Vol 192*, vol. 192, pp. 189-221.

Lukyanov, K. A., Chudakov, D. M., Lukyanov, S. and Verkhusha, V. V. (2005). Photoactivatable fluorescent proteins. *Nature Reviews Molecular Cell Biology* **6**, 885-891.

Lundmark, R. and Carlsson, S. R. (2002). The beta-appendages of the four adaptor-protein (AP) complexes: structure and binding properties, and identification of sorting nexin 9 as an accessory protein to AP-2. *Biochem J* **362**, 597-607.

Lundmark, R. and Carlsson, S. R. (2003). Sorting nexin 9 participates in clathrin-mediated endocytosis through interactions with the core components. *J Biol Chem* **278**, 46772-81.

Lundmark, R. and Carlsson, S. R. (2004). Regulated membrane recruitment of dynamin-2 mediated by sorting nexin 9. *J Biol Chem* **279**, 42694-702.

MaCaulay, S. L., Stoichevska, V., Grusovin, J., Gough, K. H., Castelli, L. A. and Ward, C. W. (2003). Insulin stimulates movement of sorting nexin 9 between cellular compartments: a putative role mediating cell surface receptor expression and insulin action. *Biochem J* **376**, 123-34.

Madin SH, Darby NB Jr. (1958) Established kidney cell lines of normal adult bovine and ovine origin. *Proc Soc Exp Biol Med.* 98(3):574-6.

Majoul, I., Schmidt, T., Pomasanova, M., Boutkevich, E., Kozlov, Y. and Soling, H.-D. (2002). Differential expression of receptors for Shiga and Cholera toxin is regulated by the cell cycle. *J Cell Sci* **115**, 817-826.

Mallard, F., Antony, C., Tenza, D., Salamero, J., Goud, B. and Johannes, L. (1998). Direct pathway from early/recycling endosomes to the Golgi apparatus revealed through the study of shiga toxin B-fragment transport. *J Cell Biol* **143**, 973-90.

Mallard, F., Tang, B. L., Galli, T., Tenza, D., Saint-Pol, A., Yue, X., Antony, C., Hong, W., Goud, B. and Johannes, L. (2002). Early/recycling endosomes-to-TGN transport involves two SNARE complexes and a Rab6 isoform. *J Cell Biol* **156**, 653-64.

Marches, O., Batchelor, M., Shaw, R. K., Patel, A., Cummings, N., Nagai, T., Sasakawa, C., Carlsson, S. R., Lundmark, R., Cougoule, C. et al. (2006). EspF of enteropathogenic Escherichia coli binds sorting nexin 9. *Journal of Bacteriology* **188**, 3110-3115.

Marcus, S. L., Wenk, M. R., Steele-Mortimer, O. and Finlay, B. B. (2001). A synaptojanin-homologous region of Salmonella typhimurium SigD is essential for inositol phosphatase activity and Akt activation. *Febs Letters* **494**, 201-207.

Marcusson, E. G., Horazdovsky, B. F., Cereghino, J. L., Gharakhanian, E. and Emr, S. D. (1994). The sorting receptor for yeast vacuolar carboxypeptidase Y is encoded by the VPS10 gene. *Cell* **77**, 579-86.

Marsman, M., Jordens I, Kuijl C, Janssen L and J., N. (2004). Dynein-mediated vesicle transport controls intracellular Salmonella replication. *Mol Biol Cell.* **15**.

Mason, D., Mallo, G. V., Terebiznik, M. R., Payrastre, B., Finlay, B. B., Brumell, J. H., Rameh, L. and Grinstein, S. (2007). Alteration of Epithelial Structure and Function Associated with PtdIns(4,5)P2 Degradation by a Bacterial Phosphatase. *J. Gen. Physiol.* **129**, 267-283.

Massol, R. H., Larsen, J. E., Fujinaga, Y., Lencer, W. I. and Kirchhausen, T. (2004). Cholera toxin toxicity does not require functional Arf6-and dynamin-dependent endocytic pathways. *Molecular Biology of the Cell* **15**, 3631-3641.

Matoba, S., Morano, K. A., Klionsky, D. J., Kim, K. and Ogrydziak, D. M. (1997). Dipeptidyl aminopeptidase processing and biosynthesis of alkaline extracellular protease from Yarrowia lipolytica. *Microbiology* **143**, 3263-3272.

Maxfield, F. R. and McGraw, T. E. (2004). Endocytic recycling. *Nat Rev Mol Cell Biol* **5**, 121-32.

Mayor, S., Presley, J. F. and Maxfield, F. R. (1993). Sorting of membrane components from endosomes and subsequent recycling to the cell surface occurs by a bulk flow process. *J Cell Biol* **121**, 1257-69.

Mazella, J. (2001). Sortilin/neurotensin receptor-3: a new tool to investigate neurotensin signaling and cellular trafficking? *Cellular Signalling* **13**, 1-6.

McLaughlin S, Wang J, Gambhir A, Murray D. (2002) PIP(2) and proteins: interactions, organization, and information flow. *Annu Rev Biophys Biomol Struct.* **31**:151-75.

McLaughlin S, Murray D. (2005) Plasma membrane phosphoinositide organization by protein electrostatics. *Nature.* **438**(7068):605-11.

McNiven, M. A., Cao, H., Pitts, K. R. and Yoon, Y. (2000). The dynamin family of mechanoenzymes: pinching in new places. *Trends in Biochemical Sciences* **25**, 115-120.

Medigeshi, G. R. and Schu, P. (2003). Characterization of the in vitro retrograde transport of MPR46. *Traffic* **4**, 802-11.

Meresse, S., Steele-Mortimer, O., Finlay, B. B. and Gorvel, J. P. (1999). The rab7 GTPase controls the maturation of Salmonella typhimurium-containing vacuoles in HeLa cells. *Embo Journal* **18**, 4394-4403.

Merino-Trigo, A., Kerr, M. C., Houghton, F., Lindberg, A., Mitchell, C., Teasdale, R. D. and Gleeson, P. A. (2004). Sorting nexin 5 is localized to a subdomain of the early endosomes and is recruited to the plasma membrane following EGF stimulation. *J Cell Sci.*

Merritt, E. A., Kuhn, P., Sarfaty, S., Erbe, J. L., Holmes, R. K. and Hol, W. G. J. (1998). The 1.25 A resolution refinement of the cholera toxin B-pentamer: evidence of peptide backbone strain at the receptor-binding site. *Journal of Molecular Biology* **282**, 1043-1059.

Merritt, E. A., Sarfaty, S., Akker, F. V. D., L'Hoir, C., Martial, J. A. and Hol, W. G. J. (1994). Crystal structure of cholera toxin B-pentamer bound to receptor G(M1) pentasaccharide. *Protein Sci* **3**, 166-175.

Meyer, C., Eskelinen, E. L., Guruprasad, M. R., von Figura, K. and Schu, P. (2001). Mu 1A deficiency induces a profound increase in MPR300/IGF-II receptor internalization rate. *J Cell Sci* **114**, 4469-76.

Meyer, C., Zizioli, D., Lausmann, S., Eskelinen, E. L., Hamann, J., Saftig, P., von Figura, K. and Schu, P. (2000). mu1A-adaptin-deficient mice: lethality, loss of AP-1 binding and rerouting of mannose 6-phosphate receptors. *Embo J* **19**, 2193-203.

Miaczynska, M. and Zerial, M. (2002). Mosaic organization of the endocytic pathway. *Experimental Cell Research* **272**, 8-14.

Michell, R. H., Heath, V. L., Lemmon, M. A. and Dove, S. K. (2006). Phosphatidylinositol 3,5-bisphosphate: metabolism and cellular functions. *Trends in Biochemical Sciences* **31**, 52-63.

Moisenovich, M., Tonevitsky, A., Maljuchenko, N., Kozlovskaya, N., Agapov, I., Volknandt, W., Bereiter-Hahn, J. and . (2004). Endosomal ricin transport: involvement of Rab4- and Rab5-positive compartments. *Histochem Cell Biol.* **121**, 429-39.

Molloy, S. S., Anderson, E. D., Jean, F. and Thomas, G. (1999). Bi-cycling the furin pathway: from TGN localization to pathogen activation and embryogenesis. *Trends Cell Biol* **9**, 28-35.

Montgomery, M. K. (2006). RNA interference: unraveling a mystery. *Nat Struct Mol Biol* **13**, 1039-1041.

Motley, A., Bright, N. A., Seaman, M. N. and Robinson, M. S. (2003). Clathrin-mediated endocytosis in AP-2-depleted cells. *J Cell Biol* **162**, 909-18.

Mukherjee, S. and Maxfield, F. R. (2004). Lipid and cholesterol trafficking in NPC. *Biochim Biophys Acta.* **1685**, 28-37.

Mullock, B. M., Bright, N. A., Fearon, C. W., Gray, S. R. and Luzio, J. P. (1998). Fusion of lysosomes with late endosomes produces a hybrid organelle of intermediate density and is NSF dependent. *J Cell Biol* **140**, 591-601.

Munro S. (2003) Lipid rafts: elusive or illusive? *Cell.* **115**(4):377-88.

Murphy, R. F. (1991). Maturation models for endosome and lysosome biogenesis. *Trends Cell Biol* **1**, 77-82.

Ni, X., Canuel, M. and Morales, C. R. (2006). The sorting and trafficking of lysosomal proteins. *Histol Histopathol* **21**, 899-913.

Ni, X. and Morales, C. R. (2006). The Lysosomal Trafficking of Acid Sphingomyelinase is Mediated by Sortilin and Mannose 6-phosphate Receptor. *Traffic* **7**, 889-902.

Nichols, B. J. (2002). A distinct class of endosome mediates clathrin-independent endocytosis to the Golgi complex. *Nature Cell Biology* **4**, 374-378.

Nichols, B. J., Kenworthy, A. K., Polishchuk, R. S., Lodge, R., Roberts, T. H., Hirschberg, K., Phair, R. D. and Lippincott-Schwartz, J. (2001). Rapid cycling of lipid raft markers between the cell surface and Golgi complex. *Journal of Cell Biology* **153**, 529-541.

Nicot, A.-S., Fares, H., Payrastre, B., Chisholm, A. D., Labouesse, M. and Laporte, J. (2006). The Phosphoinositide Kinase PIKfyve/Fab1p Regulates Terminal Lysosome Maturation in Caenorhabditis elegans. *Mol. Biol. Cell* **17**, 3062-3074.

Nicoziani, P., Vilhardt, F., Llorente, A., Hilout, L., Courtoy, P. J., Sandvig, K. and van Deurs, B. (2000). Role for dynamin in late endosome dynamics and trafficking of the cation-independent mannose 6-phosphate receptor. *Molecular Biology of the Cell* **11**, 481-495.

Niehrs, C. and Huttner, W. B. (1990). Purification and Characterization of Tyrosylprotein Sulfotransferase. *Embo Journal* **9**, 35-42.

Nielsen, M. S., Madsen, P., Christensen, E. I., Nykjaer, A., Gliemann, J., Kasper, D., Pohlmann, R. and Petersen, C. M. (2001). The sortilin cytoplasmic tail conveys Golgi-endosome transport and binds the VHS domain of the GGA2 sorting protein. *Embo J* **20**, 2180-90.

Nimnual, A. S., Yatsula, B. A. and Bar-Sagi, D. (1998). Coupling of Ras and Rac guanosine triphosphatases through the Ras exchanger Sos. *Science* **279**, 560-3.

Norris, F. A., Wilson, M. P., Wallis, T. S., Galyov, E. E. and Majerus, P. W. (1998). SopB, a protein required for virulence of Salmonella dublin, is an inositol phosphate phosphatase. *Proceedings of the National Academy of Sciences of the United States of America* **95**, 14057-14059.

Nossal R. (2001) Energetics of clathrin basket assembly. *Traffic.* **2**(2):138-47.

Nothwehr, S. F., Bruinsma, P. and Strawn, L. A. (1999). Distinct domains within Vps35p mediate the retrieval of two different cargo proteins from the yeast prevacuolar/endosomal compartment. *Mol Biol Cell* **10**, 875-90.

Nothwehr, S. F., Ha, S. A. and Bruinsma, P. (2000). Sorting of yeast membrane proteins into an endosome-to-Golgi pathway involves direct interaction of their cytosolic domains with Vps35p. *J Cell Biol* **151**, 297-310.

Nothwehr, S. F. and Hindes, A. E. (1997). The yeast VPS5/GRD2 gene encodes a sorting nexin-1-like protein required for localizing membrane proteins to the late Golgi. *J Cell Sci* **110 (Pt 9)**, 1063-72.

Nothwehr, S. F., Roberts, C. J. and Stevens, T. H. (1993). Membrane protein retention in the yeast Golgi apparatus: dipeptidyl aminopeptidase A is retained by a cytoplasmic signal containing aromatic residues. *J Cell Biol* **121**, 1197-209.

O'Brien, A. D., Tesh, V. L., Donohuerolfe, A., Jackson, M. P., Olsnes, S., Sandvig, K., Lindberg, A. A. and Keusch, G. T. (1992). Shiga Toxin - Biochemistry, Genetics, Mode of Action, and Role in Pathogenesis. *Current Topics in Microbiology and Immunology* **180**, 65-94.

Oatey, P. B., Venkateswarlu, K., Williams, A. G., Fletcher, L. M., Foulstone, E. J., Cullen, P. J. and Tavare, J. M. (1999). Confocal imaging of the subcellular distribution of phosphatidylinositol 3,4,5-trisphosphate in insulin- and PDGF-stimulated 3T3-L1 adipocytes. *Biochemical Journal* **344**, 511-518.

Orlandi, P. A. and Fishman, P. H. (1998). Filipin-dependent inhibition of cholera toxin: Evidence for toxin internalization and activation through caveolae-like domains. *Journal of Cell Biology* **141**, 905-915.

Orsel, J. G., Sincock, P. M., Krise, J. P. and Pfeffer, S. R. (2000). Recognition of the 300-kDa mannose 6-phosphate receptor cytoplasmic domain by 47-kDa tail-interacting protein. *Proceedings of the National Academy of Sciences of the United States of America* **97**, 9047-9051.

Pang, H., Le, P. U. and Nabi, I. R. (2004). Ganglioside GM1 levels are a determinant of the extent of caveolae/raft-dependent endocytosis of cholera toxin to the Golgi apparatus. *J Cell Sci* **117**, 1421-1430.

Parks, W. T., Frank, D. B., Huff, C., Renfrew Haft, C., Martin, J., Meng, X., de Caestecker, M. P., McNally, J. G., Reddi, A., Taylor, S. I. et al. (2001). Sorting nexin 6, a novel SNX, interacts with the transforming growth factor-beta family of receptor serine-threonine kinases. *J Biol Chem* **276**, 19332-9.

Parton, R. G. (1994). Ultrastructural-Localization of Gangliosides - Gm(1) Is Concentrated in Caveolae. *Journal of Histochemistry & Cytochemistry* **42**, 155-166.

Patel, J. C. and Galan, J. E. (2005). Manipulation of the host actin cytoskeleton by Salmonella -- all in the name of entry. *Current Opinion in Microbiology* **8**, 10-15.

Patki, V., Lawe, D. C., Corvera, S., Virbasius, J. V. and Chawla, A. (1998). A functional PtdIns(3)P-binding motif. *Nature* **394**, 433-4.

Pattni, K., Jepson, M., Stenmark, H. and Banting, G. (2001). A PtdIns(3)P-specific probe cycles on and off host cell membranes during Salmonella invasion of mammalian cells. *Curr Biol* **11**, 1636-42.

Pearse, B. M. F. and Robinson, M. S. (1990). Clathrin, Adaptors, and Sorting. *Annual Review of Cell Biology* **6**, 151-171.

Peden, A. A., Oorschot, V., Hesser, B. A., Austin, C. D., Scheller, R. H. and Klumperman, J. (2004). Localization of the AP-3 adaptor complex defines a novel endosomal exit site for lysosomal membrane proteins. *Journal of Cell Biology* **164**, 1065-1076.

Pelkmans, L., Burli, T., Zerial, M. and Helenius, A. (2004). Caveolin-Stabilized Membrane Domains as Multifunctional Transport and Sorting Devices in Endocytic Membrane Traffic. *Cell* **118**, 767-780.

Pelkmans, L., Kartenbeck, J. and Helenius, A. (2001). Caveolar endocytosis of simian virus 40 reveals a new two-step vesicular-transport pathway to the ER. *Nature Cell Biology* **3**, 473-483.

Perrais, D. and Merrifield, C. J. (2005). Dynamics of Endocytic Vesicle Creation. *Developmental Cell* **9**, 581-592.

Perret E, Lakkaraju A, Deborde S, Schreiner R, Rodriguez-Boulan E. (2005) Evolving endosomes: how many varieties and why? *Curr Opin Cell Biol.* **17**(4):423-34.

Peter, B. J., Kent, H. M., Mills, I. G., Vallis, Y., Butler, P. J., Evans, P. R. and McMahon, H. T. (2004). BAR domains as sensors of membrane curvature: the amphiphysin BAR structure. *Science* **303**, 495-9.

Petersen, C. M., Nielsen, M. S., Nykjaer, A., Jacobsen, L., Tommerup, N., Rasmussen, H. H., Roigaard, H., Gliemann, J., Madsen, P. and Moestrup, S. K. (1997). Molecular identification of a novel candidate sorting receptor purified from human brain by receptor-associated protein affinity chromatography. *J Biol Chem* **272**, 3599-605.

Petiot, A., Faure, J., Stenmark, H. and Gruenberg, J. (2003). PI3P signaling regulates receptor sorting but not transport in the endosomal pathway. *J Cell Biol* **162**, 971-9.

Pfeffer, S. R. (2001). Membrane transport: retromer to the rescue. *Curr Biol* **11**, R109-11.

Phillips, S. A., Barr, V. A., Haft, D. H., Taylor, S. I. and Haft, C. R. (2001). Identification and characterization of SNX15, a novel sorting nexin involved in protein trafficking. *Journal of Biological Chemistry* **276**, 5074-84.

Pizarro-Cerda, J. and Cossart, P. (2004). Subversion of phosphoinositide metabolism by intracellular bacterial pathogens. *Nature Cell Biology* **6**, 1026-1033.

Ponnambalam, S., Girotti, M., Yaspo, M. L., Owen, C. E., Perry, A. C., Suganuma, T., Nilsson, T., Fried, M., Banting, G. and Warren, G. (1996). Primate homologues of rat TGN38: primary structure, expression and functional implications. *J Cell Sci* **109**, 675-685.

Pons, V., Hullin-Matsuda, F., Nauze, M., Barbaras, R., Peres, C., Collet, X., Perret, B., Chap, H. and Gassama-Diagne, A. (2003). Enterophilin-1, a new partner of sorting nexin 1, decreases cell surface epidermal growth factor receptor. *J Biol Chem* **278**, 21155-61.

Pons, V., Peres, C., Teulie, J. M., Nauze, M., Mus, M., Rolland, C., Collet, X., Perret, B., Gassama-Diagne, A. and Hullin-Matsuda, F. (2004). Enterophilin-1 interacts with focal adhesion kinase and decreases beta1 integrins in intestinal Caco-2 cells. *J Biol Chem* **279**, 9270-7.

Ponting, C. P. (1996). Novel domains in NADPH oxidase subunits, sorting nexins, and PtdIns 3-kinases: binding partners of SH3 domains? *Protein Sci* **5**, 2353-7.

Press, B., Feng, Y., Hoflack, B. and Wandinger-Ness, A. (1998). Mutant Rab7 causes the accumulation of cathepsin D and cation-independent mannose 6-phosphate receptor in an early endocytic compartment. *J Cell Biol* **140**, 1075-89.

Racoosin, E. L. and Swanson, J. A. (1993). Macropinosome maturation and fusion with tubular lysosomes in macrophages. *J. Cell Biol.* **121**, 1011-1020.

Radice, G., Lee, J. J. and Costantini, F. (1991). H beta 58, an insertional mutation affecting early postimplantation development of the mouse embryo. *Development* **111**, 801-11.

Raiborg, C., Bache, K. G., Gillooly, D. J., Madshus, I. H., Stang, E. and Stenmark, H. (2002). Hrs sorts ubiquitinated proteins into clathrin-coated microdomains of early endosomes. *Nat Cell Biol* **4**, 394-8.

Rathman, M., Sjaastad, M. and Falkow, S. (1996). Acidification of phagosomes containing Salmonella typhimurium in murine
macrophages. *Infect Immun.* **64**, 2765-73.

Reaves, B. J., Bright, N. A., Mullock, B. M. and Luzio, J. P. (1996). The effect of wortmannin on the localisation of lysosomal type I integral membrane glycoproteins suggests a role for phosphoinositide 3-kinase activity in regulating membrane traffic late in the endocytic pathway. *J Cell Sci* **109 (Pt 4)**, 749-62.

Ren, M., Xu, G., Zeng, J., De Lemos-Chiarandini, C., Adesnik, M. and Sabatini, D. D. (1998). Hydrolysis of GTP on rab11 is required for the direct delivery of transferrin from the pericentriolar recycling compartment to the cell surface but not from sorting endosomes. *Proc Natl Acad Sci U S A* **95**, 6187-92.

Riederer, M. A., Soldati, T., Shapiro, A. D., Lin, J. and Pfeffer, S. R. (1994). Lysosome biogenesis requires Rab9 function and receptor recycling from endosomes to the trans-Golgi network. *J Cell Biol.* **125**, 573-82.

Rink, J., Ghigo, E., Kalaidzidis, Y. and Zerial, M. (2005). Rab conversion as a mechanism of progression from early to late endosomes. *Cell* **122**, 735-49.

Rojas, R., Kametaka, S., Haft, C. R. and Bonifacino, J. S. (2007). Interchangeable but Essential Functions of SNX1 and SNX2 in the Association of Retromer with Endosomes and the Trafficking of Mannose 6-Phosphate Receptors. *Mol. Cell. Biol.* **27**, 1112-1124.

Roth, T. F. and Porter, K. R. (1964). Yolk protein uptake in the oocyte of the mosquito Aedes eegypti. L. *J. Cell Biol.* **20**, 313-332.

Rudolph, M. G., Weise, C., Mirold, S., Hillenbrand, B., Bader, B., Wittinghofer, A. and Hardt, W.-D. (1999). Biochemical Analysis of SopE from Salmonella typhimurium, a Highly Efficient Guanosine Nucleotide Exchange Factor for RhoGTPases. *J. Biol. Chem.* **274**, 30501-30509.

Rusten, T. E., Rodahl, L. M. W., Pattni, K., Englund, C., Samakovlis, C., Dove, S., Brech, A. and Stenmark, H. (2006). Fab1 phosphatidylinositol 3-phosphate 5-kinase controls trafficking but not silencing of endocytosed receptors. *Molecular Biology of the Cell* **17**, 3989-4001.

Rutherford, A. C., Traer, C., Wassmer, T., Pattni, K., Bujny, M. V., Carlton, J. G., Stenmark, H. and Cullen, P. J. (2006). The mammalian phosphatidylinositol 3-phosphate 5-kinase (PIKfyve) regulates endosome-to-TGN retrograde transport. *J Cell Sci* **119**, 3944-3957.

Sabharanjak, S., Sharma, P., Parton, R. G. and Mayor, S. (2002). GPI-anchored proteins are delivered to recycling endosomes via a distinct cdc42-regulated, clathrin-independent pinocytic pathway. *Developmental Cell* **2**, 411-423.

Sachse, M., Ramm, G., Strous, G. and Klumperman, J. (2002a). Endosomes: multipurpose designs for integrating housekeeping and specialized tasks. *Histochemistry and Cell Biology* **117**, 91-104.

Sachse, M., Urbe, S., Oorschot, V., Strous, G. J. and Klumperman, J. (2002b). Bilayered clathrin coats on endosomal vacuoles are involved in protein sorting toward lysosomes. *Mol Biol Cell* **13**, 1313-28.

Saint-Pol, A., Yelamos, B., Amessou, M., Mills, I. G., Dugast, M., Tenza, D., Schu, P., Antony, C., McMahon, H. T., Lamaze, C. et al. (2004). Clathrin adaptor epsinR is required for retrograde sorting on early endosomal membranes. *Dev Cell* **6**, 525-38.

Salcedo, S. P. and Holden, D. W. (2003). SseG, a virulence protein that targets Salmonella to the Golgi network. *Embo Journal* **22**, 5003-5014.

Sandvig, K., Garred, O., Prydz, K., Kozlov, J. V., Hansen, S. H. and Vandeurs, B. (1992). Retrograde Transport of Endocytosed Shiga Toxin to the Endoplasmic-Reticulum. *Nature* **358**, 510-512.

Sandvig, K., Grimmer, S., Lauvrak, S. U., Torgersen, M. L., Skretting, G., van Deurs, B. and Iversen, T. G. (2002). Pathways followed by ricin and Shiga toxin into cells. *Histochemistry and Cell Biology* **117**, 131-141.

Sandvig, K. and Olsnes, S. (1979). Effect of Temperature on the Uptake, Excretion and Degradation of Abrin and Ricin by Hela-Cells. *Experimental Cell Research* **121**, 15-25.

Sandvig, K., Spilsberg, B., Lauvraka, S. U., Torgersen, M. L., Iversen, T. G. and van Deurs, B. (2004). Pathways followed by protein toxins into cells. *International Journal of Medical Microbiology* **293**, 483-490.

Sandvig, K. and van Deurs, B. (2002). Membrane traffic exploited by protein toxins. *Annual Review of Cell and Developmental Biology* **18**, 1-24.

Sandvig, K. and van Deurs, B. (2005). Delivery into cells: lessons learned from plant and bacterial toxins. *Gene Therapy* **12**, 865-872.

Sandvig, K. and VanDeurs, B. (1996). Endocytosis, intracellular transport, and cytotoxic action of shiga toxin and ricin. *Physiological Reviews* **76**, 949-966.

Santamaría A, Castellanos E, Gómez V, Benedit P, Renau-Piqueras J, Morote J, Reventós J, Thomson TM, Paciucci R. (2005) PTOV1 enables the nuclear translocation and mitogenic activity of flotillin-1, a major protein of lipid rafts. *Mol Cell Biol.* **25**(5):1900-11.

Schapiro, F. B., Lingwood, C., Furuya, W. and Grinstein, S. (1998). pH-independent retrograde targeting of glycolipids to the Golgi complex. *Am J Physiol Cell Physiol* **274**, C319-332.

Schmucker, D., Vorbruggen, G., Yeghiayan, P., Fan, H. Q., Jackle, H. and Gaul, U. (2000). The Drosophila gene abstrakt, required for visual system development, encodes a putative RNA helicase of the DEAD box protein family. *Mechanisms of Development* **91**, 189-196.

Schwarz, D. G., Griffin, C. T., Schneider, E. A., Yee, D. and Magnuson, T. (2002). Genetic analysis of sorting nexins 1 and 2 reveals a redundant and essential function in mice. *Mol Biol Cell* **13**, 3588-600.

Scott, C. C., Cuellar-Mata, P., Matsuo, T., Davidson, H. W. and Grinstein, S. (2002). Role of 3-Phosphoinositides in the Maturation of Salmonella-containing Vacuoles within Host Cells. *J. Biol. Chem.* **277**, 12770-12776.

Seaman, M. N. (2004). Cargo-selective endosomal sorting for retrieval to the Golgi requires retromer. *J Cell Biol* **165**, 111-22.

Seaman, M. N., Marcusson, E. G., Cereghino, J. L. and Emr, S. D. (1997). Endosome to Golgi retrieval of the vacuolar protein sorting receptor, Vps10p, requires the function of the VPS29, VPS30, and VPS35 gene products. *J Cell Biol* **137**, 79-92.

Seaman, M. N., McCaffery, J. M. and Emr, S. D. (1998). A membrane coat complex essential for endosome-to-Golgi retrograde transport in yeast. *J Cell Biol* **142**, 665-81.

Seaman, M. N. J. (2005). Recycle your receptors with retromer. *Trends in Cell Biology* **15**, 68-75.

Sechi, A. S. and Wehland, J. (2000). The actin cytoskeleton and plasma membrane connection: PtdIns(4,5)P-2 influences cytoskeletal protein activity at the plasma membrane. *Journal of Cell Science* **113**, 3685-3695.

Sekito, A., Taira, T., Niki, T., Iguchi-Ariga, S. M. M. and Ariga, H. (2005). Stimulation of transforming activity of DJ-1 by Abstrakt, a DJ-1-binding protein. *International Journal of Oncology* **26**, 685-689.

Sheetz, M. P. (2001). Cell control by membrane-cytoskeleton adhesion. *Nature Reviews Molecular Cell Biology* **2**, 392-396.

Shiba, T., Takatsu, H., Nogi, T., Matsugaki, N., Kawasaki, M., Igarashi, N., Suzuki, M., Kato, R., Earnest, T., Nakayama, K. et al. (2002). Structural basis for recognition of acidic-cluster dileucine sequence by GGA1. *Nature* **415**, 937-41.

Shin, H. W., Hayashi, M., Christoforidis, S., Lacas-Gervais, S., Hoepfner, S., Wenk, M. R., Modregget, J., Uttenweiler-Joseph, S., Wilm, M., Nystuen, A. et al. (2005). An enzymatic cascade of Rab5 effectors regulates phosphoinositide turnover in the endocytic pathway. *J Cell Biol* **170**, 607-18.

Shisheva, A. (2001). PIKfyve: the road to PtdIns 5-P and PtdIns 3,5-P(2). *Cell Biol Int* **25**, 1201-6.

Shisheva, A., Rusin, B., Ikonomov, O. C., DeMarco, C. and Sbrissa, D. (2001). Localization and insulin-regulated relocation of phosphoinositide 5-kinase PIKfyve in 3T3-L1 adipocytes. *J Biol Chem* **276**, 11859-69.

Simons, K. and Ikonen, E. (1997). Functional rafts in cell membranes. *Nature.* **387**, 569-72.

Simonsen, A., Lippe, R., Christoforidis, S., Gaullier, J. M., Brech, A., Callaghan, J., Toh, B. H., Murphy, C., Zerial, M. and Stenmark, H. (1998). EEA1 links PI(3)K function to Rab5 regulation of endosome fusion. *Nature* **394**, 494-8.

Singh, R. D., Puri, V., Valiyaveettil, J. T., Marks, D. L., Bittman, R. and Pagano, R. E. (2003). Selective caveolin-1-dependent endocytosis of glycosphingolipids. *Molecular Biology of the Cell* **14**, 3254-3265.

Sixma, T. K., Pronk, S. E., Kalk, K. H., van Zanten, B. A. M., Berghuis, A. M. and Hol, W. G. J. (1992). Lactose binding to heat-labile enterotoxin revealed by X-ray crystallography. *Nature* **355**, 561-564.

Skanland, S. S., Walchli, S., Utskarpen, A., Wandinger-Ness, A. and Sandvig, K. (2007). Phosphoinositide-regulated retrograde transport of ricin: Crosstalk between hVps34 and sorting nexins. *Traffic* **8**, 297-309.

Slepnev, V. I., De Camilli, P. and Review., D.-. (2000). Accessory factors in clathrin-dependent synaptic vesicle endocytosis. *Nat Rev Neurosci.* **1**, 161-72.

Slot, J. W., Geuze, H. J., Gigengack, S., James, D. E. and Lienhard, G. E. (1991). Translocation of the Glucose Transporter Glut4 in Cardiac Myocytes of the Rat. *Proceedings of the National Academy of Sciences of the United States of America* **88**, 7815-7819.

Smith, A. C., Cirulis, J. T., Casanova, J. E., Scidmore, M. A. and Brumell, J. H. (2005). Interaction of the Salmonella-containing Vacuole with the Endocytic Recycling System. *J. Biol. Chem.* **280**, 24634-24641.

Smith, D. C., Lord, J. M., Roberts, L. A. and Johannes, L. (2004). Glycosphingolipids as toxin receptors. *Seminars in Cell & Developmental Biology* **15**, 397-408.

Sonnichsen, B., De Renzis, S., Nielsen, E., Rietdorf, J. and Zerial, M. (2000). Distinct membrane domains on endosomes in the recycling pathway visualized by multicolor imaging of Rab4, Rab5, and Rab11. *J Cell Biol* **149**, 901-14.

Soulet, F., Yarar, D., Leonard, M. and S.L., S. (2005). SNX9 regulates dynamin assembly and is required for efficient clathrin-mediated endocytosis. *Mol Biol Cell* **16**, 2058-67.

Spangler, B. D. (1992). Structure and Function of Cholera-Toxin and the Related Escherichia-Coli Heat-Labile Enterotoxin. *Microbiological Reviews* **56**, 622-647.

Stahelin, R. V., Burian, A., Bruzik, K. S., Murray, D. and Cho, W. (2003). Membrane Binding Mechanisms of the PX Domains of NADPH Oxidase p40phox and p47phox. *J. Biol. Chem.* **278**, 14469-14479.

Stanley, K. K. and Howell, K. E. (1993). TGN38/41: a molecule on the move. *rends Cell Biol.* **3**, 252-5.

Steele-Mortimer, O., Knodler, L. A., Marcus, S. L., Scheid, M. P., Goh, B., Pfeifer, C. G., Duronio, V. and Finlay, B. B. (2000). Activation of Akt/protein kinase B in epithelial cells by the Salmonella typhimurium effector SigD. *Journal of Biological Chemistry* **275**, 37718-37724.

Steele-Mortimer, O., Meresse, S., Gorvel, J.-P., Toh, B.-H. and Finlay, B. B. (1999). Biogenesis of Salmonella typhimurium-containing vacuoles in epithelial cells involves interactions with the early endocytic pathway. *Cellular Microbiology* **1**, 33-49.

Stein, M. A., Leung, K. Y., Zwick, M., GarciadelPortillo, F. and Finlay, B. B. (1996). Identification of a Salmonella virulence gene required for formation of filamentous structures containing lysosomal membrane glycoproteins within epithelial cells. *Molecular Microbiology* **20**, 151-164.

Stender, S., Friebel, A., Linder, S., Rohde, M., Mirold, S. and Hardt, W.-D. (2000). Identification of SopE2 from Salmonella typhimurium, a conserved guanine nucleotide exchange factor for Cdc42 of the host cell. *Molecular Microbiology* **36**, 1206-1221.

Stenmark, H., Aasland, R., Toh, B. H. and D'Arrigo, A. (1996). Endosomal localization of the autoantigen EEA1 is mediated by a zinc-binding FYVE finger. *J Biol Chem* **271**, 24048-54.

Stephens, L. M. A., Hawkins, P. (2000). Phosphoinositide 3-kinases: regulation by cell-surface receptors and function of 3-phosphorylated lipids. In *Biology of Phosphoinositides*, (ed. S. Cockcroft), pp. 32-108: Oxford University Press.

Stockinger, W., Sailler, B., Strasser, V., Recheis, B., Fasching, D., Kahr, L., Schneider, W. J. and Nimpf, J. (2002). The PX-domain protein SNX17 interacts with members of the LDL receptor family and modulates endocytosis of the LDL receptor. *Embo J* **21**, 4259-67.

Stoorvogel, W., Geuze, H. J. and Strous, G. J. (1987). Sorting of endocytosed transferrin and asialoglycoprotein occurs immediately after internalization in HepG2 cells. *J Cell Biol* **104**, 1261-8.

Stoorvogel, W., Oorschot, V. and Geuze, H. J. (1996). A novel class of clathrin-coated vesicles budding from endosomes. *J. Cell Biol.* **132**, 21-33.

Stoorvogel, W., Strous, G. J., Geuze, H. J., Oorschot, V. and Schwartz, A. L. (1991). Late endosomes derive from early endosomes by maturation. *Cell* **65**, 417-27.

Sugimoto, Y., Ninomiya, H., Ohsaki, Y., Higaki, K., Davies, J. P., Ioannou, Y. A. and Ohno, K. (2001). Accumulation of cholera toxin and GM1 ganglioside in the early endosome of Niemann-Pick C1-deficient cells. *Proceedings of the National Academy of Sciences of the United States of America* **98**, 12391-12396.

Swanson, J. A. and Watts, C. (1995). Macropinocytosis. *Trends Cell Biol.* **5**, 424-8.

Takatsu, H., Katoh, Y., Shiba, Y. and Nakayama, K. (2001). Golgi-localizing, gamma-adaptin ear homology domain, ADP-ribosylation factor-binding (GGA) proteins interact with acidic dileucine sequences within the cytoplasmic domains of sorting receptors through their Vps27p/Hrs/STAM (VHS) domains. *Journal of Biological Chemistry* **276**, 28541-28545.

Takei, K., Slepnev, V. I., Haucke, V. and De Camilli, P. (1999). Functional partnership between amphiphysin and dynamin in clathrin-mediated endocytosis. *Nat Cell Biol* **1**, 33-9.

Teasdale, R. D., Loci, D., Houghton, F., Karlsson, L. and Gleeson, P. A. (2001). A large family of endosome-localized proteins related to sorting nexin 1. *Biochem J* **358**, 7-16.

Terebiznik, M. R., Vieira, O. V., Marcus, S. L., Slade, A., Yip, C. M., Trimble, W. S., Meyer, T., Finlay, B. B. and Grinstein, S. (2002). Elimination of host cell PtdIns(4,5)P-2 by bacterial SigD promotes membrane fission during invasion by Salmonella. *Nature Cell Biology* **4**, 766-773.

Thomsen, P., Roepstorff, K., Stahlhut, M. and van Deurs, B. (2002). Caveolae are highly immobile plasma membrane microdomains, which are not involved in constitutive endocytic trafficking. *Molecular Biology of the Cell* **13**, 238-250.

Tooze, J. and Hollinshead, M. (1991). Tubular early endosomal networks in AtT20 and other cells. *J Cell Biol* **115**, 635-53.

Torgersen, M. L., Skretting, G., van Deurs, B. and Sandvig, K. (2001). Internalization of cholera toxin by different endocytic mechanisms. *Journal of Cell Science* **114**, 3737-3747.

Tran, D., Carpentier, J. L., Sawano, F., Gorden, P. and Orci, L. (1987). Ligands Internalized through Coated or Noncoated Invaginations Follow a Common Intracellular Pathway. *Proceedings of the National Academy of Sciences of the United States of America* **84**, 7957-7961.

Ullrich, O., Reinsch, S., Urbe, S., Zerial, M. and Parton, R. G. (1996). Rab11 regulates recycling through the pericentriolar recycling endosome. *J Cell Biol* **135**, 913-24.

Urbe, S., Sachse, M., Row, P. E., Preisinger, C., Barr, F. A., Strous, G., Klumperman, J. and Clague, M. J. (2003). The UIM domain of Hrs couples receptor sorting to vesicle formation. *J Cell Sci* **116**, 4169-79.

Utskarpen, A., Slagsvold, H. H., Iversen, T. G., Walchli, S. and Sandvig, K. (2006). Transport of ricin from endosomes to the Golgi apparatus is regulated by Rab6A and Rab6A '. *Traffic* **7**, 663-672.

van der Sluijs, P., Hull, M., Webster, P., Male, P., Goud, B. and Mellman, I. (1992). The small GTP-binding protein rab4 controls an early sorting event on the endocytic pathway. *Cell* **70**, 729-40.

van Deurs, B., Sandvig, K., Petersen, O. W., Olsnes, S., Simons, K. and Griffiths, G. (1988). Estimation of the amount of internalized ricin that reaches the trans- Golgi network. *J. Cell Biol.* **106**, 253-267.

van Deurs, B., Tonnessen, T. I., Petersen, O. W., Sandvig, K. and Olsnes, S. (1986). Routing of internalized ricin and ricin conjugates to the Golgi complex. *J. Cell Biol.* **102**, 37-47.

van Kerkhof, P., Lee, J., McCormick, L., Tetrault, E., Lu, W., Schoenfish, M., Oorschot, V., Strous, G. J., Klumperman, J. and Bu, G. (2005). Sorting nexin 17 facilitates LRP recycling in the early endosome. *Embo J* **24**, 2851-61.

van Weert, A. W., Dunn, K. W., Gueze, H. J., Maxfield, F. R. and Stoorvogel, W. (1995). Transport from late endosomes to lysosomes, but not sorting of integral membrane proteins in endosomes, depends on the vacuolar proton pump. *J Cell Biol* **130**, 821-34.

Varlamov, O. and Fricker, L. D. (1998). Intracellular trafficking of metallocarboxypeptidase D in AtT-20 cells: localization to the trans-Golgi network and recycling from the cell surface. *J Cell Sci.* **111**, 877-85.

Verges, M., Luton, F., Gruber, C., Tiemann, F., Reinders, L. G., Huang, L., Burlingame, A. L., Haft, C. R. and Mostov, K. E. (2004). The mammalian retromer regulates transcytosis of the polymeric immunoglobulin receptor. *Nat Cell Biol* **6**, 763-9.

Vetter, I. R. and Wittinghofer, A. (2001). The guanine nucleotide-binding switch in three dimensions. *Science* **294**, 1299-304.

Vollert, C. S. and Uetz, P. (2004). The Phox Homology (PX) Domain Protein Interaction Network in Yeast. *Mol Cell Proteomics* **3**, 1053-64.

Voos, W. and Stevens, T. H. (1998). Retrieval of resident late-Golgi membrane proteins from the prevacuolar compartment of Saccharomyces cerevisiae is dependent on the function of Grd19p. *J Cell Biol* **140**, 577-90.

Waguri, S., Dewitte, F., Le Borgne, R., Rouille, Y., Uchiyama, Y., Dubremetz, J. F. and Hoflack, B. (2003). Visualization of TGN to endosome trafficking through fluorescently labeled MPR and AP-1 in living cells. *Mol Biol Cell* **14**, 142-55.

Wan, L., Molloy, S. S., Thomas, L., Liu, G., Xiang, Y., Rybak, S. L. and Thomas, G. (1998). PACS-1 defines a novel gene family of cytosolic sorting proteins required for trans-Golgi network localization. *Cell* **94**, 205-16.

Wang, Y., Pennock, S. D., Chen, X., Kazlauskas, A. and Wang, Z. (2004). Platelet-derived growth factor receptor-mediated signal transduction from endosomes. *J Biol Chem* **279**, 8038-46.

Wang, Y., Zhou, Y., Szabo, K., Haft, C. R. and Trejo, J. (2002). Down-regulation of protease-activated receptor-1 is regulated by sorting nexin 1. *Mol Biol Cell* **13**, 1965-76.

Wang, Y. J., Wang, J., Sun, H. Q., Martinez, M., Sun, Y. X., Macia, E., Kirchhausen, T., Albanesi, J. P., Roth, M. G. and Yin, H. L. (2003). Phosphatidylinositol 4 phosphate regulates targeting of clathrin adaptor AP-1 complexes to the Golgi. *Cell* **114**, 299-310.

Wassmer, T., Attar, N., Bujny, M. V., Oakley, J., Traer, C. J. and Cullen, P. J. (2007). A loss-of-function screen reveals SNX5 and SNX6 as potential components of the mammalian retromer. *Journal of Cell Science* **120**, 45-54.

Waterman, S. R. and Holden, D. W. (2003). Functions and effectors of the Salmonella pathogenicity island 2 type III secretion system. *Cellular Microbiology* **5**, 501-511.

Westergaard, U. B., Sorensen, E. S., Hermey, G., Nielsen, M. S., Nykjaer, A., Kirkegaard, K., Jacobsen, C., Gliemann, J., Madsen, P. and Petersen, C. M. (2004). Functional Organization of the Sortilin Vps10p Domain. *J. Biol. Chem.* **279**, 50221-50229.

Whyte, J. R. C. and Munro, S. (2001). A yeast homolog of the mammalian mannose 6-phosphate receptors contributes to the sorting of vacuolar hydrolases. *Current Biology* **11**, 1074-1078.

Wilcke, M., Johannes, L., Galli, T., Mayau, V., Goud, B. and Salamero, J. (2000). Rab11 regulates the compartmentalization of early endosomes required for
efficient transport from early endosomes to the trans-golgi network. *J Cell Biol.* **151**, 1207-20.

Williams, R., Schluter, T., Roberts, M. S., Knauth, P., Bohnensack, R. and Cutler, D. F. (2004). Sorting nexin 17 accelerates internalization yet retards degradation of P-selectin. *Mol Biol Cell* **15**, 3095-105.

Worby, C. A. and Dixon, J. E. (2002). Sorting out the cellular functions of sorting nexins. *Nat Rev Mol Cell Biol* **3**, 919-31.

Worby, C. A., Simonson-Leff, N., Clemens, J. C., Kruger, R. P. and Muda, M., Dixon, J.E. (2001). The sorting nexin, DSH3PX1, connects the axonal guidance receptor, Dscam, to the actin cytoskeleton. *J Biol Chem.* **276**, 41782-9.

Xu, J., Liu, D., Gill, G. and Songyang, Z. (2001a). Regulation of cytokine-independent survival kinase (CISK) by the Phox homology domain and phosphoinositides. *J Cell Biol* **154**, 699-705.

Xu, Y., Hortsman, H., Seet, L., Wong, S. H. and Hong, W. (2001b). SNX3 regulates endosomal function through its PX-domain-mediated interaction with PtdIns(3)P. *Nat Cell Biol* **3**, 658-66.

Xu, Y., Seet, L. F., Hanson, B. and Hong, W. (2001c). The Phox homology (PX) domain, a new player in phosphoinositide signalling. *Biochem J* **360**, 513-30.

Yam, P. T. and Theriot, J. A. (2004). Repeated Cycles of Rapid Actin Assembly and Disassembly on Epithelial Cell Phagosomes. *Mol. Biol. Cell* **15**, 5647-5658.

Yin, H. L. and Janmey, P. A. (2003). PHOSPHOINOSITIDE REGULATION OF THE ACTIN CYTOSKELETON. *Annual Review of Physiology* **65**, 761-789.

Yoo, K. W., Kim, E. H., Jung, S. H., Rhee, M., Koo, B. K., Yoon, K. J., Kong, Y. Y. and Kim, C. H. (2006). Snx5, as a Mind bomb-binding protein, is expressed in hematopoietic and endothelial precursor cells in zebrafish.
. *FEBS Lett.* **580**, 4409-16.

Yoshimori, T., Yamamoto, A., Moriyama, Y., Futai, M. and Tashiro, Y. (1991). Bafilomycin A1, a specific inhibitor of vacuolar-type H(+)-ATPase, inhibits acidification and protein degradation in lysosomes of cultured cells. *J Biol Chem* **266**, 17707-12.

Yu, J. W. and Lemmon, M. A. (2001). All phox homology (PX) domains from Saccharomyces cerevisiae specifically recognize phosphatidylinositol 3-phosphate. *J Biol Chem* **276**, 44179-84.

Zerial, M. and McBride, H. (2001). Rab proteins as membrane organizers. *Nat Rev Mol Cell Biol* **2**, 107-17.

Zeuschner, D., Geerts, W. J. C., van Donselaar, E., Humbel, B. M., Slot, J. W., Koster, A. J. and Klumperman, J. (2006). Immuno-electron tomography of ER exit sites reveals the existence of free COPII-coated transport carriers. *Nat Cell Biol* **8**, 377-383.

Zheng, B., Lavoie, C., Tang, T. D., Ma, P., Meerloo, T., Beas, A. and Farquhar, M. G. (2004). Regulation of Epidermal Growth Factor Receptor Degradation by Heterotrimeric G{alpha}s Protein. *Mol Biol Cell* **15**, 5538-5550.

Zheng, B., Ma, Y. C., Ostrom, R. S., Lavoie, C., Gill, G. N., Insel, P. A., Huang, X. Y. and Farquhar, M. G. (2001). RGS-PX1, a GAP for GalphaS and sorting nexin in vesicular trafficking. *Science* **294**, 1939-42.

Zhong, Q., Lazar, C. S., Tronchere, H., Sato, T., Meerloo, T., Yeo, M., Songyang, Z., Emr, S. D. and Gill, G. N. (2002). Endosomal localization and function of sorting nexin 1. *Proc Natl Acad Sci U S A* **99**, 6767-72.

Zhou, D. and Galan, J. (2001). Salmonella entry into host cells: the work in concert of type III secreted effector proteins. *Microbes and Infection* **3**, 1293-1298.

Zhou, D., Mooseker, M. S. and Galan, J. E. (1999a). Role of the S-typhimurium actin-binding protein SipA in bacterial internalization. *Science* **283**, 2092-2095.

Zhou, D. G., Chen, L. M., Hernandez, L., Shears, S. B. and Galan, J. E. (2001). A Salmonella inositol polyphosphatase acts in conjunction with other bacterial effectors to promote host cell actin cytoskeleton rearrangements and bacterial internalization. *Molecular Microbiology* **39**, 248-259.

Zhou, D. G., Mooseker, M. S. and Galan, J. E. (1999b). An invasion-associated Salmonella protein modulates the actin-bundling activity of plastin. *Proceedings of the National Academy of Sciences of the United States of America* **96**, 10176-10181.

Zhu, Y. X., Doray, B., Poussu, A., Lehto, V. P. and Kornfeld, S. (2001). Binding of GGA2 to the lysosomal enzyme sorting motif of the mannose 6-phosphate receptor. *Science* **292**, 1716-1718.

Zimmerberg, J. and McLaughlin, S. (2004). Membrane curvature: how BAR domains bend bilayers. *Curr Biol* **14**, R250-2.

Appendix

I. Primers

Cloning Primers

VPS35

5' (XhoI): GAT CTC GAG AA ATG AAG AGA TGC CTG GAC AAA AAC
3' (BamHI): GAT GGA TTC TTA AAG GAT GAG ACC TTC ATA AAT TG

Sequencing Primers

pEGFP-Seq (sense)	5'-ACTACCTGACCACCCATGCC-3'
pEGFP-Seq (antisense)	5'-TGTGGGAGGTTTTTTAAAGC-3'
SNX1 (internal, sense)	5'-TCTCCTCAAGATGTTCAACAAA-3'
VPS35 (internal 840)	5' –GCTCACCGTGAAGATGGACCTG-3'

II. Cloning Maps

1. mRFP-SNX1

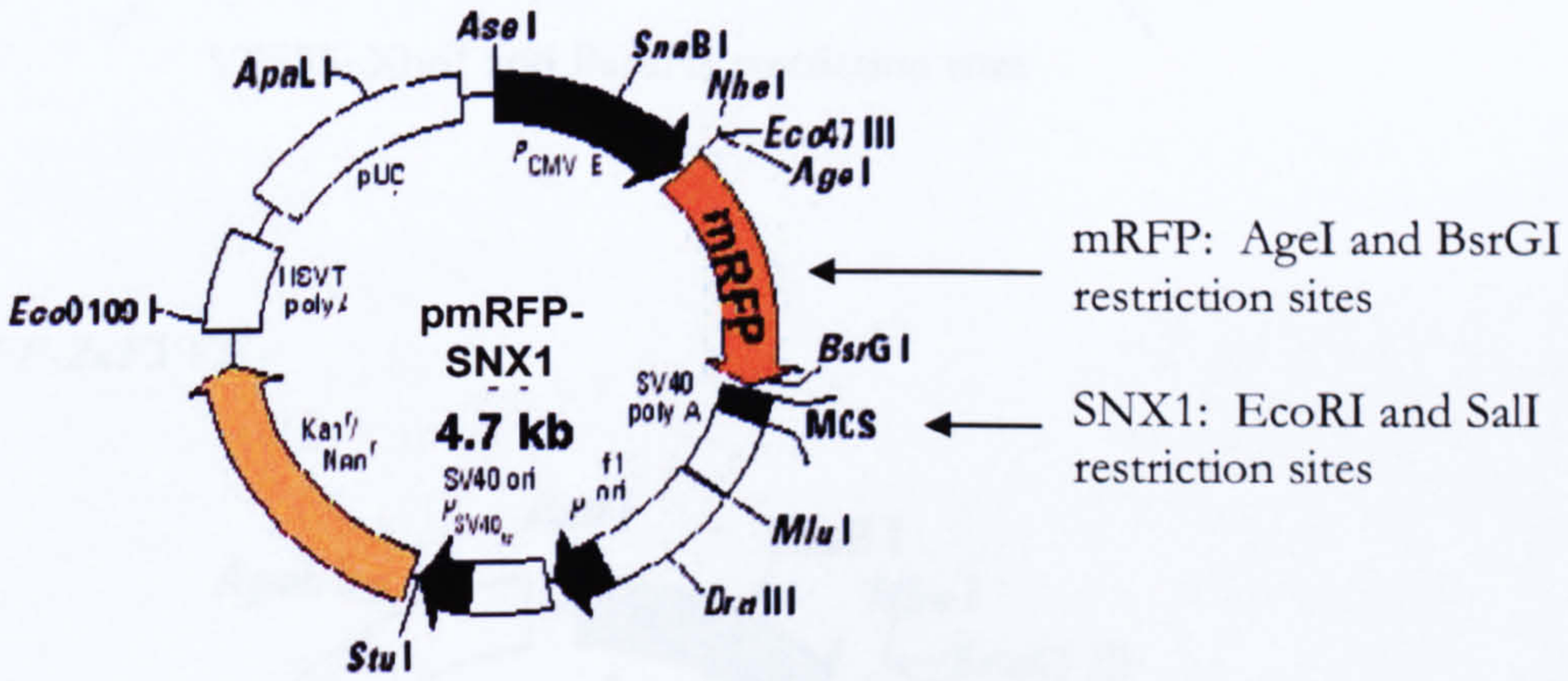

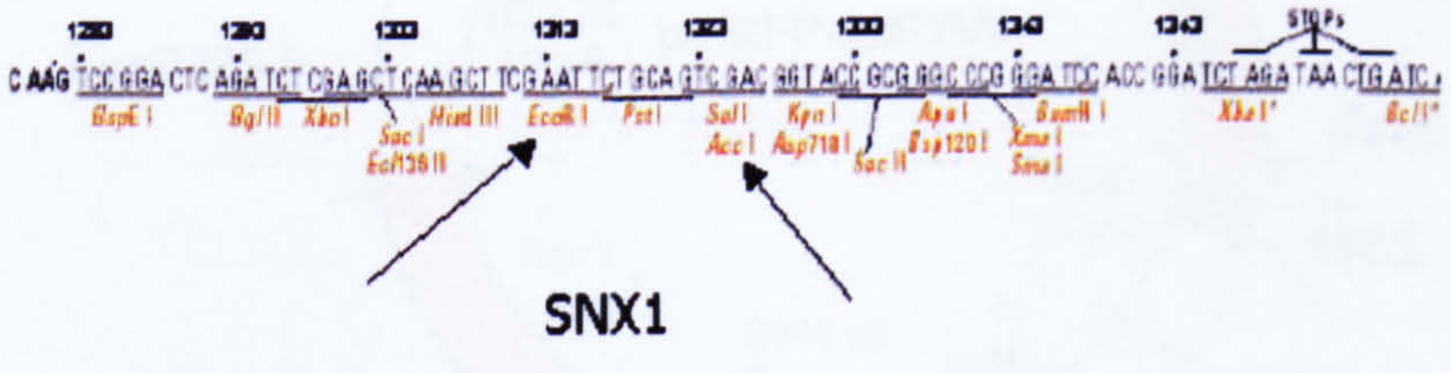

2. pEGFP-C1-VPS35

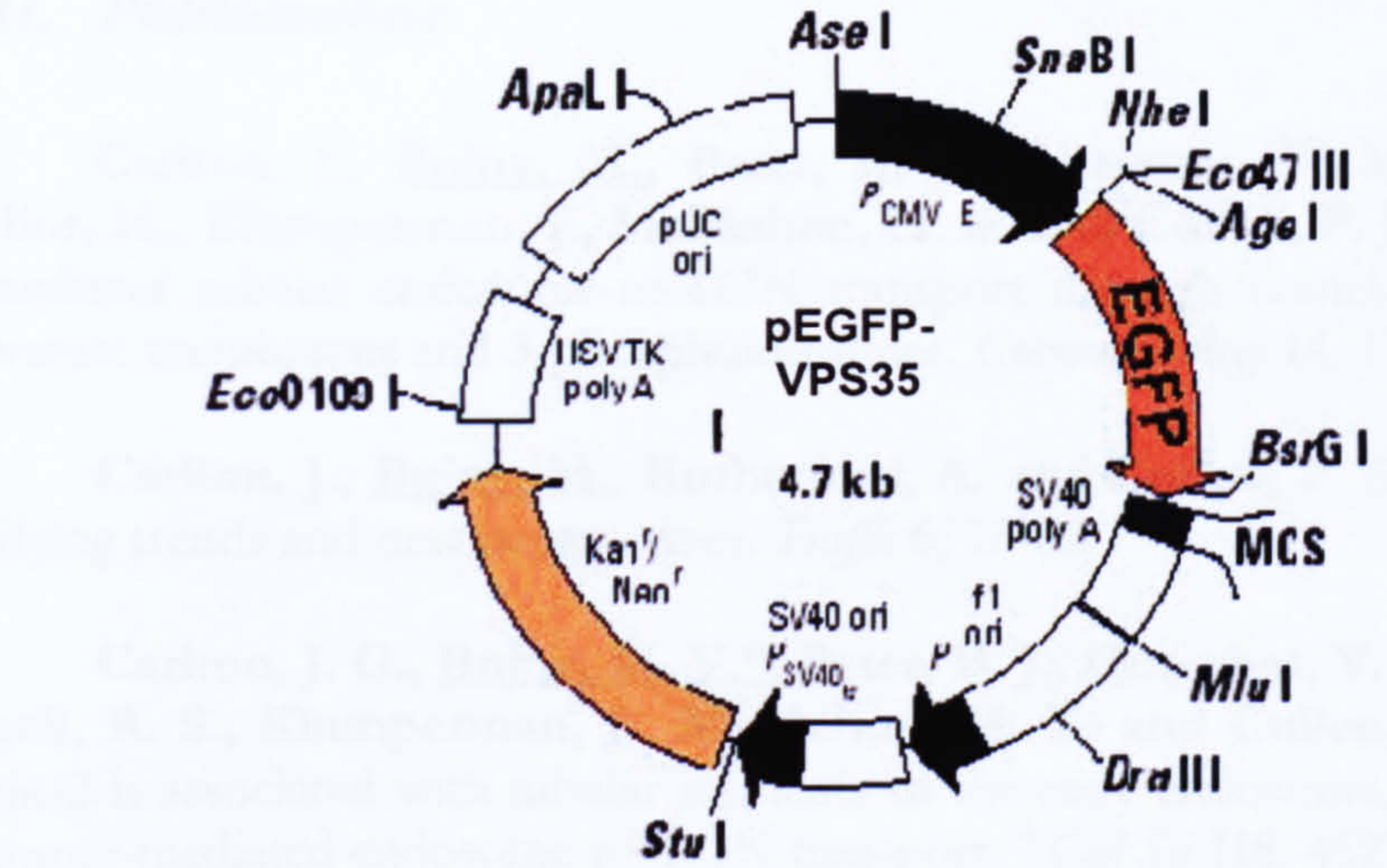

VPS35: XhoI and BamHI restriction sites

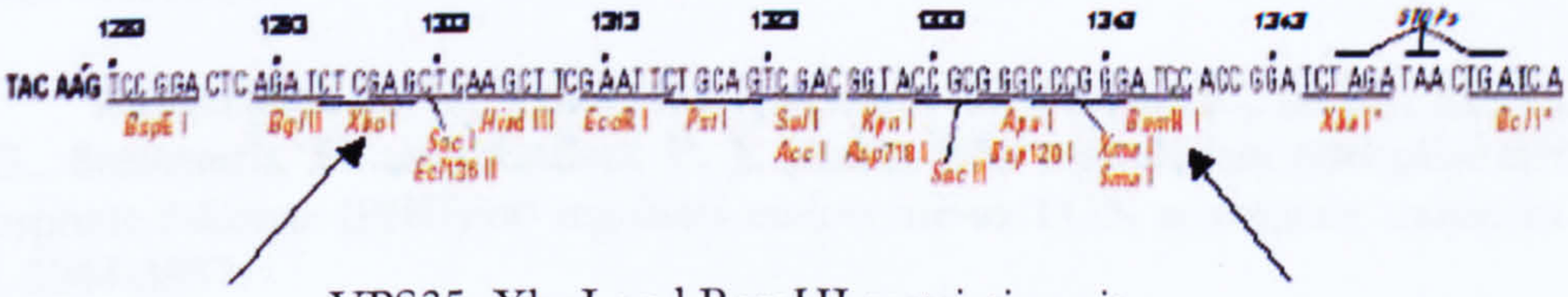

VPS35: XhoI and BamHI restriction sites

3. pmRFP-2xFYVE

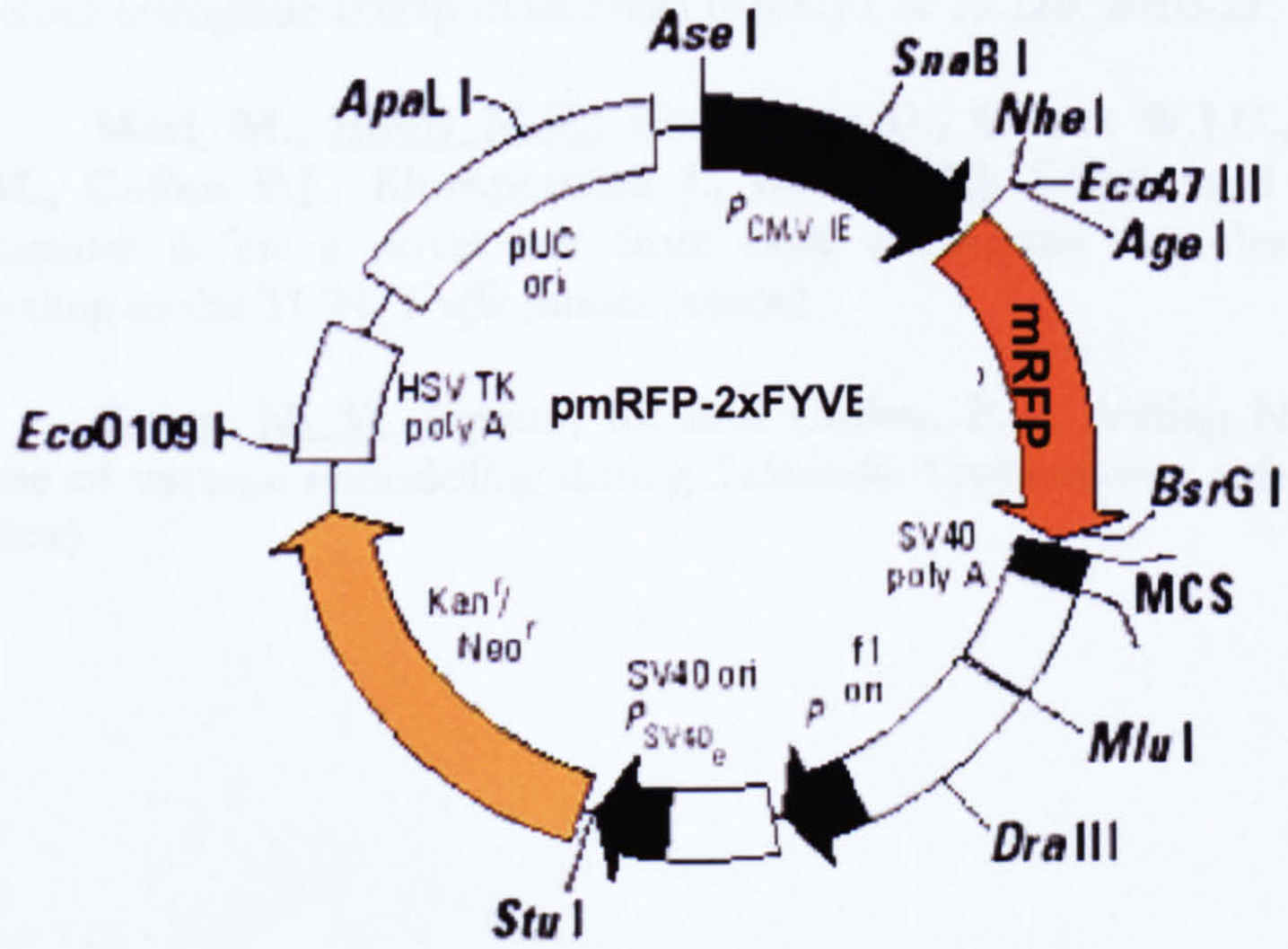

Created from pEGFP-C1-2xFYVE (Pattni et al., 2001)
GFP-coding sequence was replaced with mRFP (excised from pmRFP) using AgeI and BsrGI restriction sites (see **para. 5.2.2**)

III. Publications

Carlton, J., Bujny, M., Peter, B. J., Oorschot, V. M. J., Rutherford, A., Mellor, H., Klumperman, J., McMahon, H. T. and Cullen, P. J. (2004). Sorting nexin-1 mediates tubular endosome-to-TGN transport through coincidence sensing of high-curvature membranes and 3-phosphoinositides. *Current Biology* **14**, 1791-1800.

Carlton, J., Bujny, M., Rutherford, A. and Cullen, P. (2005a). Sorting nexins - Unifying trends and new perspectives. *Traffic* **6**, 75-82.

Carlton, J. G., Bujny, M. V.*, Peter, B. J., Oorschot, V. M. J., Rutherford, A., Arkell, R. S., Klumperman, J., McMahon, H. T. and Cullen, P. J. (2005b). Sorting nexin-2 is associated with tubular elements of the early endosome, but is not essential for retromer-mediated endosome-to-TGN transport. *J Cell Sci* **118**, 4527-4539.
* joint first author

Rutherford, A. C., Traer, C., Wassmer, T., Pattni, K., Bujny, M. V., Carlton, J. G., Stenmark, H. and Cullen, P. J. (2006). The mammalian phosphatidylinositol 3-phosphate 5-kinase (PIKfyve) regulates endosome-to-TGN retrograde transport. *J Cell Sci* **119**, 3944-3957.

Wassmer, T., Attar, N., Bujny, M. V., Oakley, J., Traer, C. J. and Cullen, P. J (2007). A loss-of-function screen reveals SNX5 and SNX6 as potential components of the mammalian retromer. *J Cell Sci* **120**, 45-54.

Bujny, M. V., Popoff, V., Johannes, L. and Cullen, P. J. The retromer component, sorting nexin-1, is required for efficient early endosome-to-*trans* Golgi network retrograde transport of Shiga toxin. *J Cell Sci* **120**, 2010-21.

Mari, M., Bujny M.V., Zeuschner D., Geerts W.J.C., Griffith J., Petersen C.M., Cullen P.J., Klumperman J., Geuze H.J. Sortilin and Mannose 6-phosphate Receptors define a novel exit from early endosomal vacuoles for SNX1-dependent recycling to the TGN. *Traffic* (under review)

Bujny, M. V., Jepson, M. and Cullen, P. J. Sorting Nexin-1 defines an early phase of vacuole remodelling during *Salmonella* Typhimurium infection. *J Cell Sci.* (under review)